The Hong Kong Polytechnic University

Department of Applied Biology and Chemical Technology

Structural and functional studies on class A β-lactamase-derived biosensors

WONG WAI TING

A thesis submitted in partial fulfilment of the requirements for the degree of Doctor of Philosophy

August 2010

Certificate of originality

I hereby declare that this thesis is my own work and that, to the best of my knowledge and belief, it reproduces no material previously published or written, nor material that has been accepted for the award of any other degree or diploma, except where due acknowledgement has been made in the text.

Wong Wai Ting

August 2010

Abstract

The extensive use of beta-lactam antibiotics in veterinary and clinical applications has led to food contamination and reduced efficacy of β-lactam antibiotics as bacteria become antibiotic-resistant due to selective pressure. The major mechanism of antibiotic resistance in bacteria is β-lactamase that inactivates the β-lactam antibiotics. Recently, our group has constructed a "switch-on" fluorescent biosensor from a β-lactamase (Chan P.-H. *et al.*; *J. Am Chem. Soc.*, **2004**, *126*, 4074) that can successfully detect trace amount of β-lactam antibiotics. In this project, the β-lactamase from *Bacillus licheniformis* 749/C (PenP) was engineered by site-directed mutagenesis to form the mutant E166C, in which the Glu166 residue in the Ω-loop is replaced with a cysteine residue. It was separately labeled with two thiol-reactive fluorophores, badan (b) and fluorescein-5-maleimide (f) to form two biosensors, PenP_E166Cb and PenP_E166Cf, respectively. This project concentrates on the study of the biosensing mechanisms of both biosensors in order to explain how they generate fluorescence changes upon β-lactam binding.

The fluorescence studies of both PenP_E166Cb and PenP_E166Cf with various β-lactams (mainly cephalosporins) reveal that the formation of enzyme-substrate complex enhances the fluorescence of the biosensors significantly. For PenP_E166Cb, the response is selective, and only the addition of oxyimino-cephalosporins gave significant enhancement in fluorescence intensity. Structural studies of PenP_E166Cb and PenP_E166Cf, as well as their antibiotic-bound intermediates show that the biosensing mechanisms in E166Cb and E166Cf are different. The results show that the E166Cb only detects oxyimino-

cephalosporins because of the steric clashes between the side chain of oxyimino-cephalosporins and the Ω-loop residues, which induces a change in the local environment around the fluorophore. But E166Cf detects all cephalosporins as the fluorescein label is likely to share a common space with the incoming β-lactam in the active site so that the fluorescein label is displaced from the active site to a more solvent exposed environment. Binding kinetics was studied by ESI-MS to investigate the binding rate of cefotaxime for PenP_E166Cb in comparison with the unlabeled enzyme E166C. We found that the flexibility of the Ω-loop in PenP_E166Cb is significantly increased and the Ω-loop changed to a new conformation after incorporation of the badan label. The new conformation results in the improved binding of cephalosporins with large side chains. Furthermore, based on the crystal structure of PenP_E166Cb, some residues that are in close proximity to the badan label were changed and the biosensing properties of the β-lactamase-based biosensor were improved.

Acknowledgement

I would like to thank my supervisor Prof. Thomas Y. C. Leung for his guidance, advice and support. In these four years, he has given me a great deal of freedom in doing research. He has taught me the passion and enthusiasm of the research science. Also, he has provided the best environment for my research. He is the kindest supervisor I have ever met.

I would like to give my deepest gratitude to my co-supervisor Dr. Y. X. Zhao. Her invaluable advice and patience throughout the course has helped me learn so much from this interesting project, especially in the study of crystallography.

I owe special thanks to Dr. H. K. Yap for his invaluable knowledge, suggestions and patience in teaching me molecular biology. He has supported me and helped me a lot in these years. Thanks for demonstrating to me various experimental techniques during my project.

I would particularly like to thank Mr. P. K. So, who taught me the use of mass spectrometry. He has given me valuable ideas and advice on experimental design.

Last but not the least, thanks are never enough to my parents and my friends, Dr. Alan Lam, Dr. Emily Tsang, Dr. Gabriel Wong, Dr. P. H. Chan, Dr. Ryan Chow, Dr. W. H. Chung, Mr. Angus Chan, Miss Kareena Tsang, Mr. Leo Lee, Miss Sammi Tsui, Miss Sandra Siu, Mr. Steve Chong, who have given me

endless support and encouragement throughout the difficult time of study. We have shared more than a few laughs along the way.

Table of Contents

Chapter 3: Characterization and functional study of the fluorescent biosensor PenP_E166Cb

Abbreviations

6xHis-tag	**Six-histidine-tagged**
badan	**6-bromoacetyl-2-dimethylaminoaphthalene**
B. licheniformis	**Bacillus licheniformis**
CD	**Circular dichroism**
CV	**Column volume**
Da	**Dalton**
DDI	**Double deionized**
DEAE	**Diethylaminoethyl**
DMF	**Dimethyul formamide**
E	**Enzyme**
EG	**Ethylene glycol**
ES	**Non-covalent enzyme-substrate complex**
ES*	**Covalent enzyme-substrate complex**
ESI-MS	**Electrospray ionization mass spectrometry**
E. coli	**Escherichia coli**
EDTA	**Ethylenediamine tetra acetic acid**
fluorescein	**Fluorescein-5-maleimide**
GdnHCl	**Guanidinium hydrochloric acid**
h	**Hours**
IPTG	**Isopropyl beta-D-thiogalactoside**
Kan^r	**Kanamycin resistance**
mAU	**Milli absorption unit**
Milli-Q	**Double-deionzed water through 0.2µm filter**
min	**Minute**
MPD	**2-Methyl-2,4-pentanediol**
M.W.	**Molecular weight**
NaCl	**Sodium Chloride**
OD_x	**Optical density at x nm wavelength**
PBPs	**Penicillin binding proteins**
PEG	**Polyethylene glycol**
PenPC	**Beta-lactamase I of Bacillus cereus 569/H**
PenP	**Beta-lactamase of Bacillus licheniformis 749/C**
ppb	**Parts per billion**
rpm	**Revolutions per minute**
s	**Second**
SDS/PAGE	**Sodium dodecyl sulphate polyacrylamide gel electrophoresis**
TB	**Terrific Bloth**
TEV protease	**tobacco etch virus protease**
Tris-HCl	**Tris(hydroxymethyl)aminomethane (pH adjusted with hydrochloric acid)**
UV	**Ultra violet light**
VIS	**Visible light**
v/v	**Volume per volume**
w/v	**Weight per volume**

List of Figures and Tables

Tables	Descriptions
1.1	Milk drug residue test detection levels
2.1	Excitation and emission parameters used in fluorescence measurement
3.1	Labeling efficiencies of PenP_E166Cb at different labeling conditions
3.2	The percentage change in fluorescence intensity and shift in wavelength maximum upon adding various β-lactams to PenP_E166Cb
4.1	X-ray data collection and structure refinement statistics for PenP_E166C, apo PenP_E166Cb and PenP_E166Cb in complex with cefotaxime
4.2	X-ray data collection and structure refinement statistics for PenP_E166Cb in complex with 7-ACA, cephaloridine and cefoxitin
5.1	(a) Primers for site-directed mutagenesis of PenP_E166Cb (b) Components for PCR reactions.
5.2	PCR reaction condition for site-directed mutagenesis
5.3	(a) Primers used and (b) PCR reaction condition for cloning of 6xHis_TEV_PenP_E166C/L169N/N104L
5.4	Reaction components for restriction digestion of PenP encoding gene
5.5	Ligation reaction of PenP gene and pRset-K
5.6	PCR reaction components for verification of the ligation reaction
5.7	PCR reaction conditions for verification of the ligation reaction
5.8	Theoretical and calculated molecular masses of (a) PenP_E166C mutants and (b) PenP_E166Cb mutants.
6.1	Labeling efficiency of PenP_E166Cf at different labeling conditions
6.2	X-ray data collection and structure refinement statistics for apo PenP_E166Cf and PenP_E166Cf in complex with cefotaxime
6.3	Kinetic parameters of the PenPC_E166C, PenPC_E166Cf and PenPC_E166Cb for the hydrolysis of cefuroxime determined by ESI-

MS

Scheme	Descriptions
1	Catalytic mechanism of penicillin binding protein
2	Catalytic mechanism of β-lactamases
3	The labeling reaction between PenP_E166C and badan
4	The labeling reaction between PenP_E166C and fluorescein-5-maleimide

Appendix	Descriptions
I	Protein sequences of all mutants done for 6xHis_TEV_PenP_E166C
II	Plasmid map for 6xHis_TEV_PenP_E166C/L169N/N104L
III	Hampton Screen Formulation CS1 and CS2

Chapter 1: Introduction

1.1 β-lactam antibiotics

β-lactams have been used for a long time to treat infectious diseases in both Gram-negative and Gram-positive bacterial infections (Poole 2004; Drawz *et al.* 2009; Fisher and Mobashery 2009). Accounting for >65% of the world antibiotic market, β-lactams target the penicillin-binding proteins (PBPs), which are responsible for cell wall biosynthesis. The β-lactam antibiotics will bind to PBPs and the peptidoglycan synthesis will be retarded. This will lead to cell death. The mechanism and function of PBPs will be further discussed in Section 1.2.

β-lactam antibiotics' ancestor is penicillin. The story started when a Scottish bacteriologist, Alexander Fleming, made an observation in an experiment (Kong *et al.* 2010). He realized that the Staphylococcus colonies on the culture plates, which are in close proximity to the mold, were transparent and seemed to be undergoing lysis. Therefore he concluded that there was something with microbial antagonistic property present. This finding led him and his colleagues to find out and purify penicillin from a strain called *Penicillium chrysogenum*. Large-scale production of penicillin for clinical trials was successfully achieved in 1941. Different forms of penicillin were produced from different production conditions, but they all contained β-lactam rings.

A β-lactam antibiotic contains a β-lactam ring, which is a lactam with a heteroatomic ring structure with three carbon atoms and one nitrogen atom. The

key component in penicillin (penam) synthesis and modification is the β-lactam nucleus, 6-aminopenicilanic acid (6-APA, Figure 1.1). By adding different side-chains to 6-APA at the C-6α position, different kinds of β-lactam agents can be produced. Therefore 6-APA is the starting block for the preparation of penicillins. The core structure and the numbering system of penicillins are shown in Figure 1.1. Penicillin G, penicillin V, ampicillin, amoxicillin, oxacillin and meticillin are some common examples of penicillins (Figure 1.1).

Cephalosporin (cepham) is another kind of β-lactam agent that contains the cephalosporin nucleus, 7-aminocephalosporanic acid (7-ACA) (Figure 1.2). It is derived from cephalosporin C from a strain of *Cephalosporium acremonium* and it is analogous to the penicillin nucleus 6-aminopenicillanic acid. Similar to 6-APA, changing of the 7-ACA side-chains on C-7α and C-3 positions would result in the development of a wide variety of antibiotic agents with potent broad-spectrum activity (Caselli *et al.* 2001). On the base of the side chain (R_2 group) on the C-7α position, cephalosporins can be divided into oxyimino-cephalosporins and non-oxyimino-cephalosporins. Cefotaxime and cefoxitin are examples of oxyimino-cephalosporins and non-oxyimino-cephalosporins, respectively. The core structure with numbering system and examples of different generations of cephalosporins are shown in Figure 1.2. The definition of generations is according to the antibiotics' antimicrobial spectrum.

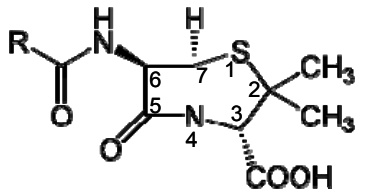

Core structure of penicillins

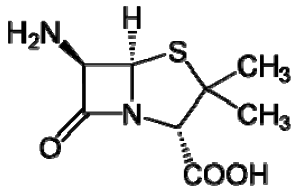

6-APA

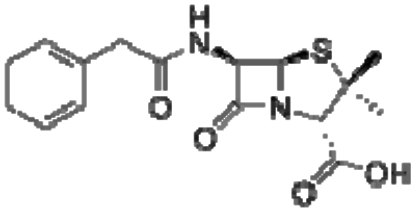

penicillin G

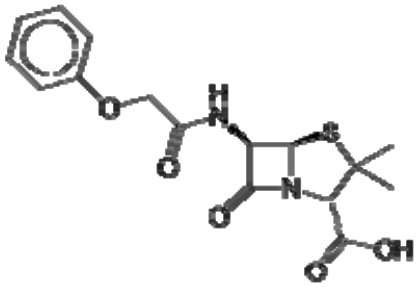

penicillin V

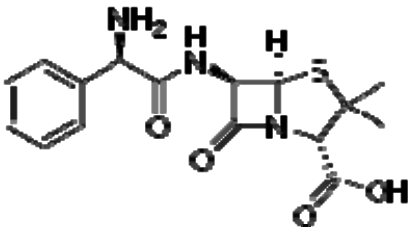

ampicillin

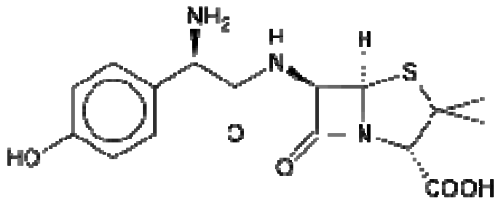

amoxicillin

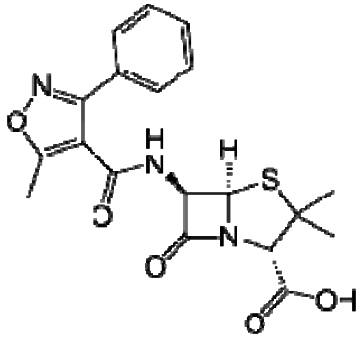

oxacillin

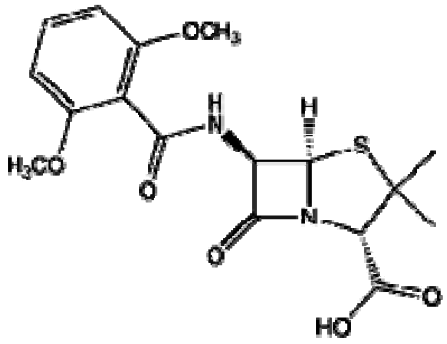

meticillin

Figure 1.1: Chemical structures of some penicillins (penams).

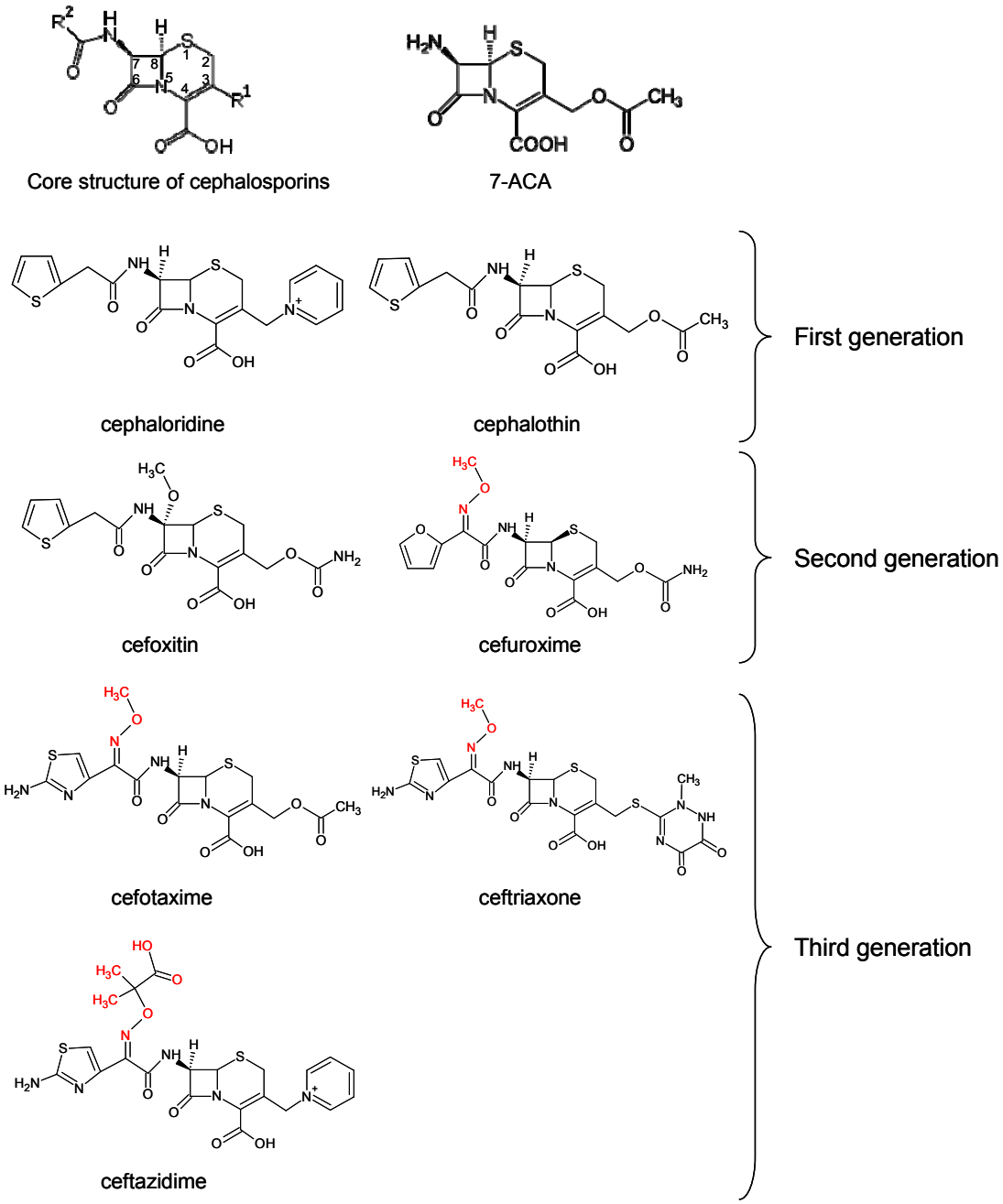

Figure 1.2: Chemical structures of some cephalosporins (cephems).

1.2 Penicillin binding proteins

The cell wall is essential for bacteria to preserve cell shape and rigidity, and to resist intracellular pressure of different atmospheres that occurs inside the cell. The cell wall is a highly cross-linked peptidoglycan layer comprised of repeating unit of alternating disaccharide, N-acetyl glucosamine and N-acetyl muramic acid. The disaccharides are always terminated by two D-alanine residues. The cross-linking of the peptidoglycan units is catalysed outside the cytoplasmic membrane by an enzyme called cell-wall transpeptidases (Wilke *et al.* 2005).

The transpeptidase enzymes have a serine active site for acylation and deacylation to achieve the catalytic cycle. They are called penicillin binding proteins (PBPs) because β-lactam antibiotics can inhibit the cell-wall transpeptidases efficiently. PBPs catalyze the polymeriazation of the glycan strand (transglycosylation) and the cross-linking between glycan chains (transpeptidation) (Sauvage *et al.* 2008). After PBP acylation, the long-lived acyl-PBP species will cross-link to the amino group of the neighbouring chain, generating a single polymeric macromolecule. The mechanism of the peptidoglycan crosslinkng is shown in Figure 1.3 (Fisher *et al.* 2005).

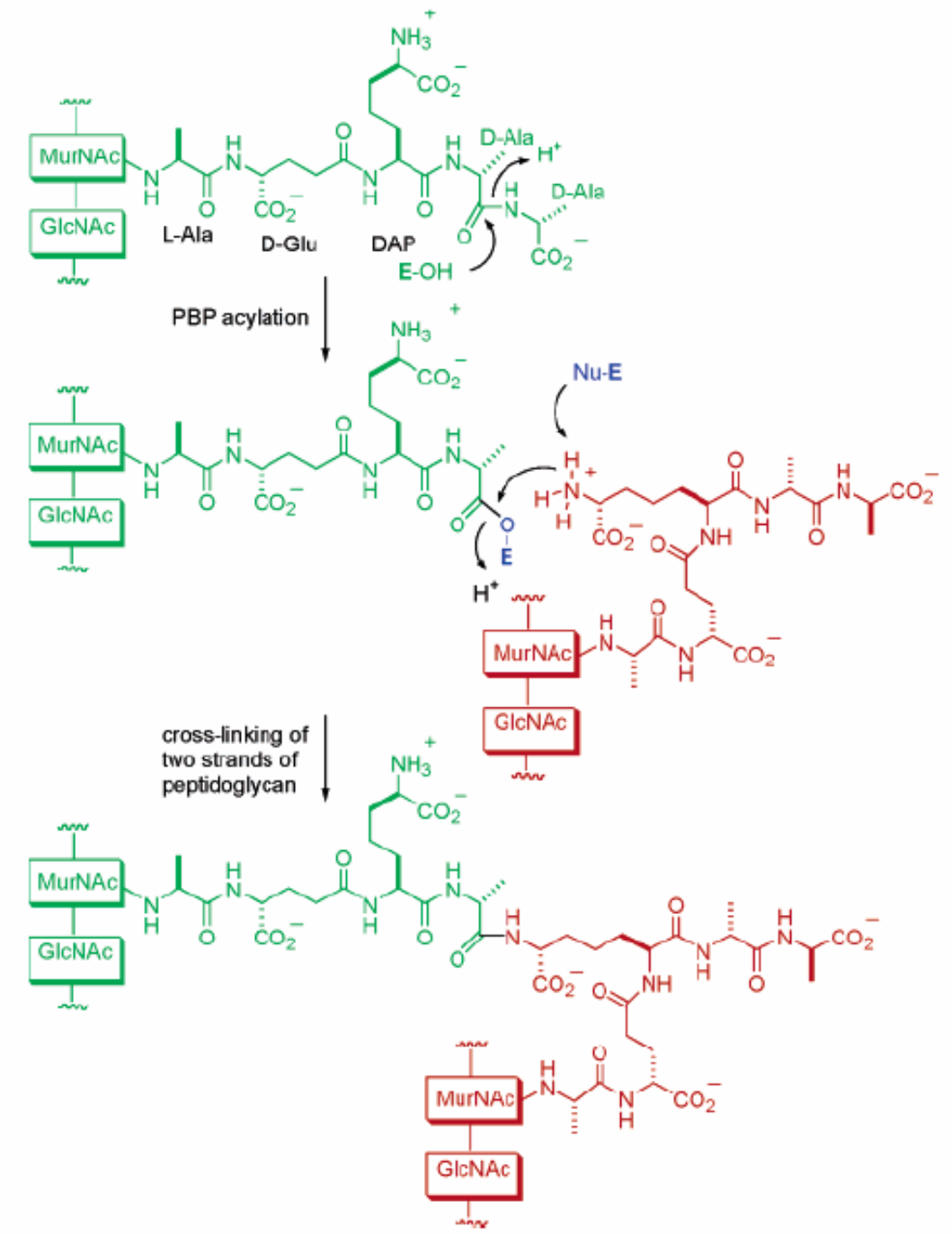

Figure 1.3: Schematic diagram of the mechanism of peptidoglycan cross-linking in cell wall biosynthesis. (Obtained from: Fisher, J.F., Meroueh, S.O., and Mobashery, S. 2005. Bacterial resistance to β-lactam antibiotics: compelling opportunism, compelling opportunity. Chem Rev 105: 398, Scheme 2)

PBPs can be classified into two categories: high molecular weight (HMW) PBPs and low molecular weight (LMW) PBPs. HMW PBPs are responsible for peptidoglycan polymerization and insertion into pre-existing cell wall (Goffin and Ghuysen 1998). They belong to class A or class B PBPs depending on the structure and the catalytic activity of the N-terminal domain (Sauvage *et al.* 2008). LMM PBPs are usually called class C PBPs. The classification of HMW PBPs is shown in Figure 1.4.

(a)

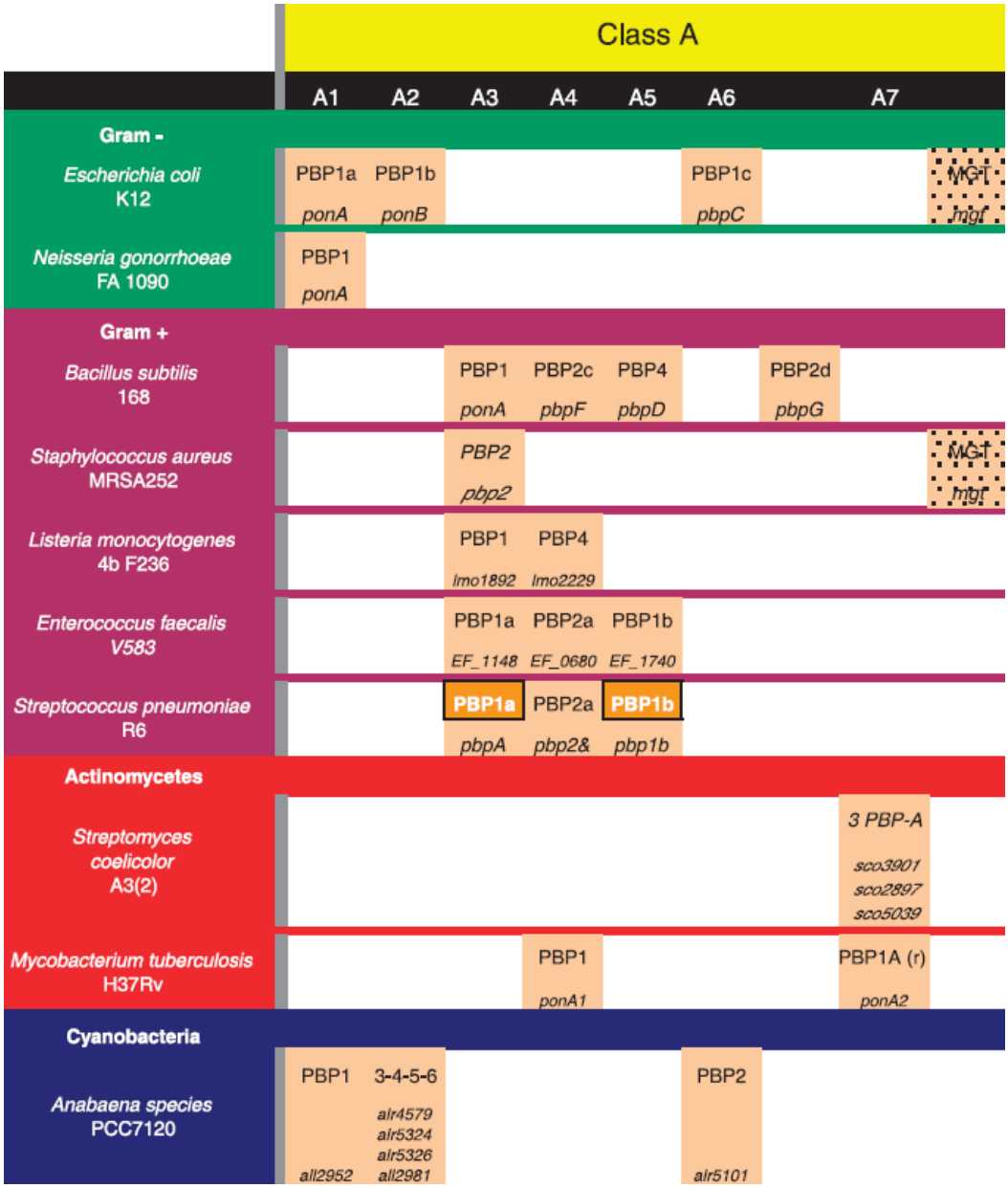
Class A
A1
A2
A3
A4
A5
A6
A7
Gram -
Escherichia coli K12
PBP1a ponA
PBP1b ponB
PBP1c pbpC
MGT mgt
Neisseria gonorrhoeae FA 1090
PBP1 ponA
Gram +
Bacillus subtilis 168
PBP1 ponA
PBP2c pbpF
PBP4 pbpD
PBP2d pbpG
Staphylococcus aureus MRSA252
PBP2 pbp2
MGT mgt
Listeria monocytogenes 4b F236
PBP1 lmo1892
PBP4 lmo2229
Enterococcus faecalis V583
PBP1a EF_1148
PBP2a EF_0680
PBP1b EF_1740
Streptococcus pneumoniae R6
PBP1a pbpA
PBP2a pbp2&
PBP1b pbp1b
Actinomycetes
Streptomyces coelicolor A3(2)
3 PBP-A sco3901 sco2897 sco5039
Mycobacterium tuberculosis H37Rv
PBP1 ponA1
PBP1A (r) ponA2
Cyanobacteria
Anabaena species PCC7120
PBP1 all2952
3-4-5-6 alr4579 alr5324 alr5326 all2981
PBP2 alr5101

(b)

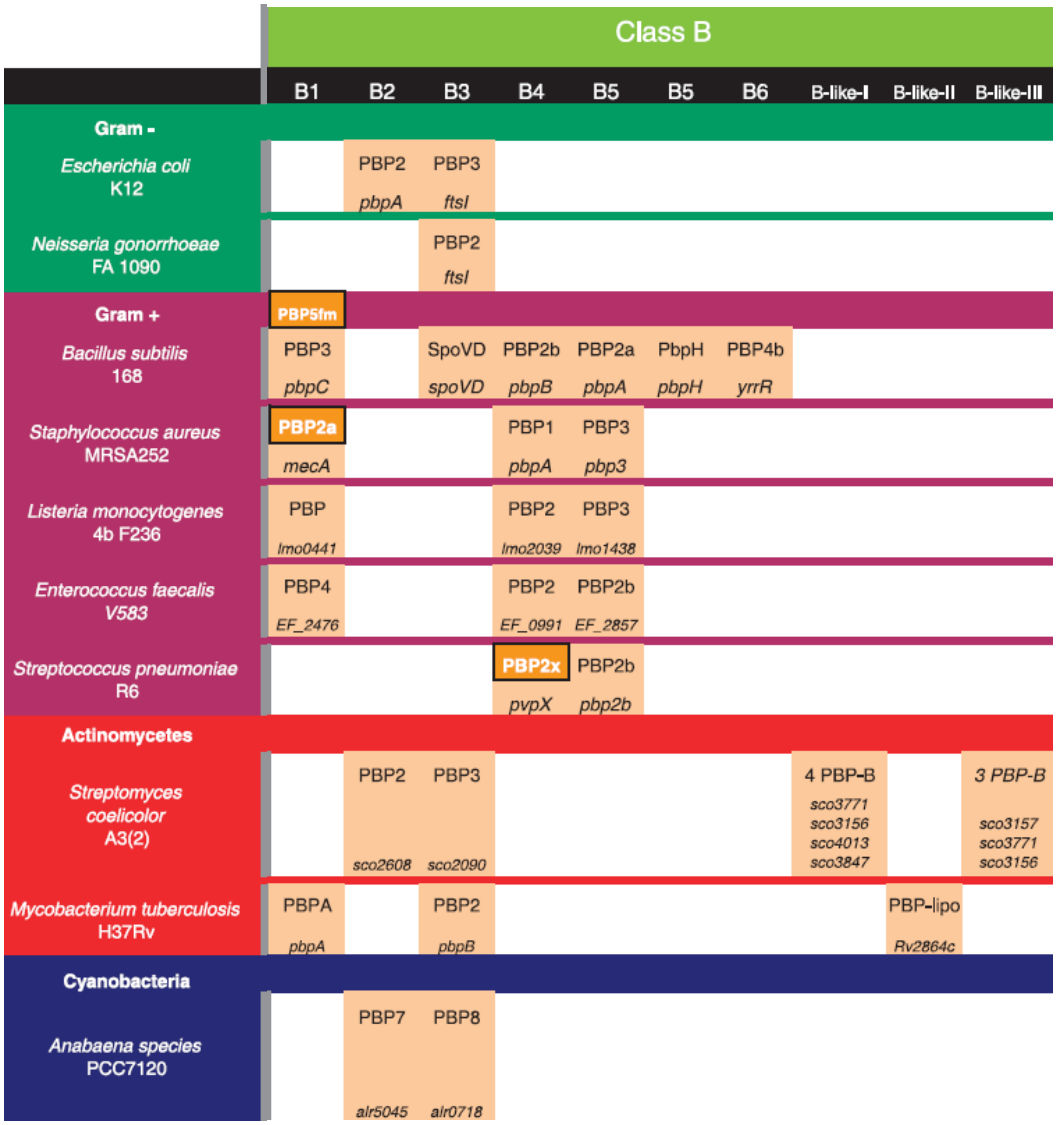

Figure 1.4: HMW PBPs classification. Complete set of (a) class A and (b) class B HMW PBPs from 10 bacteria. The two class subdivisions are adapted from Goffin & Ghuysen (1998). The name of the PBP is given with its encoding gene (for most PBPs) (Obtained from: Sauvage, E., Kerff, F., Terrak, M., Ayala, J.A., and Charlier, P. 2008. The penicillin-binding proteins: structure and role in peptidoglycan biosynthesis. FEMS Microbiol Rev 32: 235, Figure 1).

Since β-lactam antibiotics are highly similar in stereochemical properties to the D-alanine-D-alanine substrate for transpeptidases, β-lactams can bind to the active site of the PBPs covalently and form penicilloyl-enzyme complexes. As a result, the active site is blocked and the normal transpeptidase catalysis is stopped and inhibited. The cell wall peptidoglycan is no longer highly cross-linked and thus the bacteria will be highly susceptible to cell death (Wilke *et al.* 2005). The following reaction scheme shows how PBP reacts with β-lactam antibiotics to form the acyl-enzyme intermediate. The reaction follows the Michaelis-Menten mechanism:

Scheme 1:

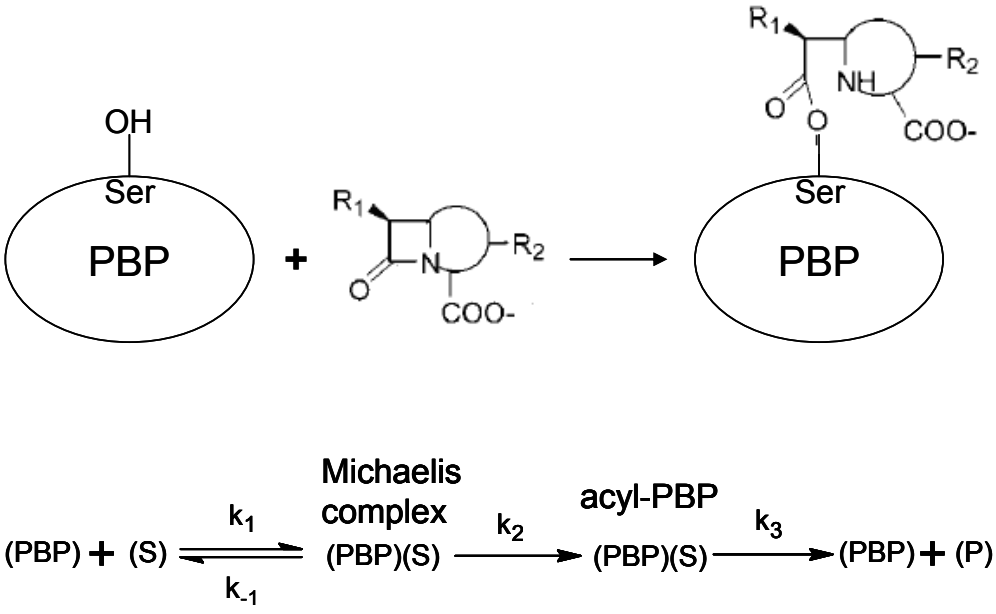

where (S) is the β-lactam, (PBP)(S) before k_2 is the non-covalent Michaelis complex of PBP and β-lactam, (PBP)(S) after k_2 is the covalent complex of PBP and β-lactam and P is the hydrolyzed β-lactam. k_1, k_{-1}, k_2 and k_3 are the rate constant. k_2 is the acylation rate constant and k_3 is the deacylation rate constant. The k_3 in PBP is very small.

The rate constants for different types of PBPs to react with β-lactams have been studied widely by mass spectrometry (Mouz *et al.* 1999; Di Guilmi *et al.* 2000; Llinas *et al.* 2005). For example, the deacylation rate constants of *Streptococcus pneumoniae* PBP2x mutants in complex with β-lactam antibiotics were determined by electrospray ionization mass spectrometry (Di Guilmi *et al.* 2000). The determination of all rate constants is essential for a better understanding of the mechanism of resistance of PBPs to β-lactams. The k_3 values of three different PBPs (S-PBP2x, R-PBP2x and T338P (S-PBP2x mutation Thu338Pro)) complexed with two different antibiotics (benzylpenicillin and cefotaxime) were determined. It was found that the mutations on S-PBP2x present a marginally affected deacylation rate for the two antibiotics compared with the wild-type S-PBP2x one.

There were also some structural studies on the PBPs (Lee *et al.* 2001; Lim and Strynadka 2002; Yamada *et al.* 2007; Job *et al.* 2008). For example, the structure of a PBP complexed with a cephalosporion was resolved at a resolution of 1.2 Å (Lee *et al.* 2001). The cephalosporin was incorporated into the active site serine of D-alanyl-D-alanine carboxypeptidase/transpeptidase (EC) from *Streptomyces sp.* strain R61. This structure demonstrated how the two peptide strands are sequestered in the presence of the antibiotic and so the mechanism of the cross-linking reaction could be probed.

The structure of PBP2a from *S. aureus* (SauPBP2a) was determined at 1.8 Å resolution (Lim and Strynadka 2002). The newly discovered PBP2a is more resistant to antibiotics with normal lethal concentrations used clinically because

it has low affinity to β-lactams. The acyl-PBP complexes of SauPBP2a with nitrocefin, penicillin G and methicillin were also determined. All these structures together reveal changes in the conformation of SauPBP2a with different substrates and important chemical interactions between PBP2a and the substrates.

1.3 β-lactamases

Due to attacks of antimicrobial agents, bacteria become resistant to β-lactam antibiotics by three mechanisms: alteration of the antibiotic binding site in PBPs, alteration of permeability or efflux pumps to expel β-lactams, and most commonly, production of β-lactam hydrolyzing β-lactamases enzymes that degrade the β-lactams prior to attacking the target site (Neu 1992; Wilke *et al.* 2005). The β-lactamase is classified into four major classes, classes A to D, by the Amber classification scheme, a classification that bases on amino acid sequence similarity (Bonomo and Rice 1999; Fisher *et al.* 2005; Wilke *et al.* 2005). Class A β-lactamases are described as "Penicillinases" as their ability to catalyse penicillin hydrolysis is greater than that of cephalosporins (Fisher *et al.* 2005). Penicillinases include the Gram-negative plasmid penicillinase TEM/SHV, the *P. aeruginosa* PER/OXA/TOHO cephalosporinases, and the CTX-M carbapenemase subclasses; Class B β-lactamases are the metallo-β-lactamases; Class C β-lactamases are the chromosomal cephalosporinases with mechanism similar to class A β-lactamases, involving both active site acylation and hydrolytic deacylation. The crystal structures show that the active site residues Ser64, Lys67, Lys315 and Tyr150 in class C β-lactamases correspond to Ser70, Lys73, Lys315 and Ser130 in class A β-lactamases respectively; Class D β-lactamases are oxacillinases. Class A, C, and D β-lactamases all use serine as the catalytic residue in the active site, while the hydrolysis of β-lactam proceeds via an acyl-enzyme intermediate. Class B β-lactamases are very different from classes A, C and D β-lactamases in terms of protein sequence, folding and catalytic mechanism (Wilke *et al.* 2005). They are subdivided into three subclasses, B1, B2 and B3. One or two zinc ions bound onto the catalytic centre

of the enzyme will coordinate with the nucleophilic hydroxide, which is the attacking nucleophile responsible for β-lactam hydrolysis. There is no covalent intermediate in the catalytic mechanism (Page 2000).

Class A β-lactamases contain a Ω-loop, which is a secondary structural element that associates with the active site, and contains the catalytic residue Glu166. Gly166 is important for the deacylation step in the catalytic mechanism (Palzkill and Botstein 1992; Palzkill *et al.* 1994; Banerjee *et al.* 1998; Therrien *et al.* 1998). Studies about the functional and structural roles of the Ω-loop have been carried out (Palzkill *et al.* 1994; Huang *et al.* 1996). For example, deletion of the 16-residue Ω-loop in *Staphylococcus aureus* PC1, encompassing residues 163-178, was produced and and the crystal structure of the mutant was determined and refined at 2.3 Å (Banerjee *et al.* 1998). Initially, penicillin is better substrate for the wild type β-lactamases than cephalosporin. However, the deletion of the Ω-loop led to the enzyme's only acting on cephalosporins, including third generation ones. Because of the deletion of Glu166 that is situated on the Ω-loop and the disappearance of nucleophilic water site that is associated with the Ω-loop, the hydrolysis of the acyl-enzyme intermediate was prevented. The crystal structure demonstrated that the overall fold of the mutant enzyme was similar to that of the wild type β-lactamase. However, there were a few local adjustments in the vicinity of the missing Ω-loop.

β-lactamases that are capable of hydrolyzing the extended-spectrum cephalosporins have been continuously discovered worldwide. They contain single or several mutations compared with the wild-type β-lactamases (Huang *et al.* 1996). The evolution of this kind of new β-lactamases, which are called

extended-spectrum β-lactamases (ESBLs), is due to the widespread use of β-lactam antibiotics in the past few decades (Lee *et al.*). ESBLs are resistant to penicillins, first-, second-, and third-generation cephalosporins, and most aztreonam (Paterson and Bonomo 2005). The SHV-type and TEM-type class A ESBLs are more commonly found in clinical isolates than other type of ESBLs. SHV-1 shares 68 percent of amino acid sequence homology with TEM-1 and they have similar overall structures. Both SHV-type and TEM-type ESBLs have one or more amino acid substitutions around the active site (Salverda *et al.*; Knox 1995; Jacoby and Munoz-Price 2005).

In order to retain antimicrobial activity, combination therapies in which β-lactam antibiotics are coupled with β-lactamase inhibitors are used so that the enzyme inhibitors will permanently inactivate the β-lactamase in the periplasmic space and the antibiotics can attack the target PBPs. The ability to treat different bacterial infections in the community and hospitals has been advanced with the use of the β-lactam antibiotics/β-lactamase inhibitor combinations, such as ampicillin/sulbactam, piperacillin/tazobactam and amoxicillin/clavulanate (Bonomo and Rice 1999). Novel compounds like succinic acid derivatives and substituted penam sulfones have been reported in recent years (Wilke *et al.* 2005). However, quite a large number of β-lactamases are discovered in the clinic that are resistant to inactivation by β-lactamase inhibitors. It was found that a single amino acid mutation can cause resistance to combinations of β-lactam/ β-lactamase inhibitors, such as the amino acid substitution at Ambler position Arg244 in class A TEM and resistance of SHV β-lactamases to ampicillin/clavulanate (Thomson *et al.* 2007). Therefore novel inhibitors with strategic chemical properties are needed instantly to fight against the evolution of

inhibitor resistant β-lactamases.

1.4 Mechanism of β-lactam hydrolysis

Bacterial class A β-lactamases are very powerful enzyme to bind to a large variety of β-lactam antibiotics and hydrolyze them efficiently. The hydrolysis reaction resembles the PBPs' catalytic reaction. It involves two steps and the mechanism is shown in Scheme 2, where E is the enzyme, S is an antibiotic substrate, ES is the non-covalent enzyme-substrate complex, ES* is the acyl-enzyme adduct and P is the hydrolyzed product devoid of antibacterial activity. k_1, k_{-1}, k_2 and k_3 are the rate constants. k_2 is the acylation rate constant and k_3 is the deacylation rate constant (Chan *et al.* 2004).

Scheme 2

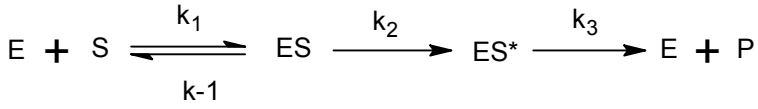

It is well known that the mechanism of β-lactamases mainly involves acylation and deacylation, where acylation is common in serine-β-lactamases and PBP, and deacylation is only observed in serine-β-lactamase (Figure 1.5). A precovalent encounter complex is first formed by non-covalent binding (A) (ES), and then becomes an acylated tetrahedral intermediate (B), which is in high-energy. A transiently stable covalent acyl-enzyme intermediate (ES*) is formed (C) afterwards. A hydrolytic water (D) in close proximity will then attack onto the carbonyl carbon on the acyl-enzyme to form a high-energy deacylation intermediate (E). Since k_3 is a very fast process, the ester-linkage of ES* will be hydrolyzed rapidly. When it collapses, the hydrolytic product is produced (F) (Minasov *et al.* 2002).

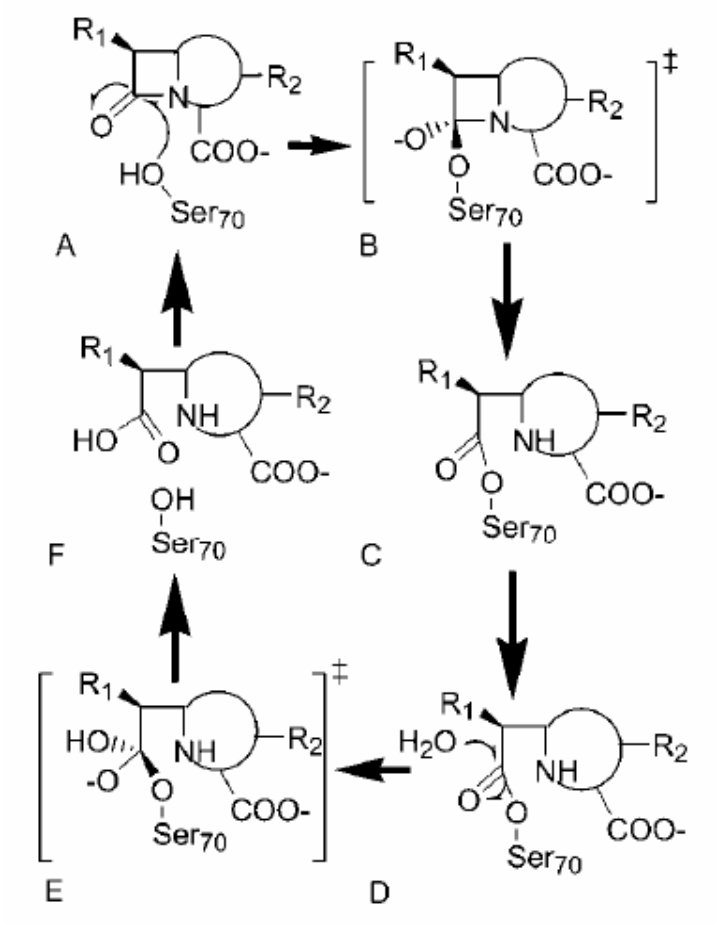

Figure 1.5: The reaction cycle of TEM-1 β-lactamase. The two states in braces represent the acylation and deacylation tetrahedral high energy intermediates (Obtained from: Minasov, G., Wang, X., and Shoichet, B.K. 2002. An ultrahigh resolution structure of TEM-1 β-lactamase suggests a role for Glu166 as the general base in acylation. *J Am Chem Soc* **124:** 5333-5340, Figure 1)

Candidates for the catalytic base to activate the serine nucleophile in acylation have been discussed for many years. The mechanisms are mainly divided into the following categories:

1) Lys73 as a general base for acylation

In the crystal structure of the molecular complex of penicillin G with a

deacylation-defective mutant of the RTEM-1 β-lactamase, the H-bond of Lys73Nζ and Ser70Oγ , which is originally present in the free structure, is no longer present but changes to Lys73Nζ and Ser130Oγ (Strynadka *et al.* 1992). Lys73 has a depressed proton affinity (pKa) and a neutral side-chain amino group so that it can act as a general base to abstract the proton on Ser70Oγ and assist in the nucleophilic attack of Ser70Oγ on the carbonyl-carbon of the substrate, so that the first tetrahedral intermediate is formed. The proton transfers from Ser70Oγ to Lys73Nζ, from Lys73Nζ to Ser130Oγ, and from Ser130Oγ to nitrogen of the leaving group.

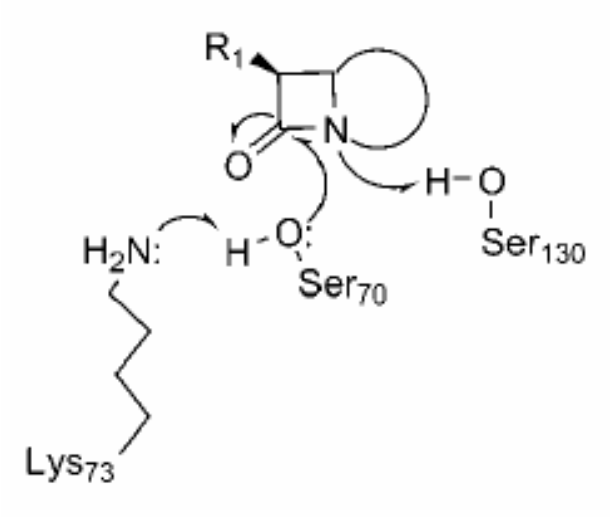

Figure 1.6: Proposed role of Lys73 as the catalytic base in acylation (obtained from: Minasov, G., X. Wang, *et al.* (2002). "An ultrahigh resolution structure of TEM-1 β-lactamase suggests a role for Glu166 as the general base in acylation." *J Am Chem Soc* **124**(19): 5333-40, Figure 2c)

2) Glu166 as an ultimate catalytic base for acylation

In the ultrahigh resolution structure of TEM-1 β-lactamase in complex with an acylation transition-state analogue, it can be observed that the Glu166 proton is hydrogen-bonded to Wat1004, while Wat1004 is a water molecule

which is hydrogen-bonded to the nucleophilic Ser70. The proton was shuttled from Ser70 to the water molecule, then finally to the Glu166 (Minasov *et al.* 2002).

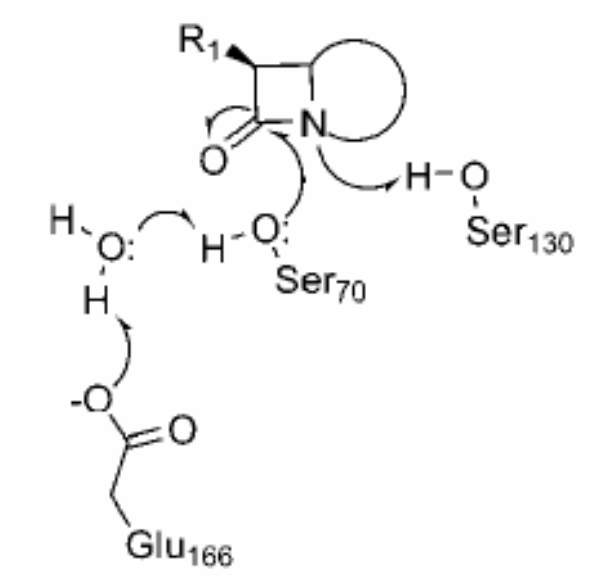

Figure 1.7: Proposed role of Glu166 as the catalytic base in acylation (obtained from: Minasov, G., X. Wang, *et al.* (2002). "An ultrahigh resolution structure of TEM-1 β-lactamase suggests a role for Glu166 as the general base in acylation." *J Am Chem Soc* **124**(19): 5333-40, Figure 2b)

3) Dual participation of Glu166 and Lys73 as general bases for acylation

With the use of ab initio quantum mechanical/molecular mechanical (QM/MM) calculations augmented by extensive molecular dynamics simulations, the general base promotion of Ser70 is not only Lys73 but also Glu166 in the serine acylation mechanism for the class A TEM-1 β-lactamase upon binding with penicillanic acid (Meroueh *et al.* 2005). Meroueh *et al.* (2005) claimed that both pathways can occur at the same time and so there is a dual participation of Glu166 and Lys73 in a concerted base promotion of Ser70. This study found that the Lys73 general base pathway only has a slightly higher energy than the

pathway involving Glu166 carboxylate as the general base, so the two pathways are competing favorably.

4) Glu166 as a general base in deacylation

Deacylation is initiated by a general-base-assisted nucleophilic attack of deacylating water (Strynadka *et al.* 1992). Many studies have proposed that the general base is Glu166 carboxylate, which can accept a proton from the catalytic water (Herzberg and Moult 1987; Jacob *et al.* 1990; Adachi *et al.* 1991; Escobar *et al.* 1994). The carboxylate group of Glu166 forms H-bond with the deacylating water molecule and with the side chain amide nitrogen of Asn170. The proton abstracted by the Glu166 is transferred back to Ser70Oγ so that the active site can be regenerated as the C7-Ser70Oγ bond is cleaved. It is believed that the Asn170 helps to direct the water molecule to the Glu166 and plays an important role in deacylation mechanism since site-directed mutagenesis on Asn170 to other residues has led to a large deduction in the deacylation rate (Lewis *et al.* 1997).

5) Lys73 as a proton donor in deacylation

Glu166 is not the only residue involved in deacylation since the distance between Ser70Oγ and Glu166Oε is too far away in the acyl-enzyme tetrahedral intermediate structure (Hata *et al.* 2006). Lys73 may also be involved in deacylation since it is located between Ser70 and Glu166. Mutation of Lys73 to alanine in the β-lactamase from *Bacillus licheniformis* gives rise to a significant reduction in the turnover rate and catalytic efficiency, and deacylation is a rate-limiting step in the reaction of penicillins (Lietz *et al.* 2000). This result reflects that the role of Lys73 as a proton donor in deacylation is more critical

than that in acylation. The major role of Lys73 is to donate a proton to the lactam N in the acylation reaction and to the Oγ of Ser70 in the acyl-enzyme in the deacylation reaction. Lietz *et. al* (2000) claimed that both Glu166 and Lys73 are important to each other for a fully efficient catalytic activity to occur, by maintaining an optimum electrostatic environment for the reaction.

1.5 Detection of β-lactam antibiotics in food

The β-lactams are one of the three largest antibiotics classes (the others are the macrolides and fluoroquinolones) widely used to treat bacterial infections in humans and livestock (Mitchell *et al.* 1998). However, it is essential to limit the use of antibiotics in the farming industries so that contamination of food can be minimized. It has been found that antibiotics are given to patients more often than recommended by guidelines set by federal and other healthcare organizations. This is becoming a big issue because bacteria have become resistant to those antibiotics. About 70 percent of bacteria that cause infections in hospitals are resistant to at least one of the most commonly used drugs that treat infections.

In order to detect antibiotics in food or human plasma, traditional analytical methods like mass spectrometry (Riediker and Stadler 2001), high performance liquid chromatography (McWhinney *et al.* 2010; Pires de Abreu *et al.* 2003) and capillary electrophoresis (CE) (Serrano and Silva 2007), are commonly used. These methods can give accurate results and can detect trace amounts of antibiotics in high sensitivity. However, there are many disadvantages of these methods, such as tedious sample preparation processes, complexity in using the machines and the high cost and maintenance of the machines.

Some simpler, faster and cheaper screening tests have been developed and sold as commercial kits for the detection of trace amounts of antibiotics in food . For example, the Charm test and the Penzym test are widely used to screen β-lactams in milk and have been approved by the US Food and Drug

Administration (FDA). The FDA recognizes six widely used β-lactam antibiotics (penicillin, ceftiofur, cloxacillin, cephapirin, amoxicillin, and ampicillin) in lactating dairy cattle that are the most likely to leave residues in milk if misused. Table 1.1 shows different screening tests for drug residues in milk. It can be seen that there are no universal screening tests that can detect all the targeted antibiotics at the safe level.

The Penzyme III Test is an enzymatic test for detection of β-lactam antibiotics in raw milk. It is based on an enzyme called DD-carboxypeptidase, which is inhibited by β-lactam antibiotics. If β-lactam antibiotics are present in a milk sample, the pre-added DD-carboxypeptidase in an assay tube will be inactivated after its mixing and incubating with the milk. A tablet containing the color reagent is then added to the reaction mixture. The intensity of the color generated is proportional to the remaining activity of the enzyme in the tube. By comparing with the standard colors provided, the amount of the β-lactam antibiotic is determined quantitatively. This test kit is available from Neogen (www.neogen.com).

Other examples of tests that can detect β-lactam antibiotics in raw, commingled bovine milk at or below the U.S. FDA-established tolerance/safe levels are the SNAP test and the Charm test. Most of these tests have the same working principles monitoring non-inhibited PBPs and generating the color change after adding some coloring reagents. Although these tests are convenient and speedy, most of them are semi-quantitative. Moreover, since they are not directly measuring the amount of β-lactams as competitive assays are involved, misleading or false positive results may be obtained since the fewer the

β-lactams there are, the higher the PBPs' activity and the higher the signal there will be.

Table 1.1: Milk drug residue test detection levels[a] (obtained from Memoranda of Information M-I-96-1: Milk Monitoring with Antimicrobial Drug Screening Tests, *http://www.fda.gov/Food/FoodSafety/Product-SpecificInformation/MilkSafety/CodedMemoranda/MemorandaofInformation/ucm082165.htm*)

Drug	PEN	AMP	AMOX	CLOX	CEPH	CEFT
Tolerance/Safe Level PPB	5	10	10	10	20	50
TEST						
Charm I/Cowside II Test for Cloxacillin	ND[b]	ND[b]	ND[b]	10	ND[b]	ND[b]
Charm II Test for Cloxacillin	ND[b]	ND[b]	ND[b]	10	ND[b]	ND[b]
Charm II Tablet Competitive Assay	4.8	9	10	70[c]	4.5	25
Charm Farm Test	5	10	10	40	20	25
Charm II Tablet Sequential Assay	4.8	8	10	50[c]	4.5	23
Charm II Tablet Transit Test	4.8	9	10	80[c]	4.5	13
Charm Rapid Inhibition Test	3	4.5	4.5	25[c]	16	50
Charm I/Charm II Tablet Test	4.8	10	10	50[c]	8	40
Charm II Tablet Quantitative Assay	4.8	8	10	10	4.5	23
Charm B. Stearothermophilus Disk Assay	5	6.5	10	48[c]	11	75[c]
Delvotest P	3	10	8	30[c]	8	50
Delvo-X-PRESS	5	10	10	50	10	10
Lactek B-L	5	10	8	8	16	ND[b]
Lactek CEF	ND[b]	ND[b]	ND[b]	ND[b]	ND[b]	50
Penzyme III Test	5	10	8	80[c]	8	80
Penzyme Milk Test	5	10	8	80	8	80
SNAP Test	5	10	10	50[c]	8	50

a - PPB which can be detected by test 90 percent of time with 95 percent confidence.

b - ND indicates not detected at 100 ppb.

c - Precise 90/95% levels were not determined for these sensitivities that are significantly above the tolerance/safe level.

PEN = Penicillin, AMP = Ampicillin, AMOX = Amoxicillin, CLOX = Cloxacillin, CEPH = Cephapirin, CEFT = Ceftiofur

1.6 β-lactamase-based biosensor

It is an emerging approach to design fluorescent biosensors in order to detect small ligands or ions (e.g. phosphate ions, retinoic acid, aminoglycoside antibiotics, amino acids, etc) (Hirshberg *et al.* 1998; de Lorimier *et al.* 2002; Donato and Noy 2006; Chu *et al.* 2008) and to study dynamic protein interactions, conformational changes and electrostatic character of proteins (Weiss 2000; Cohen *et al.* 2002; Michalet *et al.* 2006; Loving and Imperiali 2008). Fast and simple methods that can provide quantitative analysis are developed. Our research group has developed a novel and β-lactamase based fluorescent biosensor called PenPC_E166Cf, which is more sensitive, simple and quantitative and without tedious sample pre-treatment and without using expensive instruments and reagents (Chan *et al.* 2004).

The β-lactamase based biosensor is produced by mutagenesis of β-lactamase I from *Bacillus cereus* 569/H (PenPC), E166C, in which the Glu166 residue in the Ω loop is replaced with a cysteine residue, and then by the labeling of the cysteine residue with an environmental sensitive fluorophore, fluoescein-5-meleimide. It is noted that the mutation still allows the enzyme to undergo acylation with β-lactam antibiotics, but the deacylation step is much slower than that of the wild type enzyme. This may be due to the fact that Glu166 is responsible for activating the water molecule in the hydrolysis of β-lactam ring (Leung *et al.* 1994). The catalytic efficiency of this mutant was found to be over 1800-fold lower that that of the wild-type enzyme. This serves the purpose to detect the covalently bound acyl enzyme more easily by analyzing technique (Chan *et al.* 2004; Chan *et al.* 2005).

It has been reported that the Ω-loop is a flexible loop composed of a loosely packed 17-residue (residues 163 - 178) segment and is adjacent to the active site of β-lactamase for hydrolysis of the β-lactam ring (Banerjee *et al.* 1998). The choice of labeling at position 166 is attributed to the flexible loop and its proximity to the active site. In addition, the deacylation activity of the enzyme is depicted at the same time and this is an advantage for biosensing. Thus, upon binding to the β-lactam antibiotics at the active site, the local environment of the fluorophore will change that may result in significant changes in the fluorescence signal.

Beside β-lactamase I from *Bacillus cereus* 569/H (PenPC), some other β-lactamases can also be used as biosensors. In this project, β-lactamase of *Bacillus licheniformis* 749/C (PenP) labeled with badan was studied. The β-lactamase is encoded by a single chromosomal gene (Gray and Chang 1981). It has a much higher melting temperature (T_m) than other β-lactamases so that it is a more stable biosensor (Fitter and Haber-Pohlmeier 2004). The structure of badan and the reaction scheme between PenP and badan is shown in Scheme 3.

Scheme 3

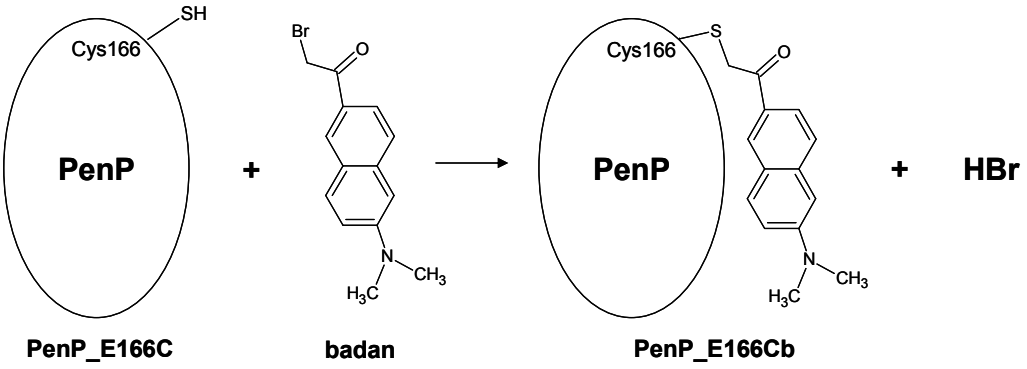

Scheme 3: The labeling reaction between PenP_E166C and badan.

1.7 Structural studies by X-ray crystallography

X-ray crystallography is the most favored technique to determine the structures of proteins and biological macromolecules for years. To obtain a three dimensional molecular structure, protein crystallization, mounting crystal, data collection, data processing, refinement and model building should be carried out step by step (Smyth and Martin 2000).

Protein crystallization:

The sample should be purified well since purity is the most important prerequisite for crystallizability. Protein will crystallize when the protein concentration increases in a suitable environment composed of certain amount of crystallizing agent with correct pH. Crystal growth in solution starts with nucleation of a microscopic crystallite and then a larger crystal is formed from the growth of the crystallite. When the concentration of protein or the crystallizing agent increases, supersaturation has been reached. Supersaturation can be divided into metastable phase, nucleation phase and precipitation phase while crystal only will grow in the first two phases. Different variables like pH, concentration, buffer, precipitant (like PEG), salt and temperature can be adjusted in order to obtain the best crystallization condition for a specific protein. There are several methods to achieve protein crystallization, the most common being the hanging drop vapour diffusion method. The set-up for this method is shown in Figure 1.8. The sample drop is 50/50 (v/v) mixture of protein solution and the reservoir solution is suspended from a glass coverslip. There is a net loss of water from the drop because of the difference in the vapour pressure of water inside the drop and over the reservoir. The sample drop is observed with an

electronic microscope daily to see if there is any crystal grown. Commercial kits are available for screening of crystallization conditions with different combinations of precipitant, buffer, pH and salt included in standard solutions.

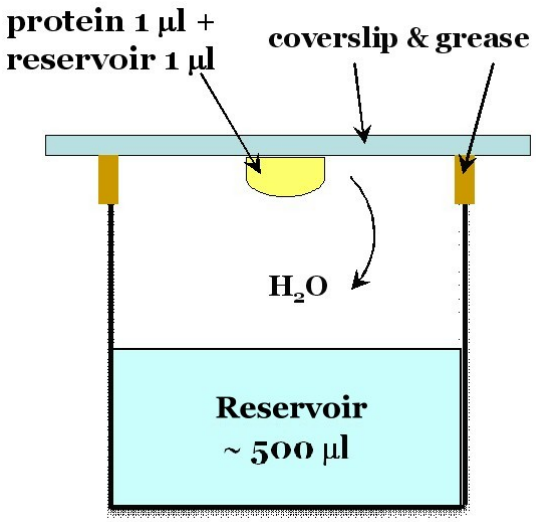

Figure 1.8: The set-up of Hanging drop vapour diffusion method.

Mounting crystal:

When the crystal is ready for data collection, it is mounted onto a goniometer by a tiny loop and then fast-frozen by liquid nitrogen. Crystal is soaked in a cryoprotective agent prior to mounting to avoid ice ring from occurring during data collection or cracking of crystal during the flash-frozen step. The goniometer can be accurately positioned and rotated so that the alignment of crystal is within the X-ray beam.

Data collection:

When the crystal is mounted, it will be exposed to the X-ray beam and it will scatter the X-rays into reflections on a photographic film. A crystal is actually composed of many repeating units of protein molecules so that proteins

with different arrangements will result in different intensities and patterns of spots on the film. To collect all the information of a structure, the crystal is rotated degree by degree and an image is recorded at every degree. The number of degrees needed depends on the space group of the crystal as a higher symmetry space group requires fewer degrees of image.

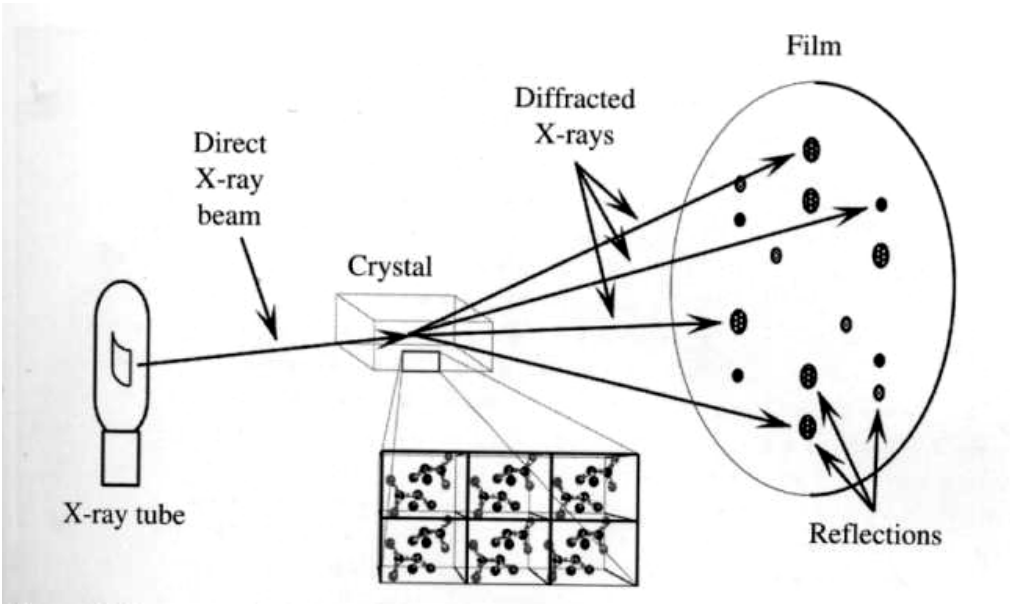

Figure 1.9: Schematic diagram on X-ray crystallographic data collection (obtained from: Rhodes, G. (2000), "Crystallography Made Crystal Clear: A Guide for Users of Macromolecular Models", Academic Press, 2nd edition, p.11, Figure 2.5).

Data processing:

For data processing, some well-developed programs and software packages can be used so that data can be processed and the electron density map can be calculated more quickly. Data processing includes indexing the reflections, identifying the unit cell of the crystal, determining the cell symmetry and space group, integrating the spots, and merging and scaling the images. This process

will give a single file containing all the information required for further processing. Molecular replacement is a commonly used technique to solve the phase problem by using an atomic model with known structure as a template to build a new model for the new crystal. The sequence identity between the known structure and the unknown one should be more than 30%. An electron density map will be generated after obtaining the amplitude information and phase information from experimental data and from the model structure.

Refinement and model building:

The structure can be refined either manually or automatically by a computer so that the structure can match the electron density well. The modified structure is used as a new model for the refinement. To determine whether the structure has been improved or not, the R-factor and R_{free}-factor are used. The R-factor is an expression of discrepancy between the crystallographic model and the experimental X-ray diffraction data. 95% of data is used to refine the model and calculate the R-factor. The remaining 5% data is not included in the refinement and used to calculate the R_{free}-factor. In a good refined structure at high resolution (<2 Å), both the R-factor and the R_{free}-factor can be as low as 0.2. It tells how well the refined structure predicts the observed data. Water and some other solvent molecules can be added to the structures until no extra electron density is found.

X-ray crystallography has been widely used in determining the crystal structures of different β-lactamases (Eidam *et al.*; Schneider *et al.*; Knox and Moews 1991; Banerjee *et al.* 1998; Crichlow *et al.* 1999; Brown *et al.* 2009). For example, the acyl-enzyme adduct can be crystallized to better understand how

the class A β-lactamase interact with β-lactam antibiotics. Crystal soaking can be performed to form the acyl-enzyme intermediate. After soaking the crystal into ligand solution for a moment, the ligand molecule diffuses into the interior of the protein crystal through solvent channels and bind to the protein. There were some studies on crystallization of class A β-lactamases. It was found that the deletion of Ω-loop from a class A β-lactamase did not change the overall folding of the protein but local adjustments in the vicinity of the missing loop were observed (Banerjee *et al.* 1998). The β-strand had a new degree of conformational flexibility as it is displaced inward toward the active site space and became inconsistent with the penicillin binding. The crystal structure of β-lactamase of *Bacillus licheniformis* 749/C, the enzyme that we studied, was reported (Knox and Moews 1991). It was refined with X-ray diffraction data up to 2 Å resolution. The enzyme was crystallized at pH 5.5 from polyethylene glycol (M_r 8,000) and it is a wild-type enzyme without labeled with any fluorophores. The crystal was in space group $P2_1$ with 2 molecules in an asymmetric unit. It can be used as the starting model to refine the structure of PenP_E166Cb. This enzyme was crystallized at the same pH value but with different polyethylene glycols (M_r 6,000) (Dideberg *et al.* 1985). In addition, the crystal structures of the BS3 Class A β-lactamase and the acyl-enzyme adduct formed with cefoxitin were reported (Fonze *et al.* 2002). It was revealed that the geometry of the active site was perturbed upon substrate binding, generating a different conformation of the Ω-loop.

An ultrahigh resolution (0.88 Å) of the structure of CTX-M-9 β-lactamase was published by Chen *et al.* (Chen *et al.* 2007). With this ultrahigh resolution structure, the alternate residue conformation and the hydrogen atoms

for the side chains can be accurately identified. Moreover, it can reveal the protonation states and hydrogen-bonding partners of all the active site residues so that more hints would be given for the mechanism of the enzyme.

X-ray crystallography was also used to study the interaction between the β-lactamase and the β-lactamase inhibitory protein. For example, the structure of β-lactamase inhibitory protein (BLIP-II) in complex with the TEM-1 β-lactamase had been determined at 2.3 Å (Lim *et al.* 2001).

1.8 Functional studies by mass spectrometry

Electrospray ionization mass spectrometry (ESI-MS) can be used to analyse organic compounds, biochemicals and metals. It is used extensively in studying protein–protein interactions because of its several advantages over conventional analytical techniques. For example, spectrophotometric based methods require chromogenic samples and the rate of the reaction progress is measured by changes in the absorbance of the reaction mixture. This limits the choice of the samples that can be analysed.

Comparatively, ESI-MS can analyse a wider range of compounds as samples do not have to be chromogenic. Compared with HPLC and GC analysis, the ESI-MS does not have to get rid of a large amount of solvents present and does not cause thermal degradation to compounds. On top of that, ESI-MS gives faster analysis than many of the conventional analytical techniques. Lastly, since it is highly sensitive and can detect trace amounts of samples, only a low concentration of sample (μM range) is needed for analysis so that some of the valuable sample can be saved.

In this project, ESI-MS was used to study the binding reactions between the β-lactamase-based biosensor and the β-lactam antibiotics, penicillin G and cefotaxime. Upon acidic quenching, the enzyme is unfolded and the reaction is stopped. The non-covalently bound enzyme-substrate complex (ES) will be dissociated into free enzyme and substrate. The covalently bound acyl enzyme (ES*) intermediate can be detected and quantified by the mass spectrometer.

The mass spectrometry used in this project is a Quadrupole – Time of Flight (Q-TOF) mass spectrometry equipped with an electrospray ionization source (Micromass Q-TOF 2).

Electrospray ionization

Electrospray ionization in mass spectrometry is used to produce ions in the gas phase so that the ions can be analysed. It takes place under atmospheric pressures and temperatures. The sample solution is first pumped through a stainless steel capillary needle, which is maintained at several kilovolts with respect to a cylindrical electrode surrounding the needle. A charged spray of fine droplets is formed and passes through a desolvating capillary, where the solvent is evaporated and the charges are attached to the analyte molecules. As solvent is evaporated, the droplets become smaller and their charge density becomes greater. The charges are concentrated and ion ejection occurs due to the coulombic repulsion at a critical radius. The droplets become very small. After that, desorption of ions into the ambient gas occurs (Skoog *et al.* 1998). The mechanism of the electrospray process is shown in Figure 1.10.

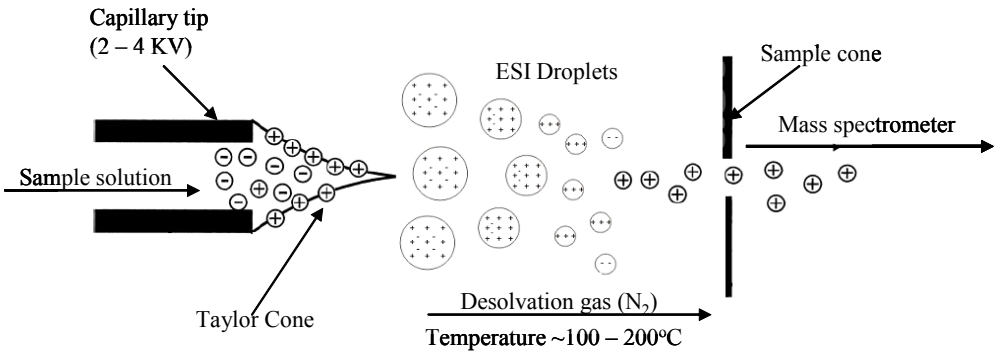

Figure 1.10: The electrospray process in mass spectrometry

Quadrupole Time-of-Flight (Q-TOF) Mass analyzer

In the Q-TOF mass spectrometer, the quadrupole mass analyser is placed in front of the Time-Of-Flight mass analyzer. The quadrupole mass analyser is used to separate ions according to their mass to charge ratio. It is made up of four rods with a circular or hyperbolic section. The ions are separated by altering the voltage applied to the four rods. After the ions have been separated, they arrive the Time-Of-Flight mass analyzer. The samples are bombarded with laser-generated photons and then ionized. The ions are then accelerated into a filed-free drift tube by an electric field pulse. The time it takes the ions to reach the detector is measured. Heavier ions take a longer time to reach the detector. Finally, the detector counts the number of ions that have arrived and measures the time for the ions to arrive (time of flight). Figure 1.11 shows a schematic diagram for the system. The following equations are used to measure the mass to charge ratio of the ions, given that an ion with mass (m) and charge (q) and spends time (t) to travel through a distance (d) to reach the detector:

$$t = d/v$$

$$mv^2/2 = qV = E$$

$$t^2 = (m/q)\,(d^2/2V), \text{ as } m/z = kt^2$$

where V is the accelerating voltage applied and E is the potential energy. Since the term $d^2/2V$ is a constant, the time of flight t depends on the m/q of the ions only.

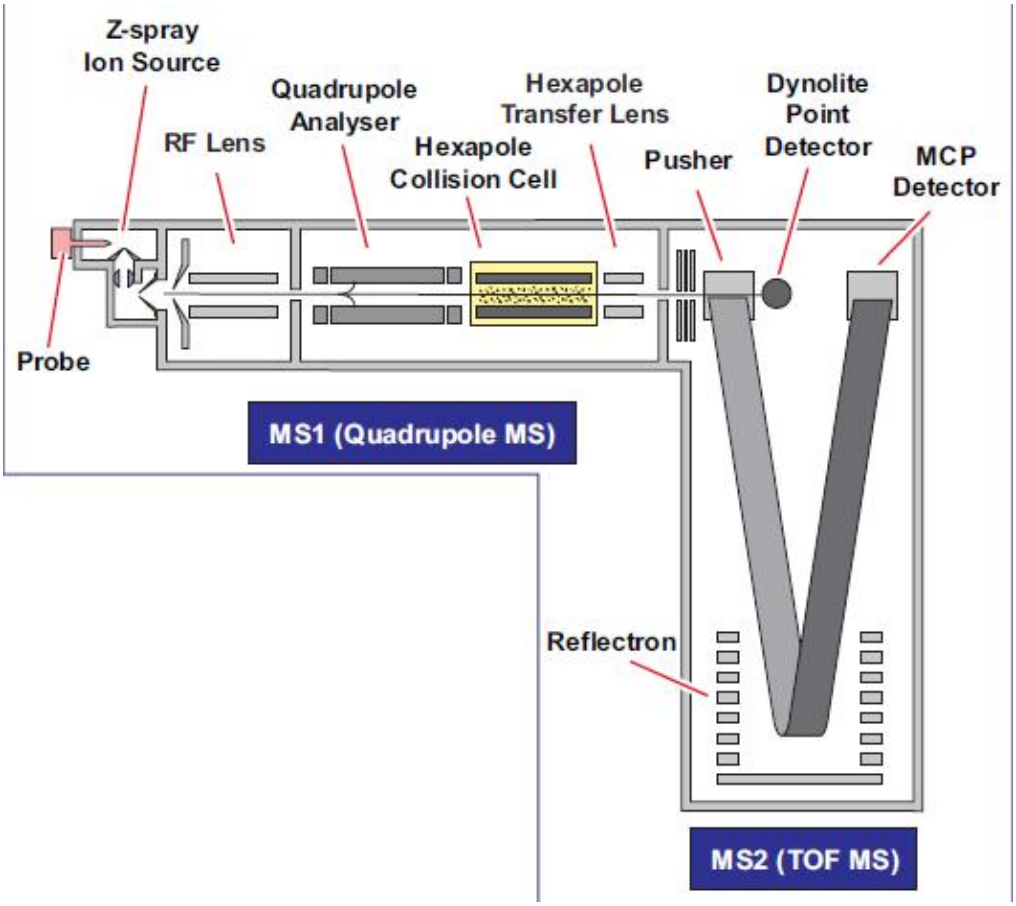

Figure 1.11: Schematic diagram of the Q-TOF (Micromass) mass spectrometer (from the operation manual of Q-TOF 2 (Waters))

There were many previous studies on the β-lactamases by mass spectrometry. For example, the masses of the reaction intermediates of class A β-lactamases PC1 with tazobactam (TZB), a potent penicillanic sulfone inhibitor, were determined by ESI/MS. After the inactivation of the PC1 by TZB, new molecular masses were observed, which had mass increments of 52, 70 and 88 Da relative to the uninhibited PC1 (Yang *et al.* 2000).

High performance liquid chromatography (HPLC) analysis was used in conjunction with the ESI/MS in order to find out the amino acid residues that are involved in the binding of TZB. After digestion of the reaction intermediates with

endoproteinase Glu-C and trypsin, the peptides were separated by HPLC and analysed by ESI/MS so that the amino acid residues corresponding to the mass increments could be found. From the HPLC result, the mechanism of the reaction can be figured out. The 52-Da adduct, which should be the propiolylated enzyme after acylation, was identified for the peptide composed of amino acid residue Ser-70. The formation of 70-Da adduct was formed after the interaction of Ser-130 with the acylated intermediates and the displacement of hydrolysed TZB. The 80-Da adduct was due to the hydrolysis of the 70-Da adduct.

In addition, there was an MS study about inhibition of *Escherichia coli* TEM-2 β-lactamases by Clavulanic acid. The study showed that the inhibition of class A β-lactamses by clavams (Clavulanic acid) and sulfones (Sulbactam) are very similar to each other. The mass increments of 52, 70 and 88 Da can also be found in the case of Clavulanic acid (Brown *et al.* 1996).

1.9 Aims of study

Antibiotics like penicillins and cephalosporins are commonly used against serious bacterial infections. Different methods were designed in order to detect various antibiotics and to avoid overuse of antibiotics in the farming industry and clinical applications. In this project, instead of using the previously developed PenPC_E166Cf biosensor, the PenP β-lactamase of *Bacillus licheniformis* 749/C was chosen due to its higher thermostability and availability of the X-ray crystal structure. To develop a sensitive PenP-based biosensor, the mechanism of this biosensor was studied by X-ray crystallography, in addition to kinetic studies by electrospray ionization mass spectrometry (ESI-MS) and fluorescence analysis. To study the structure of the PenP_E166C that has been labeled with the two fluorophores, badan and fluorescein-5-maleimide, and also that of the acyl-enzyme intermediate upon binding with different antibiotics, the enzyme should be in high purity. In this project, the enzyme was labeled and purified through a series of purification process. The structures obtained from X-ray crystallography will be more convincing than from molecular modelling. The structural and functional data obtained from the study will help to improve the biosensors both for antibiotic detection and for the discovery of new effective drugs against bacterial infection.

Chapter 2: Materials and Methodology

2.1 Materials

2.1.1 Bacterial strains

E. coli BL21 (DE3) was used as a host for the over-expression of β-lactamase mutants (Wang *et al.* 2010; Wood 1966; Moffatt and Studier 1987; Studier *et al.* 1990).

2.1.2 Plasmids

Plasmid pRset-K was modified from pRset-A from Invitrogen by replacing the ampicillin resistant gene by a kanamycin resistant marker from pET28 (Novagen). Map of the plasmid is shown in Figure 2.1.

2.1.3 DNA manipulation reagents

PCR reaction and site-directed mutagenesis were performed by PfuUltra High-Fidelity DNA Polymerase (Strategene). Primers used in PCR were purchased from Sigma-Proligo. dNTPs and *Dpn*I were purchased from Bioneer and Promega, respectively.

2.1.4 Media

Tryptone, yeast extract and nutrient agar were purchased from Oxoid. Luria-Bertani (LB) was purchased from Usb and it was used for transformation and preparation of *E. coli* competent cells. Terrific Broth (TB) medium was prepared by addition of 12 g tryptone, 24 g yeast extract and 4 ml glycerol into

900 ml double-deionized water and autoclaved (Kloos *et al.* 1999; Tartoff *et al.* 1987; Vakulenko and Golemi 2002). A 100 ml of sterile solution of 0.17 M KH_2PO_4, 0.72 M K_2HPO_4 was added into the TB medium. The TB medium was used for expression of PenP mutants. The nutrient agar plates containing 50 μg/ml kanamycin were prepared by addition of 1 ml kanamycin (10 mg/ml) into 200 ml sterilized molten agar at < 60 ℃.

2.1.5 Chemicals

Penicillin G, ampicillin, cefotaxime, ceftriaxone, ceftazidime, cefoxitin, cephalothin, cephaloridine, cefuroxime, 7-ACA, kanamycin, ammonium acetate, formic acid, myoglobin from horse heart, sodium hydroxide, were purchased from Sigma Co. Isopropylthiogalactoside (IPTG) was purchased from TaKaRa. TrisHCl, guanidine hydrochloride (GdnHCl), sodium chloride, potassium phosphate were purchased from Usb. A Crystal Screen kit was obtained from Hampton Research. 6-bromoacetyl-2-dimethylaminoaphthalene (badan) was purchased from Invitrogen.

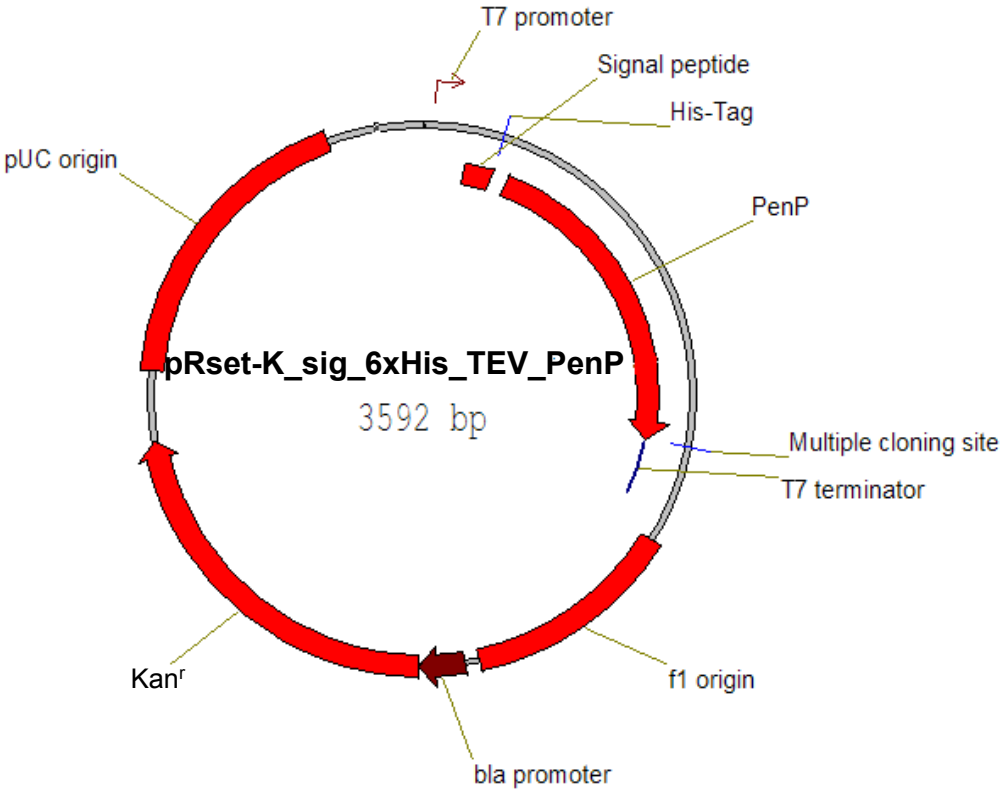

Figure 2.1.1: Plasmid map of pRset-K_sig_6xHis_TEV_PenP. A signal peptide followed by 6 codons of the 6xHis-tag was added before the 5' end of NdeI site of pRset-K. The PenP gene was cloned between the *Nde*I and *Hind*III sites of pRset-K. A TEV cleavage site was added to replace the *Nde*I site between the 6xHis-tag and PenP gene.

2.2 Subcloning of the β-lactamase gene into expression vector

2.2.1 The subcloning steps

pRset-K was used as the vector for expression of β-lactamase. The nucleotide sequence of the TEM-1 β-lactamase signal peptide followed by 6 codons of His was then added before the 5' end of NdeI site of pRset-K by PCR method. PenP gene without original signal peptide was cloned between the *Nde*I and *Hind*III sites of pRset-K for the expression of β-lactamase. To remove the 6xHis-tag of the expressed protein by TEV protease, a TEV cleavage site was added to replace the *Nde*I site between 6xHis and PenP gene by site directed mutagenesis kit from Stratagene to produce protein with the sequence HHHHHHENLYFQ_PenP. The cloning was done by Dr. H. K. Yap and Mr. C. L. Chan. Map of the plasmid is shown in Figure 2.1.1. The vector was named "pRset-K_sig_6xHis_TEV_PenP".

2.2.2 Preparation of *E. coli* competent cells

E. coli TOP10 and *E. coli* BL21 (DE3) strains were cultured in 5 ml sterilized LB medium overnight at 37 ℃ with shaking at 280 rpm. 200 μl of overnight culture was added to 100 ml sterilized LB medium. It was incubated at 37 ℃ with shaking (280 rpm) until A_{600} reaches 0.3-0.4. Cells were harvested by centrifugation at 4000 rpm for 20 min at 4℃. The cell pellets were resuspended in 10 ml of sterilized ice-cooled 100 mM $CaCl_2$ and kept on ice for 30 min. After that the cells were centrifuged at the same condition again. After centrifugation, the cell pellets were resuspended in 1 ml of ice-cold $CaCl_2$ with 15% glycerol and mixture was aliquoted into 10 eppendoff tubes. The competent cells were stored at -80 ℃ immediately.

2.2.3 Transformation of competent cells

5 μl of PCR product or 2 μl of purified plasmid DNA was added into 100 μl competent cell when the cells were just melted. The mixture was mixed and incubated in ice for 10 min. Then the competent cell was heat-shocked at 42℃ for 30 s. After heat-shock, the cells were put on ice and incubated for 2 more min. LB medium (500 ml) was added to the cells, and incubated at 37℃ with 280 rpm agitation for 1 h. The cells were plated on nutrient agar with 50 μg/ml kanamycin and incubated at 37℃ for overnight.

Single colonies were picked and transferred into LB medium for overnight growth. The plasmids from the pelleted cells were prepared by Miniprep Kit from Qiagen. The screening of the purified DNA was subjected to

DNA sequencing provided by Life Scientific. The plasmid DNAs with the correct sequence were then transformed into *E. coli* BL21 (DE3) competent cells, followed by expression and purification.

2.3 Site-directed mutagenesis

The 6xHis_TEV_PenP_E166C mutants were prepared by QuickChange Site-Directed Mutagenesis Kits from Strategene. Primers used for the specific mutagenesis are listed in Chapter 5.2.1. The primers should have a melting temperature (T_m) greater than or equal to 78 ℃. The reaction components, the reaction conditions and the procedures for transformation are described in the same section.

2.4 Expression and purification of β-lactamase mutants

2.4.1 Expression of β-lactamase mutants from *E. coli*

A small amount of bacterial glycerol stock of *E. coli* BL21 (DE3) transformed with the desired pRset-K plasmid was inoculated into 5 ml TB medium (4.5 ml of TB medium, 0.5 ml of phosphate solution) with 50 μg/ml kanamycin in a universal bottle. The seed culture was grown at 37 ℃, 280 rpm for overnight but less than 16 h. Overnight culture (1 ml) was added to 200 ml of TB medium (180 ml of TB medium, 20 ml of phosphate solution) with 50 μg/ml kanamycin in a 1L non-baffled flask. Adequate aeration was ensured by filling the flask with 20% capacity only. Four 1L-flasks were prepared and totally 800 ml of culture medium was incubated at 37 ℃ with shaking (280 rpm) until A_{600} reaches 0.8-1.0. Then filtered IPTG (isopropylthiogalactoside) with final concentration of 200 μM was added and the culture solutions were incubated at 30 ℃ with shaking for overnight again.

On the next day, the culture was transferred to two 400 ml-centrifuge bottles and centrifuged using a JA-10 rotor at 4 ℃, 9,000 rpm for 20 min. The supernatant was collected and filtered through 0.45 μm and 0.2 μm filter before the buffer exchange process. Buffer exchange with starting buffer for nickel affinity column (0.5 M sodium chloride, 0.02 M sodium phosphate) was performed by amicon stirred cell and the volume of the supernatant was reduced for injection into the column.

2.4.2 Protein purification by nickel affinity chromatography and anion exchange chromatography

Before loading the sample to the nickel affinity column, the sample was filtered through 0.45 μm and 0.2 μm filter again. The column used was a 5 ml HiTrap™ chelating HP column from GE Healthcare. Two columns were connected in series to prevent from overloading of the sample. The column was first injected with 0.1 M nickel (II) sulphate and washed with milli-Q water in order to remove the unbound nickel ions. Then it was pre-equilibrated with starting buffer (0.5 M sodium chloride, 0.02 M sodium phosphate, pH 7.4). Sample was loaded to the column and the column was washed with 10 column volume (CV) of starting buffer to remove the unbound proteins. Elution was performed with an imidazole gradient from 0 M to 0.5 M in 7 CV. Fractions showing positive UV absorbance at 280 nm were analyzed by SDS-PAGE to check for the purity. The fractions containing the target protein were pooled and buffer exchange was carried out for the next chromatographic process. Regeneration buffer (0.05 M EDTA, 0.02 M sodium phosphate, pH 7.4) was used to wash away the nickel and regenerate the column.

The sample was buffer-exchanged with starting buffer for DEAE cellulose column (20 mM Tris-HCl, 25 mM NaCl, pH 7.5). The column used was a 5ml DEAE Sepharose™ FF column from GE Healthcare. The column was pre-equilibrated with the starting buffer. After loading the sample onto the column, it was washed with 25 CV starting buffer to collect the desired proteins. Elution was performed with a gradient of 25 mM NaCl to 500 mM NaCl in 10 CV. Fractions showing positive UV absorbance at 280 nm were analyzed by

SDS-PAGE to check for the purity. The fractions containing the target protein were pooled and concentrated by ultra-amicon. The protein solution was aliquoted and stored at -20 ℃ for future use. The target protein was named "6xHis_TEV_PenP_E166C".

2.4.3 Protein gel electrophoresis (SDS/PAGE)

In order to check for the molecular masses and purity of the proteins, the proteins were separated by sodium dodecyl sulphate (SDS)/polyacrylamide gel electrophoresis (PAGE) in a Mini-PROTEIN III dual slab cell (Bio-Rad Laboratories). The polyacrylamide gel was a composition of 12% stacking gel layered on top of 12% resolving gel. The protein samples (10 μl) were mixed with same amount of loading buffer containing reducing agent, β-mercaptoethanol and SDS. The mixture was boiled in water for about 5 min and was loaded onto the gel. The low-range marker from Bio-Rad was used for determination of molecular weight of proteins. Electrophoresis was carried out in running buffer at 200 V for 54 min. After electrophoresis, the gel was stained with Coomassie Blue R-250 staining solution (25% methanol, 10% acetic acid and 0.06% Coomassie blue R-250) for a few minutes with agitation. The gel was destained with destaining solution (10% acetic acid and 10% methanol) with agitation until the bands on the gel are clearly appeared and the background of the gel was clear. The gel was cleaned with DDI water for several times and dried with gel drying films (Promega).

2.4.4 Protein concentration determination

Bradford assay was used to determine the concentration of proteins in this project. 200 µl of Bradford Reagent Dye (Bio-Rad Laboratories) was mixed with 800 µl of protein samples diluted with water. The mixture was allowed to stand for 10 min and taken to the spectrophotometer to measure the absorbance at 595 nm. A standard protein curve was obtained by using different concentrations of bovine serum albumin (Sigma) in a range of 0-10 µg/ml.

2.5 Cleavage of the 6xHis-tag

2.5.1 Cleavage of the 6xHis-tag by TEV protease

The pMAL-c2 plasmid of TEV protease was provided by Mr. C. C. Leung. The expression and purification of TEV protease was done by Mr. Po Kai Ting. By trial-and-error, the cleavage was carried out by adding TEV protease into 6xHis_TEV_PenP_E166C solution at a concentration ratio of 1 to 20 in order to optimize the cleavage (1 mg of TEV protease can digest 20 mg of 6xHis_TEV_PenP_E166C) (Phan *et al.* 2002; Shih *et al.* 2005).

The 6xHis_TEV_PenP_E166C protein was dissolved in 50 mM Tris-HCl buffer at pH 7.5 and appropriate amount of TEV protease, β-mercaptoethaol (final conc.: 1 mM) was added to the protein solution. The concentration of 6xHis_TEV_PenP_E166C protein was adjusted to 2 mg/ml. The mixture was stirred at 280 rpm, 30 ℃ for about 6 h. Samples at different time points during digestion were collected for protein gel electrophoresis.

2.5.2 Purification of protein after cleavage of 6xHis-tag by nickel affinity chromatography

After TEV protease digestion, the protein cleavage mixture was loaded onto the HiTrap™ chelating nickel affinity column (GE Healthcare) to remove undigested protein, TEV protease and the 6xHis-tag. After equilibrating the column, 10-column volume of starting buffer was used to wash away proteins that do not bind onto the column. Elution was performed to elute 6xHis-tagged proteins and 6xHis-tag. Eluates showing UV absorbance were anlayzed by SDS/PAGE to check for purity. The fractions containing digested PenP_E166C were pooled and checked for protein concentration and stored at -20 ℃ for future use. The protein with the 6xHis-tag removed was named “PenP_E166C” in this project.

2.6 Labeling of β-lactamase

2.6.1 Traditional method of labeling

1 mg of freeze-dried protein was dissolved in 2 ml of 6M GdnHCl (pH adjusted to 7–7.5 with potassium hydroxide) and it was allowed to stand at room temperature for 30 min in order to unfold the β-lactamase protein. A ten-fold molar excess of fluorophore, with concentration of 20 mM, was dissolved in DMF and added to the protein solution drop by drop. The mixture was stirred at room temperature for 3 to 4 h in darkness (Owenius *et al.* 1999).

After labeling reaction, the mixture was dialysed against 1 L of 50 mM potassium phosphate buffer (pH 7.0) at 4 ℃ with the use of dialysis tubing having 12 kDa cut-off size in order to remove excess fluorophore. Replacement with new buffer was performed regularly for at least 6 times. Refolding of protein was carried out at the same time as GdnHCl was removed from the reaction mixture during dialysis.

2.6.2 Optimization of labeling conditions

The effects of concentration of GdnHCl, temperature and time were examined. 1 mg of freeze-dried protein was dissolved in 6 M, 4 M, 2 M and 0 M GdnHCl respectively. The dilution was performed by Tris buffer (20 mM Tris-HCl and 50 mM NaCl). A 10-fold molar excess of badan/fluorescein was dissolved in DMF and added to the protein solution. The reaction mixture was allowed to shake at 25 ℃ for 1 h. For the protein solution without using GdnHCl, the duration of reaction tested were 30 min, 1 h and 2 h. The conditions of 37 ℃ were also tested.

The reaction mixture was then dialysed against 2 L DDI water at 4 ℃. Other conditions of dialysis were remained the same as the traditional method. The labeling efficiency of reaction was checked by ESI-MS and the secondary structures of the proteins were studied by circular dichroism spectrometry. The labeled protein was named “PenP_E166Cb” for badan-labeled protein and “PenP_E166Cf” for fluorescein-labeled protein in this project.

2.6.3 Secondary structure study by circular dichroism spectrometry

Circular dichroism (CD) spectra were measured by the Jasco 810 spectropolarimeter. Buffer exchange of the protein samples with DDI water was performed by dialysis. The protein sample (0.1-0.2 mg/ml) was added to the 200 µl-water-jacketed cylindrical cell with a path length of 1.0 mm. Scanning was carried at a scan speed of 200 nm/min at room temperature. The measurement range was 190 – 250 nm (far-UV region).

2.7 Fluorescence studies of fluorophore-labeled β-lactamases

2.7.1 Fluorescence scanning experiment

The fluorescence scanning spectra were obtained by Perkin-Elmer LS50B spectrofluorimeter at 25 ℃ in 50 mM potassium phosphate (pH 7.0). Antibiotics were weighed accurately with an electronic balance and subsequently made up with 50 mM phosphate buffer (pH 7) to appropriate volume to give a 0.1 M stock solution. This stock solution was used to prepare different working antibiotic solutions by serial dilutions with the same buffer.

445 μl of phosphate buffer (50 mM, pH 7) was added into a quartz cuvette with a 1-cm excitation path length and measured as blank. 50 μl of PenP_E166Cb/PenP_E166Cf solution (1 μM) was added to the cuvette. The mixture was scanned from 410 nm to 600 nm in order to obtain a scanning spectrum for the baseline. Then a 5 μl of the working antibiotic solutions was added to the enzyme solution to give a reaction mixture containing the desired antibiotic concentration and 0.1 μM PenP_E166Cb/PenP_E166Cf enzyme. The reaction mixture was mixed immediately before measurement and it was scanned over the same wavelengths after incubation for 100 s. The excitation and emission parameters for both fluorophores, badan and fluorescein, are shown in Table 2. 1.

2.7.2 Time-dependent fluorescence measurement

The buffer, protein and antibiotics were mixed together as described in 2.7.1. A 1,000 s fluorescence emission spectrum was traced at a fixed wavelength after the incubation of antibiotics to the protein solution. The excitation wavelength for time-dependent fluorescence measurements was set at 380 nm for badan and 494 nm for fluorescein. The emission wavelength chosen was the one which gives largest change in fluorescence intensity in the scanning spectrum. This can be observed from the initial scanning measurement in the previous section. The scanning speed was 250 nm/min. All measurements were performed at room temperature.

Table 2.1: Excitation and emission parameters used in fluorescence measurement.

		badan	**fluorescein**
Excitation wavelength (nm)		380	494
Emission Wavelength (nm)	**Scanning**	410-600	500-600
	Time-dependent measurement	500	515
Slit width (nm)		10	5

2.8 ESI-MS studies of β-lactamase

2.8.1 Determination of molecular mass and purity

The protein was buffer-exchanged with 20 mM ammonium acetate (pH 7.0) for at least four cycles with the use of Amicon Ultra-4 (NMWL = 10,000) centrifugal filter devices (Millipore). 70 μl of 1 μM PenP_E166Cb (in 20 mM ammonium acetate buffer, pH 7.0) was mixed with 70 μl of 2% (v/v) formic acid in CH_3CN to the enzyme solution in order to unfold the protein, giving a mixture in buffer/CH_3CN (1:1 v/v) containing 1% (v/v) formic acid (pH ≈ 2). Then the sample was injected into the mass spectrometer at a flow rate of 5 μl/min with a syringe pump (Harvard Apparatus, model 22). 600-1800 m/z range was scanned to obtain the multiply charged mass spectrum that contains the multiply-charged protein ion peaks. The capillary voltage and cone voltage were set to 3 kV and 30 V, respectively. Nitrogen was used as the desolvation gas, cone gas and nebulizing gas, while the nebulizing gas was fully opened. The desolvation gas and cone gas were adjusted to 400 and 50 L/h, respectively. 10 μM horse heart myoglobin (M_α = 16950.5 Da) was used to calibrate the m/z axis externally. The average molecular mass of the enzyme was obtained by de-convolution of the raw multiply charged spectra using the MassLynx 4.1 Transform Program (Micromass, Altrincham, Cheshire, U.K.). From the spectrum obtained, the purity of the protein mixture can be estimated.

2.8.2 Determination of labeling efficiency

The labeling efficiency was calculated by the masses of PenP_E166C and PenP_E166Cb, which was determined by electrospray mass spectrometry. It was calculated by the following formula:

$$\frac{Relative\ intensity\ of\ labeled\ protein}{Relative\ intensity\ of\ labeled\ protein + Relative\ intensity\ of\ unlabeled\ protein} x\ 100\%$$

2.8.3 Detection of covalent acyl-enzyme substrate complex in reaction with β-lactam antibiotics

The PenP_E166C and PenP_E166Cb mutants were buffer-exchanged as described in 2.8.1. The covalent acyl enzyme–substrate complexes formed by PenP_E166Cb and β-lactam antibiotics can be detected by ESI-MS. The enzyme-substrate binding reaction was initiated by mixing 70 μl of 5 μM PenP_E166Cb (in 20 mM ammonium acetate buffer, pH 7.0) with 70 μl of 10 μM antibiotic (in 20 mM ammonium acetate buffer, pH 7.0). The reaction was allowed to take place at room temperature. At desired time intervals, the reaction was quenched by adding 140 μl of 8% formic acid in CH_3CN to the enzyme solution in order to unfold the protein, giving a reaction mixture in buffer/CH_3CN (1:1 v/v) containing 4% formic acid (pH ≈ 2). The sample was then ready for injection into the mass spectrometer and the determination of molecular mass of the acyl-enzyme intermediate is stated in Section 2.8.1.

2.8.4 Kinetic study on binding by quench-flow system

For short reaction times (down to 10 ms), the reaction was initiated and quenched by a quench-flow system (Biologic SFM-400/Q, Claix, France). The instrumentation of quench-flow system is stated in Section 3.2.9. Two major peaks are shown in the resulting ESI spectrum, which are attributed to the free enzyme E and the enzyme-substrate complex ES*, respectively. The relative amount of ES* can be expressed as the ratio of the amount of ES* to the total amount of the enzyme, $[ES^*]/[E_{total}]$, where [ES*] is the peak intensity of peak B and $[E_{total}]$ (= [E] + [ES*]) is the sum of peak intensities of peak A and B in the transformed mass spectrum.

2.9 X-ray crystallographic studies of β-lactamases

2.9.1 Crystallization of β-lactamase

The β-lactamase protein solution was concentrated by Amicon Ultra-4 (NMWL = 10,000) centrifugal filter devices (Millipore) to 20 mg/ml and diluted to 10 mg/ml. Crystallization of the protein was performed by hanging drop vapour diffusion method. Crystal Screen^{TM} (CS) and Crystal Screen 2^{TM} (CS2) (Hampton Research) were used firstly, which contains 98 different crystallization conditions. They are shown in Appendix III.

500 μl of crystal screen reagent (CS 1-50, CS2 1-48) were added to 98 different reservoirs of the VDX^{TM} plate. 1 μl of the protein solution was mixed with 1 ul of the reservoir solution on a coverslip. In order to examine two different concentrations of protein solution at the same time, two drops were pipetted onto the same coverslip. The coverslip was inverted and sealed onto the pre-greased edge of the reservoir immediately to avoid evaporation. The mixture was allowed to equilibrate with the environment of the reservoir. The procedure was repeated for the 98 crystal screen reagents in different wells of the plate. The plates were incubated at 18 ℃ incubator free of vibration.

The drops were examined under a stereo microscope (10 to 100X magnification) after the crystal screens were set afterwards. The conditions that produced crystals were recorded and optimized with similar conditions (pH, salt type, salt concentration, precipitant type, precipitant concentration, sample concentration, temperature, additives, and other crystallization variables) were

tried in order to improve the crystal's shape, size and quality.

To obtain crystals of acyl-enzyme intermediates upon binding with antibiotics, soaking experiment was performed. After the crystal of apo enzyme was produced, the crystal was taken out by a cryoloop carefully and transferred to an antibiotic solution, which is a mixture of 18 µl of reservoir solution that crystallized the protein and 2 µl of antibiotic solution (100 mM) in order to obtain a final concentration of 0.01 M. The crystal was allowed to incubate in the solution for 20 min. Then it was ready for mouting onto the X-ray machine and data collection.

2.9.2 Structure determination

The crystal was taken out from the drop by a cryoloop and transferred into a cryoprotected mother liquor (containing 20% of ethylene glycol/glycerol that prevents from ice-ring formation) for a few seconds. The crystal was picked up by the cryoloop and mounted onto a goniometer head inside the X-ray machine so that the crystal orientation could be set precisely. The loop with crystal was dipped into nitrogen gas once stood on the goniometer head to increase molecular order in the crystals and improve diffraction. Data collection was collected on the Rigaku MicroMax^{TM}-007HF and processed by CrystalClear 1.3.5 SP2. The molecular replacement and structure refinement were done by CCP4 package 6.0.0 program suite (Potterton *et al.* 2003).

Chapter 3: Characterization and functional study of the fluorescent biosensor PenP_E166Cb

3.1 Introduction

β-lactamase-based fluorescent biosensor is a biosensor that utilizes class A β-lactamase to detect the presence of β-lactam antibiotics. The biosensor generates a change in fluorescence signal upon binding with various β-lactams due to the changing of the fluorophore's surrounding environment. We tested a wide range of β-lactams, mainly cephalosporins that contain a more bulky side chain group. There are many different kinds of fluorophores. The fluorophores we used belong to a thiol reactive fluorophore so that they react with the unique thiol group of Cys on the protein mutant.

The fluorophore badan (6-bromoacetyl-2-dimethylaminoaphthalene), belongs to the family of naphthalene-type fluorophores that are widely used for the study of protein structure with conformational analysis and ligand binding (Koehorst *et al.*; Cohen *et al.* 2005; Vazquez *et al.* 2005; Venkatraman *et al.* 2007). Badan belongs to "haloalkyl derivative" (iodoacetamide) in thio-reactive probes. The labeling reaction of badan is shown in Scheme 3 in Chapter one. The badan not only causes the change in the fluorescence emission intensity, but also induces a spectral shift with a change in the wavelength maximum if the environment it encounters upon ligand binding is different from before. When the badan is moved to a more non-polar environment, there will be a shift in the emission spectrum to a shorter wavelength (Owenius *et al.* 1999; Schindel *et al.*

2001; Koehorst *et al.* 2008). It is believed that the protein together with the fluorophore would undergo a conformational change after addition of antibiotic to the active site of the protein. This conformational change should alter the solvent accessibility of the fluorophore, which can be used to detect the presence of antibiotics. Another fluorophore, called fluorescein (fluorescein-5-maleimide), was also used in our study. This fluorophore is described in detail in Section 6.1.

In addition to the fluorescence measurement, characterization of the biosensor by mass spectrometry was also performed in order to study the purity and identity of the β-lactamase mutants. SDS/PAGE accompanied with mass spectrometry is a common composition technique to identify the purity of protein. The binding affinity of the β-lactamase-based biosensor is also important. After the conjugation of fluorophore near to the active site of the protein, a conformational change in the flexible Ω-loop might be resulted. This kind of change may alter the binding kinetics of the protein towards various β-lactams. Therefore, mass spectrometry in conjunction with a quench flow system can be performed to study the amount of the substrate-bound protein at desired time intervals. The more the substrate-bound protein (ES*) is formed within a time interval, the higher is the binding efficiency. Therefore, by comparing the binding rate before and after the conjugation of fluorophore to the protein, the effect of the fluorophore on the binding efficiency of the protein can be studied.

3.2 Methods

3.2.1 Subcloning of the gene encoding 6xHis_TEV_PenP and site-directed mutagenesis

This part was done by Dr. H. K. Yap and Mr. C. L. Chan. After site-directed mutagenesis, 6xHis_TEV_PenP_E166C was constructed.

3.2.2 Preparation and purification of the 6xHis_TEV_PenP_E166C mutant

The mutant was expressed and purified with the same procedures as described in Section 2.4.

3.2.3 Removal of the 6xHis-tag from the 6xHis_TEV_PenP_E166C mutant

TEV protease was used to cleave the 6xHis-tag from the 6xHis_TEV_PenP_E166C mutant.

3.2.4 Purification of PenP_E166C by gel filtration chromatography

Prior to crystallization, the protein solution was concentrated by Amicon® Ultra-4 centrifugal filter devices (Millipore NMWL = 10,000) to less than 1 ml and loaded to a Superdex™ 75 gel filtration column (GE Healthcare). The running buffer contained 20 mM Tris-HCl, 50 mM NaCl, pH 7.5. The flow-rate was 1 ml/min. The target protein was eluted out at approx. 0.5-column

volume. The related fractions were pooled and concentrated by ultra-filtration to 20 mg/ml.

3.2.5 Labeling of β-lactamase mutants

After optimization of the labeling conditions of β-lactamase mutants by badan, the optimum labeling conditions were found. The optimization procedures are described in Section 2.6.2. GdnHCl (2 M; pH adjusted to 7 – 7.5 with potassium hydroxide) was added to the protein solution and the final protein concentration was adjusted to about 1 mg/ml. The protein solution was incubated at room temperature for 30 min to unfold the protein. A ten-fold molar excess of 6-bromoacetyl-2-dimethylaminoaphthalene (badan), with a concentration of 20 mM, was dissolved in DMF and added to the protein solution drop by drop. The mixture was shaked at 300 rpm at room temperature for 2 h in dark, and then dialysed against 1 L of 50 mM potassium phosphate buffer (pH 7.0) at 4℃ overnight with the use of dialysis tubing (12 kDa cut-off size) in order to remove the excess dye. Buffer exchanges were carried out regularly during dialysis. After buffer exchange for 3 times, the protein solution was concentrated by Amicon Ultra and subjected to gel filtration chromatography (Section 3.2.4).

3.2.6 Determination of molecular mass, purity and labeling efficiency

The molecular mass, purity and labeling efficiency were determined using ESI-MS (Sections 2.8.1 and 2.8.2). The calculated molecular mass of 6xHis_TEV_PenP_E166C, TEV protease digested PenP_E166C and labeled

PenP_E166Cb were 31,225 Da, 29,608 Da and 29,818 Da, respectively.

3.2.7 Fluorescence scanning experiment and time-dependent fluorescence measurement

Different kinds of β-lactam antibiotics were used for the fluorescence scanning measurement for PenP_E166Cb, namely penicillin G, ampicillin, 7-ACA, cefotaxime, ceftazidime, cephalothin, ceftriaxone, cefoxitin, cefuroxime and cephaloridine. The concentration used for all antibiotics was 10^{-4} M to get a saturated fluorescence signal. The details of the measurement are described in Section 2.7.1. In addition, the fluorescence scanning spectrum for PenP_E166Cb in complex with cefotaxime was done in more detail because cefotaxime is a third generation and oxyimino-cephalosporins (with a large methoxyimino-moiety on R2 side-chain group) and it has a fast respond towards our biosensor. Different concentrations of cefotaxime were tested (2 x 10^{-8} M, 5 x 10^{-8} M, 1 x 10^{-7} M, 1 x 10^{-6} M). For the time-dependent fluorescence measurement, cefotaxime was also chosen to be the candidate. The details are described in Section 2.7.2. The concentrations used in this measurement were the same as those used in the scanning measurement.

3.2.8 Detection of covalent acyl-enzyme substrate complex in reaction with cefoxitin

Scanning spectrum shows that cefoxitin gives only a very small change in fluorescence signal to the enzyme. In order to confirm that cefoxitin can react and bind to the fluorophore-labeled β-lactamase, ESI-MS was performed and the method used is described in Section 2.8.3. The reaction mixture was allowed to incubate at room temperature for 3 min prior to the addition of the quenching reagent.

3.2.9 Kinetic study on the binding of cefotaxime by quench-flow system

The amount of the covalently bound acyl-enzyme intermediate of PenP_E166Cb with the addition of cefotaxime (ES*) at desired time intervals was determined by ESI-MS as described in Section 2.8. Since the reaction of PenP_E166Cb and cefotaxime is very rapid, a quench-flow system was used prior to ESI-MS analysis so that the reaction could be quenched mechanically and immediately in a very short time down to the milli-second level.

Figure 3.1 shows the schematic diagram of a SFM-400/Q quench-flow system used in this project. This instrument is composed of four syringes (S1, S2, S3, and S4). S1 was not used in the study, while S2 and S3 were filled with protein and substrate, respectively. S4 was filled with quenching reagent that contains formic acid. The four syringes are actuated by four independent stepping motors, which are controlled by the Bio-Kine software.

To start the enzymatic reaction, the enzyme was injected via syringe S2 and the substrate was injected via syringe S3. The enzyme and the substrate were mixed in a mixer and then introduced to the delay line. In order to control the reaction time, the flow rates of the reactants in the delay line were altered by the computer program. After passing through the delay line, the reaction mixture reached the second mixer so that it was mixed with the quenching reagent from syringe S4. The quenched reaction mixture was collected by a collection syringe and then analyzed by ESI-MS.

The protocol of the analysis of the covalent acyl-enzyme substrate complex is described in Sections 2.8.3 and 2.8.4. Both PenP_E166C and PenP_E166Cb were subjected to kinetic analysis with the addition of penicillin G and cefotaxime. S2 was filled with 10 ml of 5 μM PenP_E166C or PenP_E166C (in 20 mM ammonium acetate buffer, pH 7.0) and S3 was filled with 10 ml of 10 μM antibiotic (in 20 mM ammonium acetate buffer, pH 7.0). S4 was filled with 10 ml of 8% formic acid in CH_3CN. After obtaining different [ES*] values according to different reaction time, a plot of [ES*]/[E_{total}] against time was generated.

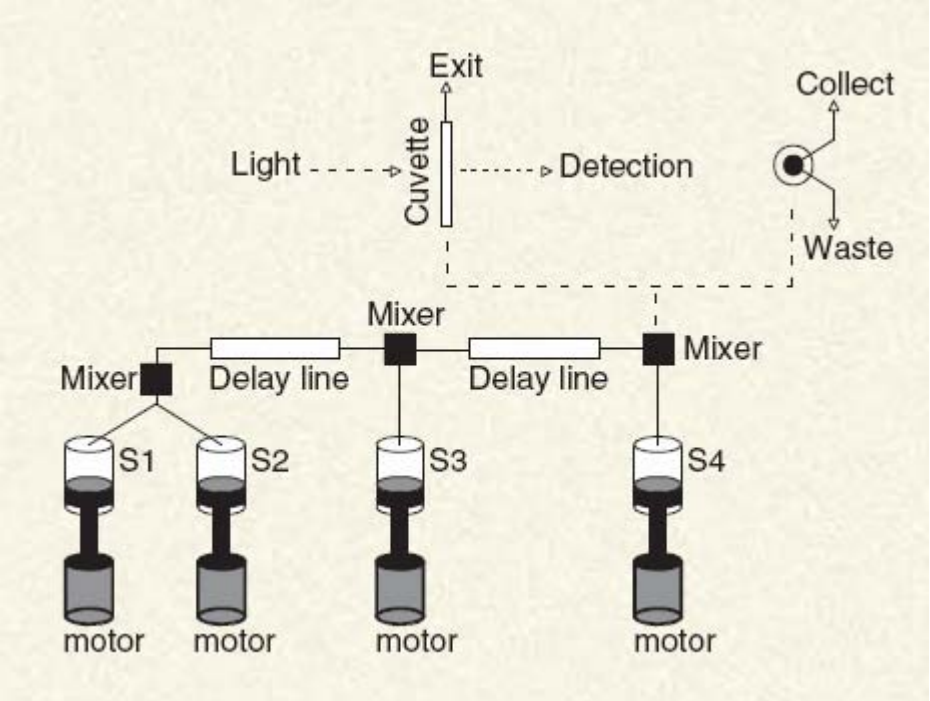

Figure 3.1: Schematic diagram of the SFM-400/Q quench-flow system (taken from the catalog of BioLogic Science Instruments, www.instrument.com.cn/download.asp?url=/Show/Literature/C10515.pdf)

3.3 Results

3.3.1 Preparation and purification of the 6xHis_TEV_PenP_E166C mutant

Figure 3.2 is the elution profile of the protein from nickel affinity column. A large broad peak was observed during the elution process. The fractions containing the washed out portion and the large peak were analysed by SDS/PAGE (Figure 3.3). Besides the target protein that had the size of about 30,000 Da, there were other proteins present in fractions 4 to 9. These fractions were pooled.

By Bradford analysis that measures the protein concentration, it can be calculated that a total of 428 mg protein, including 6xHis_TEV_PenP_E166C, was obtained when 800 ml of bacterial culture grown in TB medium was prepared. However, the SDS/PAGE gel shows impurities of the pooled fractions. Therefore another column was used in order to purify the target protein.

Figure 3.4 (a) shows the protein elution profile from DEAE cellulose column. SDS/PAGE analysis is shown in Figure 3.4 (b). The large peak in Figure 3.4 (a) refers to the target protein while the small peak should be the impurities. From the Bradford assay, it was calculated that after the DEAE cellulose column, 228 mg of 6xHis_TEV_PenP_E166C was finally obtained. The purity and molecular mass were further confirmed by mass spectrometry.

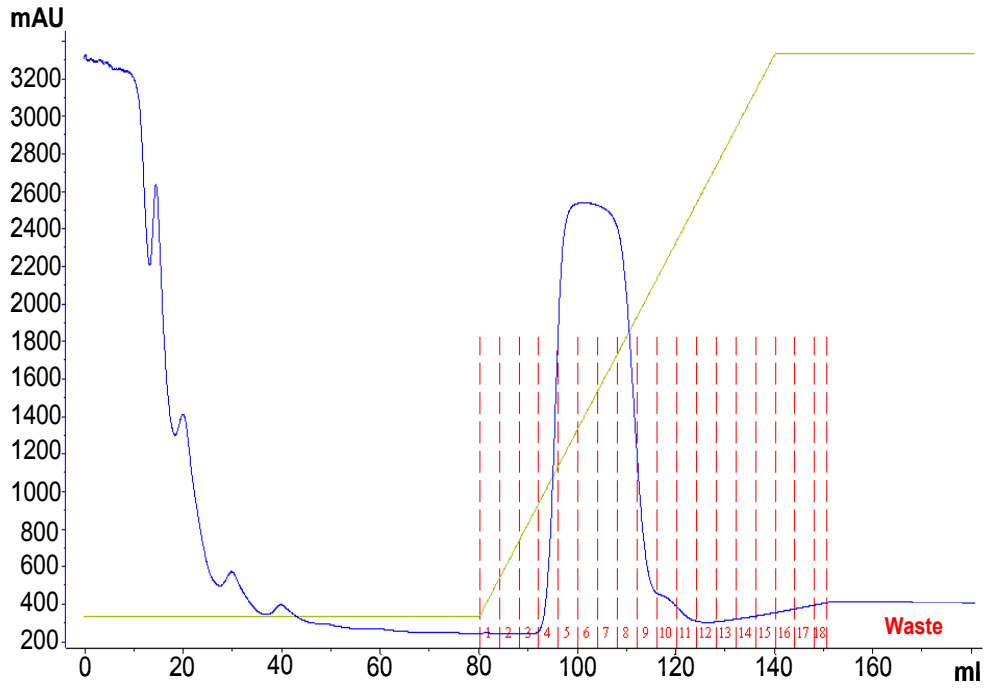

Figure 3.2: Elution profile of 6xHis_TEV_PenP_E166C from nickel affinity chromatography using 5ml HiTrap^{TM} chelating HP column from GE Healthcare. The column was washed with 8 column-volumes of starting buffer (0.02 M sodium phosphate and 0.5 M NaCl) and elution was performed with an imidazole gradient of 0 M - 0.5 M, which is shown as a slope. Protein was detected using absorbance at a wavelength of 280 nm in mAU (milli absorption unit).

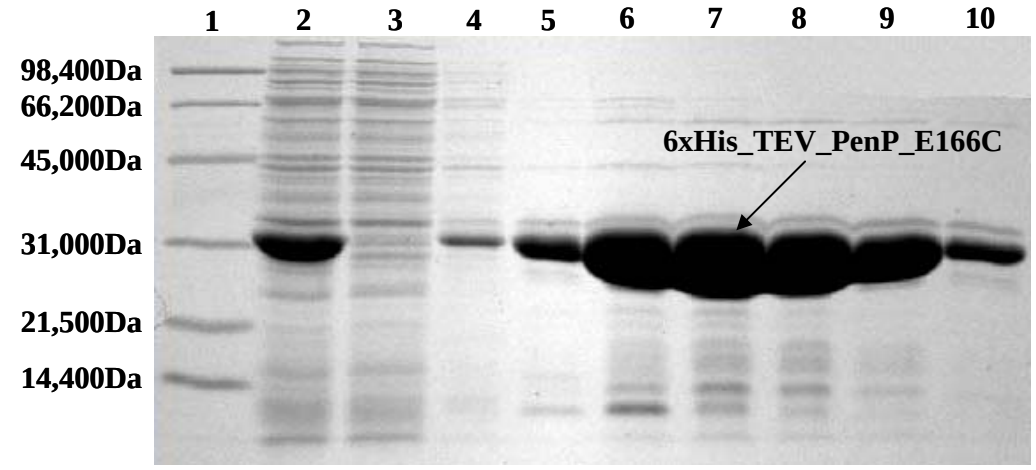

Figure 3.3: 12% SDS/PAGE analysis of the column fractions from nickel affinity chromatography for 6xHis_TEV_PenP_E166C. Lane 1 is the low range molecular weight marker; lane 2 is the sample before loading to the column; lane 3 is the flow-through during sample injection; lane 4 is the unbound protein washed out from the column; lanes 5 to 10 are the column fractions from 4 to 9, respectively.

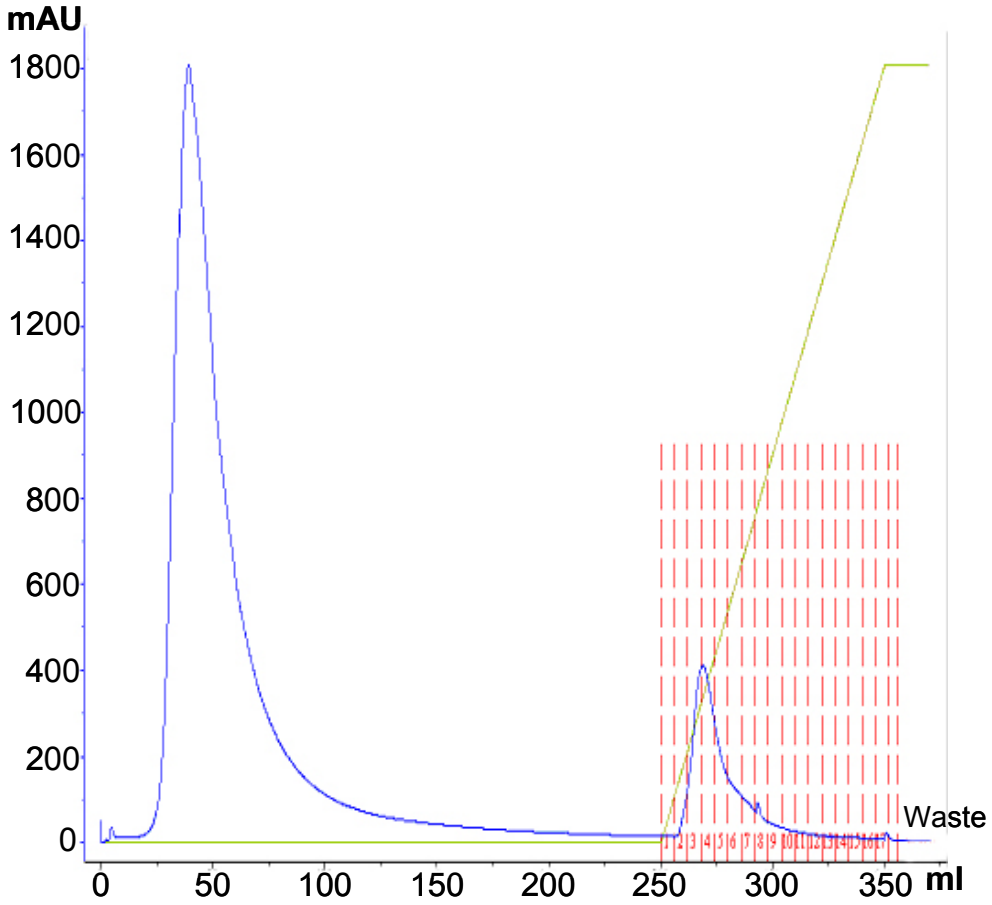

Figure 3.4: (a) Elution profile of 6xHis_TEV_PenP_E166C from DEAE cellulose chromatography using 5ml DEAE Sepharose^{TM} FF column from GE Healthcare. The column was washed with 25 column-volumes of starting buffer (0.02 M Tris-HCl, 0.05 M NaCl) and elution was performed with NaCl gradient (0.05 M - 0.5 M), which is shown as a slope. Protein was detected using absorbance at 280 nm in mAU (milli absorption unit).

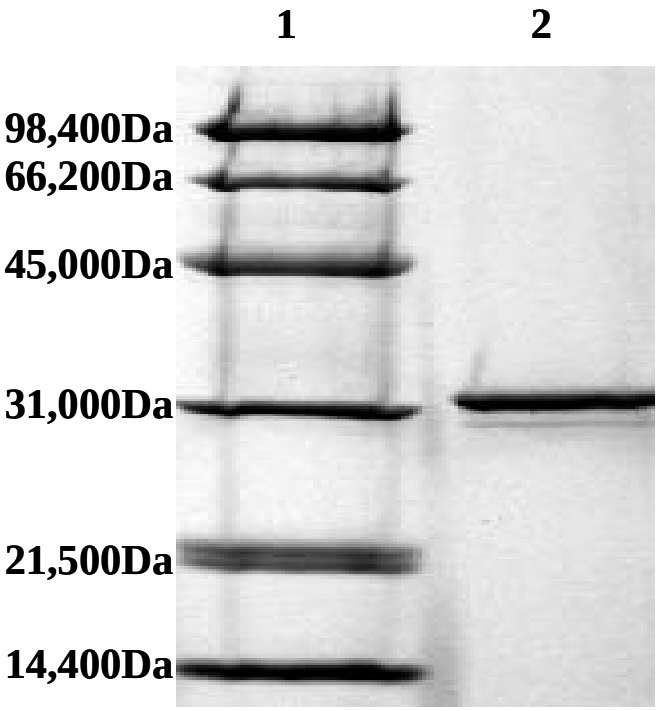

Figure 3.4: (b) 12% SDS/PAGE analysis of 6xHis_TEV_PenP_E166C from DEAE column. Lane 1 is the low-range molecular weight marker and lane 2 is the loosely bound protein washed out from the DEAE cellulose column.

3.3.2 Removal of the 6xHis-tag from 6xHis_TEV_PenP_E166C

The 6xHis tag was cleaved from 6xHis_TEV_PenP_E166C by TEV protease with the method described in Section 2.5.1. To optimize the cleavage conditions, samples at 0 h, 2 h, 4 h and 6 h during digestion reaction were collected and analyzed by SDS/PAGE. Figure 3.5 shows that the uncleaved 6xHis_TEV_PenP_E166C has a molecular size of ~31,000 Da. Start from 2 h, most of the protein has been digested as the band corresponding to the uncleaved protein becomes lighter and there is a small down-shifted band with lower molecular mass, which is the digested protein.

After the TEV digestion, the reaction mixture was loaded onto the nickel affinity column. The purification profile is shown in Figure 3.6. It can be seen that there are a large broad peak and several small peaks from fractions A1 to A10 and fractions B12 to B8, respectively. Fractions B12 to B8 were included in the elution gradient.

Samples in the fractions of the peaks were analyzed by SDS/PAGE and shown in Figure 3.7. Bands with a molecular size of about 30,000 Da correspond to our target protein. It can be seen that the bands in lanes 2 to 5 of Figure 3.7 have a lower molecular size than that in lane 8. Therefore the first large broad peak should be the digested PenP_E166C with 6xHis-tag removed while the band at lane 8, which has a larger molecular size, should be the undigested 6xHis_TEV_PenP_E166C. The digested PenP_E166C did not bind to the nickel affinity column as the 6xHis-tag was cleaved while the undigested 6xHis_TEV_PenP and the TEV protease were bound to the column.

Lanes 2 to 5 show that the digested PenP_E166C was very pure since only one band is observed on each lane. Thus fractions A2 to A8 were pooled.

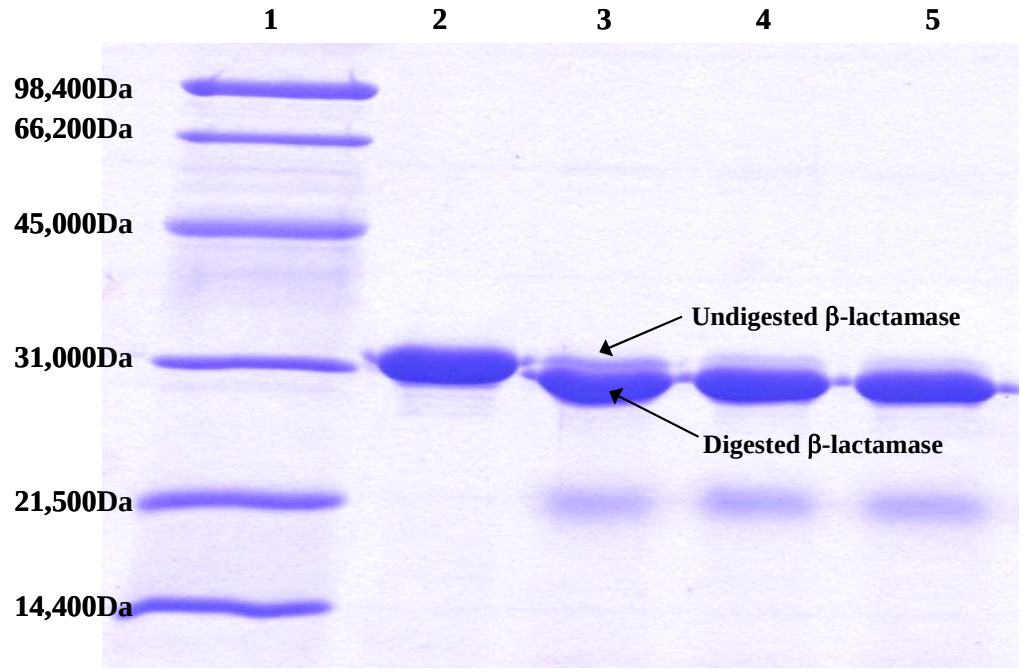

Figure 3.5: 12% SDS/PAGE analysis of 6xHis-cleaved β-lactamases by TEV protease at different incubation time points. Lane 1 is the low range marker (14400 Da to 98400 Da); lane 2 is the uncleaved β-lactamase; lanes 3 to 5 are the samples at 2 h, 4 h, 6 h during digestion reaction respectively.

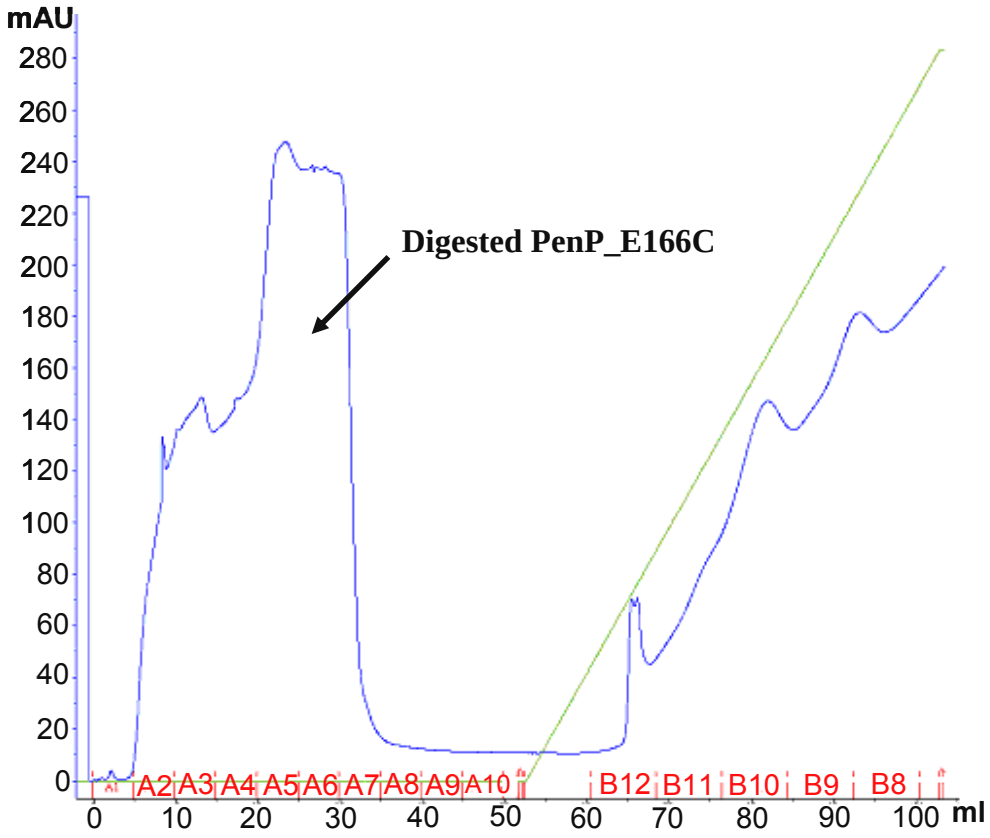

Figure 3.6: Elution profile of TEV protease digested 6xHis_TEV_PenP_E166C from nickel affinity chromatography. The column was washed with 10 column-volumes of starting buffer (0.02 M sodium phosphate and 0.5 M NaCl). Elution was performed with an imidazole gradient of 0 M - 0.5 M, which is shown as a slope. Protein was detected using absorbance at a wavelength of 280 nm in mAU (milli absorption unit).

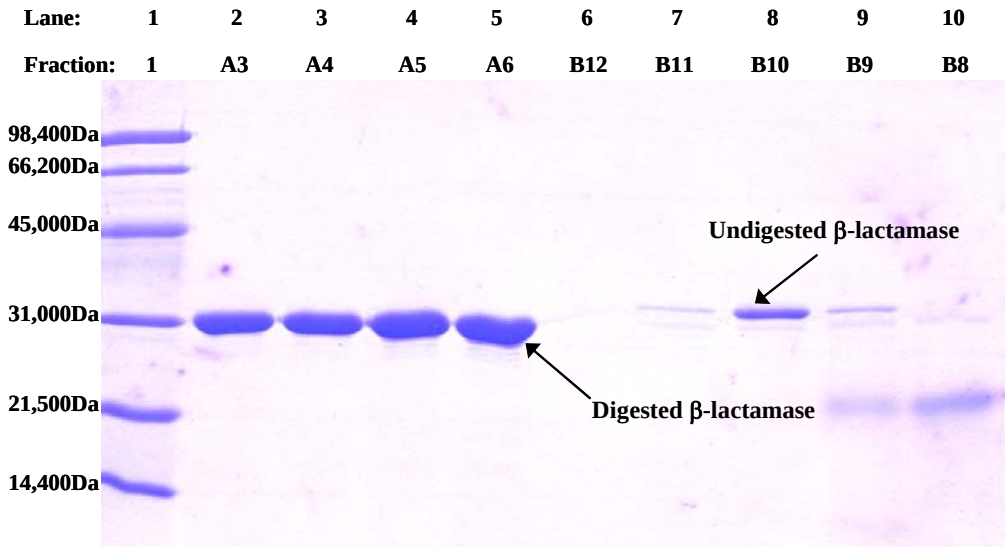

Figure 3.7: 12% SDS/PAGE analysis of the column fractions from nickel affinity chromatography for 6xHis_TEV_PenP_E166C after TEV protease digestion. Lane 1 is the low range marker. Lanes 2 to 5 correspond to fractions A3 to A6; lanes 6 to 10 correspond to fractions B12 to B8, respectively.

3.3.3 Purification of PenP_E166C by gel filtration chromatography

After the cleavage of the 6xHis-tag from 6xHis_TEV_PenP_E166C, gel filtration chromatography was performed to further purify the protein by size exclusion method. Figure 3.8 shows the elution profile while Figure 3.9 shows the SDS/PAGE analysis for the elution profile. There is a large peak at about 11 ml elution volume corresponding to PenP_E166C. It was then confirmed by SDS/PAGE analysis, which shows that fractions 6 – 9 have thick bands at the molecular weight around 30,000 Da.

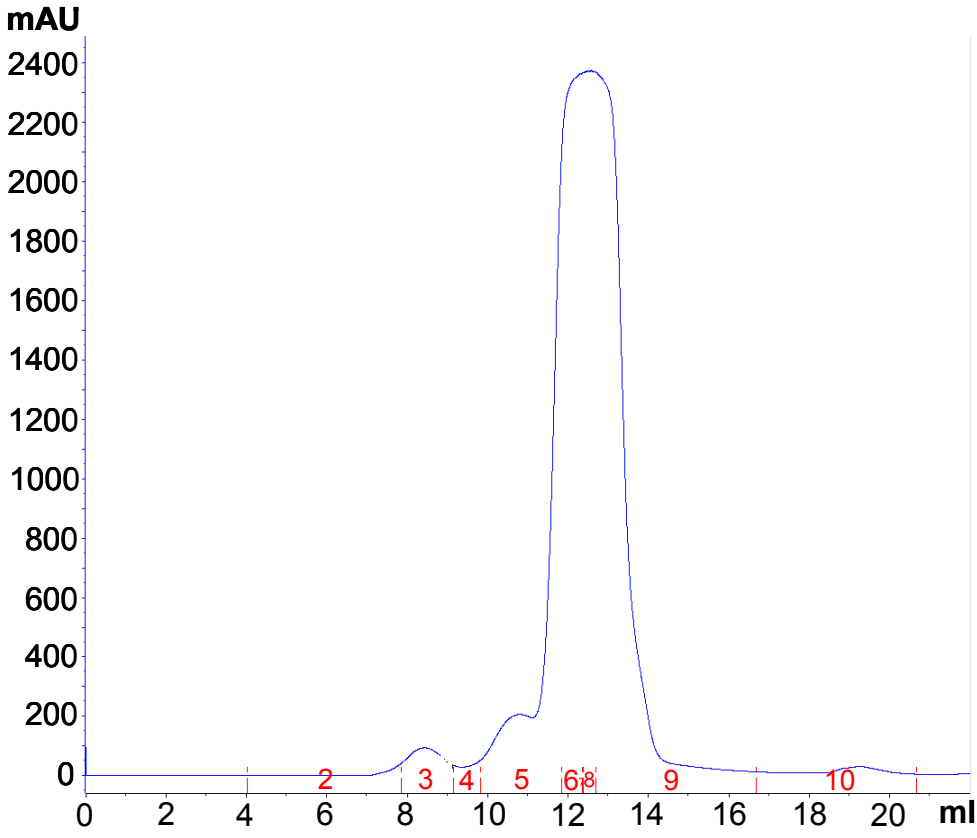

Figure 3.8: Elution profile of the gel filtration chromatography for PenP_E166C using a Superdex™ 75 gel filtration column (GE Healthcare). The running buffer contained 20 mM Tris-HCl, 50 mM NaCl, pH 7.5. The red numbers are the

fraction numbers.

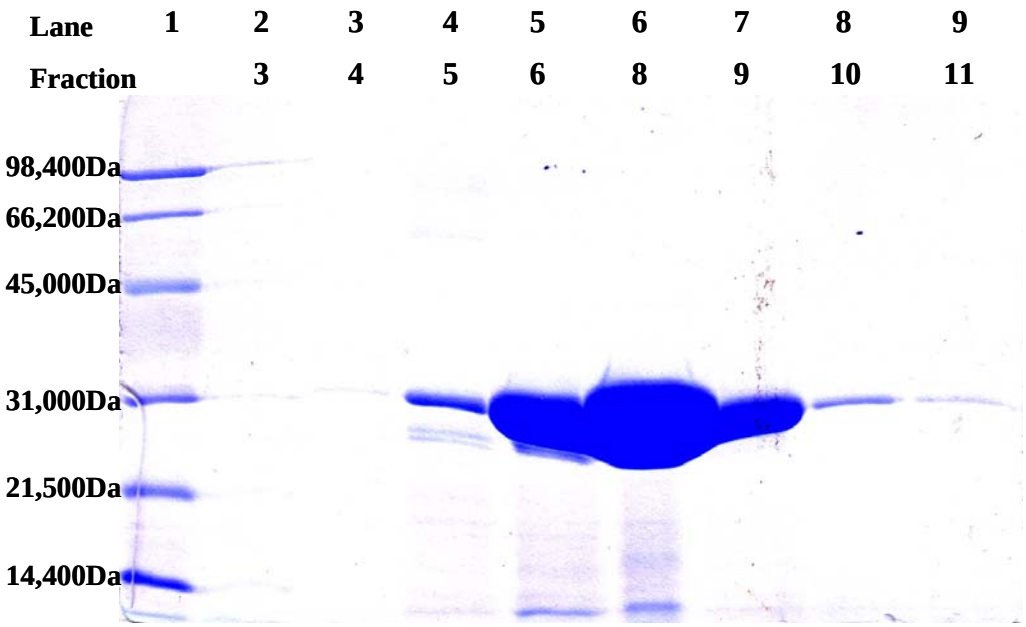

Figure 3.9: 12% SDS/PAGE analysis of the column fractions from gel filtration chromatography for PenP_E166C after TEV protease digestion. Lane 1 is the low range molecular weight marker; lanes 2 to 9 represent fractions 3 to 11, respectively.

3.3.4 Optimization of labeling condition

PenP_E166C, without the 6xHis-tag, was labeled with badan. After labeling, the solution turned yellow, which was a good indicator in the labeling process. Precipitation was observed during the labeling process, which might be due to excessive badan.

The best labeling condition was derived from the result of using different concentrations of GdnHCl, different reaction times and temperatures for labeling. The labeling efficiencies of the different conditions were calculated and listed in Table 3.1 according to the equation shown in Section 2.8.2. When GdnHCl was used to unfold the protein prior to a one-hour labeling reaction, 100% labeling efficiency was achieved. In the mass spectra, no peak of unlabeled PenP_E166C can be found. However, if no GdnHCl was used, the labeling efficiency was dramatically reduced to less than 20%, no matter how long the labeling process was. The mass spectrum from the sample without GdnHCl before labeling is shown in Figure 3.10 and that of using 4 M GdnHCl before labeling is shown in Figure 3.11. The small peaks associated with peak B in Figure 3.10 and Figure 3.11 may be due to the salt adducts and small amount of impurities after labeling. When the temperature was increased from 25 ℃ to 37 ℃, the labeling efficiency was increased by about 10%.

Table 3.1: Labeling efficiencies of PenP_E166Cb at different labeling conditions.

Conc. of GdnHCl	Labeling duration			Temperature
	30 min	1 h	2 h	
6 M GdnHCl	---	100%	---	**25 ℃**
4 M GdnHCl	---	100%	---	
2 M GdnHCl	---	100%	---	
0 M GdnHCl	16%	16%	16%	
	26%	29%	---	**37 ℃**

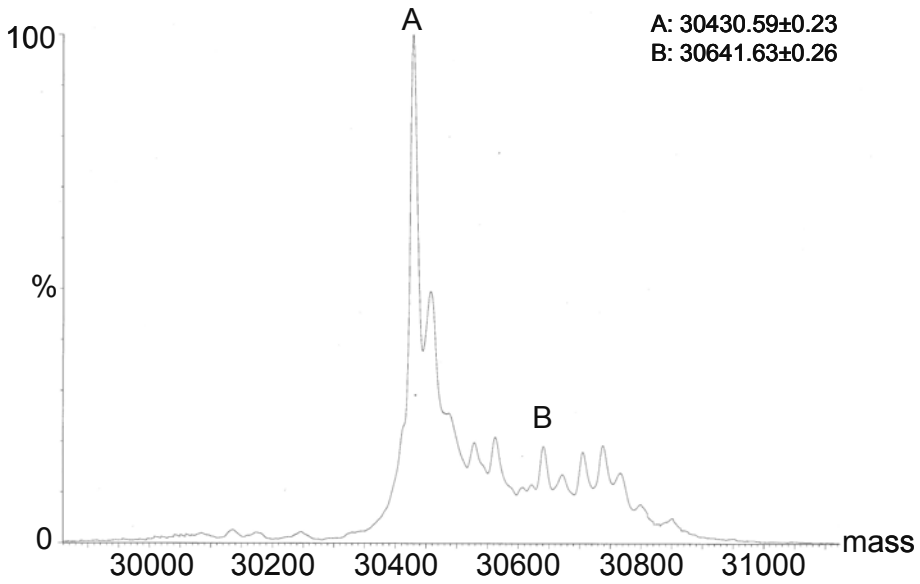

Figure 3.10: Transformed mass spectrum of 6xHis_PenP_E166Cb after labeling by badan at 25 ℃ for 1 h. No GdnHCl was used before the labeling process. A is the unlabeled enzyme and B is the labeled enzyme.

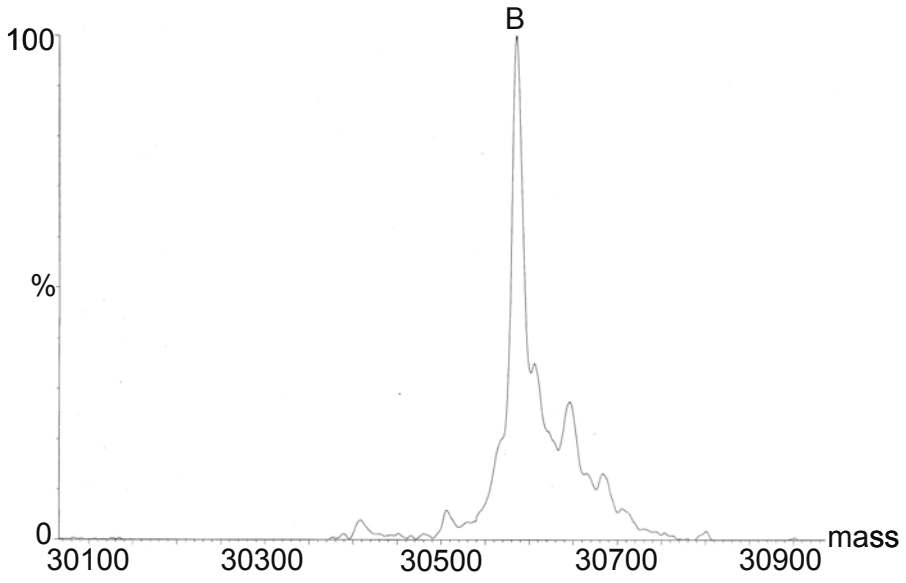

Figure 3.11: Transformed mass spectrum of 6xHis_PenP_E166Cb after labeling by badan at 25 ℃ for 1 h. GdnHCl (4 M) was used to unfold the protein before labeling. A is the unlabeled enzyme (not detected) and B is the labeled enzyme.

3.3.5 Determination of molecular mass, purity and labeling efficiency

The molecular mass of 6xHis_TEV_PenP_E166C, TEV protease digested PenP_E166C and labeled PenP_E166Cb were confirmed by ESI-MS. The method was described in Section 2.8.1. As shown in the transformed mass spectrum in Figure 3.12 (a), the measured molecular mass is 31,225.4 Da, which is in good agreement with the theoretical average molecular mass (31,225.3 Da) calculated based on the primary amino acid sequence. This confirms that the glutamic acid at the 166 position of the 6xHis_TEV_PenP wild-type β-lactamase was successfully mutated to cysteine by site-directed mutagenesis to become 6xHis_TEV_PenP_E166C.

The transformed mass spectrum of the TEV Protease-digested PenP_E166C (see Figure 3.12 (b)) shows that the measured molecular mass is 29,607.0 Da while the calculated mass is 29,607.4 Da. This implies that the 6xHis-tag was successfully removed by TEV protease digestion.

After the cleavage of the 6xHis-tag, the protein was subsequently labeled with badan. The transformed mass spectrum of the labeled PenP_E166Cb shows a single peak with a molecular mass value of 29,819.0 Da, which is 212 Da higher than E166C. The mass increment of 209 Da is due to an addition of a badan molecule. The measurement shows that the badan was incorporated into the PenP_E166C mutant with a stiochiometry of 1:1 and the protein was labeled with badan in 100% labeling efficiency. Figure 3.12 (c) shows the results for the protein that was unfolded with 2M GdnHCl prior to labeling.

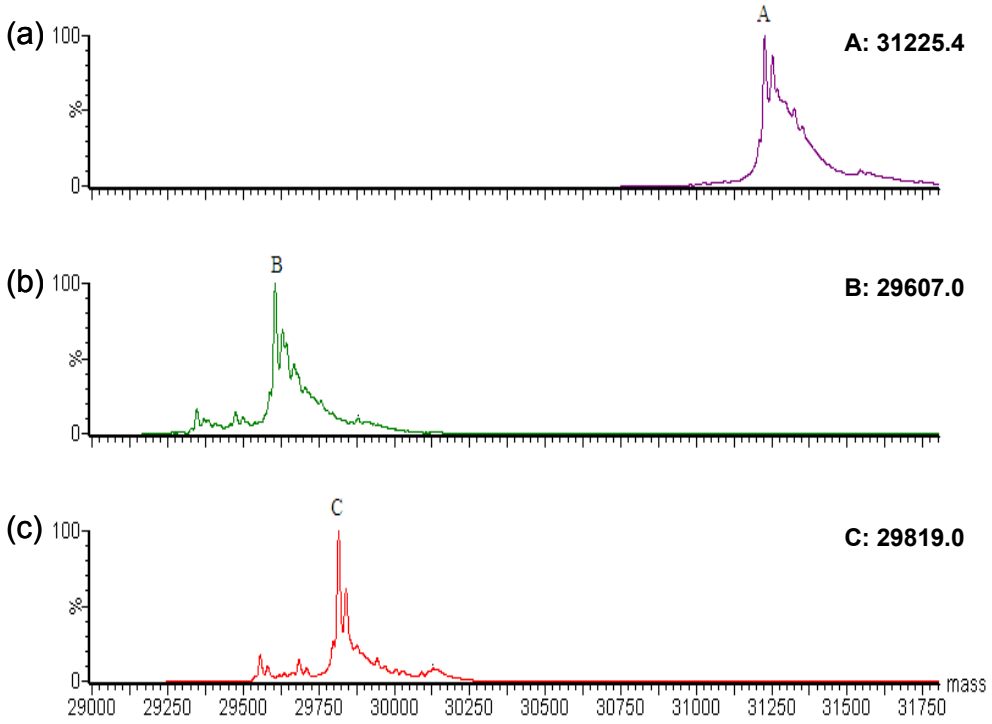

Figure 3.12: De-convoluted ESI mass spectra of (a) 6xHis_TEV_PenP_E166C, (b) TEV protease digested PenP_E166C and (c) labeled PenP_E166Cb.

3.3.6 Secondary structure study by circular dichroism spectrometry

Far-UV circular dichroism spectrometry was used to study the secondary structure of PenP_E166Cb unfolded with different concentrations of GdnHCl according to the method described in Section 2.6.3. Figure 3.13 shows that the spectra of all the refolded proteins from all the unfolding conditions are highly similar to one another. This indicates that the concentration of GdnHCl would not affect the refolding of the protein. The conditions used in each spectrum are shown. The x-axis refers to the scanning wavelength and the y-axis refers to the absorptivity. There are variations of maximum and minimum absorptivity among the four spectra. This should be due to the small variations in protein concentrations among the four samples.

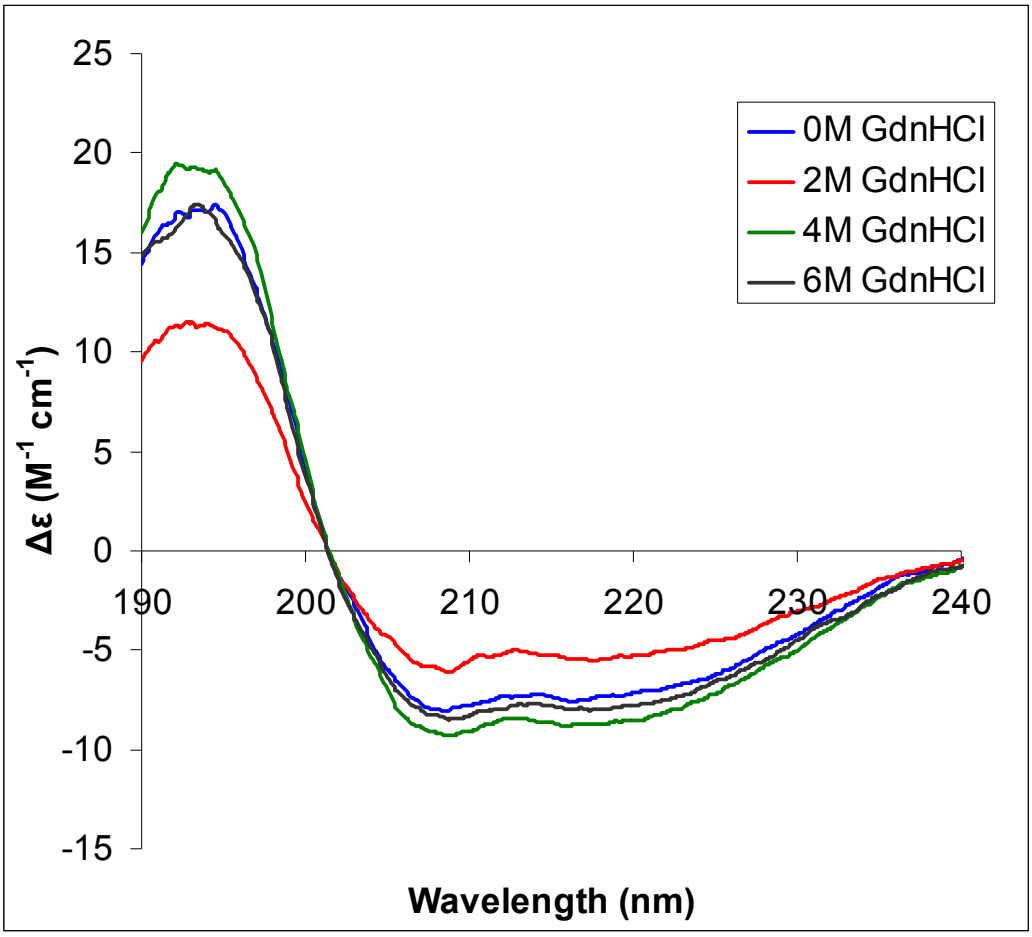

Figure 3.13: Far-UV circular dichroism spectra of PenP_E166Cb after labeling, using different concentrations of GdnHCl for unfolding. All labeling reactions were performed at 25 ℃ and labeled for 1 h. Scanning was performed at a scan speed of 200 nm/min at room temperature over the scan range of 190-250 nm.

3.3.7 Purification of PenP_E166Cb by gel filtration chromatography

After the labeling reaction of PenP_E166C, gel filtration chromatography was performed to further purify the protein by size exclusion method. In addition, excess badan and DMF can be removed by this method. Figure 3.14 shows the elution profile. There is a large peak at about 11 ml elution volume representing PenP_E166Cb. It was confirmed by ESI-MS, which shows that the protein solution is pure enough to proceed to crystallization. The mass spectra are shown in Figure 3.12.

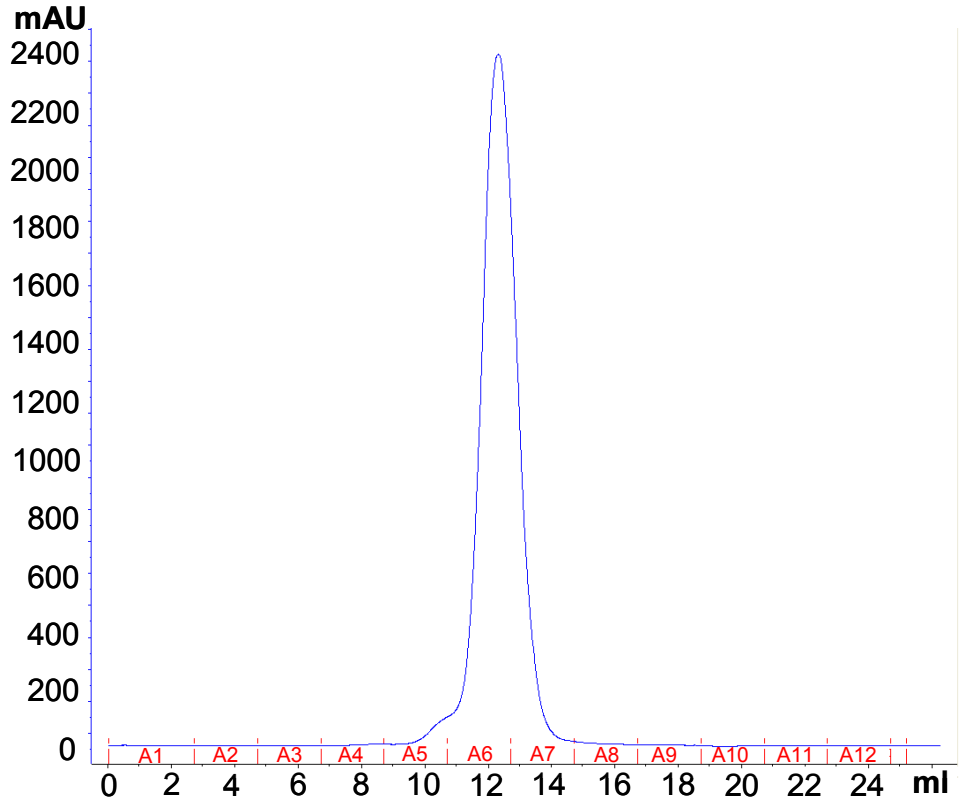

Figure 3.14: Elution profile of the gel filtration chromatography for PenP_E166Cb using Superdex^{TM} 75 gel filtration column (GE Healthcare). The running buffer contained 20 mM Tris-HCl, 50 mM NaCl, pH 7.5.

3.3.8 Fluorescence scanning spectra and time-dependent fluorescence spectrum

The scanning spectra of different β-lactam antibiotics for PenP_E166Cb (1×10^{-7} M), namely penicillin G, ampicillin, 7-ACA, cefotaxime, cefuroxime, ceftazidime, ceftriaxone, cefoxitin, cephaloridine and cephalothin are shown in Figure 3.15 and Figure 3.16. Figure 3.15 shows the antibiotics that can generate positive changes in fluorescence signal, while Figure 3.16 shows the antibiotics that give non-significant fluorescence signal changes upon binding. Changes of fluorescence intensity are considered "positive" when the percentage change is larger than 10%. The antibiotics added were in a concentration of 1×10^{-4} M so that a saturated fluorescence signal could be achieved. The percentage change in the fluorescence intensity is calculated by the largest difference of the fluorescence intensities before and after binding with β-lactam at the same emission wavelength.

The percentage change in fluorescence intensity and shift in wavelength maximum upon the addition of various β-lactams are summarized in Table 3.2. The result shows that pencillin G, ampicillin, cefotaxime, cefuroxime, ceftazidime and ceftriaxone gave an enhancement in fluorescence intensity, while penicillin G, cefotaxime and ceftriaxone generated a significant blue-shift of wavelength at the maximum change of fluorescence signal. The cefuroxime gave a smaller change in fluorescence intensity than the other antibiotics.

7-ACA, cefoxitin, cephaloridine and cephalothin did not generate significant changes in the fluorescence signal, both in the fluorescence intensity

and the wavelength at emission maximum. The fluorescence change was less than 10% upon the addition of these antibiotics.

We focused on cephalosporins and fluorescence measurement was be done in detail for the binding of PenP_E166Cb and cefotaxime, as cefotaxime contains diverse side chain groups of the cephem nucleus. Different concentrations of cefotaxime were used in measurement to investigate the sensitivity of the biosensor and the relationship between the the concentrations of the antibiotics and the emitted fluorescence intensity. The fluorescence scanning spectra of PenP_E166Cb in the presence of 2 x 10^{-8} M, 5 x 10^{-8} M, 1 x 10^{-7} M and 1 x 10^{-6} M cefotaxime are shown in Figure 3.17.

The concentrations used in the time-dependent measurement were the same as those used in the scanning measurement. The time-dependent profile is shown in Figure 3.18. It can be seen that the fluorescence signal rose instantaneously upon the addition of the antibiotic to the protein mixture. The increase in fluorescence signal became steady at around 50 s for lower concentrations of cefotaxime (e.g. 2 x 10^{-8} M). The fluorescence signal reached a plateau and did not drop back to the baseline in the first 1,000 s for all antibiotic concentrations. The slightly slanted fluorescence signal for certain cefotaxime concentrations (e.g. 5 x 10^{-8} M) might be due to a branched pathway mechanism of the acyl-enzyme complex (Escobar *et al.* 1994; Zawadzke *et al.* 1996; Vanwetswinkel *et al.* 2000) or the instability of the fluorescence machine. The time-dependent profile of PenPC_E166Cf (1 x 10^{-7} M) in complex with cefuroxime (1 x 10^{-6} M) is also included in the same figure for comparison.

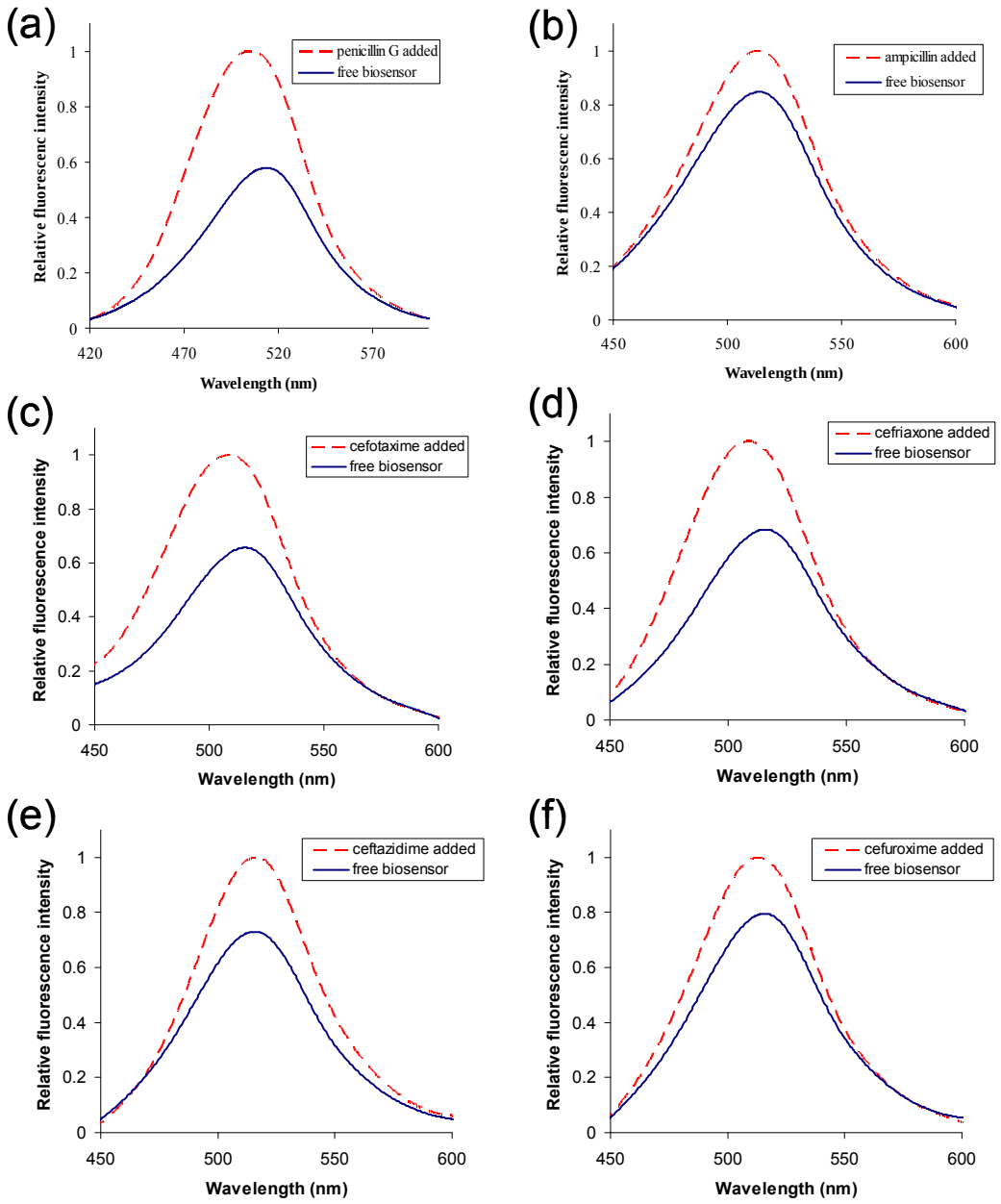

Figure 3.15: Fluorescence scanning spectra of PenP_E166Cb (0.1 μM) in the presence of 0.1 mM (a) penicillin G, (b) ampicillin, (c) cefotaxime, (d) ceftriaxone, (e) ceftazidime, and (f) cefuroxime.

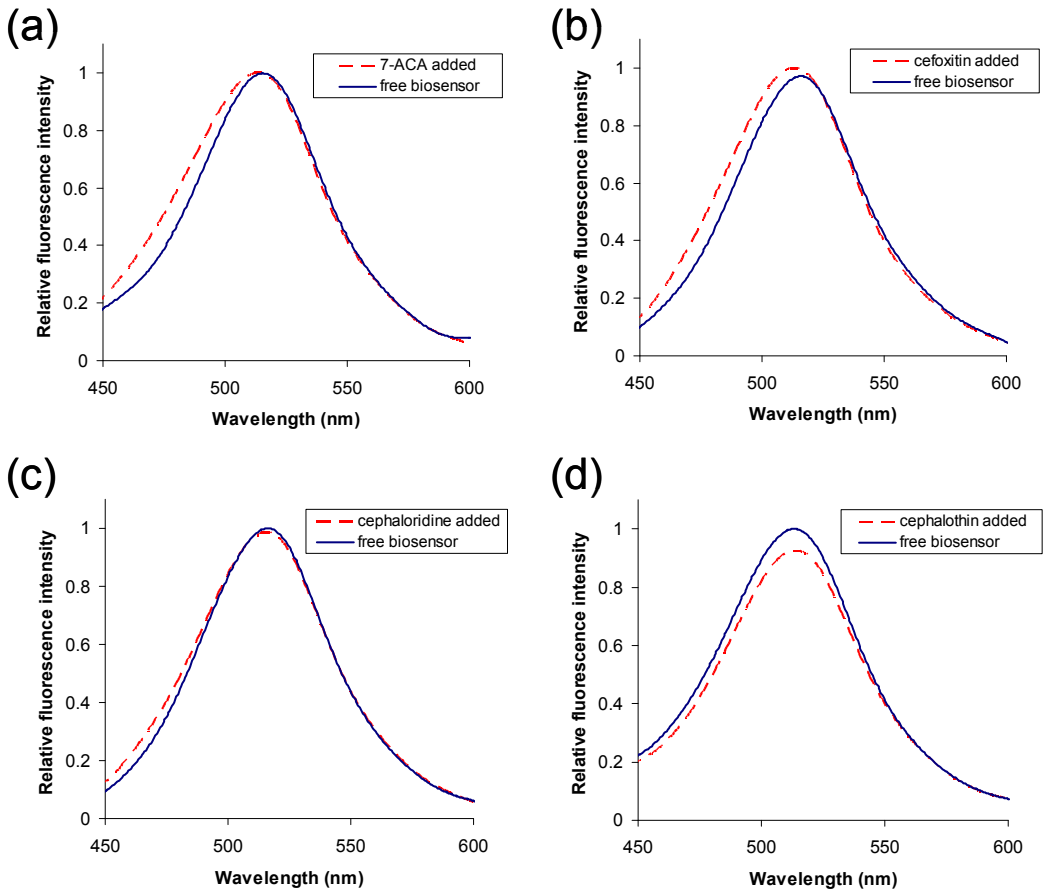

Figure 3.16: Fluorescence scanning spectra of PenP_E166Cb (0.1 μM) in the presence of 0.1 mM (a) 7-ACA, (b) cefoxitin, (c) cephaloridine, and (d) cephalothin.

Table 3.2: Percentage change in fluorescence intensity and shift in wavelength maximum upon adding various β-lactams

β-lactam	Emission maximum	Percentage change in fluorescence intensity
penicillin G	-9 nm	+98%
ampicillin	-0.5 nm	+18%
7-ACA	-1 nm	-1%
cefotaxime	-8 nm	+71%
cefuroxime	-1 nm	+14%
ceftazidime	-0.5 nm	+38%
ceftriaxone	-8 nm	+63%
cefoxitin	-2 nm	+2%
cephaloridine	---	+0%
cephalothin	---	-7%

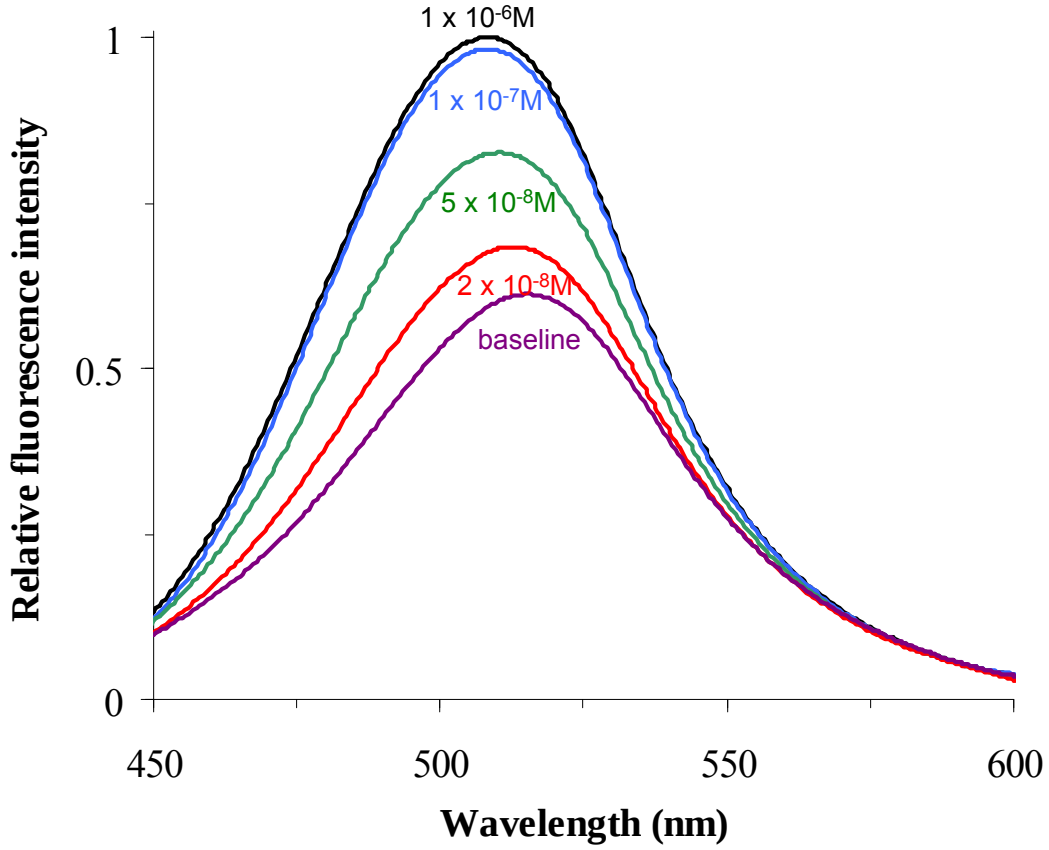

Figure 3.17: Fluorescence scanning spectrum of PenP_E166Cb (0.1 μM) in the presence of 2 x 10^{-8} M, 5 x 10^{-8} M.1 x 10^{-7} M and 1 x 10^{-6} M cefotaxime.

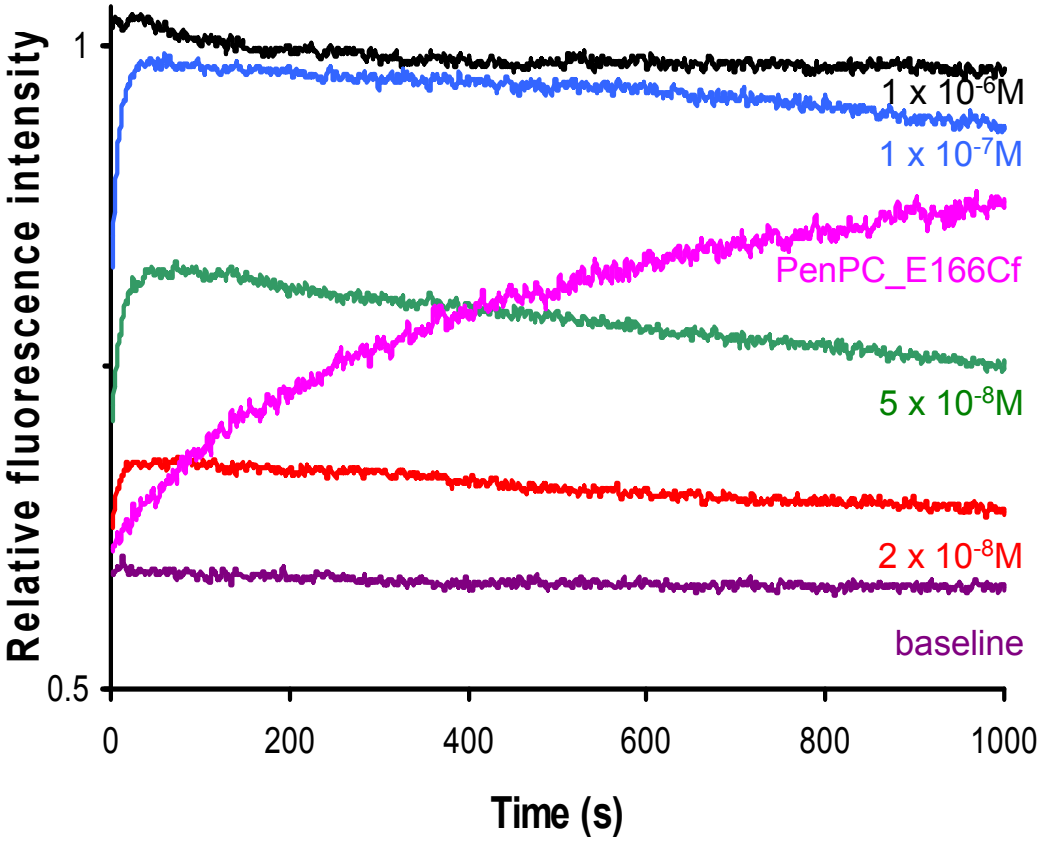

Figure 3.18: Time-dependent fluorescence spectra of PenP_E166Cb (0.1 μM) in the presence of 2 x 10^{-8} M, 5 x 10^{-8} M, 1 x 10^{-7} M and 1 x 10^{-6} M cefotaxime. Time-dependent fluorescence profile of PenPC_E166Cf (0.1 μM) in complex with cefotaxime (1 x 10^{-6} M) is also included.

3.3.9 Detection of covalent acyl-enzyme substrate complex in reaction with cefoxitin

To confirm that the antibiotic cefoxitin can react and bind to the fluorophore-labeled β-lactamase, ESI-MS was performed and the method used is described in Section 2.8.3. Formic acid was used before injecting the sample into the mass spectrometer to unfold the protein. When the protein is unfolded, the non-covalent protein-substrate complex will be dissociated, while the covalently bound protein-substrate complex can be retained as the protein and ligand are linked by a stable covalent bond. Therefore, in our experiment, the covalently bound acyl-enzyme intermediate of PenP_E166Cb can be detected by this unfolding method.

The mass spectrum of the reaction mixture is shown in Figure 3.19. The free badan-labeled 6xHis_PenP_E166Cb has a molecular mass of 30,642 Da and the antibiotic cefoxitin has a molecular mass of 428 Da. There is only a small peak of free enzyme (A) but an intense peak with mass increment of 368 Da, which is supposed to be the acyl-enzyme intermediate (ES*) in reaction with cefoxitin. This indicates that there is a loss of 60 Da upon binding, which should be due to a loss of $–OCONH_2$ moiety on the C3 position of cefoxitin. The loss of a moiety of $–OCOCH_3$ at the same position was also observed in a previous ESI-MS study of the reaction between TEM-1 β-lactamase and cefotaxime (Saves *et al.* 1995). The C3 leaving group is very common after the acylation of cephalosporins to β-lactamases (Faraci and Pratt 1986; Strynadka *et al.* 1994).

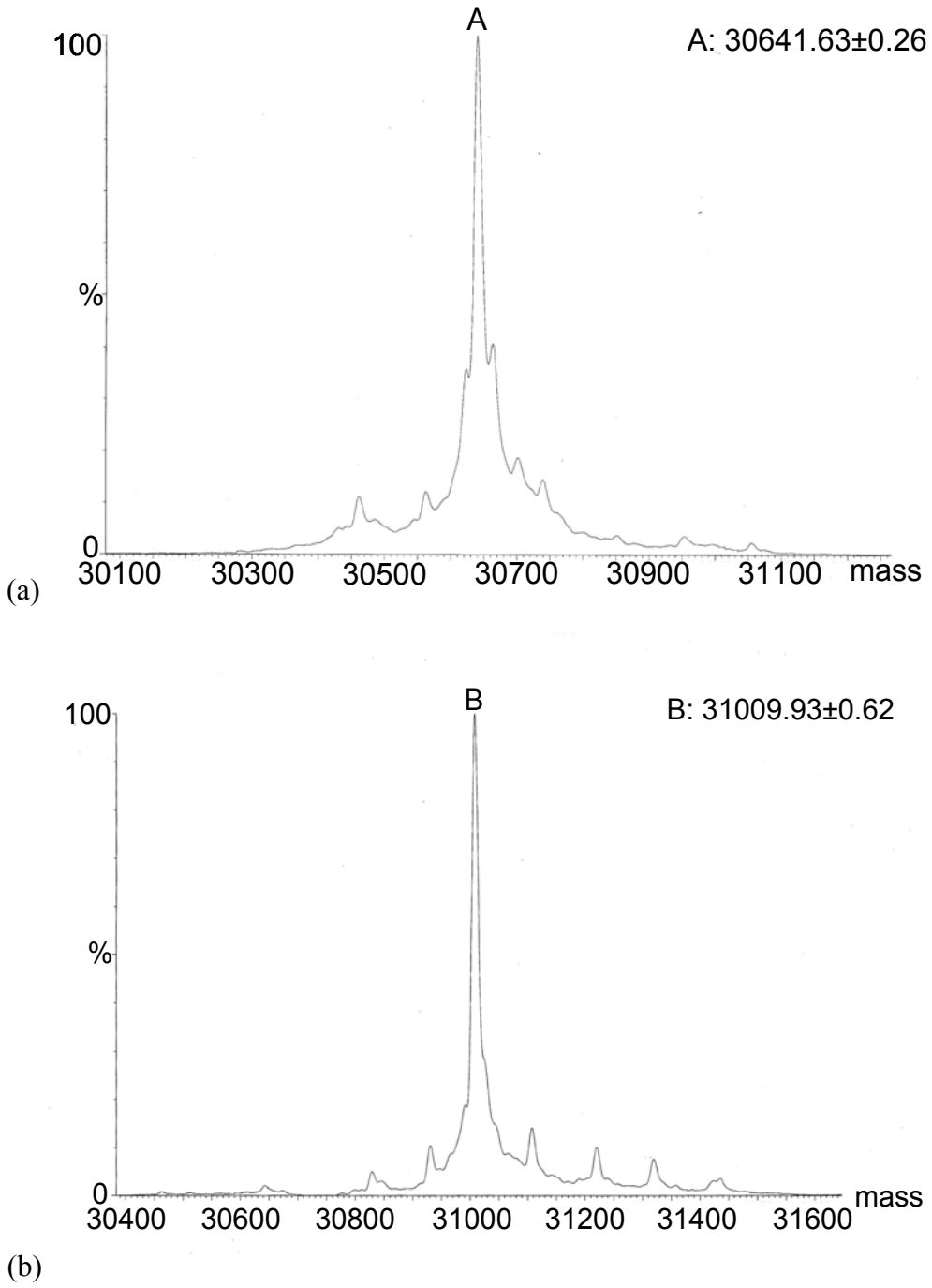

Figure 3.19: Transformed mass spectra acquired after incubation of 6xHis_PenP_E166Cb (5 μM) with cefoxitin (50 μM) in 20 mM ammonium acetate (pH 7.0). Peaks A and B correspond to the free enzyme E and the covalent acyl enzyme-substrate complex ES*, respectively.

3.3.10 Kinetic study on binding by quench-flow system

The binding rate of PenP_E166C and PenP_E166Cb were studied by mass spectrometry with the help of a quench-flow system because of the fast reaction time that is close to the millisecond level. Preliminary analysis of the binding experiment shows that when a 1:2 molar ratio of PenP_E166Cb to β-lactams was used, all of the PenP_E166Cb was found to be bound with the β-lactams in only one second so that the linear region of increasing amount of ES* was missing. Therefore it is impossible to mix and quench the solutions solely by hands. Two antibiotics, cefotaxime and penicillin G, were used in this kinetic study (Figure 3.20).

It was found that the binding rate of cefotaxime to PenP_E166Cb was significantly faster PenP_E166C, as the reaction time to achieve a maximum amount of ES* was reduced from more than 10 s to 1 s. Therefore the binding efficiency of cefotaxime was enhanced after the labeling of the enzyme. For penicillin G, the binding rate of PenP_E166Cb was in the same magnitude order to that of PenP_E166C, which means that the effect of labeling on the binding rate for penicillin G was not observable in this range of reaction time. Figure 3.21 is the transformed mass spectra acquired after incubation of 6xHis_PenP_E166Cb and 6xHis_PenP_E166C with cefotaxime and penicillin G at different time intervals.

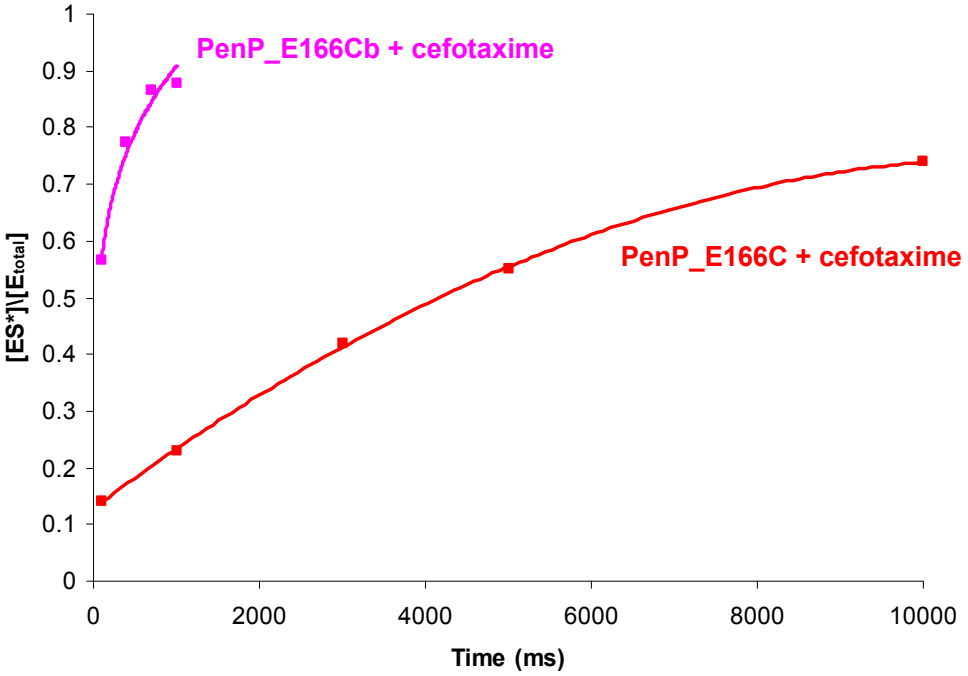

(a)

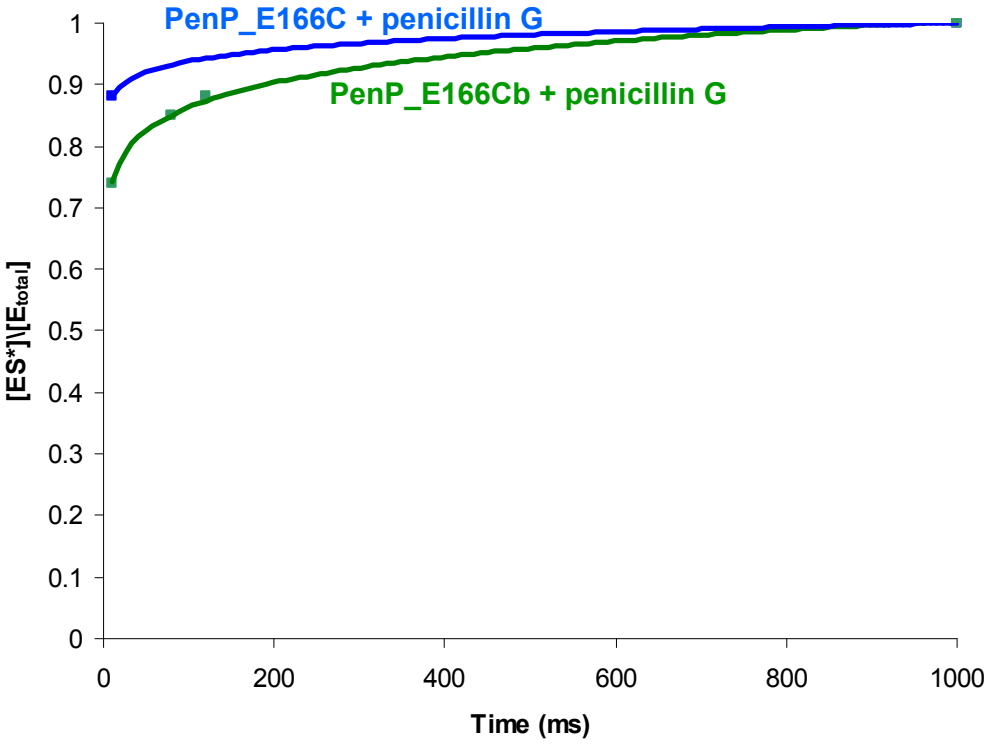

(b)

Figure 3.20: ESI-MS study on the binding rate of PenP_E166C and PenP_E166Cb with (a) cefotaxime and (b) penicillin G.

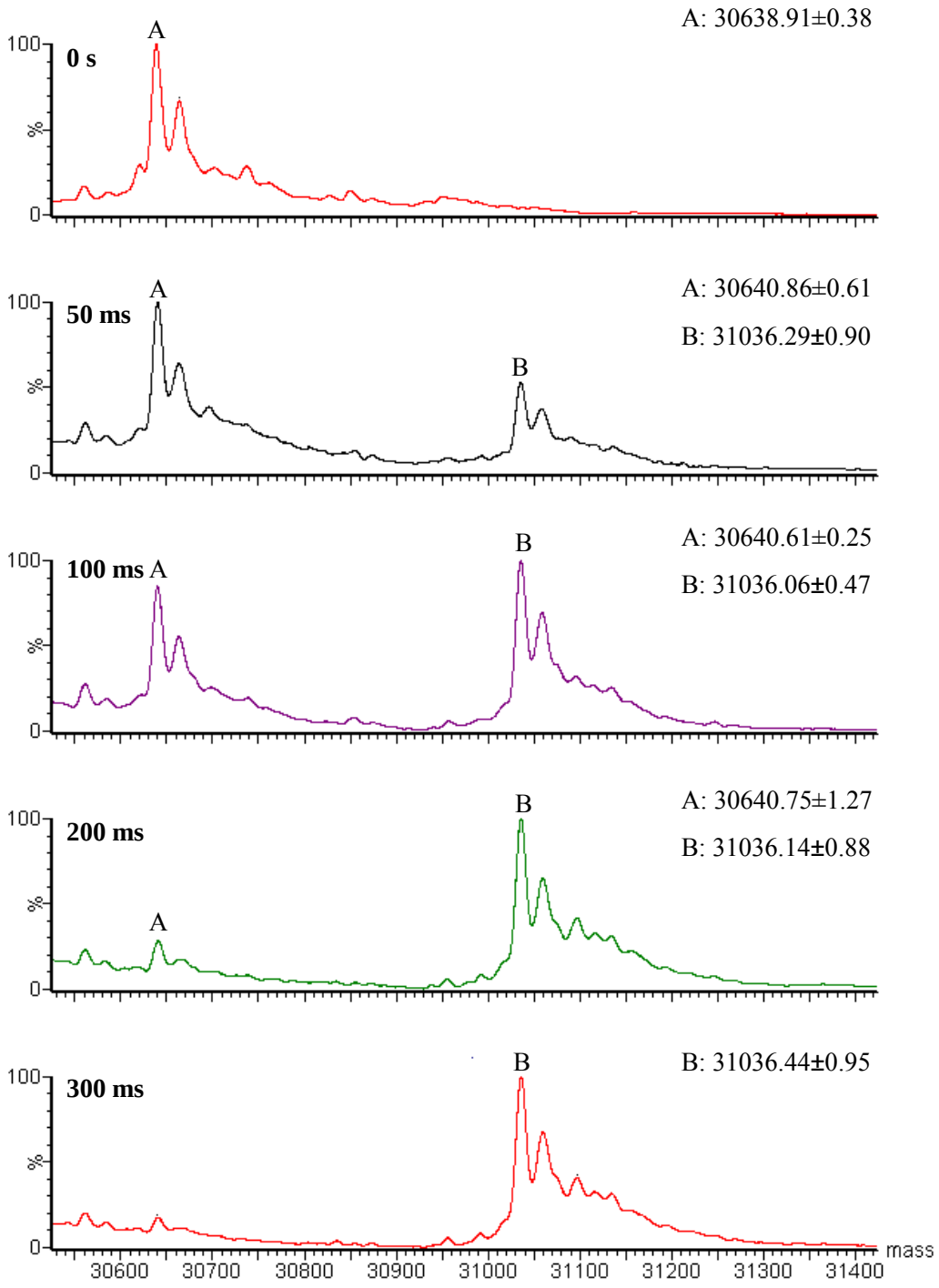

Figure 3.21: (a) Transformed mass spectra acquired after incubation of 6xHis_PenP_E166Cb (5 μM) with cefotaxime (10 μM) in 20 mM ammonium acetate (pH 7.0) at different time intervals. Peaks A and B correspond to the free enzyme E and the covalent acyl enzyme-substrate complex ES*, respectively.

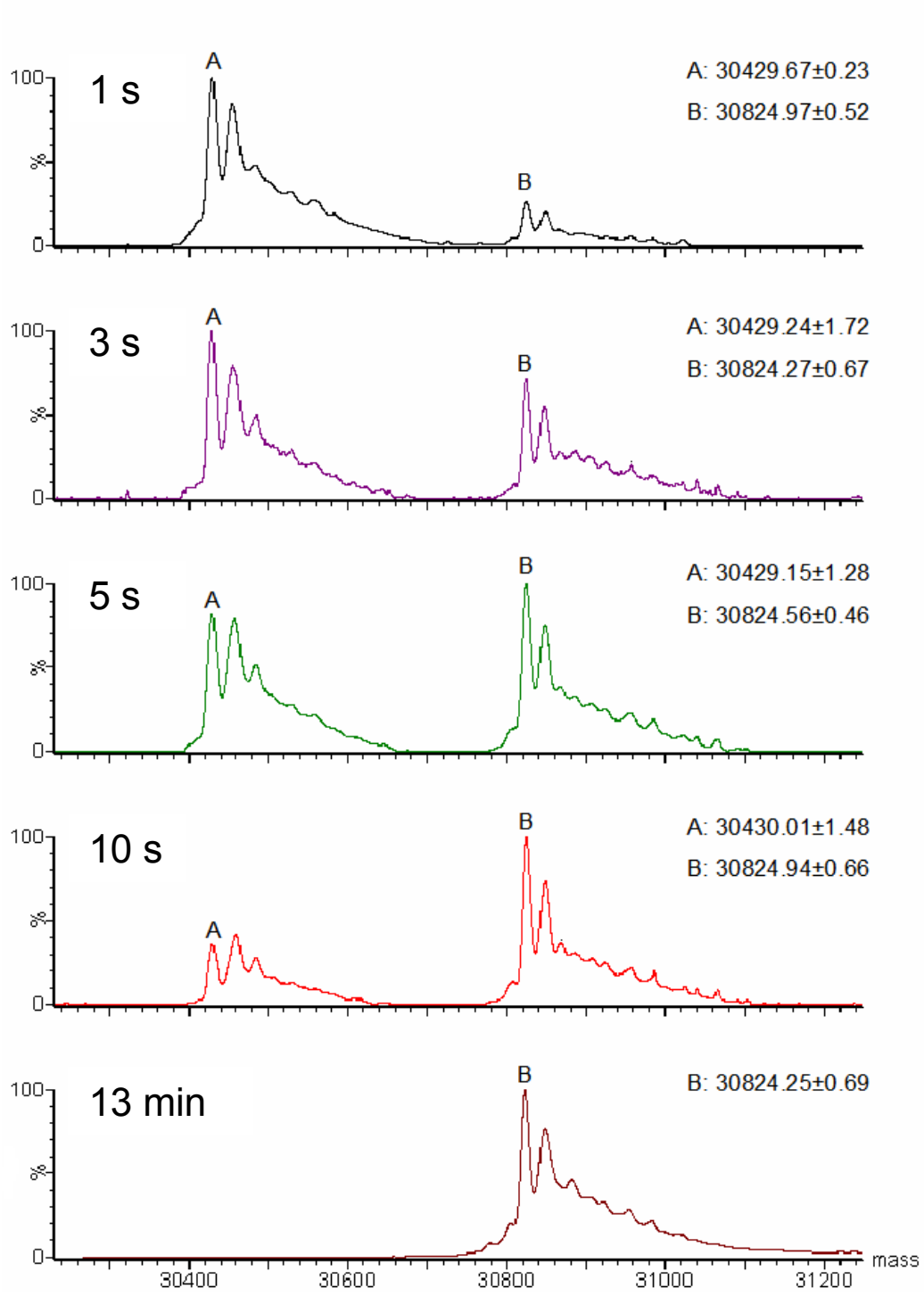

(b): Transformed mass spectra acquired after incubation of 6xHis_PenP_E166C (5 μM) with cefotaxime (10 μM) in 20 mM ammonium acetate (pH 7.0) at different time intervals. Peaks A and B correspond to the free enzyme E and the covalent acyl enzyme-substrate complex ES*, respectively.

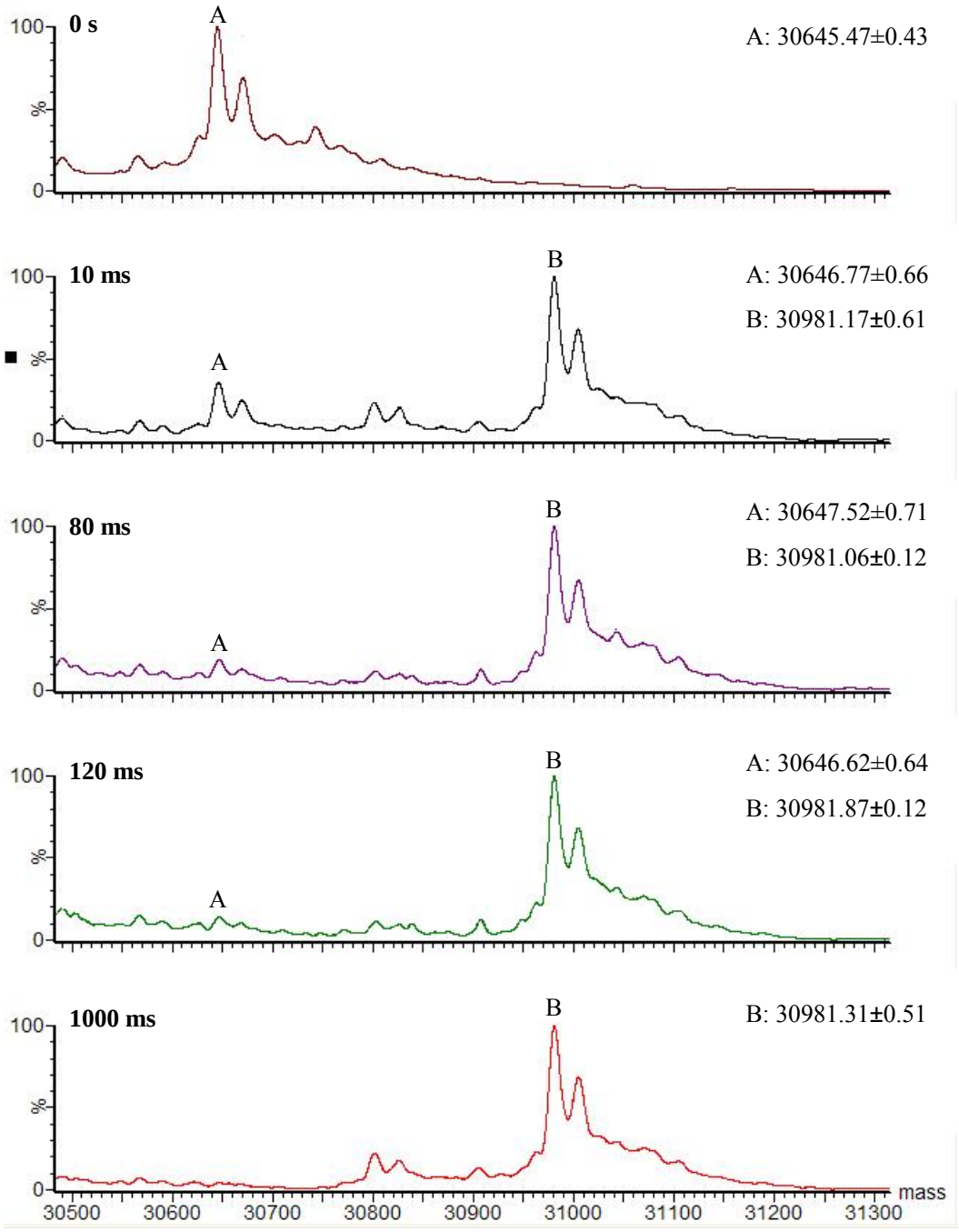

(c): Transformed mass spectra acquired after incubation of 6xHis_PenP_E166Cb (5 μM) with penicillin G (10 μM) in 20 mM ammonium acetate (pH 7.0) at different time intervals. Peaks A and B correspond to the free enzyme E and the covalent acyl enzyme-substrate complex ES*, respectively.

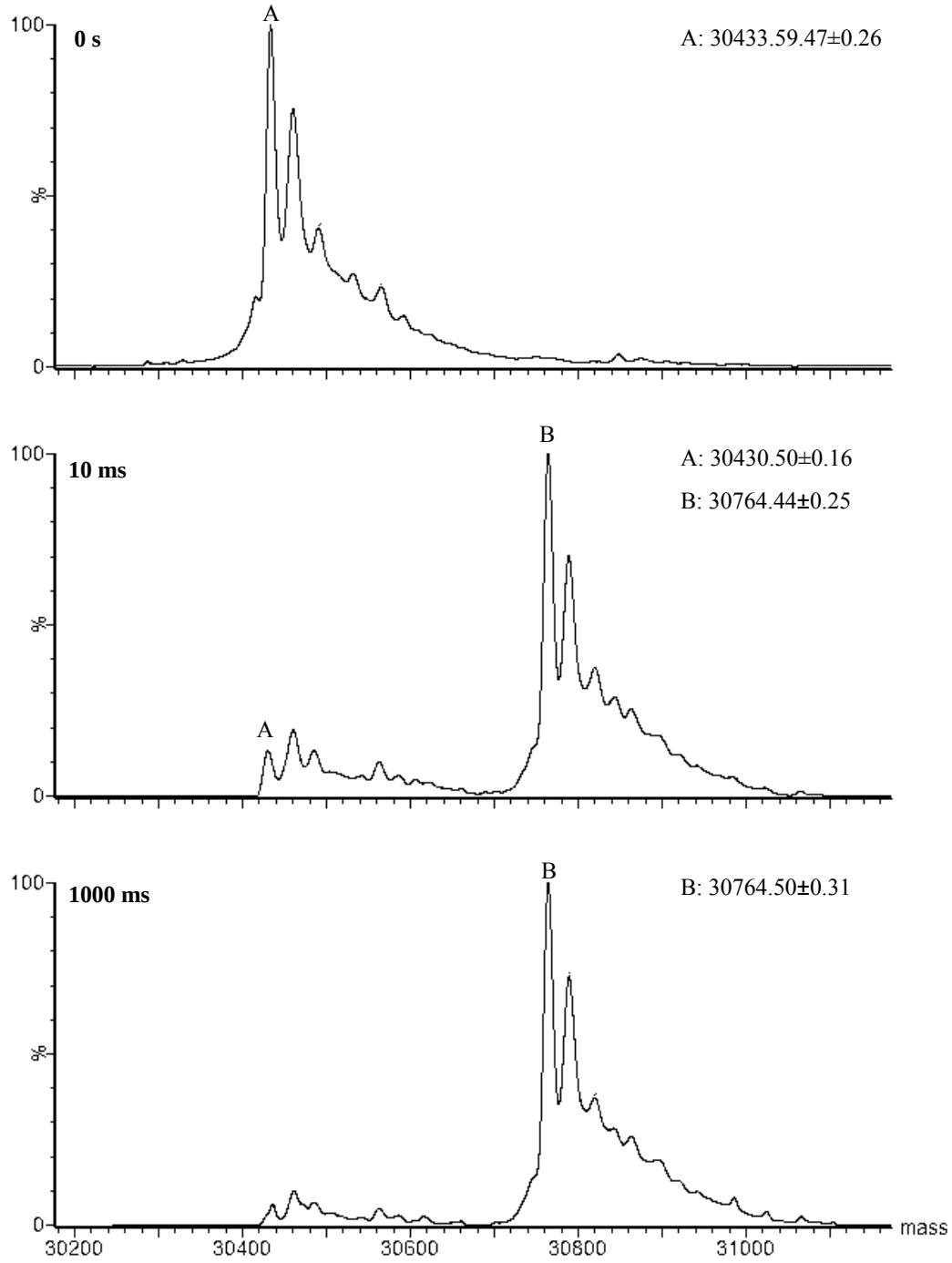

(d): Transformed mass spectra acquired after incubation of 6xHis_PenP_E166C (5 μM) with penicillin G (10 μM) in 20 mM ammonium acetate (pH 7.0) at different time intervals. Peaks A and B correspond to the free enzyme E and the covalent acyl enzyme-substrate complex ES*, respectively.

3.4 Discussion

3.4.1 Preparation of the biosensor

A series of purification steps were performed to purify the β-lactamase based biosensor to a high quality. As shown in Section 3.3.4, a series of badan labeling conditions have been tested. The result shows that GdnHCl is essential to unfolding the protein prior to the addition of the badan to the protein solution. We have finally chosen the lowest concentration of GdnHCl (2 M) in the experiment based on the assumption that the effect on the overall unfolding of the protein will be minimum when a lower concentration of GdnHCl is used. It is believed that the protein would be refolded back to the original conformation after removing the GdnHCl. However, precipitation was always observed during the buffer exchange process. This may be due to the reduced solubility of badan after the removal of DMF. Some of the protein was lost after labeling, possibly due to the miss folding of the protein in the refolding process.

To test whether the folding after labeling was correct or not, circular dichroism studies were performed. The result shows that the protein refolded in a normal manner and the fluorophore did not affect the overall folding of the protein. Even at high unfolding GdnHCl concentration (6M), the protein secondary structures were similar to the native protein after refolding. This indicates that if the protein is unfolded by the GdnHCl, it can refold back into its original conformation. The binding of PenP_E166Cb with cefoxitin indicates that the folding of the protein is correct and the enzyme mutant activity is maintained.

High labeling efficiency (~ 100%) should be achieved because it is not easy to separate PenP_E166Cb from PenP_E166C by chromatography as they have similar properties, such as a molecular mass with just 211 Da difference. The presence of the unlabeled PenP_E166C may cause the risk of crystallization of the enzyme without the presence of fluorophore. Homogeneity is important in crystallization since the protein molecules have to come close to each other in order to pack together to form first a lattice and then a crystal. Despite numerous attempts, the protein with an N-terminal 6xHis-tag could not crystallize well. However, when the 6xHis-tag was cleaved from the protein by TEV protease, single crystals were obtained with the same crystallization conditions. Removing the 6xHis-tag might help to produce good crystals (Kim *et al.* 2001).

3.4.2 Fluorescence signal of the labeled PenP_E166Cb

The changes in fluorescence signal upon addition of 10 different β-lactam antibiotics were investigated. Six antibiotics were tested, namely penicillin G, ampicillin, cefotaxime, cefuroxime, ceftazidime and ceftriaxone, producing positive fluorescence changes. A blue-shift of wavelength at maximum change of fluorescence signal is usually accompanied by an increase in fluorescence intensity, most obviously in the case of penicillin G, cefotaxime and ceftriaxone. This might be due to a change in the polarity of the environment in proximity to the fluorophore (badan) after the binding of the β-lactam antibiotics. The common feature of the cephalosporins that gave positive changes in fluorescence signal (cefotaxime, cefuroxime, ceftazidime and ceftriaxone) is a bulky branched group at the C7 position with the methoxyimini moiety. These cephalosporins, named oxyimino-cephalosporins, produce fast, instantaneous and measurable fluorescence changes. This is a significant improvement for sensing β-lactams over the PenPC_E166Cf biosensor previously published because of the immediate fluorescence response upon addition of cephalosporins. For example, PenP_E166Cb is instantaneous and PenPC_E166Cf takes 2000 s at 1 x 10^{-6} M cefotaxime to reach maximum emission intensity. The different functional groups at the C3 position do not affect the fluorescence signal. For example, cefotaxime and ceftriaxone have different R1 groups at the C3 position but their fluorescence signals were highly similar, which should be due to the same side chain group at the C7 position. Therefore the side chain group at the C7 position directly contributes to the resulting fluorescence signal.

On the other hand, four of the tested antibiotics did not generate any

positive changes in fluorescence signal (7-ACA, cefoxitin, cephaloridine and cephalothin), or any changes in wavelength at emission maximum. All these four antibiotics belong to non-oxyimino-cephalosporins containing non-branched side chain group with only a thiozoldine ring at the C7 position. Similar to the oxyimino-cephalosporins, the change in the functional group at the C3 position (e.g. cefoxitin and cephalothin) would not affect the weak fluorescence profile. It can be concluded that the presence of the bulky branched group at the C7 position with the methoxyimini moiety is the critical factor for the positive change in fluorescence intensity. The differentiation of the cephalosporins by PenP_E166Cb is shown in Figure 3.22.

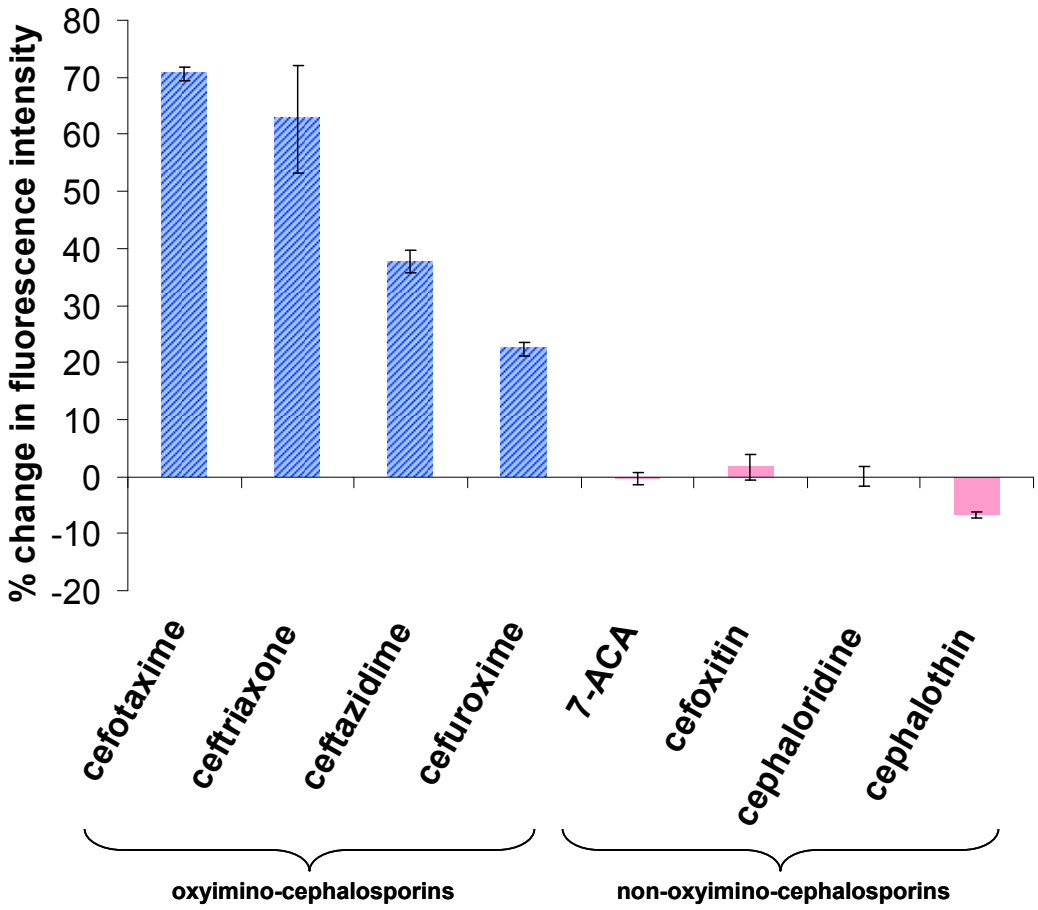

Figure 3.22: Differentiation of oxyimino- and non-oxyimino-cephalosporins (1 x 10^{-4} M) by the change in fluorescence intensity in PenP_E166Cb (1 x 10^{-7} M).

The standard deviations were calculated from a total of three trials for each antibiotic.

A range of concentrations of cefotaxime, from 2 x 10^{-8} M to 1 x 10^{-6} M, were used in both the fluorescence scanning measurement and the time-dependent fluorescence measurement. Cefotaxime was studied in more detail because it is a very common β-lactam antibiotic and it contains diverse side chain groups of the cephem nucleus. In addition, it generates the best fluorescence signal among all cephalosporins. The result shows that there was a strong correlation between the increase in fluorescence signal and the increasing concentration of the antibiotic so that the biosensor was sensitive to the change in the antibiotic concentration. The time-dependent fluorescence profile with different antibiotic concentrations reflects that the increase in fluorescence intensity was due to the increasing amount of the acyl-enzyme intermediate ES*, which is time-dependent and substrate-concentration-dependent (Figure 3.23). Therefore when a maximum amount of ES* was formed, the fluorescence signal reached a plateau and did not drop back to the baseline in the first 1,000 s because of the dramatically impaired deacylation rate (k_3) of the complex compared to the wild-type enzyme. A more stable ES* would lead to a longer plateau of signal, which is usually desirable in biosensing.

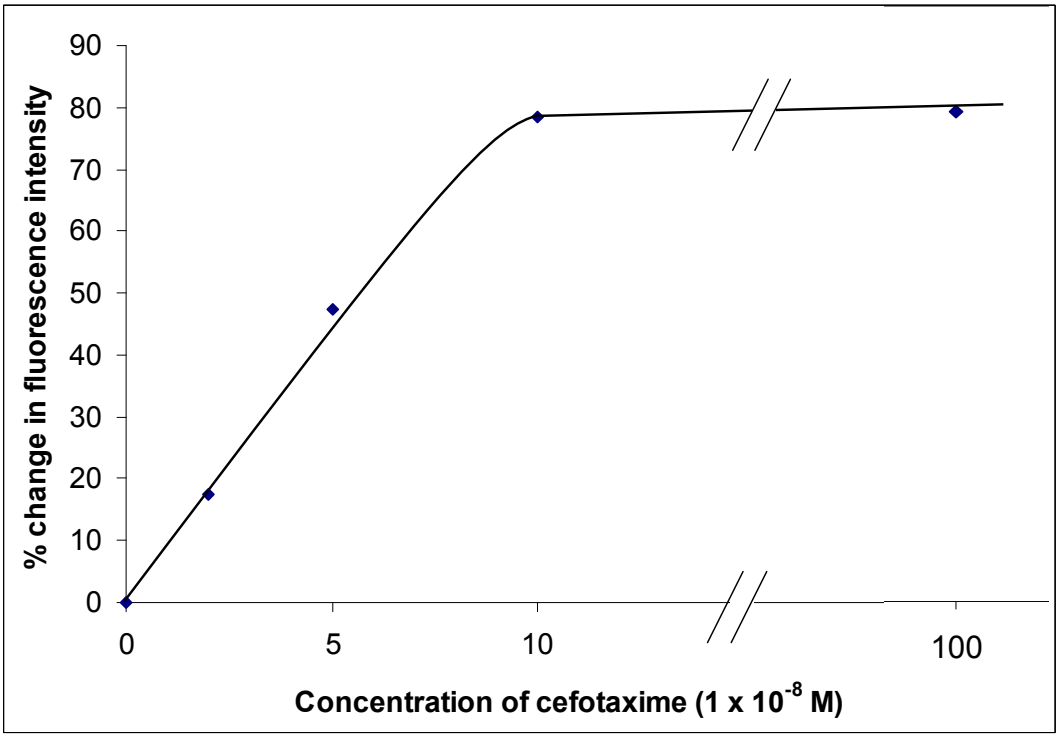

Figure 3.23: Relationship between the change in fluorescence intensity of PenP_E166Cb (1 x 10^{-7} M) against different concentrations of cefotaxime (2 x 10^{-8} M, 5 x 10^{-8} M, 1 x 10^{-7} M and 1 x 10^{-6} M)

3.4.3 Kinetic study on the binding of cefotaxime showing improved binding rate by conjugation of fluorophore

It is interesting to investigate the effect of the conjugation of fluorophore to the binding kinetics of the protein. However, the kinetic parameters (e.g. K_d, k_2) are difficult to obtain because of the limitation of the quench-flow machine as some of the reaction rates are too high for high antibiotic concentrations (e.g. > 2 molar excess). Therefore we can just compare the binding rates of PenP_E166C and PenP_E166Cb by simple binding curves (amount of [ES*] formed VS time) at the same concentration of β-lactams.

It is surprising to note that the binding rate of cefotaxime to PenP_E166Cb was significantly improved when compared to PenP_E166C. This means after conjugation of a fluorophore onto the Ω-loop, the binding rate of cefotaxime was enhanced, which might be due to the increased flexibility of the Ω-loop that allowed the large side chain of the cefotaxime to accommodate and bind to the active site of the protein. The oxyimino group and the thiozolyl ring of cephalosporins were less hindered by the surroundings so that the antibiotic binds to the active site more readily. This result is consistent with the prediction that the mutations on Arg164 and Asp179 would enlarge the active site and hence improve the binding affinity for cephalosporins with large beta functionalities (Vakulenko *et al.* 1999). It was shown that there will be severe steric interactions between the large side chain of β-lactams and the secondary structural element in the Ω-loop that are next to the active site, which cause the low binding affinity of the substrates to the enzyme. In our result, the binding rate of cefotaxime to PenP_E166Cb was comparable to that of penicillin G, while penicillin G is a

good substrate for class A β-lactamases. However, the binding of penicillin G to PenP_E166Cb was not enhanced by the presence of fluorophore. The faster binding rate for cephalosporins with large side chains on C7 position is a good characteristic of a biosensor because it can give fast responses.

3.5 Concluding remarks

The PenP β-lactamase mutant E166C was successfully expressed, purified and labeled with badan to form PenP_E166Cb. The labeled mutant was characterized with fluorescence spectrometry after addition of different cephalosporins. About half of the tested β-lactam antibiotics showed positive changes in fluorescence intensity immediately after the addition of the substrates to the protein solution. It was found that the PenP_E166Cb differentiated the cephalosporins by generating significant enhancements in fluorescence intensity for oxyimino cephalosporins instead of for non-oxyimino ones.

The binding kinetics of penicillin G and cefotaxime for both PenP_E166C and PenP_E166Cb were investigated by mass spectrometry with a quench flow system. It was found that after conjugation of a badan fluorophore onto the Ω-loop of PenP β-lactamase, the binding rate of cefotaxime was significantly improved when compared to the one without the fluorophore. The improved binding might be due to the increased flexibility of badan-linked Ω-loop.

Chapter 4: Structural study of PenP_E166Cb

4.1 Introduction

It is presumed that the fluorescence change in the previous β-lactamase-based biosensor PenPC_E166Cf upon binding with β-lactam antibiotic is due to the movement of fluorescein on the flexible Ω-loop to a more polar environment after the incoming antibiotic has occupied the same space with fluorescein in the active site. However, this hypothesis has not yet been confirmed by X-ray crystallography and has only been supported by molecular modeling in the previous study (Chan *et al.* 2004). In the molecular modeling results, it was shown that the fluorescein molecule was initially lying inside the substrate-binding pocket and close to the active site. After binding of penicillin G, the fluorescein moves out and becomes more exposed to the solvent, which leads to an increase in the fluorescence intensity. Molecular modeling can give us an overview and a few speculations regarding the mechanism of binding and fluorescence change, but fails to provide any definitive answer.

To further confirm the proposed biosensing mechanism, X-ray crystallography was carried out so that the environment that the fluorophore experiences before and after binding with β-lactam antibiotics can be investigated. The structural results are likely to show some detailed information on the protein conformation after conjugation of a fluorophore, the hydrophobicity and the polarity of the environment around the fluorophore, the positions of the fluorophore before and after binding, and whether there is an

interaction of the fluorophore with the protein. Such information can help us to understand the mechanism of β-lactam antibiotic biosensing and understand how the changing environment leads to a change in fluorescence signal.

In this project, we have chosen the PenP β-lactamase-based biosensor instead of using the previous PenPC_E166Cf for structural studies because the PenP β-lactamase-based biosensor was found to be more thermostable and could generate good fluorescent signals upon addition of antibiotic. The melting temperature (T_m) of PenP is the highest among all characterized β-lactamases (Vanhove *et al.* 1995; Fitter and Haber-Pohlmeier 2004), which is an advantage for crystallization. Moreover, since crystallization needs a large amount of protein, the high expression level of PenP and the simple purification method indicate that PenP is a good starting material (Frate *et al.* 2000). More importantly, the availability of the crystal structures in the literature (PDB ID: 4BLM and 1MBL) (Knox and Moews 1991; Knox *et al.* 1993) give us examples for crystallization conditions and a template for resolving crystal structure in high identity by molecular replacement. After obtaining the crystal structure of the fluorophore labeled PenP_E166C, the initial and final environments of the fluorophore after adding various β-lactams can be studied. Then the biosensor can be subjected to site-directed mutagenesis on different sites. Some sites may be critical to changes in fluorescence signals in order to improve the sensitivity and the sensing spectrum of the biosensor.

4.2 Methods

4.2.1 Crystallization of PenP_E166C, PenP_E166Cb and PenP_E166Cb in complex with various β-lactam antibiotics

The crystallizations of PenP_E166C and PenP_E166Cb were performed using the method described in Section 2.9.1. The method of structure determination is described in Section 2.9.2. The structures of PenP_E166C and PenP_E166Cb are compared.

To obtain crystals of PenP_E166C, PenP_E166Cb and PenP_E166Cb in complex with various β-lactam antibiotics, the proteins were extensively purified to obtain a high purity. The best crystallization conditions for the growth of each crystal were found. The procedures of crystallization are described in detail in Section 2.9.1. Five β-lactam antibiotics (cefotaxime, cefuroxime, 7-ACA, cefoxitin and cephaloridine) were used in the soaking experiment in order to obtain the crystal structure of the acyl-enzyme intermediate complex.

4.2.2 Confirmation of the desired protein crystals

To confirm that the crystal was successfully grown from the labeled protein, the fluorescence levels of the crystals were checked with the use of SDS/PAGE gel electrophoresis (McLachlin and Dunn 1996). The crystals were spun at 13,000 rpm for 5 min and the supernatant was removed. New stabilizing solution was added (solution of crystallization condition) and the crystals were washed five times by repeating this procedure. A small portion of supernatant was taken out for gel electrophoresis at the last time of washing (Figure 4.2, lane 2). Tris-HCl buffer pH 7.5 (50 mM) was added to dissolve the crystals and SDS/PAGE gel electrophoresis was performed. The low-range marker from Bio-Rad was used to determine the molecular weight of proteins. After electrophoresis, the gel was exposed to UV light and fluorescence image of the gel band was taken. The gel was then stained with Coomassie Blue R-250 staining solution for a few minutes and destained with a destaining solution with agitation.

4.3 Results

4.3.1 Crystallization of PenP_E166C and PenP_E166Cb

The hanging drop vapour diffusion method was performed as described in Section 2.9.1. Crystal Screen™ (CS) and Crystal Screen 2™ (CS2) (Hampton Research) were used in order to screen the initial crystallization conditions. From the 98 different conditions, it was observed that conditions CS #9 (0.2 M ammonium acetate, 0.1 M sodium citrate tribasic dihydrate at pH 5.6, 30% w/v PEG 4000), CS #10 (0.2 M ammonium acetate, 0.1 M sodium acetate trihydrate at pH 4.6, 30% w/v PEG 4000), CS #22 (0.2 M sodium acetate trihydrate, 0.1 M Tris HCl at pH 8.5, 30% w/v PEG 4000) and CS #41 (0.1 M Hepes sodium at pH 7.5, 10% v/v 2-propanol, 20% w/v PEG 4000) produced crystals of PenP_E166Cb.

It was noted that the flattened crystal formed at CS #41 was large enough to be seen by naked eyes without using the microscope. However, not all crystals from these four conditions could be used for data analysis, as some of them were too small or formed in bundles. Since single crystal is essential for a successful data analysis, optimization of crystallization conditions was performed by altering the pH of the buffer, adding different salt and additives (e.g. glycerol, ethylene glycol and PEG 400), and changing the % w/v of precipitant. For example, different molecular weights of PEG, such as 4000, 6000 and 10,000, were used to illustrate the effects of PEG on crystallization of PenP_E166Cb. It was found that only an increase in pH value of 0.3 showed a large effect on the crystallization process.

After optimization, it was found that the PenP_E166C protein crystallized at 0.1 M Hepes sodium at pH 7.5, 25% w/v PEG 4000, with a protein concentration of 15 mg/ml. It has been reported that the *Bacillus licheniformis* BS3 β-lactamase crystal was obtained at 25% w/v PEG 6000 in 100 mM sodium acetate buffer (pH 5.0) (Knox and Moews 1991; Fonze *et al.* 2002). Another study showed that the enzyme crystallized at pH 5.5 from PEG 8000 (Knox and Moews 1991). These conditions were quite similar to the conditions that we have tested. Both conditions contained PEG and sodium salts. Crystals of PenP_E166Cb were grown in a concentration of 20 mg/ml, at 0.1 M Hepes sodium at pH 7.5, 25% w/v PEG 4000 and 5% v/v 2-propanol, while the % v/v 2-propanol could be varied from 0 – 10%. The single crystals of PenP_E166Cb were slightly tinted in a light yellow colour due to the presence of the badan. The crystals of both PenP_E166C and PenP_E166Cb were taken to the X-ray machine for data analysis. Figure 4.1 shows some of the crystals grown from different crystallization conditions.

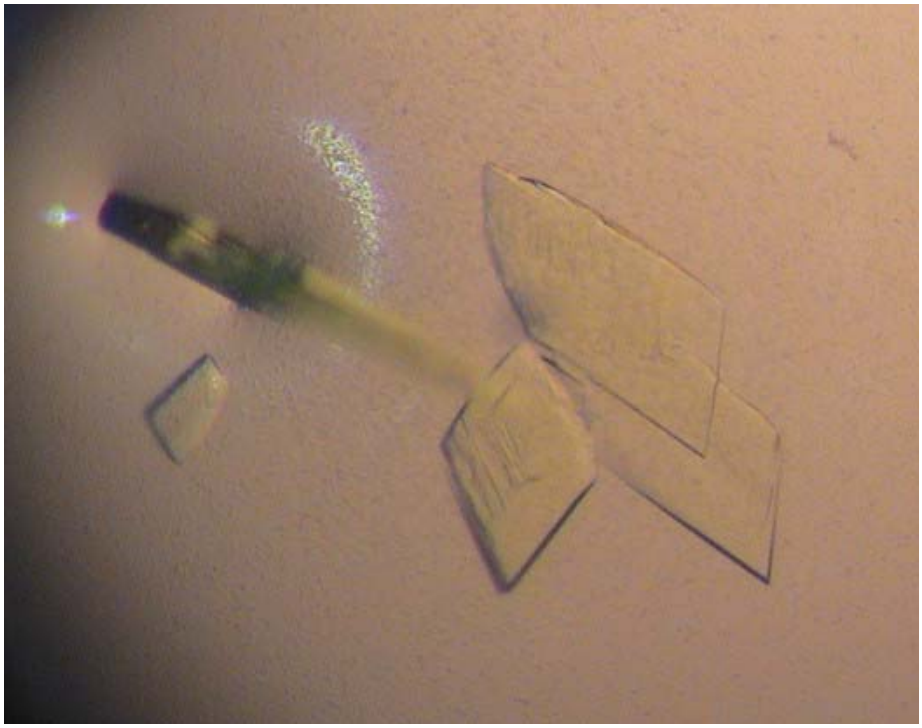

Figure 4.1: (a) Crystals of PenP_E166Cb formed by Hampton Screen CS #41 (0.1 M Hepes sodium at pH 7.5, 10% v/v 2-propanol, 20% w/v PEG 4,000), 20 mg/ml of protein.

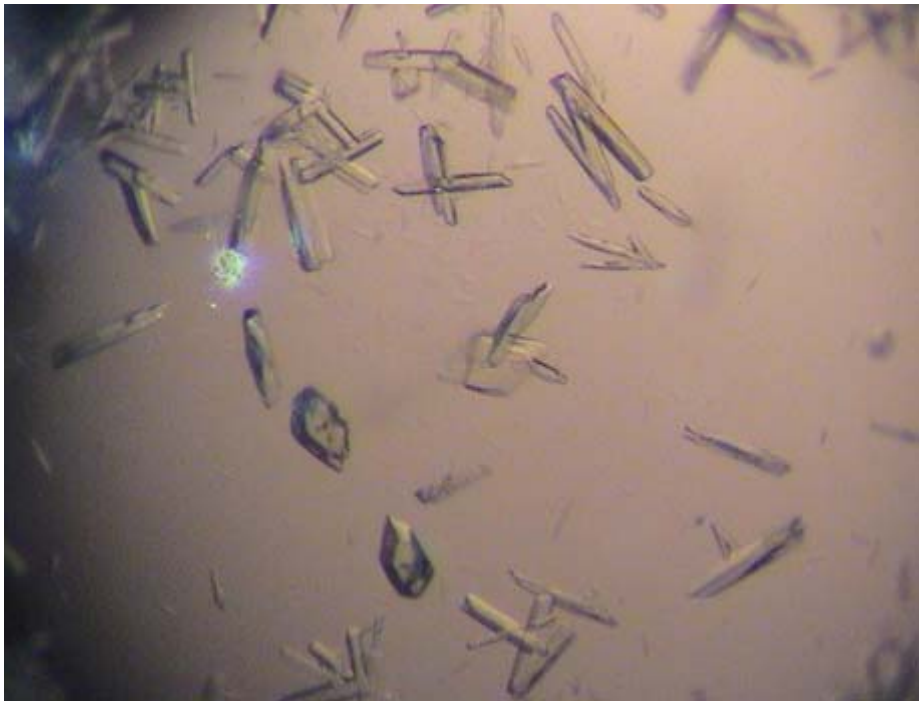

Figure 4.1: (b) Crystals of PenP_E166Cb grown at 0.5 M NH_4 acetate, 30% w/v PEG 4,000, 0.1 M Hepes at pH 6.9, 15 mg/ml of protein.

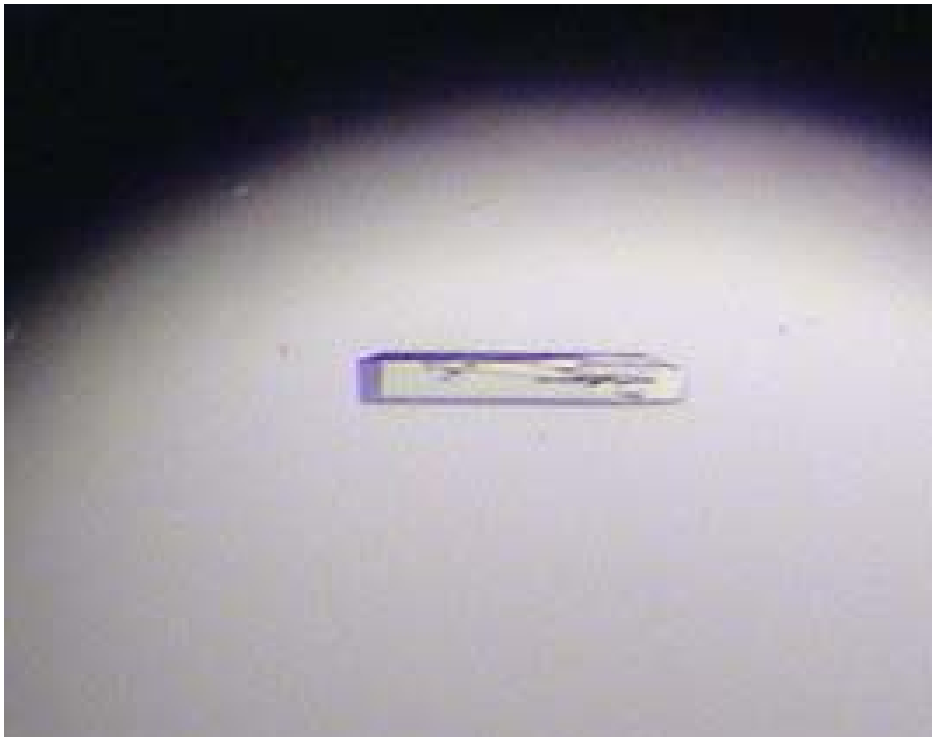

Figure 4.1: (c) Crystals of PenP_E166Cb grown at 0.5 M NH_4 acetate, 20% w/v PEG 10,000, 0.1 M Hepes at pH 7.2, 15 mg/ml of protein.

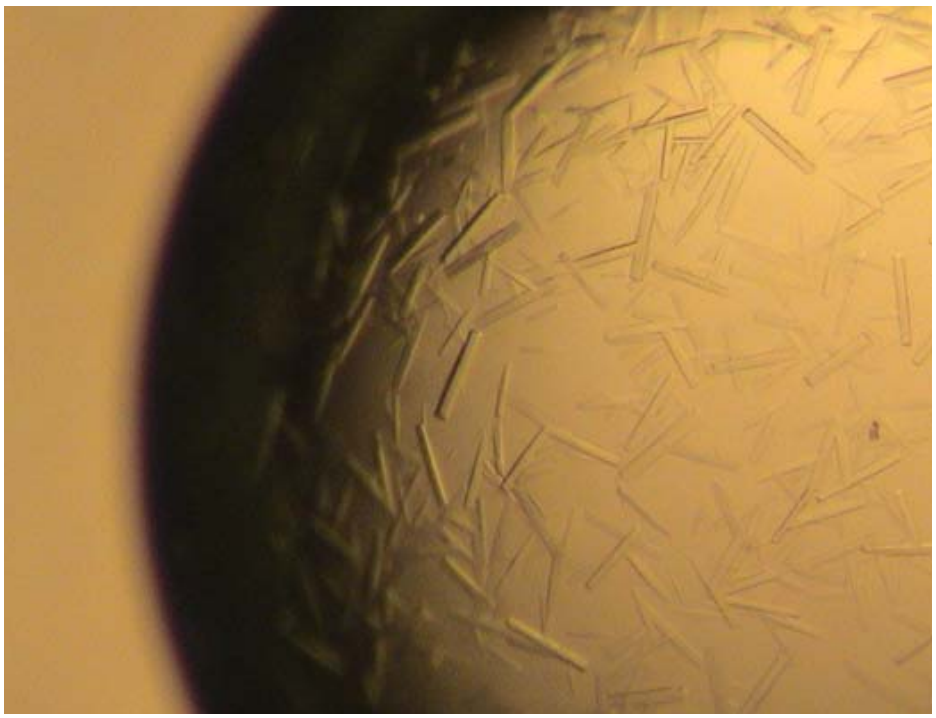

Figure 4.1: (d) Crystals of PenP_E166Cb grown at 0.5 M NH_4 acetate, 25% w/v PEG 6,000, 0.1 M Hepes at pH 6.9, 7.5 mg/ml of protein.

4.3.2 Confirmation of the desired protein crystals

Crystals grown were confirmed to be the PenP_E166Cb instead of unlabeled PenP_E166C because the PenP_E166Cb crystals have a light yellow colour due to the presence of fluorophore. In addition, the crystals of PenP_E166Cb were purified by a series of resuspension and centrifugation steps for the analysis of the molecular weight and fluorescence property by SDS/PAGE under UV exposure. Crystals chosen for confirmation were grown at the same conditions as those for data analysis.

The SDS/PAGE of the washed crystals of PenP_E166Cb and the fluorescence image of the same polyacrylamide gel are shown in Figure 4.2. Lane 1 on the left is the low range marker. Lane 2 is the supernatant after final washing of the crystal. In theory, the supernatant should not contain any solution of PenP_E166Cb since the crystal was washed several times. It is in agreement with the experimental result of the SDS/PAGE analysis since no band was observed in the middle lane. Lane 3 is the melted crystals. The melted crystals contained a band at the correct molecular mass of about 30,000 Da, which suggests that the crystals should be composed of PenP_E166Cb. This band was found to fluoresce when the same polyacrylamide gel was exposed to the UV light. This means that the crystals are the targeted protein PenP_E166Cb, which contains a fluorescent badan molecule.

(a)

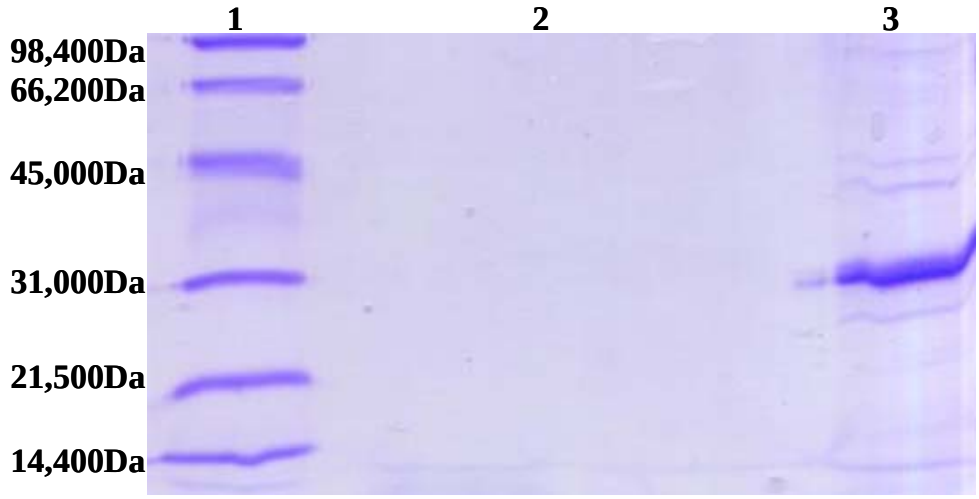

(b)

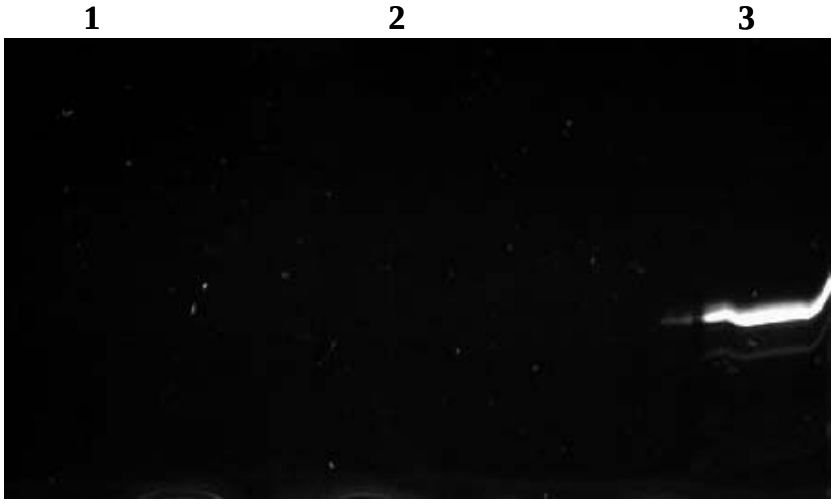

Figure 4.2: (a) SDS/PAGE of the purified crystal of PenP_E166Cb. Lane 1 is the marker: rabbit muscle phosphorylase b (97,400), bovine serum albumin (66,200), hen egg white ovalbumin (45,000), bovine carbonic anhydrase (31,000), soybean trypsin inhibitor (21,500), hen egg white lysozyme (14,400); lane 2 shows the supernatant after final wash of the crystal; lane 3 is the purified crystal of PenP_E166Cb. (b) Fluorescence image of the same polyacrylamide gel.

4.3.3 Crystal structure of PenP_E166C

The crystal dataset of PenP_E166C has a resolution of up to 2.5 Å was collected and the structure determination was done by molecular replacement (Phaser) in the CCP4 package 6.0.0 (Potterton *et al.* 2003), using the known structure of PenP (PDB databank ID: 4BLM) as the search model. The crystal belongs to the monoclinic group $P2_1$ with cell parameter: a = 43.0 Å, b = 92.4 Å, c = 66.1 Å. The X-ray data collection statistics for PenP_E166C is shown in Table 4.1. There are two molecules per asymmetric unit.

The crystal structure of PenP_E166C is shown in Figure 4.3. The structure of the wild-type PenP β-lactamase is superimposed with the PenP_E166C in Figure 4.4. The RMSD of all atoms on chain A between the two structures are 0.346 Å. It can be seen that the modification of glutamic acid to cysteine does not have any impacts on the conformation of other parts of the protein. Figure 4.5 shows the B-factors of all atoms calculated by the CCP4 suite.

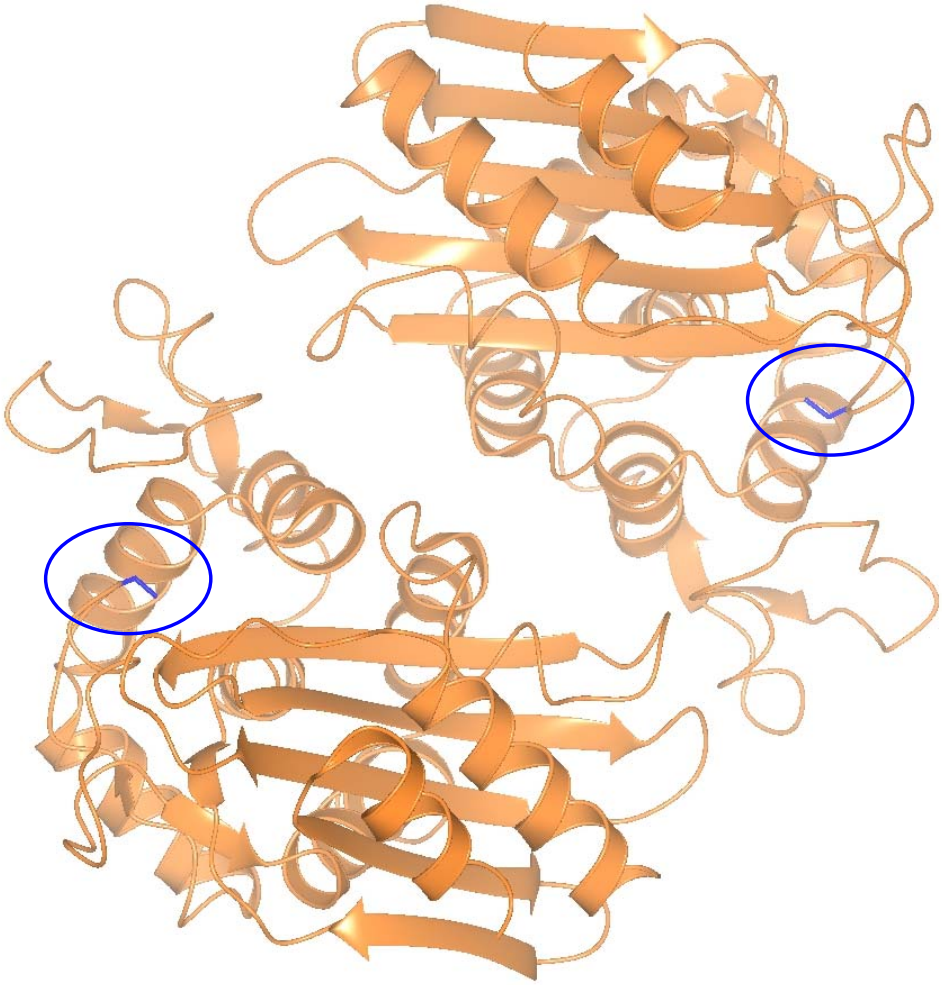

Figure 4.3: The crystal structure of PenP_E166C is shown in orange. Two molecules are observed in an asymmetric unit. The Cys166 residues in the two molecules are circled and the side chains are presented in stick and displayed in blue.

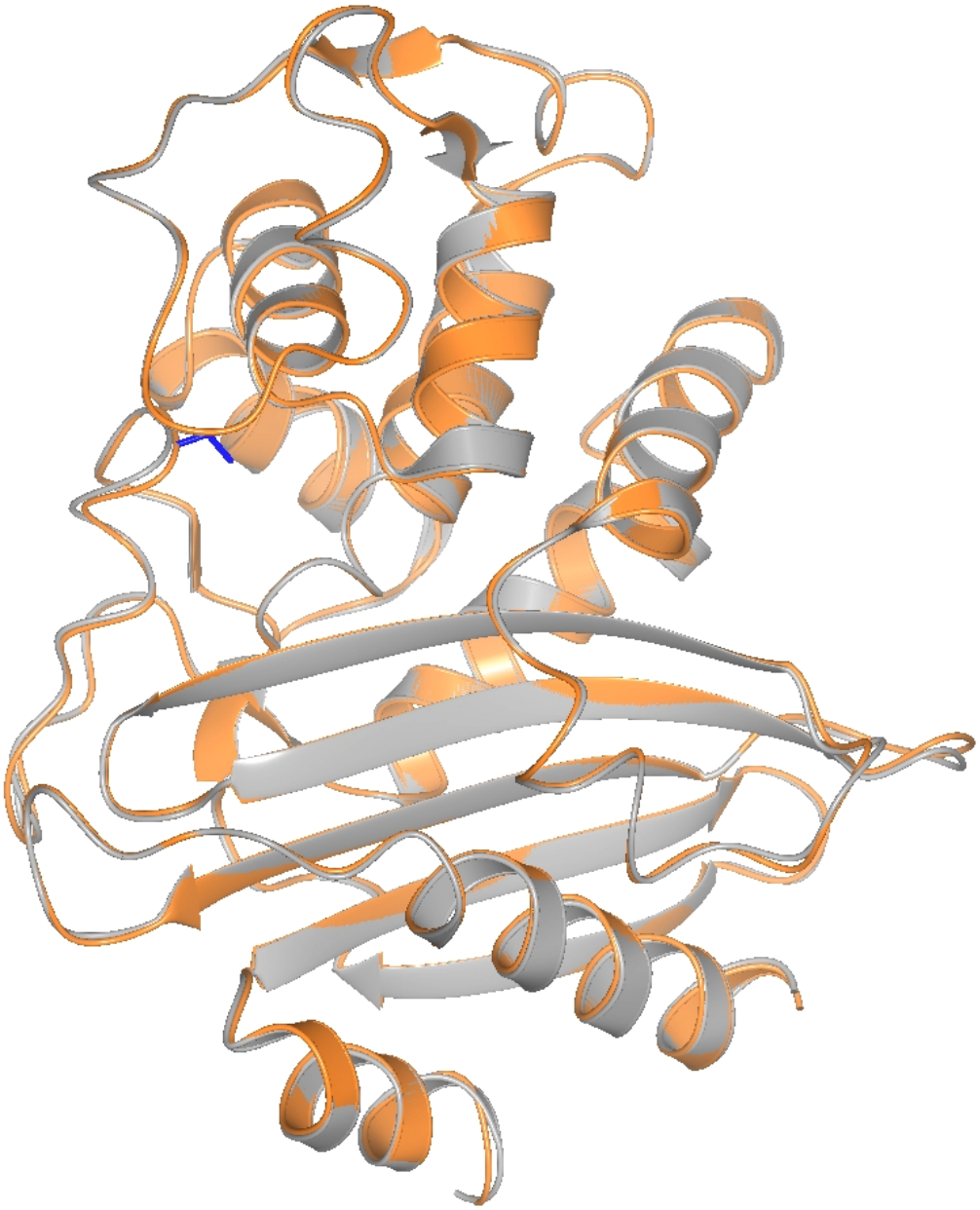

Figure 4.4: The crystal structure of PenP_E166C (in orange) superimposed with the wild-type PenP (PDB databank ID: 4BLM) (in grey). The Cys166 residue is displayed in blue.

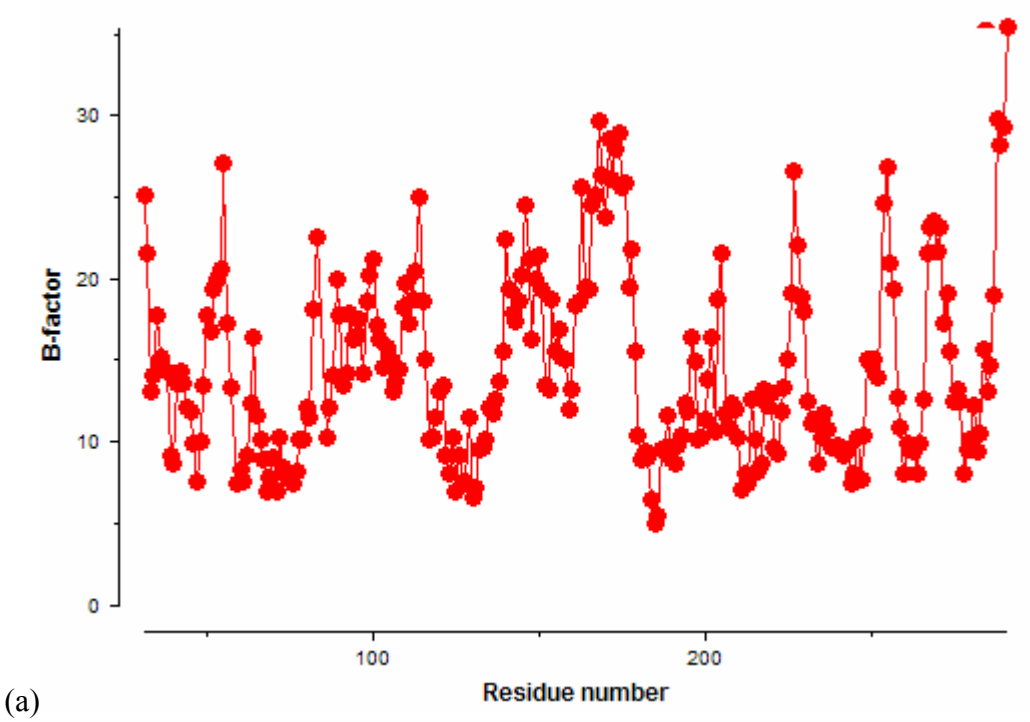

(a)

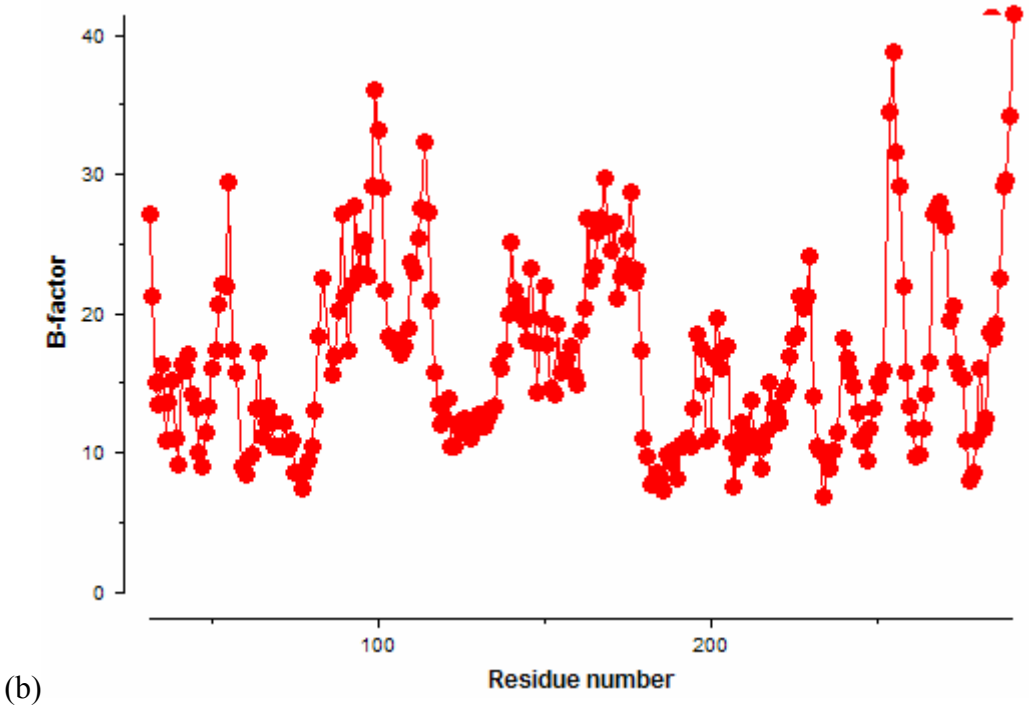

(b)

Figure 4.5: Average B-factors of all atoms in (a) chain A and (b) chain B of PenP_E166C. The y-axis is the value of B-factor and the x-axis is the protein residue number.

4.3.4 Crystal structure of apo PenP_E166Cb

The crystal dataset of PenP_E166Cb has a resolution of up to 1.7 Å and the structure determination was done by molecular replacement (Phaser) in the CCP4 package 6.0.0 (Potterton *et al.* 2003), using the known structure of PenP (PDB databank ID: 4BLM) as the search model. The crystal belongs to the monoclinic group $P2_1$ with cell parameter: a = 43.8 Å, b = 91.3 Å, c = 66.5 Å. There are two molecules per asymmetric unit. The crystallographic data and refinement statistics are shown in Table 4.1.

The badan molecules were generated by the Monomer Library Sketcher in the CCP4 package 6.0.0 and PRODRG (Schuttelkopf and van Aalten 2004). They were modeled onto the PenP structure after careful inspection of the f_o-f_c and $2f_o$-f_c electron density maps. The two badan molecules are in different locations and orientations. One of the badans is located nearer to and pointing to the antibiotic binding site. It is called the "near" badan in this project. The distance between the dimethyl group of this badan and the -OH group of Ser70 is 7.8 Å. The $2f_o$–f_c electron density map for the omega loop region and the f_o-f_c omit maps of the two badan molecules are shown in Figure 4.7 and Figure 4.8. The badan is obviously covalently linked with the cysteine residue by the continuous connectivity of the electron density cloud between the carbon atom of the naphthalene group of the badan and the sulphur atom of the cysteine residue. The other badan in another molecule (molecule B) is located a little bit further and pointing away from the antibiotic binding site. It is termed the "far" badan and is shown in green (Figure 4.8). The dimethyl group of this "far" badan is 11.9 Å away from the -OH group of Ser70.

To compare the two different locations of badan in the two molecules, molecules A and B are superimposed and shown in Figure 4.9. The naphthalene groups of the "near" badan and the "far" badan are oriented in plane to each other. It can be described as a badan molecule swinging in plane with a pendulum motion. The swinging angle between the two badan molecules is approximately 30°.

It can be observed that the naphthalene plane of the badan molecule is situated between the two molecular surfaces of PenP_E166Cb, which are residues 103-104 and residues 167-170. The badan is closest to these two surfaces and is sandwiched between them. The dimethyl amino group of the naphthalene ring projects toward the solvent and is more exposed to the outside. By the CCP4 package program, the solvent accessible areas for the "near" badan and the "far" badan were calculated as ~120 $Å^2$ and ~200 $Å^2$, respectively. On the other hand, the average B-factors for both chains in PenP_E166Cb structure show that Ω-loop had a higher B-factor than other part of the protein (>50 against 20-40) (Figure 4.6). The two badan molecules in the structure also had high B-factor values among all amino acids (58 in chain A and 75 in chain B, respectively).

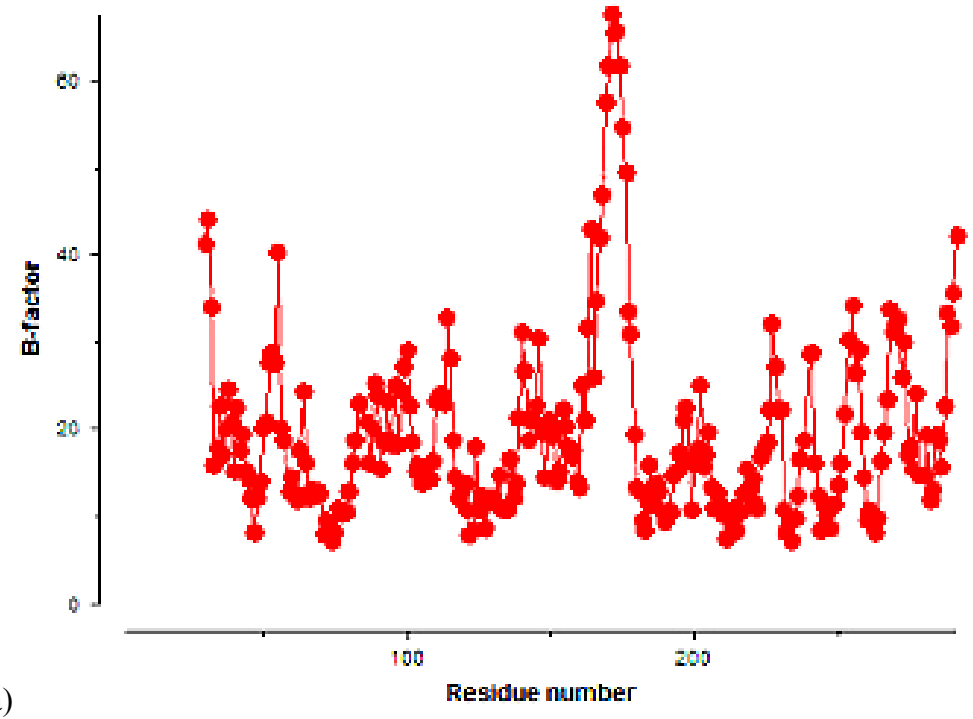

(a)

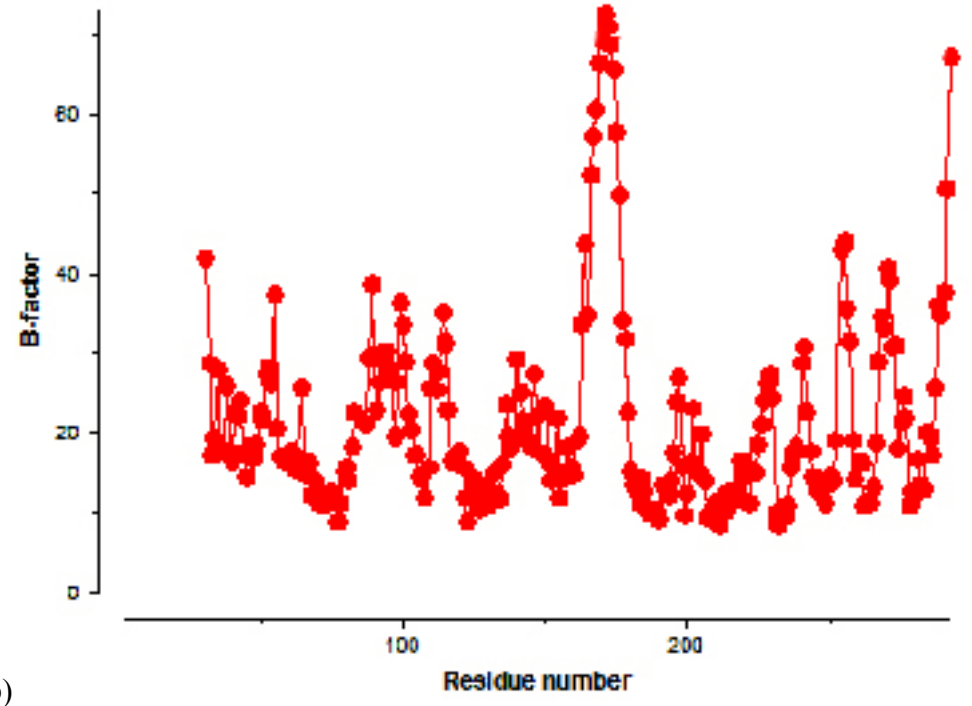

(b)

Figure 4.6: Average B-factors of (a) chain A and (b) chain B of PenP_E166Cb. The y-axis is the value of B-factor and the x-axis is the protein residue number.

Table 4.1: X-ray data collection and structure refinement statistics for PenP_E166C, apo PenP_E166Cb and PenP_E166Cb in complex with cefotaxime and cephaloridine

	E166C	E166Cb	E166Cb+ cefotaxime
Soaking condition			
Soaking solution	---	---	0.01M cefotaxime in 25% (w/v) PEG 4k, 0.1M Hepes pH 7.2
Soaking duration	---	---	20 min
Data collection			
Space group	$P2_1$	$P2_1$	$P2_1$
Unit cell parameters (Å)			
a	43.02	43.49	43.30
b	92.41	91.01	91.50
c	66.08	66.16	66.15
Resolution range (Å)	46.2-2.5 (2.6-2.5)	42.1-1.9 (2.0-1.9)	45.8-1.9 (2.0-1.9)
No. of total reflections	80428	152034	156015
No. of unique reflections	17617	39194	39490
I/σ	8.1 (4.0)	7.9 (2.4)	7.3 (2.2)
Completeness (%)	98.6 (86.9)	99.6 (99.6)	99.5 (96.3)
R_{merge} (%)	8.8 (17.0)	6.5 (26.1)	10.4 (17.8)
Structure refinement			
Resolution (Å)	41.63-2.50	40.06-1.95	40.00-1.90
R_{cryst}/R_{free} (%)	25.8/20.8	21.0/26.9	19.7/24.6
r.s.m.d. bonds (Å)/angles (°)	0.011/1.538	0.020/1.875	0.012/1.615
No. of reflections			
Working set	16489	34444	37382
Test set	890	1831	1983
No. of atoms			
Protein atoms	4001	4437	4382
Water molecules	94	199	127
Average *B*-factor (Å^2)			
Main chain	15.745	20.190	19.082
Side chain	16.688	22.580	22.606

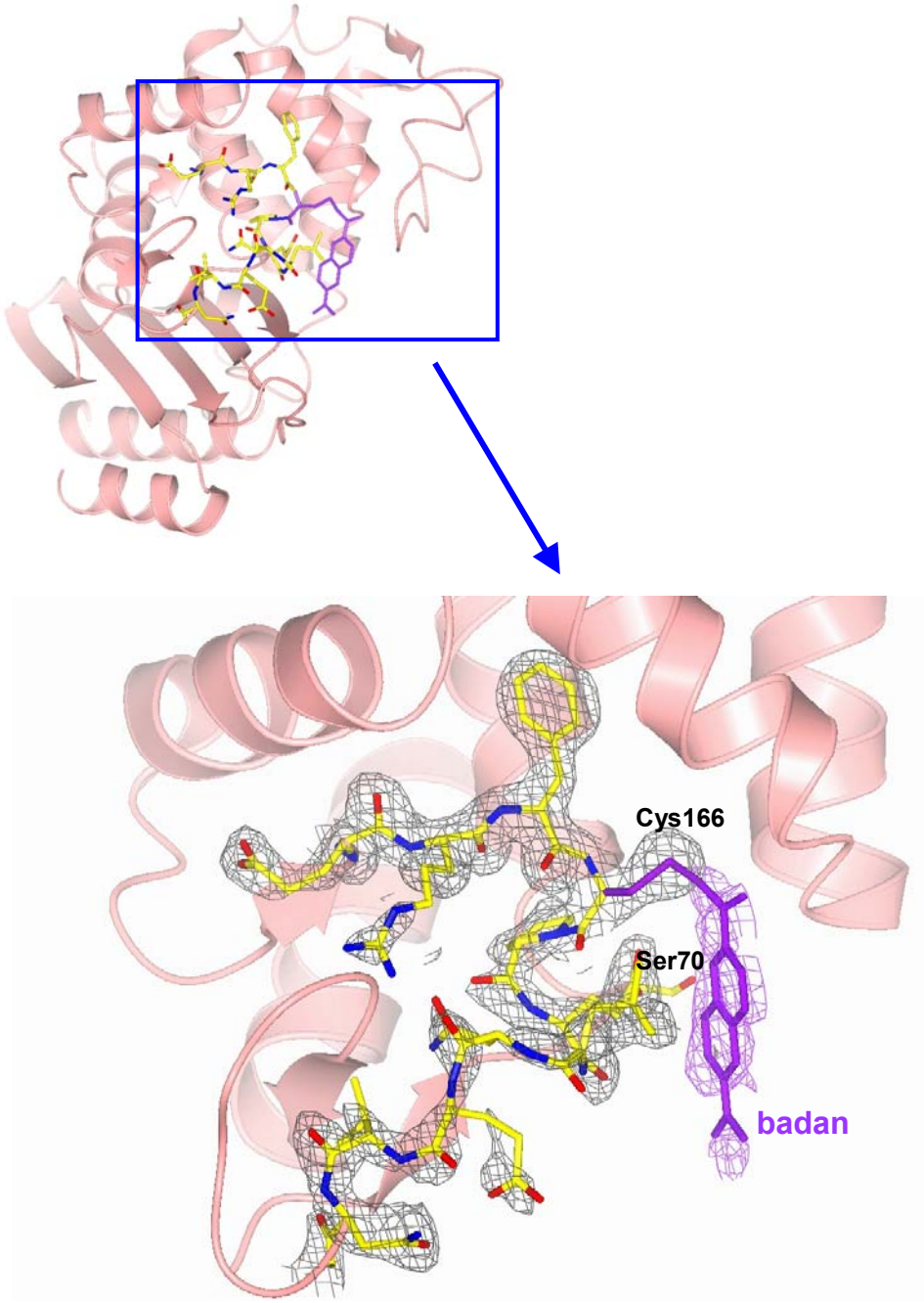

Figure 4.7: The f_o-f_c omit map showing the "near" badan molecule and the $2f_o$-f_c map showing the residues 163-173 on Ω loop. Structure of PenP-E166Cb is shown in pink. Residues on Ω loop (163-173) and the key catalytic residue for acylation (Ser70) are displayed in cpk colour scheme. The "far" badan is shown in purple cylinder model. The f_o-f_c map of badan is contoured at 2.0 σ and the $2f_o$-f_c map of the residues 163-173 is contoured at 1.0 σ.

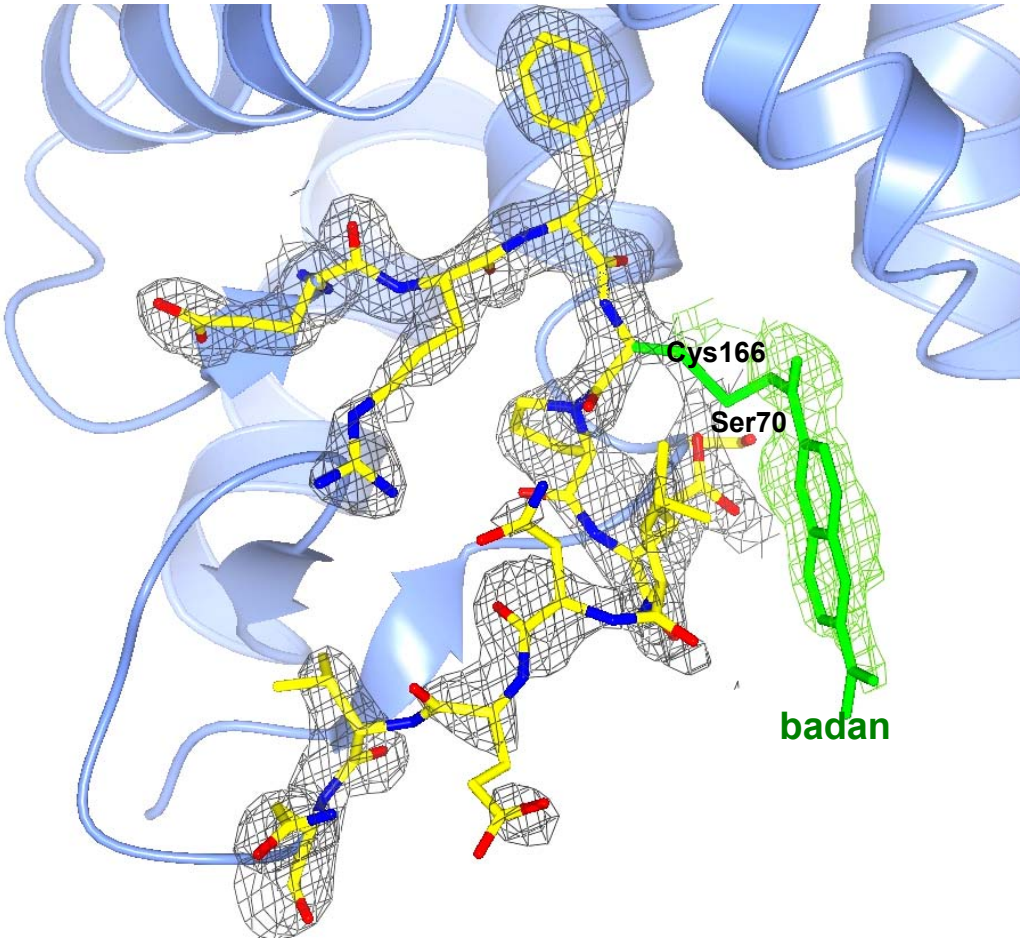

Figure 4.8: The f_o-f_c omit map showing the "far" badan molecule and the $2f_o$-f_c map showing the residues 163-173 on Ω loop. Structure of PenP-E166Cb is shown in blue. Residues on Ω loop (163-173) and the key catalytic residue for acylation (Ser70) are displayed in cpk colour scheme. The "far" badan is shown in green cylinder model. The f_o-f_c map of badan is contoured at 2.0 σ and the $2f_o$-f_c map of the residues 163-173 is contoured at 1.0 σ.

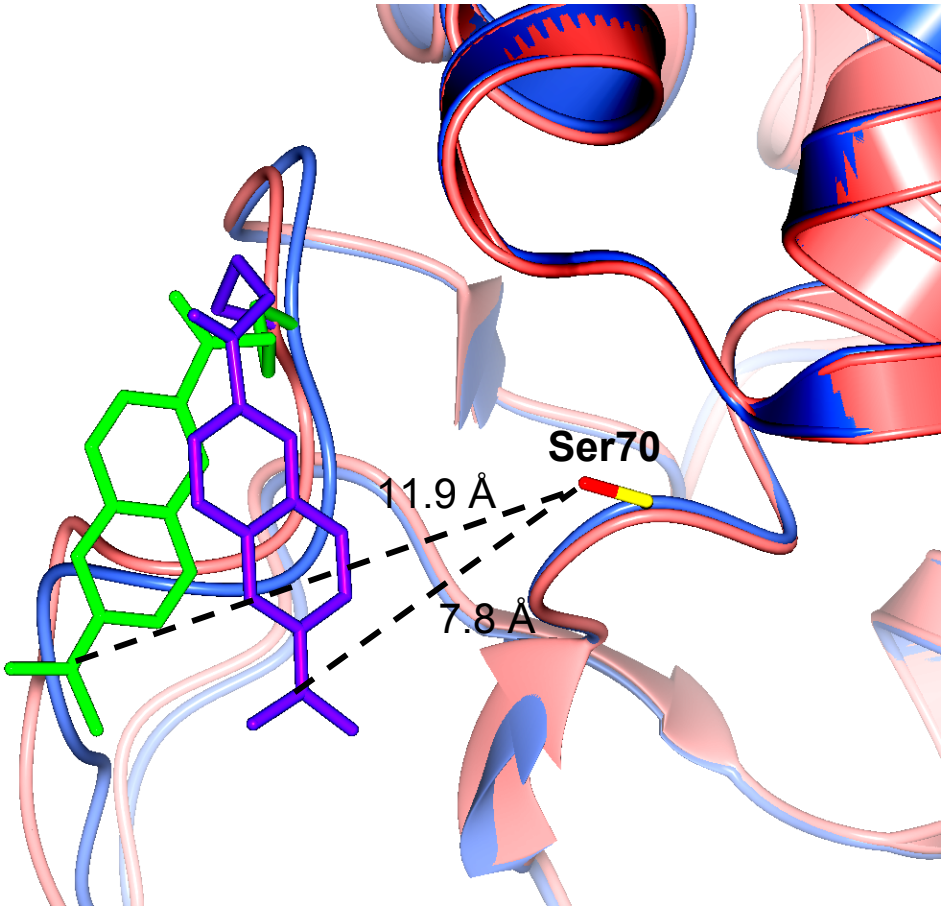

Figure 4.9: Superimposition of molecules A and B in the apo structure of PenP_E166Cb by aligning all the main chain Cα atoms. Ser70 is shown in cpk. The "near" and "far" badans are in purple and green, respectively. The protein body of "near" badan and that of the "far" badan are shown in pink and blue, respectively. The "far" badan sways 30 degrees in plane from the "near" badan.

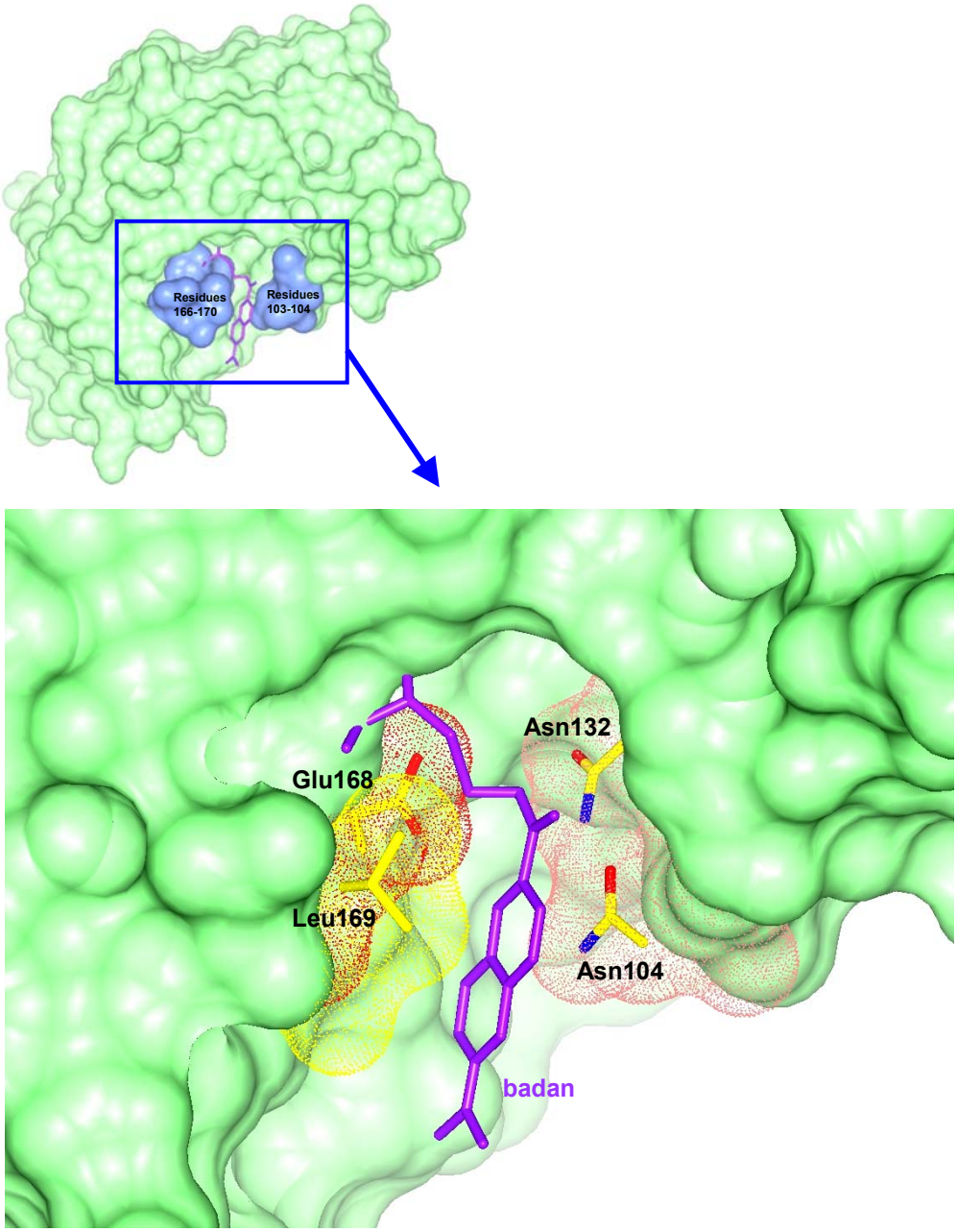

Figure 4.10: Surface docking groove showing the interface between the badan molecule (the "near" badan is used) and the PenP_E166Cb, which is shown in green. Residues 103-104 and 167-170 are displayed in blue surface in the upper picture. Badan and four residues located within 4.5 Å from badan are shown in cpk stick model and labeled. The surface profile of the four residues is presented as mesh model and colored according to their polarity (Yellow: hydrophobic; Red: acidic; Pink: polar).

4.3.5 Crystal structures of PenP_E166Cb in complex with cefotaxime and cefuroxime

The structure of the PenP_E166Cb in complex with cefotaxime was obtained at the resolution of 1.8 Å. The crystallographic data and refinement statistics are shown in Table 4.1. Cefotaxime and cefuroxime were transferred to the crystal by the soaking method. Figures 4.11 (a) and 4.12 (a) show the electron density maps of badan and cefotaxime in PenP_E166Cb-cefotaxime complex structure. The f_o-f_c omit map indicates the presence of the badan molecule and the cefotaxime. Figures 4.11 (a) and 4.12 (a) are the "near" badan and "far" badan, respectively. For the "near" badan, the green dash line represents disordering of Glu168 and Leu169 after binding because of the poor electron density obtained in this region. It can be observed that there is a linkage between the Oγ atom of Ser70 and the C8 of the β-lactam ring in cefotaxime, indicating that cefotaxime is covalently bound to the active site residue Ser70 as stated in the literature (Shimamura *et al.* 2002).

There is a difference in position between the "near" and "far" badans upon binding with cefotaxime. Figures 4.11 (b) and 4.12 (a) show the movement of the "near" and "far" badan induced by the binding of cefotaxime. For the "far" badan, nearly no change in position is observed with the addition of cefotaxime (Figure 4.12 (a)). The methoxyimino group of cefotaxime is pointing to the protein interior and causes steric clash with the Glu168, giving the result of restructuring of Ω-loop (Figure 4.12 (b)). The Cα of Glu168 is displaced by 2.4 Å and the side-chain is flipped by about 180° from the antibiotic binding site to completely solvent exposed. The Leu169 was originally next to badan molecule

but becomes packed into the interior of PenP_E166Cb structure near the B3 β strand after binding with cefotaxime. Residues 170-174 has an alternative loop conformation that is more extended to the solvent.

The "near" badan has moved to a new position after binding to cefotaxime to avoid the steric clash between itself and the aminothiozale ring of cefotaxime. It is 3.5 Å away from its original position and is close to the position of the "far" badan (Figure 4.11 (b)). The Ω-loop also adopts a new conformation after the binding of cefotaxime. However, the electron density map in some regions of the Ω-loop are disordered.

Figure 4.13 (a) demonstrates the surface docking groove showing the interface between the badan molecule and PenP_E166Cb with cefotaxime. The badan remains lodged in the surface groove surrounded by the residues Asn104, Asn132 and Glu168 as observed in the apo structure. However, since the position of Glu168 is changed, the original position of Glu168 is now replaced by the methoxyimini group of cefotaxime. The positions of Asn104 and Asn132 are not changed. There is a change in the polarity of the local environment of badan upon binding with cefotaxime. The surface accessible area (SAA) of badan after binding of cefotaxime is about 157 $Å^2$, which is calculated by the AreaIMol in the CCP4Interface 1.4.4 program.

The structure of PenP_E166Cb in complex with cefuroxime was also resolved for further confirmation of the binding mode of antibiotic. The structure in complex with cefuroxime was obtained at the resolution of 1.8 Å. The binding mode will be discussed in Section 4.3.8. In Figure 4.13 (b), cefuroxime is clearly

visible in the $2f_o$-f_c map. Like cefotaxime, it can be observed that there is a linkage between the Oγ atom of Ser70 and the C8 of the β-lactam ring in cefuroxime, suggesting that cefuroxime is covalently bound to the active site residue Ser70. The Ω-loop is shown in dash line because of the poor electron density obtained.

(a)

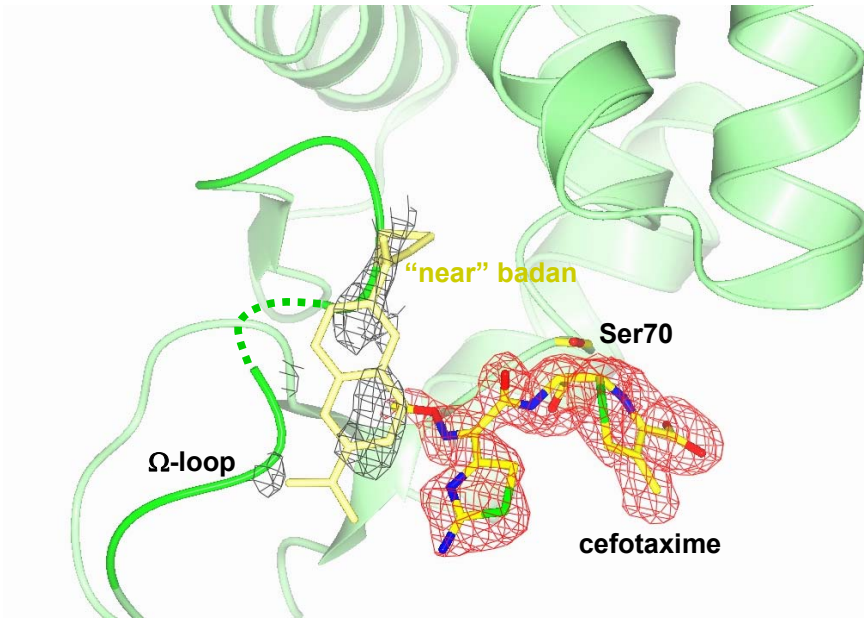

(b)

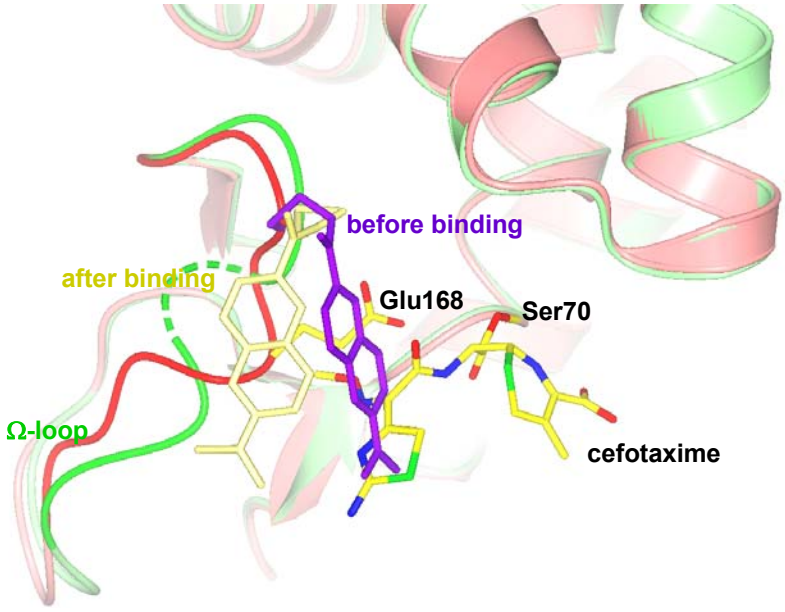

Figure 4.11: (a) The f_o-f_c omit map of the "near" badan contoured at 1.5 σ and that of cefotaxime contoured at 2 σ in PenP_E166Cb-cefotaxime complex structure. The green dash line represents disordering of Glu168 and Leu169 because of the poor electron density obtained in this region. Ser70, cefotaxime and badan are displayed in cpk stick model. (b) The "near" badan molecule before and after binding with cefotaxime. Badan before binding is shown in purple while after binding is shown in yellow. The Ω-loop before and after binding is shown in red and green, respectively.

(a)

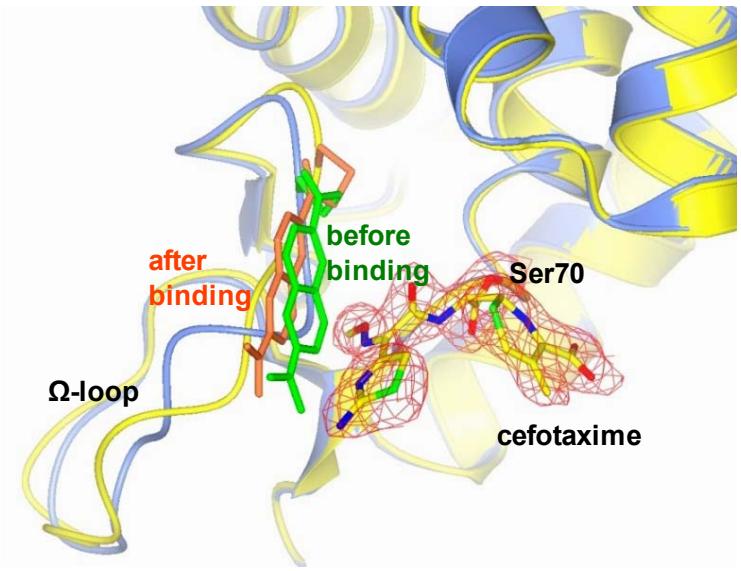

(b)

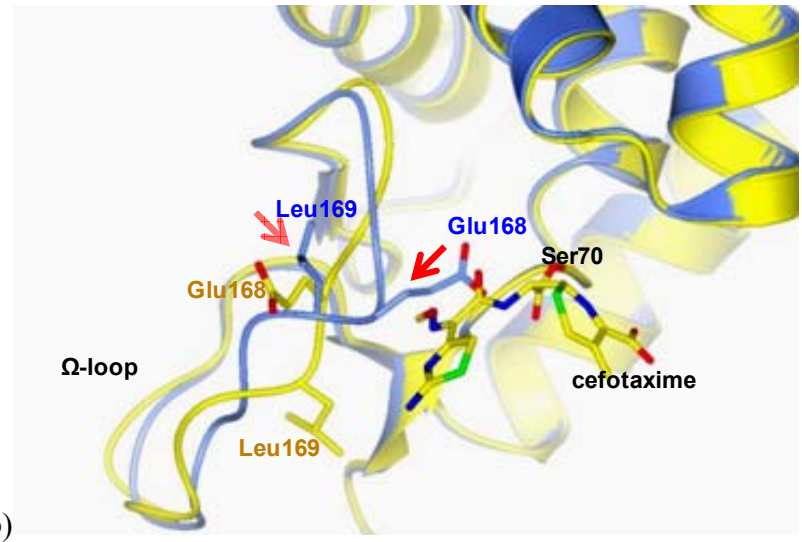

Figure 4.12: (a) The f_o-f_c omit map of cefotaxime in PenP_E166Cb-cefotaxime complex structure and the "far" badan molecule before and after binding with cefotaxime. The map is contoured at 1.0 σ. Ser70 and cefotaxime are displayed in cpk stick model. Badan before binding is shown in green while after binding is shown in orange. (b) The induced conformational change of the Ω-loop upon acylation of cefotaxime. The Ω-loop before and after binding was shown in blue and yellow, respectively. Residues Glu168 and Leu169 are shown in cpk stick model. The main chain carbon is shown in the same color with the corresponding Ω-loop. Badan fluorophore was omitted for clarity of the figure. The arrows indicate the induced conformational change of certain residues.

(a)

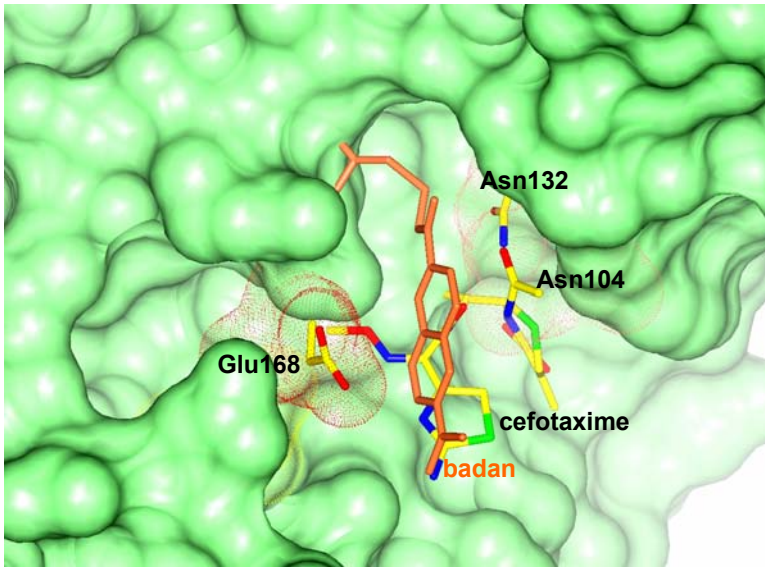

(b)

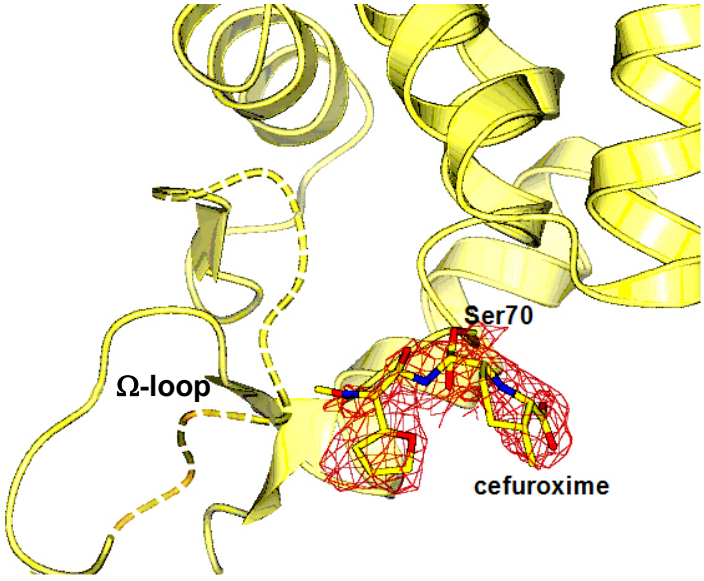

Figure 4.13: (a) Surface docking groove showing the interface between the badan molecule and PenP_E166Cb with cefotaxime, which is shown in green. Badan and four residues located within 4.5 Å from badan are shown in cpk stick model and labeled. The surface profile of the four residues is presented as mesh model and colored according to their polarity (Yellow: hydrophobic; Red: acidic; Pink: polar). The Leu169 is buried inside the protein so that it can not be shown in the figure. (b) The $2f_o–f_c$ map of cefuroxime contoured at 1 σ. The Ω-loop is shown in dash line because of the poor electron density. Cefuroxime and Ser70 are displayed in cpk stick model.

4.3.6 Crystal structures of PenP_E166Cb in complex with 7-ACA, cefoxitin and cephaloridine

All the three antibiotics (7-ACA, cefoxitin and cephaloridine) were transferred to the crystal by soaking method. The X-ray data collection and structure refinement statistics for PenP_E166Cb in complex with 7-ACA, cephaloridine and cefoxitin is shown in Table 4.2. The structure of the PenP_E166Cb in complex with 7-ACA was obtained at a resolution of 1.9 Å. Figures 4.14 (a) shows the electron density map of badan and 7-ACA in PenP_E166Cb-7-ACA complex structure. The badan and 7-ACA are very clear on the f_o-f_c omit map. From the connectivity of the electron density between the 7-ACA and Ser70, it can be confirmed that the Oγ atom of Ser70 and the C8 of the β-lactam ring in 7-ACA are linked together. Only the "far" badan is shown because both of the "far" and "near" badans have almost no change in position upon binding of 7-ACA. Figure 4.14 (b) shows the "far" badan molecule before and after binding of 7-ACA. It can be seen that the position of badan is unchanged in terms of the distance to the Ser70. Not only does the badan molecule not show any change in its position, but neither does Glu168.

The structure of PenP_E166Cb in complex with cefoxitin was obtained at a resolution of 2 Å. The electron density map of the cefoxitin in PenP_E166Cb-cefoxitin complex structure is displayed in Figure 4.15. Like the previous antibiotics that have been described, the Oγ atom of Ser70 and the C8 of the β-lactam ring in cefoxitin are linked. Nearly the whole Ω-loop is not resolved because of the broken electron density obtained between Glu163 and Gly175. Therefore, the badan and the key residues for restructuring of Ω-loop are

absent in this structure.

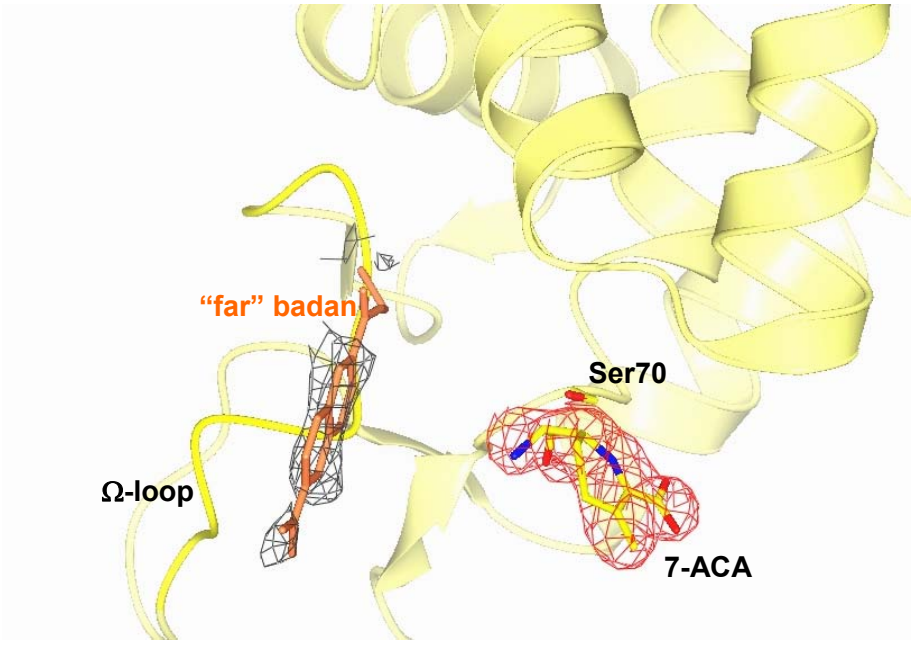

(a)

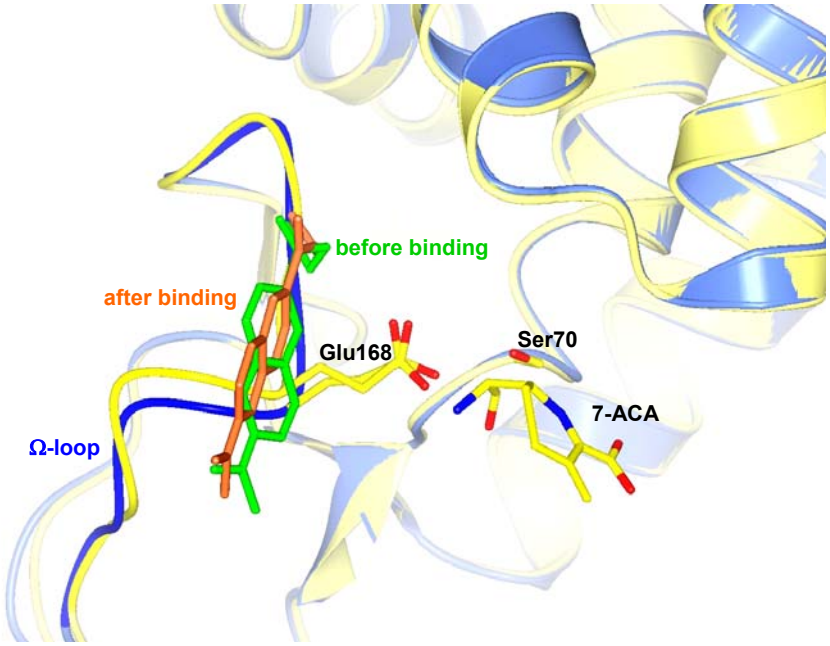

(b)

Figure 4.14: (a) The f_o-f_c omit map of the "far" badan and 7-ACA in PenP_E166Cb-7-ACA complex structure. The map is contoured at 2.0 σ. Ser70, 7-ACA and badan are displayed in cpk stick model. (b) The "far" badan molecule before and after binding with 7-ACA. Badan before binding is shown in green and after binding is shown in orange. The Ω-loop before and after binding is shown in blue and yellow, respectively. Residue Glu168 is shown in stick model.

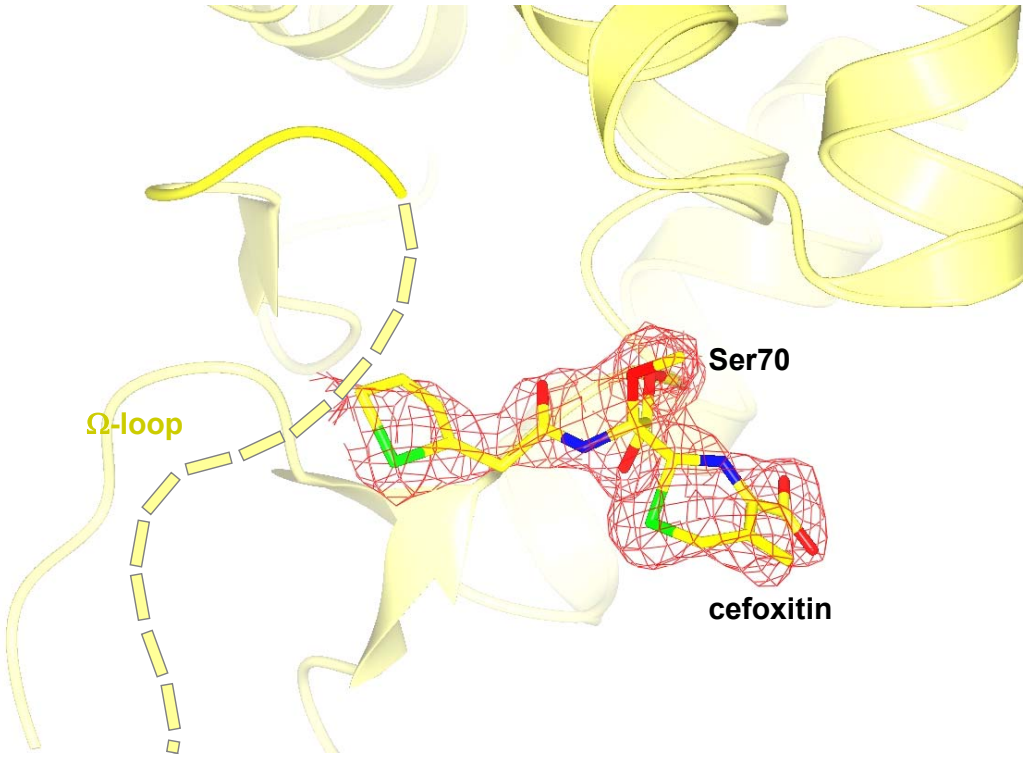

Figure 4.15: The $2f_o$-f_c electron density map of the cefoxitin in PenP_E166Cb-cefoxitin complex structure. The map is contoured at 1 σ. The yellow dashed line represents residues 163-175 because of the poor electron density obtained in this region. Ser70, cefoxitin and badan are displayed in cpk stick model.

The complex structure of PenP_E166Cb with cephaloridine was obtained at a resolution of 1.8 Å. The crystallographic data and refinement statistics are shown in Table 4.2. The f_o-f_c omit map of the cephaloridine in the complex structure is displayed in Figure 4.16 (a). It is clearly shown that the Oγ atom of Ser70 and the C8 of the β-lactam ring in cephaloridine are linked, with the C3 leaving group lost.

In this structure, it is without doubt that the Glu168 does not have a steric clash with the side chain of cephaloridine so that Glu168 remains at a similar position as before binding. Both the "near" and "far" badans are invisible in this structure and residues from Leu169 to Val174 are missing because of the discontinuous electron density obtained in this region. The badan is roughly "modeled" in Figure 4.16 (a) using the "far" badan in the free structure of PenP_E166Cb. The solvent accessible area of badan at the "far" position in this model is about 180 $Å^2$. The SAA is only changed a little when compared to the structure of PenP_E166Cb.

Figure 4.16 (b) is the superimposition of PenP_E166Cb and the PC1 β-lactamase in the presence of cephaloridine (PDB ID: 1GHM). PC1 is the only class A β-lactamase with the crystal structure resolved after binding with cephaloridine. The conformations of residues 103 – 105 of PenP_E166Cb and PC1 are slightly different. Residue 104 in PenP_E166Cb is asparagine while that in PC1 is alanine. One extra H-bond, which is formed between the side chain of Asn104 and the acylamide of cephaloridine, is observed in PenP_E166Cb-cephaloridine complex structure (Schneider *et al.*; Chen and Herzberg 2001).

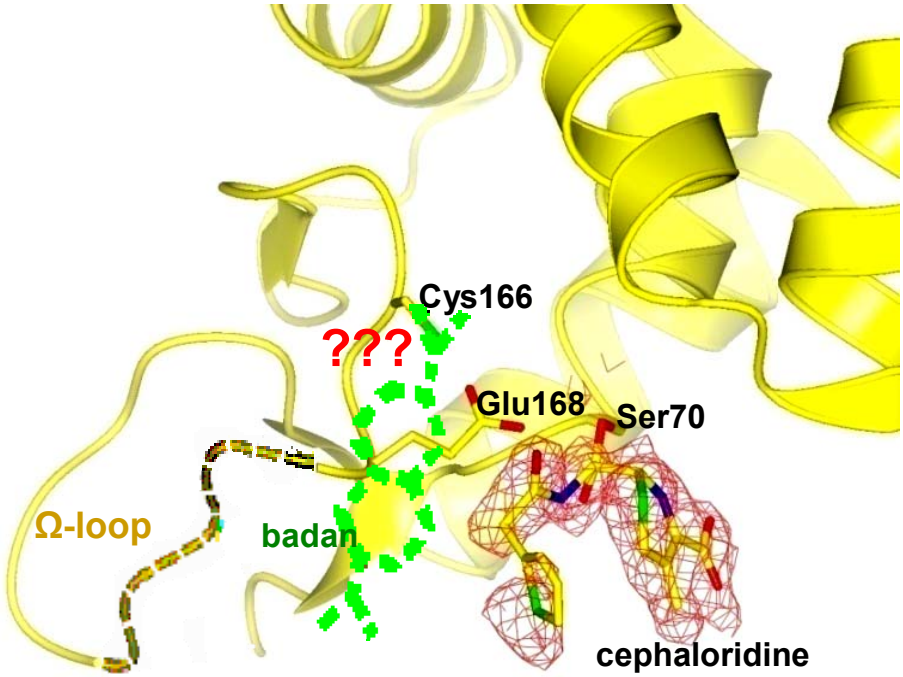

(a)

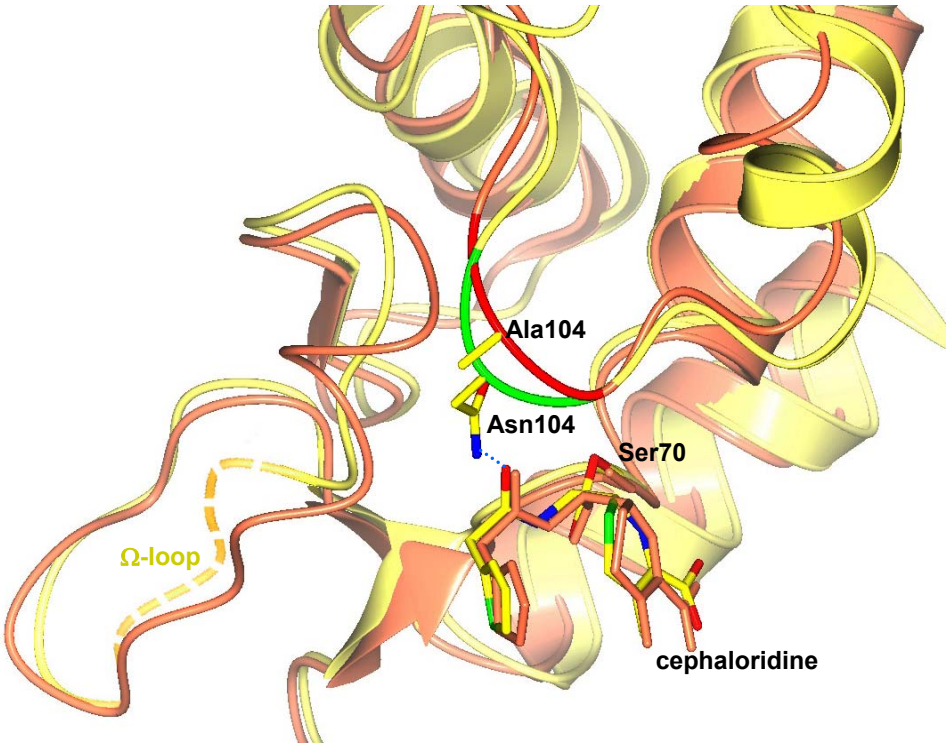

(b)

Figure 4.16: (a) The f_o–f_c omit map of cephaloridine in PenP_E166Cb-cephaloridine complex structure. The map is contoured at 1 σ. The "far" badan is invisible and the main body of the protein is displayed in yellow. Cephaloridine, Ser70, Glu166 and Glu168 are displayed in cpk. The yellow dot line represents residues Leu169 to Val174 after binding because of the

poor electron density obtained in this region. (b) Overlaid structures of PenP_E166Cb (lemon) and PC1 (coral) with cephaloridine. Residues 103 – 105 of PenP_E166Cb and PC1 are shown in green and red, respectively. Residues 70, 104 and cephaloridine are displayed in cpk cylinder model. The blue dot line represents the H-bond between side chains of N104 and the acylamide of cephaloridine.

Table 4.2. X-ray data collection and structure refinement statistics for PenP_E166Cb in complex with 7-ACA, cephaloridine and cefoxitin

	E166Cb+ 7-ACA	E166Cb+ cephaloridine	E166Cb+ cefoxitin
Soaking condition			
Soaking solution	0.01M 7-ACA in 25% (w/v) PEG 4k, 0.1M Hepes pH 7.2	0.01M cephaloridine in 25% (w/v) PEG 4k, 0.1M Hepes pH 7.2	0.01M cefoxitin in 25% (w/v) PEG 4k, 0.1M Hepes pH 7.2
Soaking duration	15 min	20 min	20 min
Data collection			
Space group	$P2_1$	$P2_1$	$P2_1$
Unit cell parameters (Å)			
a	43.23	43.33	43.19
b	91.93	91.73	91.64
c	66.04	66.11	66.06
Resolution range (Å)	45.96-1.90 (1.96-1.90)	64.06-1.79 (1.86-1.79)	45.82-1.99 (2.06-1.99)
No. of total reflections	150973	165897	154553
No. of unique reflections	38935	46065	33336
I/σ	25.3 (9.9)	19.9 (5.2)	17.6 (5.5)
Completeness (%)	98.2 (94.8)	97.8 (89.5)	98.0 (93.4)
R_{merge} (%)	3.3 (7.5)	3.7 (15.6)	5.1 (11.6)
Structure refinement			
Resolution (Å)	38.1-1.9	64.2-1.8	39.9-2.0
R_{cryst}/R_{free} (%)	19.6/23.6	21.9/26.5	20.0/24.3
r.s.m.d. bonds (Å)/angles (°)	0.012/1.631	0.011/1.699	0.012/1.567
No. of reflections			
Working set	36830	43511	31438
Test set	1949	2334	1690
No. of atoms			
Protein atoms	4411	4389	4281
Water molecules	87	364	270
Average *B*-factor (Å^2)			
Main chain	16.388	23.518	20.576
Side chain	18.623	25.468	23.205

4.3.7 Comparison of crystal structures of PenP_E166C and PenP_E166Cb

Crystals of PenP_E166C were grown at similar crystallization conditions as PenP_E166Cb. The two structures are superimposed so that the conformational change of the Ω-loop and other parts of the protein can be investigated. In general, the structure of PenP_E166Cb is identical to that of PenP_E166C. The RMSDs of all atoms on chain A and chain B between the two structures are 1.17 Å and 1.30 Å, respectively. The RMSDs of the main chain atoms on chain A and chain B are 0.93 Å and 0.95 Å, respectively. Close inspection of the differences in the two structures reveals that the conformations of the Ω-loops are very different from each other. The new configuration of Ω-loop in PenP_E166Cb structure is displayed in Figure 4.17. It can be seen that besides the Ω-loop, other parts of the protein can be overlaid very well, including some catalytic important residues, Ser70, Lys73, Ser130 and Lys234. All these residues are next to the active site and are important to both the acylation and deacylation of the enzyme (Jacob *et al.* 1990; Lenfant *et al.* 1991; Lietz *et al.* 2000; Thomas *et al.* 2005).

(a)

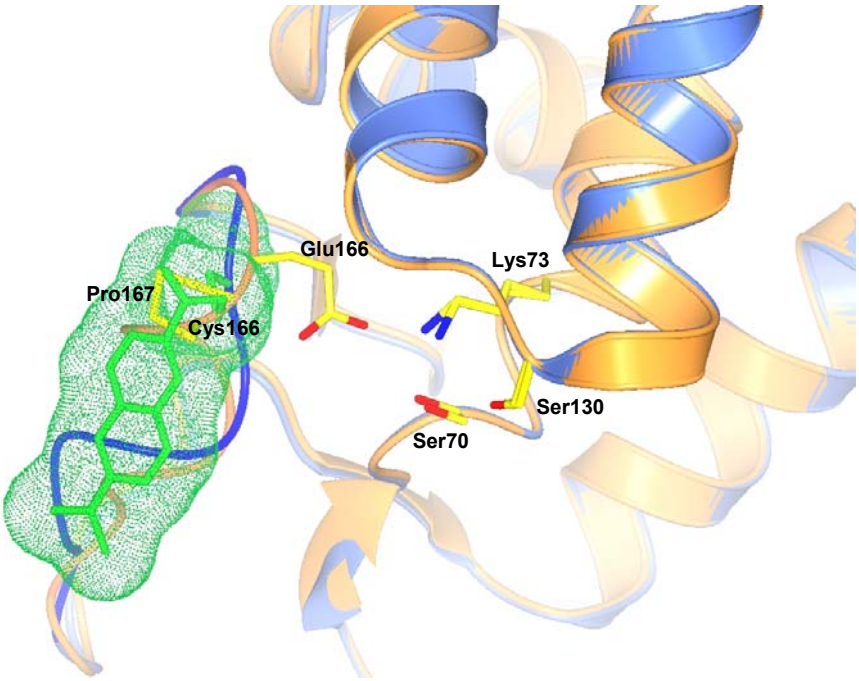

(b)

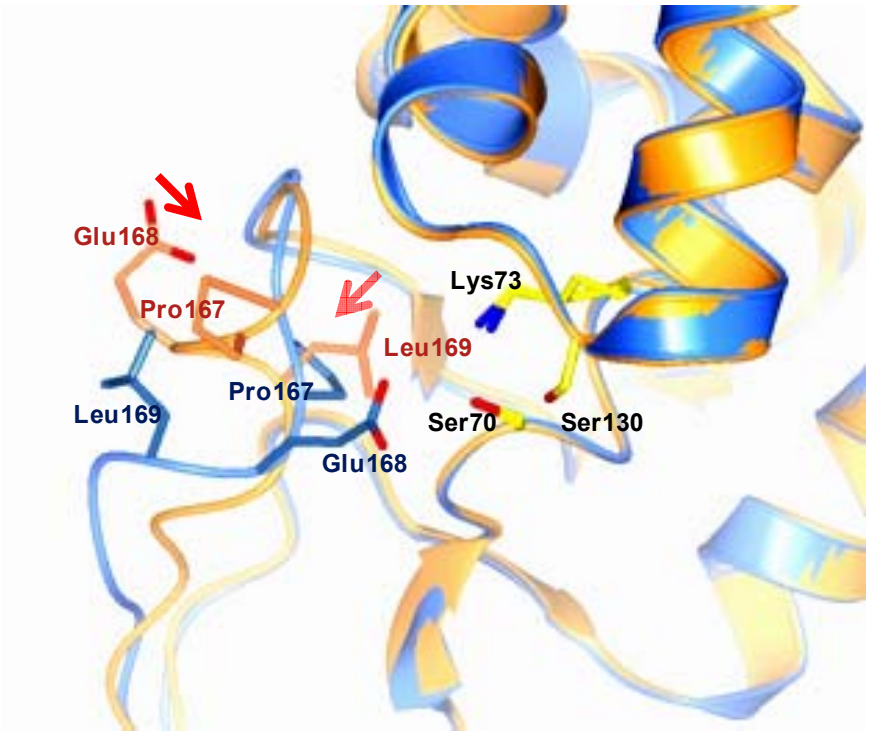

Figure 4.17: New configuration of Ω-loop in PenP_E166Cb structure. (a) The location of badan fluorophore and the residue E166Cb in PenP_E166Cb. Structures of PenP_E166Cb and PenP_E166C are shown in blue and orange, respectively. Residues on Ω-loop (Glu166 and Pro167) and key catalytic residues

for acylation (Lys73, Ser70 and Ser130) are displayed in cpk colour scheme. Badan fluorophore is presented as both stick model and surface-profile model. (b) Residues on Ω-loop (Pro167, Glu168 and Leu169) and key catalytic residues for acylation (Lys73, Ser70 and Ser130) are displayed in cpk color scheme. Badan fluorophore was not shown for clarity of the figure. The arrows indicate the induced conformational change of certain residues.

Figure 4.17 (b) is the superimposition of the structures of PenP_E166C (orange) and PenP_E166Cb (blue). It can be seen that the Ω-loop adapts a new conformation, where the helix is unwound and becomes an extended loop. The loop looks like rotating for about 30°, while the Cys166, Pro167, Glu168 and Leu169 are all being shifted to new positions. Because of the conjugation of a bulky badan molecule on Cys166, the residue 166 has moved for about 30° to become more solvent assessable to avoid steric clashes. The new position of Cys166 overlaps with the original position of Pro167 in the PenP_E166C structure, while the Cα atom of Pro167 has moved for about 5 Å from the solvent exposing position to the protein interior, which is occupied by Leu169 in the wild-type structure (Figure 4.17 (b)). The Cα atom of Glu168 has shifted down for about 4 Å. Its side chain was originally exposed to the solvent but now is pointing to the active site. It is just about 2 Å next to the Asn170 in the PenP_E166C structure. The new position of Leu169 is more solvent exposed than the original position. Asn170 is now much further away from the active site and it occupies the same position of Arg164 in PenP_E166C structure. Moreover, the electron density for residues Asn170 to Pro174 is disordered. The average B-factor for residues Asn170 to Pro174 in PenP_E166Cb is higher than that in PenP_E166C (63.5 VS 25.7 in chain A). Residues from Gly175 to Asp179 are

remained the same and are not affected by the conjugation of the fluorophore. It is noteworthy that the hydrogen bonding between Arg164 and Asp179 in PenP_E166C is lost in the PenP_E166Cb structure, while the side chain of Arg164 is totally disordered in this structure.

4.3.8 Comparison of cefotaxime binding modes for PenP_E166Cb and other β-lactamases

From the structures of PenP_E166Cb-cefotaxime complex, Toho1-cefotaxime complex (PDB code: 1IYO), and the GC1-cefotaxime complex (PDB code: 1RGZ), the cefotaxime binding modes can be compared. Figure 4.18 shows the superimposition of the three structures involved. It can be observed that the binding mode of cefotaxime in PenP_E166Cb is similar to that in GC1 and Toho-1. The C8 atom on the β-lactam ring of cefotaxime is covalently linked to the Oγ atom of Ser70 while the COO^- group on C4 of cefotaxime, which is on the R1 side group, forms extensive hydrogen bonds with the protein residues proximal to the antibiotic. However, the orientation of the oxyimino moiety in Toho-1 is different from that in both GC1 and PenP_E166Cb (Crichlow *et al.* 1999; Shimamura *et al.* 2002). The methoxyimino side chain in Toho-1 is pointing away from the active site but those in GC1 and PenP_E166Cb are pointing into the active site, and share the same position with the Glu168 in the free structure. In the structure of PenP_E166Cb-cefuroxime (Figure 4.13 (b)), it can be seen that the binding mode of cefuroxime is the same as cefotaxime, with the oxyimino group inserted into the protein interior of PenP_E166Cb.

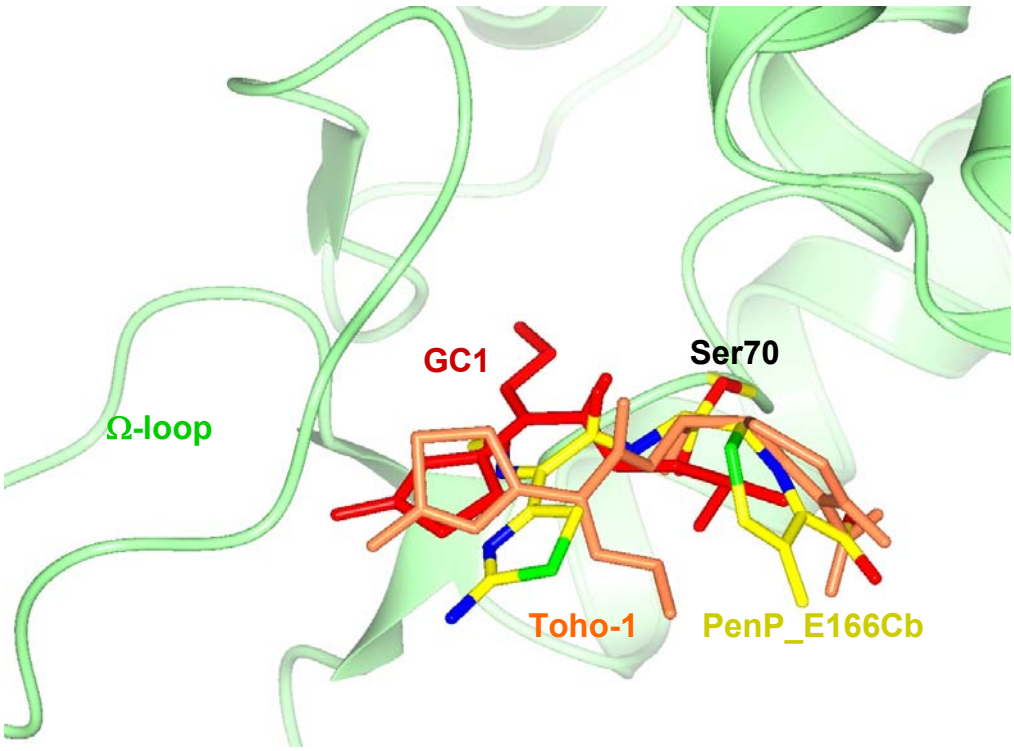

Figure 4.18: Comparison of cefotaxime binding modes in PenP_E166Cb (cpk color) with those in Toho-1 (coral) and GC1 (red). Ser70 is also displayed in cpk color.

4.4 Discussion

4.4.1 Crystal structure of PenP_E166Cb

It is surprising to note that the locations of badan, which were named “near” and “far”, in the two molecules of PenP_E166Cb are different. It is inferred that the badan is tethered to the cysteine residue and swayed at certain angles. The “near” badan is prevented from adopting the “far” orientation because of the proximity of a molecule from the neighboring symmetry-related unit cell, a restriction that does not apply to the "far" badan. Apparently, the badan molecules do not have specific interactions with the surrounding protein atoms.

The difference of the solvent accessible areas of the two badans calculated by the CCP4 program (Potterton *et al.* 2003) are due to the different orientations, while the “far” badan is further away from the antibiotic binding site and is more exposed to the solvent so that it has a higher SAA value (~200 $Å^2$). If the total surface area of badan molecule is about 400 $Å^2$, 200 $Å^2$ means that about half of the badan is buried by protein atoms of PenP_E166Cb. The badans are considered as largely polar since they are situated in a surface groove formed by residues 167-170 of Ω-loop that contain charged side chain and residues 132, 103-104 on the other side of the protein that contain the polar side chains. Also, five water molecules are found near to the badan molecules. The B-factors calculated for the badan molecules imply that the two badan molecules are highly thermodynamic when compare to other amino acids. This further supports that badan is changing its orientation between the “near” and “far”

locations. Badan in chain A has a lower B-factor than that in chain B, which also suggests that the location of the "near" badan is restrained by the neighbouring molecule of the symmetry-related unit cell while the "far" badan is freer to movement.

Our finding on the two positions of fluorophore is similar to the MDCC labeled *Escherichia coli* phosphate binding protein, as the crystal structure shows that there are two diastereoisomers with different orientations are present in the crystal, which also suggests that the fluorophore is more mobile than the bulk of the protein (Hirshberg *et al.* 1998). However, the finding of the fluorophore-labeled structure is not very common in the literature and it suggests that the highly dynamic nature of the fluorophore that conjugated to a protein through a cysteine residue maybe very useful in sensing the change in the local environment upon binding of a ligand in proximity to the fluorophore.

4.4.2 Crystal structures of PenP_E166Cb in complex with cefotaxime and cefuroxime

In the fluorescence result of different cephalosporins, it can be observed that the PenP_E166Cb detected the cephalosporins selectively, while only oxyimino-cephalosporins can generate a significant fluorescence change. The structural study of PenP_E166Cb in complex with both oxyimino- and non-oxyimino- cephalosporins suggests that the selective fluorescence response may be attributed to the changing locations of the badan molecule and/or of the surrounding protein residues that determine the local environment of badan.

It is supposed that the binding of cefotaxime to the active site of PenP_E166Cb will affect the "near" and "far" badan molecules differently. Since the "far" badan is further away from the active site than the "near" badan is, the binding of cefotaxime would not cause a big movement of the "far" badan. The SAA of the "far" badan was changed from ~200 $Å^2$ to ~160 $Å^2$. However, the SAA of the "near" badan was roughly increased from ~120 $Å^2$ to ~160 $Å^2$ since it has adopted the "far" position upon addition of cefotaxime. Because of the close proximity of the "near" badan, the "near" badan would be "kicked" away from the active site by the incoming cefotaxime that contains a large side chain to avoid the steric clash. Also, the spatial displacement of the "near" badan did not change the local polarity of the environment. In this case, the SAA of the "far" and "near" badans were counterbalanced. Therefore the change in fluorescence signal upon addition of cefotaxime should not be due to the change in position of the badan molecule solely.

On top of that, the methoxyimino moiety of the cefotaxime had a big impact on the configuration of the Ω-loop. Since it was pointing to the interior of the protein body, it would have a steric clash with the Glu168 in PenP_E166Cb. The clash gave rise to the movement of the Glu168 from its original position to a fully solvent exposed position. Not only did the Glu168 move, the residues next to this region also had reconfigurations, for example Leu169 and Asn170. Since the Glu168 became further away from the protein interior and the badan molecule, the electrostatic effect of Glu168 exerted on the local environment was reduced. The side chain of Glu168 was fully solvent exposed and led to a decrease in the polarity of the local environment of badan. Therefore the change in the Ω-loop configuration was the main reason for the change in solvent accessible area calculated by the CCP4 program since the surrounding environment of the badan molecule was different upon addition of cefotaxime. Details on the change in the Ω-loop configuration will be discussed in Section 4.4.4.

Similarly, cefuroxime has a very close structure with cefotaxime as it also belongs to oxyimino-cephlosporins that contains the methoxyimino moiety (Ayad *et al.* 1999; Mouz *et al.* 1999; Romano *et al.* 2000). So the binding of oxyimino-cephlosporins would also induce a change of Ω-loop configuration and hence a change in fluorescence signals.

4.4.3 Crystal structures of PenP_E166Cb in complex with 7-ACA, cefoxitin and cephaloridine

It has been shown that the fluorescence changes were apparently smaller upon addition of non-oxyimino cephalosporins like 7-ACA, cefoxitin and cephaloridine. All these cephalosporins are lack of the bulky methoxyimino moiety. The small change in the fluorescence signal was not because of the lack of acylation of the antibiotics since the MS results and the crystal structures show that the antibiotic was bound to the active site of PenP_E166Cb. Hydrogen bonds between the carboxylate groups of these cephalosporins with the protein residues were still present. It is suggested that the lack of the methoxyimino moiety was the main factor for the observed fluorescence results.

In the structure of PenP_E166Cb-cephaloridine complex, the configuration of the Ω-loop in PenP_E166Cb did not change as the one in PenP_E166Cb-cefotaxime complex structure. It retained the same configuration with the free PenP_E166Cb. Therefore, Glu168, the key residue in determining the fluorescence signal changes in the cefotaxime-complexed structure, was not displaced by the incoming cephaloridine. It is because cephaloridine does not have the branched oxyimino moiety that exerts special clash with Glu168. Although the two badans in the PenP_E166Cb-cephaloridine complex structure were invisible, it can be imagined that the badan would not move significantly as in the cefotaxime case. The superimposition of the PenP_E166Cb-cephaloridine complex structure and the PenP_E166Cb free structure shows that the “far” badan would not be affected by the acylation of cephaloridine since it was further away from the binding site while the “near” badan would be spacially displaced

by the cephaloridine. Similar to the case in cefotaxime, the “near” badan may be displaced to a new position that resembles to the “far” position. Therefore the movement of the two badan molecules would be counterbalanced and it was not sufficient to cause the change in fluorescence intensity. The lack of electron density obtained for badan and also some of the residues in Ω-loop suggests that the badan and the disappearing part of the Ω-loop were highly dynamic upon binding of cephaloridine. Since the position of the key residue Glu168 did not change, it can be deduced that the overall change of the polarity in the surrounding environment was very small, which gave rise to the insignificant changes in the fluorescence signal.

The Ω-loop of the PenP_E166Cb-7-ACA complex structure was highly similar to the free PenP_E166Cb. Also, the positions of the badan before and after binding with 7-ACA were very close to each other too. It is suggested that the small size of 7-ACA did not exert a change in the local environment of the badan molecule. In the structure of PenP_E166Cb-cefoxitin complex, the Ω-loop was totally disordered, which suggests that the Ω-loop became highly dynamic upon addition of cefoxitin. Since cefoxitin has a similar structure with cephaloridine, same biosensing theory could be applied to the case in cefoxitin: the insignificant changes in the positions of badan after binding and in the polarity of the local environment caused the negligible changes in the fluorescence signal.

4.4.4 Comparison of crystal structures of PenP_E166C and PenP_E166Cb

From the calculated RMSD value of all atoms between the free PenP_E166Cb and the unlabeled PenP_E166C, it can be concluded that the conjugation of badan to Cys166 would not have large effects on the conformation of the protein folding. This result was in agreement with the circular dichroism results obtained before. However, the Ω-loop region shows the most significant structural differences as described in the "results" section, especially in the N-terminal part (residues 165-171). From the electron density data obtained in this region, it is certain that the Ω-loop adapted a new conformation. This maybe due to the highly dynamic nature of the Ω-loop after the conjugation of a dynamic fluorophore. The result of the average B-factor calculated by the CCP4 program shows that the Ω-loop region was more flexible in the presence of badan than the PenP_E166C one. In addition, the poor electron density obtained in the Ω-loop region also supports the finding about the high flexibility of the Ω-loop. Besides the structural finding for the Ω-loop, the kinetic study on the binding of cefotaxime also shows that the Ω-loop in PenP_E166Cb is much more flexible than that in PenP_E166C.

After linking a bulky badan molecule to Cys166, the residue 166 could not stay at the original position and so it moved to a more solvent accessible position to avoid steric clashes with other residues in the crowded area. The cis peptide bond between Glu166 and Pro167 in the wild-type enzyme is important in the folding and locking of Ω-loop into a tightly packed position (Vanhove *et al.* 1996). However, in the PenP_E166Cb structure, this cis peptide bond was replaced by a trans peptide bond so that the flexibility of the Ω-loop was

increased when compared to the wild-type PenP.

It has been reported that Asn170 contributes to the rate of deacylation of the antibiotic in class A β-lactamases since a replacement of Asn170 by leucine would disrupt the deacylation reaction by displacing the hydrolytic water molecule (Lewis *et al.* 1997) and the mutant N170Q would also impair the deacylation by blocking access to the water molecule (Zawadzke *et al.* 1996). In the structure of PenP_E166Cb, Asn170 moved to a position that was further away from the active site. Therefore it should be deduced that the deacylation in PenP_E166Cb would be altered because of the absence of the Asn170. However, the deacylation rate of PenP_E166Cb was highly similar to that of PenP_E166C (Figure 4.19), which means that the role of Asn170 maybe replaced by other amino acids around that region. From the crystal structure of PenP_E166Cb, Glu168 has roughly overlapped with the original position of Asn170 in the PenP_E166C. Both the carbonyl group of Asn170 in PenP_E166C and the carboxylic group of Glu168 in PenP_E166Cb were at a hydrogen bond distance with the catalytic water molecule. The presence of Glu168 may counterbalance the disappeared role of Asn170 for holding the water molecule. In the PC1 β-lactamase, it has been reported that the double mutant E166Q/N170D would help to restore the deacylation that was impaired by the removal of catalytically important Glu166 (Chen and Herzberg 1999). Aspartate has a similar side chain group with glutamate so that glutamate may also help to restore the deacylation.

Since Asn170 in PenP_E166Cb occupied the same position with Arg164 in the PenP_E166C structure, the native hydrogen bond formed between Arg164 and Asp179 was disrupted because the side chain of Arg164 in PenP_E166Cb

was largely disordered. The lost of this hydrogen bond, which is a structural integrity in the Ω-loop, led to the increased flexibility of the Ω-loop by decreasing the stability of the Ω-loop (Vakulenko *et al.* 1999; Kurokawa *et al.* 2003). It was found that site-directed mutagenesis of Arg164 and Asp179 disrupted the hydrogen bond and increased the binding affinity of the enzyme for some originally poor substrates with large side chains. This resembles to our study that a more flexible Ω-loop in PenP_E166Cb can relieve the steric clashes with the incoming antibiotics with large side chain like cefotaxime because the Ω-loop was not tightly packed onto the protein body, thus increasing the binding rate.

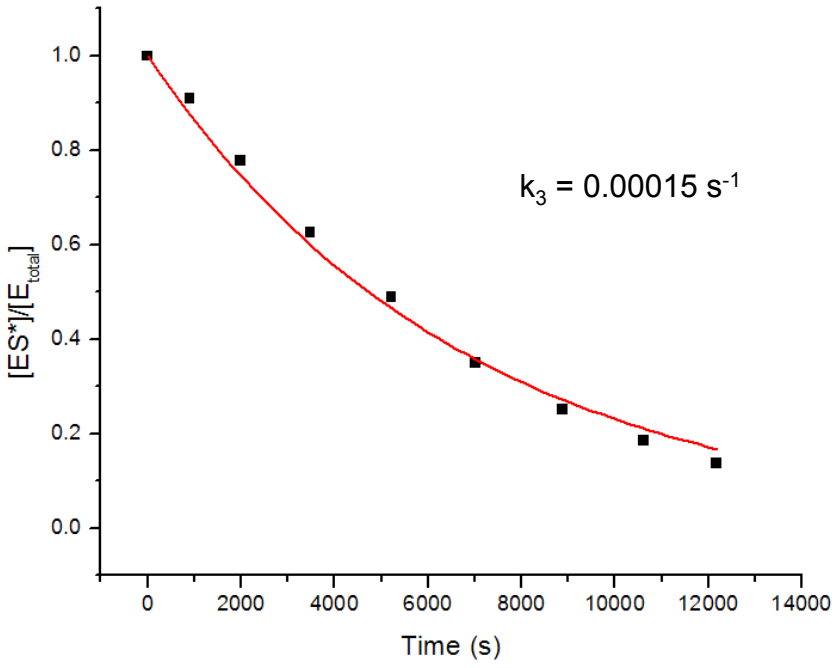

(a)

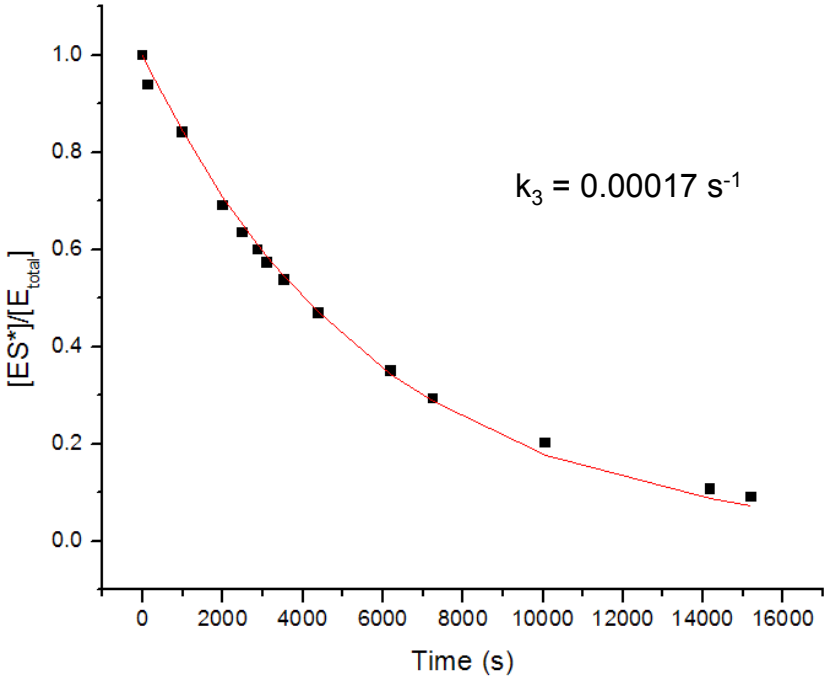

(b)

Figure 4.19: Time course for the deacylation of 2.5 μM (a) PenP_E166C and (b) PenP_E166Cb, in the presence of 5 μM cefotaxime by ESI-MS. The solid lines represent the fit of the experimental data to the equation $[ES^*]/[E_{total}]=\exp-(k_3t)$, from which the k_3 values were determined (Chan *et al.* 2008). Buffer: 20 mM ammonium acetate (pH 7.0).

4.4.5 Comparison of cefotaxime binding modes for PenP_E166Cb and other β-lactamases

The overlapping structures of PenP_E166Cb-cefotaxime complex, Toho1-cefotaxime complex and the GC1-cefotaxime complex show that the binding mode of cefotaxime can be different on different class A β-lactamases. The binding modes of the six-membered ring of the cefotaxime in the three structures were highly similar to each other in terms of the orientation. The differences in the orientations of the methoxyimino side chain described in Section 4.3.8 might be due to the high flexibility of the Ω-loop in PenP_E166Cb.

The binding mode in the PenP_E166Cb-cefotaxime complex structure resembled that in the class C extended-spectrum β-lactamase GC1, with the bulky oxyimino group of cefotaxime pointing to the active site (Schneider *et al.*; Nukaga *et al.* 2004). This new binding mode has never been reported for any class A β-lactamases because it is supposed that the bulky oxyimino moiety would experience a steric hindrance induced by the Ω-loop nearby. In Toho-1, the methoxyimino side chain is pointing away from the active site and hence the steric hindrance is reduced (Shimamura *et al.* 2002; Ibuka *et al.* 2003). However, in the extended-spectrum β-lactamase GC1, a mutated Ω-loop adopts an alternative conformation that allows the side chain to be more buried inside and leading to higher efficiency in inactivating third-generation cephalosporins.

Similarly, in PenP_E166Cb, the increase in flexibility of the Ω-loop would likely explain its reconfiguration upon binding of the oxyimino-cephalosporins as well as the novel binding mode unforeseen in class

A β-lactamases. Its resemblance to the extended spectrum class C β-lactamases in terms of binding mode may suggest new insight into antibiotic resistance, antibiotic binding and drug discovery.

4.5 Concluding remarks

The crystal structures of the apo PenP_E166Cb, the PenP_E166Cb complexed with two oxyimino-cephalosporins including cefotaxime and cefuroxime, and the PenP_E166Cb complexed with three non-oxyimino-cephalosporins including 7-ACA, cephaloridine and cefoxitin were determined. Two positions, “near” and “far”, of badan were found in the apo PenP_E166Cb structure. The badan attached to the 166 position was described to be highly dynamic and it adopted multiple conformations near the active site.

It is found that PenP_E166Cb could detect cephalosporins selectively. Our data supports that the significant fluorescence change upon adding oxyimino-cephalosporins was not due to the spacial displacement of the badan molecule by the incoming antibiotic but due to the change in the configuration of the key residues on Ω-loop in proximity to the badan molecule that causes a change in the polarity of the local environment, for example Glu168. Non-oxyimino-cephalosporins do not have the branched methoxyimino moiety to displace the key residues so that there was no or weak fluorescence changes.

The comparison of PenP_E166C and the badan labeled PenP_E166Cb shows that the conjugation of a badan molecule to the cysteine residue caused a change in the conformation of the Ω-loop. The Ω-loop became more flexible and more susceptible to the binding of cephalosporins with large side chain. The binding of cefotaxime to PenP_E166Cb was about 10 times faster than the unlabeled PenP_E166C.

The structural study of this biosensor not only provides a good model for how the biosensing mechanism is carried out upon binding of substrates in proximity to the conjugated fluorophore, but also be a good example that the conjugation of a fluorophore increases the flexibility of Ω-loop that may broaden the antibiotic binding spectrum of the biosensor. The data can povide some insights on the rational design of a fluorophore-based biosensor.

Chapter 5: Improvement of the badan-labeled biosensor by site-directed mutagenesis

5.1 Introduction

From the crystal structure of PenP_E166Cb, it has been shown that several amino acids are in proximity to the badan molecule and also the active site. Site-directed mutagenesis can be performed to investigate the effect of those residues on the surrounding environment of badan and it is expected that this will cause a change in the fluorescence signal.

Site-directed mutagenesis was performed by the QuikChange® Site-Directed Mutagenesis Kit from Stratagene. This kit offers fast and simple method and no specialized vectors are needed in the process. A pair of synthetic oligonucleotide primers (5'→3' forward primer and 3'→5' reverse primer) that contains the desired mutation was used to anneal to the supercoiled double-stranded DNA (dsDNA) vector with target site for mutation. After the thermal cycling performed by the provided DNA polymerase, the oligosynthetic primers are extended to opposite directions and mutated plasmids are generated in nicked circular strands. The nicks can be repaired by transformation of the mutated dsDNA into supercompetent *E. coli* cells. The methylated, nonmutated parental DNA template is digested with DpnI. After transformation, miniprep can be done to purify the desired plasmid and the DNA sequence of the plasmid can be checked to confirm site-directed mutagenesis. The overview of the method is shown in Figure 5.1.

In this project, it was found that Asn104, Glu168 and Leu169 were the closest residues to the badan molecule (see Chapter 4). These residues are located within 5 Å to the badan molecule. The naphthalene plane of the badan molecule is situated between the two surfaces of the protein body of PenP_E166Cb and lodged in the surface groove surrounded by Asn104, Glu168 and Leu169. Glu168 amd Leu169 are situated on one side of badan, whereas Asn104 is situated on another side. Glu168 is a conserved residue in many class A β-lactamases. But it was found that Glu168 does not involve in deacylation as Glu166 since the conversion of Glu168 to Asp168 gave fully active enzyme (Madgwick and Waley 1987). Asn 104 was found to form unique interaction with acylamide side chain of cephalosporins and it is a conserved residue in CTX-M-type ESBLs (Shimamura *et al.* 2002). It was thought to be involved in binding β-lactam substrates (Knox 1995). The lack of Asn104 may cause a lower oxyimino-cephalosporinase activity. On the other hand, it was found that residue 169 on the Ω-loop is important in influencing substrates (Ma *et al.* 2005). Substitution of Leu169 to arginine in SHV-57 β-lactamase is important for substrate specificity and causes ceftazidime resistance.

An amino acid with a hydrophobicity opposite to that of the wild-type but with similar side chain lengths was chosen. For example, the polar Asn104 was changed to the hydrophobic Leu104 because we expected the more hydrophobic environment would lead to an increase in the fluorescence signal. The Glu168 was changed to Asn168 and Leu168 to investigate the effect of the removal of electrostatic effect exerted by Glu168. In contrast, the hydrophobic Leu169 was changed to the charged Asn169 and Asp169 (Monera *et al.* 1995) to see whether

the fluorescence signal would decrease when the overall environment was electrostatic. It is aimed to construct a potent and sensitive biosensor with a broad scanning spectrum. Various mutants were studied and the biosensing mechanisms were discussed.

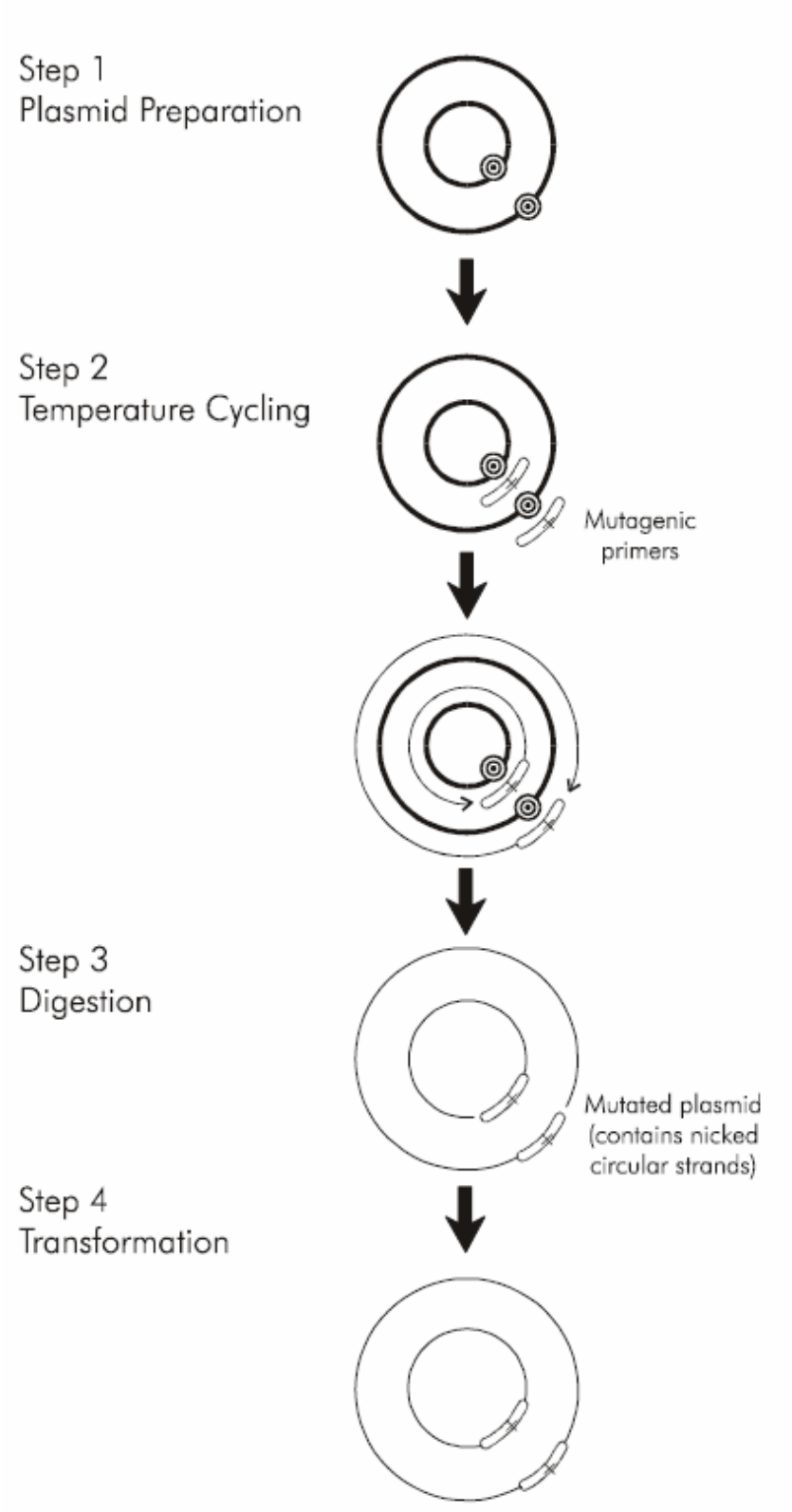

Figure 5.1: Overview of the QuikChange® site-directed mutagenesis method (QuikChange® Site-Directed Mutagenesis Kit instruction manual, p.4, Stratagene).

5.2 Methods

5.2.1 Site-directed mutagenesis of 6xHis_TEV_PenP_E166C

In order to do site-directed mutagenesis, the iProof™ High-Fidelity PCR Kit was used. All single mutagenesis were done by using the plasmid pRset-K-6xHis_TEV_PenP_E166C as template. The mutagenesis of 6xHis_TEV_PenP_E166C/L169N/N104L was done by using the plasmid pRset-K-6xHis_TEV_PenP_E166C/N104L as template. The sequences for the mutants involved are shown in Appendix I. The primers used for different mutants and the components for the PCR reactions are listed in Tables 5.1 (a) and (b), respectively. PCR reaction conditions are shown in Table 5.2.

Table 5.1: (a) Primers for site-directed mutagenesis of PenP_E166Cb (b) Components for PCR reactions.

(a)

Mutant	Primers	Sequence	T_m (℃)
E168N	E168Nf	CCCGAACGATTCTGCCCAAACTTAAATGAAGTGAATCCG	83
	E168Nr	CGGATTCACTTCATTTAAGTTTGGGCAGAATCGTTCGGG	83
E168L	E168Lf	GAACGATTCTGCCCACTGTTAAATGAAGTGAAT	77
	E168Lr	ATTCACTTCATTTAACAGTGGGCAGAATCGTTC	77
L169N	L169Nf	CGATTCTGCCCAGAGAACAATGAAGTGAATCCG	81
	L169Nr	CGGATTCACTTCATTGTTCTCTGGGCAGAATCG	81
L169D	L169Df	CGATTCTGCCCAGAGGATAATGAAGTGAATCCG	81
	L169Dr	CGGATTCACTTCATTATCCTCTGGGCAGAATCG	81
N104L	N104Lf	CGTGATGATCTTGTACTGTACAACCCGATTACG	80
	N104Lr	CGTAATCGGGTTGTACAGTACAAGATCATCACG	80
L169N/N104L	L169Nf	CGATTCTGCCCAGAGAACAATGAAGTGAATCCG	81
	L169Nr	CGGATTCACTTCATTGTTCTCTGGGCAGAATCG	81

(b)

5X iProof HF reaction buffer	10 µl
DNA template (100 ng/µl)	1 µl
Forward primer (0.1 µg/µl)	1 µl
Reverse primer (0.1 µg/µl)	1 µl
dNTPs (10 mM)	1 µl
ddH_2O	35 µl
iProof HF polymerase (2 U/µl)	1 µl
Total volume	50 µl

Table 5.2: PCR reaction conditions for site-directed mutagenesis

Segment	Cycles	Temperature (℃)	Time
1	1	98	1 min
2	20	98	10 s
		55	30 s
		72	30 s/kb of plasmid length
3	1	4	Infinity

After the PCR reactions, 1 μl of the DpnI restriction enzyme (10 U/μl) was added directly to each amplification reaction. The reaction mixtures were incubated at 37℃ for overnight to digest the parental (i.e. nonmutated) supercoiled dsDNA. After the DpnI digestions, 5 μl of the DpnI-treated DNAs were transformed into TOP10 competent cell (F- *mcr*A △(*mrr-hsd*RMS-*mcr*BC) φ80*lac*Z△M15 △*lac*X74 *rec*A1 *ara*D139 △(*araleu*) 7697 *gal*U *gal*K *rps*L (StrR) *end*A1 *nup*G, Invitrogen) following the method stated in Section 2.2.3 and several colonies were picked for sequence checking. 2 μl of the plasmids with correct sequences were transformed into *E. coli* BL21 (DE3) for expression of proteins.

For 6xHis_TEV_PenP_E166C/L169N/N104L, the signal peptide encoding sequence in the vector was removed by introducing a NdeI restriction site before the TEV site by PCR method and cloning the segment TEV_PenP_E166C/L169N/N104L (with NdeI site) into the pRSET-K vector (with 6xHis). Therefore in 6xHis_TEV_PenP_E166C/L169N/N104L, methionine (DNA sequence: ATG) was added between the 6xHis-tag and the TEV cleavage site. The primers used and the PCR reaction are shown in Table 5.3. pRAT-R bound to the T7 terminator's 3' flanking region.

Table 5.3: (a) Primers used and (b) PCR reaction conditions for cloning of 6xHis_TEV_PenP_E166C/L169N/N104L.

(a)

Primers	Sequence	T_m (℃)
6xHis(NdeI)TEV	GAGATATACATATGCATCACCCATCACCATCATGAGAACCTGTATTTC	83
pRAT-R	GCTTAATGCGCCGCTACAGG	57

(b)

Segment	Cycles	Temperature (℃)	Time
1	1	98	30 s
2	25	98	10 s
		68	30 s
		72	30 s
3	1	72	5 min
4	1	4	Infinity

After PCR reaction, the PCR product was subjected to DNA gel electrophoresis and the gel with the identified band (~1,000 bp) was sliced with a razor under UV illumination. The sliced agarose gel was purified by the illustra GFX PCR DNA and Gel Band Purification Kit from GE Healthcare. It was used for the isolation and concentration of DNA fragments from PCR mixtures, DNA-containing agarose gel bands or restriction digestions. Firstly, the sample was added with capture buffer to denature protein and dissolve agarose gel. The capture buffer-sample mix was added to the illustra GFX MicroSpin column so that the DNA bound to the column membrane. Afterwards, washing buffer was added to the column to remove salt or other contaminants from the membrane-bound DNA. After washing, nuclease-free water was used to elute the purified DNA from the column. The basic steps involved in this kit are shown in

Figure 5.2. The sample was eluted with 50 µl nuclease-free water and it was double digested with NdeI and HindIII (NEB) as shown in Table 5.4.

Table 5.4: Reaction components for restriction digestion of PenP encoding gene.

10X NEBuffer 2	5 µl
PenP segment	43 µl
NdeI (20,000 units/ml)	1 µl
HindIII (20,000 units/ml)	1 µl
Total	50 µl

The DNA concentration of the sample was measured by absorbance at 280 nm. The ligation of the PenP gene to the vector pRset-K was performed by T4 DNA ligase (Invitrogen) and set as shown in Table 5.5.

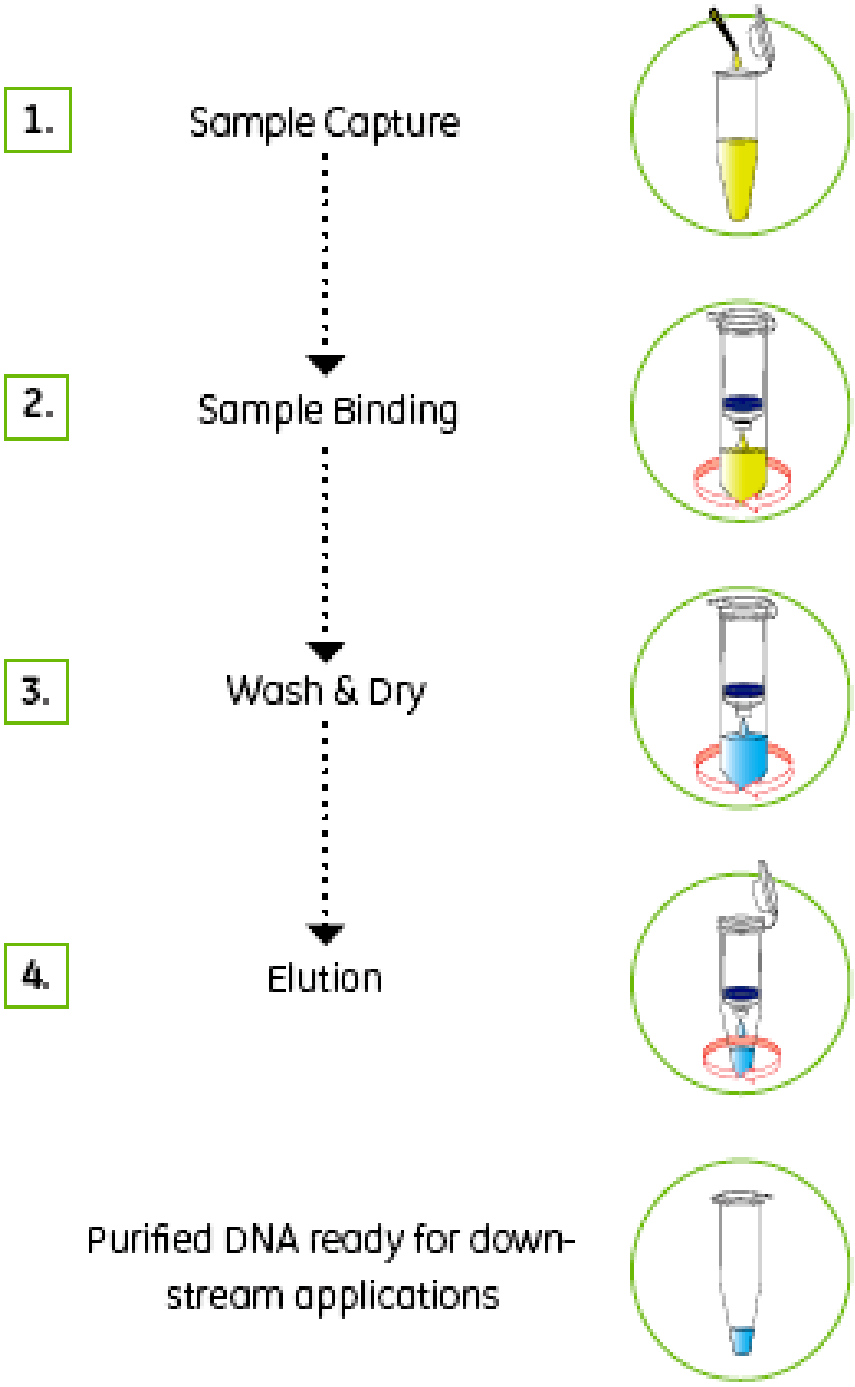

Figure 5.2: The basic steps in the illustra GFX PCR DNA and Gel Band Purification Kit (illustra GFX PCR DNA and Gel Band Purification Kit, product booklet, p. 12, GE Healthcare).

Table 5.5: Ligation reaction of PenP gene and pRset-K.

5X DNA Ligase Reaction buffer	4 μl
PenP segment	0.3 μl
pRSET-K (from Leung's group)	1 μl
T4 DNA Ligase (5 U/μl)	1 μl
DDI water	13.7 μl
Total	20 μl

The ligation was incubated at room temperature for 2 h. After ligation, 3 μl of the plasmid was transformed into TOP10 competent cell following the method stated in Section 2.2.3 and 7 colonies were picked for checking of ligation. Sterilized toothstick was used to pick part of the colony to 10 μl of sterilized water (*). The sample was incubated at 94℃ for 5 min for lysing cell before the PCR reaction. Same primers were used for the PCR reaction and the reaction is shown in Table 5.6. Taq DNA polymerase from Bioneer was used.

Table 5.6: PCR reaction components for verification of the ligation reaction.

5X iProof HF reaction buffer	10 μl
DNA sample*	10 μl
6xHis(NdeI)TEV (0.1 μg/μl)	1 μl
pRAT-R (0.1 μg/μl)	1 μl
dNTPs (10 mM)	1 μl
ddH_2O	25 μl
Taq DNA polymerase (5 U/μl)	1 μl
Total volume	50 μl

Table 5.7: PCR reaction conditions for verification of the ligation reaction.

Segment	Cycles	Temperature (℃)	Time
1	1	94	30 s
2	25	94	30 s
		50	30 s
		72	50 s
3	1	72	1 s
4	1	4	Infinity

All the seven samples were subjected to DNA gel electrophoresis and the bands were identified under UV illumination. If the PCR is successful with the two designed primers, the ligation is successful. The corresponding colony was transformed into *E. coli* BL21 (DE3) for expression of protein. The plasmid map for 6xHis_TEV_PenP_E166C/L169N/N104L is shown in Appendix II.

5.2.2 Preparation and purification of the mutants

The preparation and purification of the mutants were performed as follows: A small amount of bacterial glycerol stock of *E. coli* BL21 (DE3) containing the desired pRset-K plasmid was inoculated into 5 ml TB medium (4.5 ml of TB medium, 0.5 ml of phosphate solution) with 50 μg/ml Kanamycin in an universal bottle. The seed culture was grown at 37℃, 280 rpm for overnight but less than 16 h. 0.2 ml of the overnight culture was added to 10 ml of TB Bloth (9 ml of TB medium, 1 ml of phosphate solution) with 50 μg/ml kanamycin in a universal bottle. The culture medium was incubated at 37℃, 280 rpm until A_{600} reached 0.8-1.0. Then filtered IPTG (isopropylthiogalactoside) with final concentration of 200 μM was added and the culture solutions were incubated at 30℃ with shaking at 280 rpm for overnight again. On the next day, the culture was centrifuged using a desktop centrifuge at 4℃, 10,000 rpm for 10 min. The supernatant was collected and filtered through 0.45 μm filter and then purified by spin column.

The spin column was filled with immobilized Ni^{2+} chelating resin (HiTrap Chelating Sepharose Fast Flow, GE Healthcare). The column was first added with 0.5 ml of DDI water and spun at 3,000 rpm for 15 s under 4℃ by microcentrifuge. 0.1 M nickel (II) sulphate was added subsequently and DDI water was used to wash away the excess nickel ions. The column was equilibrated with starting buffer (0.5 M NaCl, 0.02 M sodium phosphate, pH 7.4) by adding the starting buffer to the column and spinning for three times. Once the column was prepared, the protein sample was added to the column and continuous spinning was performed until all the sample has been loaded to the

column. Theoretically 1 ml of the gel can bind 10 mg of protein. After the sample had been loaded onto the column, starting buffer was added three times in order to wash away the unbound proteins. Then, 10% of elution buffer (0.5 M NaCl, 0.02 M sodium phosphate, 0.5 M imidazole, pH 7.4) was added to the column to remove non-specific proteins. Afterwards, 100% of elution buffer was used to elute the protein with at least two consecutive spinning. Regeneration buffer (0.05 M EDTA, 0.02 M sodium phosphate, pH 7.4) was used to wash away the nickel and regenerate the column. The eluted protein sample was subjected to buffer exchange with 20 mM ammonium acetate (pH 7.0) by ultra-filtration and stored at -20℃ for future use.

5.2.3 Labeling of β-lactamase mutants

The methods for labeling of the mutants are the same as those for labeling 6xHis_TEV_PenP_E166C by badan, as described in Section 3.2.5. Each mutant protein (3 mg) was used for labeling.

5.2.4 Determination of molecular masses of the mutants

The determination of molecular mass, purity and labeling efficiency of the mutants were done by ESI-MS, following the procedures described in section 2.8.1 and 2.8.2. The calculated molecular mass of 6xHis_TEV_PenP_E166C/E168L, 6xHis_TEV_PenP_E166C/E168N, 6xHis_TEV_PenP_E166C/L169D, 6xHis_TEV_PenP_E166C/L169N, 6xHis_TEV_PenP_E166C/N104L, 6xHis_TEV_PenP_E166C/L169N/N104L are 31,209 Da, 31,210 Da, 31,227 Da, 31,226 Da, 31,224 Da, 31,357 Da, respectively. The calculated molecular mass of labelled mutant, namely 6xHis_TEV_PenP_E166Cb/E168L, 6xHis_TEV_PenP_E166Cb/E168N, 6xHis_TEV_PenP_E166Cb/L169D, 6xHis_TEV_PenP_E166Cb/L169N, 6xHis_TEV_PenP_E166Cb/N104L, 6xHis_TEV_PenP_E166Cb/ L169N/ N104L are 31,421 Da, 31,422 Da, 31,439 Da, 31,438 Da, 31,436 Da, 31,569 Da, respectively. The calculated molecular masses were calculated using the ProtParam application on ExPASy Proteomics (http://au.expasy.org/tools/protparam.html).

5.2.5 Fluorescence scanning experiment with addition of various β-lactams

Different kinds of β-lactam antibiotics were used for the fluorescence scanning measurement for all the mutants, including 7-ACA, cefotaxime, ceftazidime, cephalothin, ceftriaxone, cefoxitin, cefuroxime and cephaloridine. The concentrations used for all antibiotics were 10^{-4} M, in order to get a saturated fluorescence signal. In PenP_E166Cb, the fluorescence signals were always saturated at a concentration of 10^{-4} M. This indicates an excess of substrate was used. The details of the measurement are described in Section 2.7.1.

5.3 Results

5.3.1 Determination of molecular mass values of the labeled mutants

The molecular mass values of all the mutants and the labeled mutants are shown in the de-convoluted ESI mass spectra (Figures 5.3 - 5.8). All the mutants were successfully expressed and purified with correct molecular mass. The de-convoluted mass spectra show that the proteins have high purity. It demonstrates that a badan molecule (212 Da) was successfully labeled on each protein and the labeling efficiencies were all approx. 100%. In each spectrum, there are some peaks with comparable intensities next to the original peak. They may be the salt adducts that are usually observed between protein and small molecules derived from buffer or impurities such as Na^+ and K^+ during electrospray ionization (Tolic *et al.* 1998; Vedadi *et al.* 2006). However, the identity of the adducts produced is often unknown (Tolic *et al.* 1998). The theoretical and calculated molecular mass values of the PenP_E166C mutants and the PenP_E166Cb mutants are shown in Table 5.8.

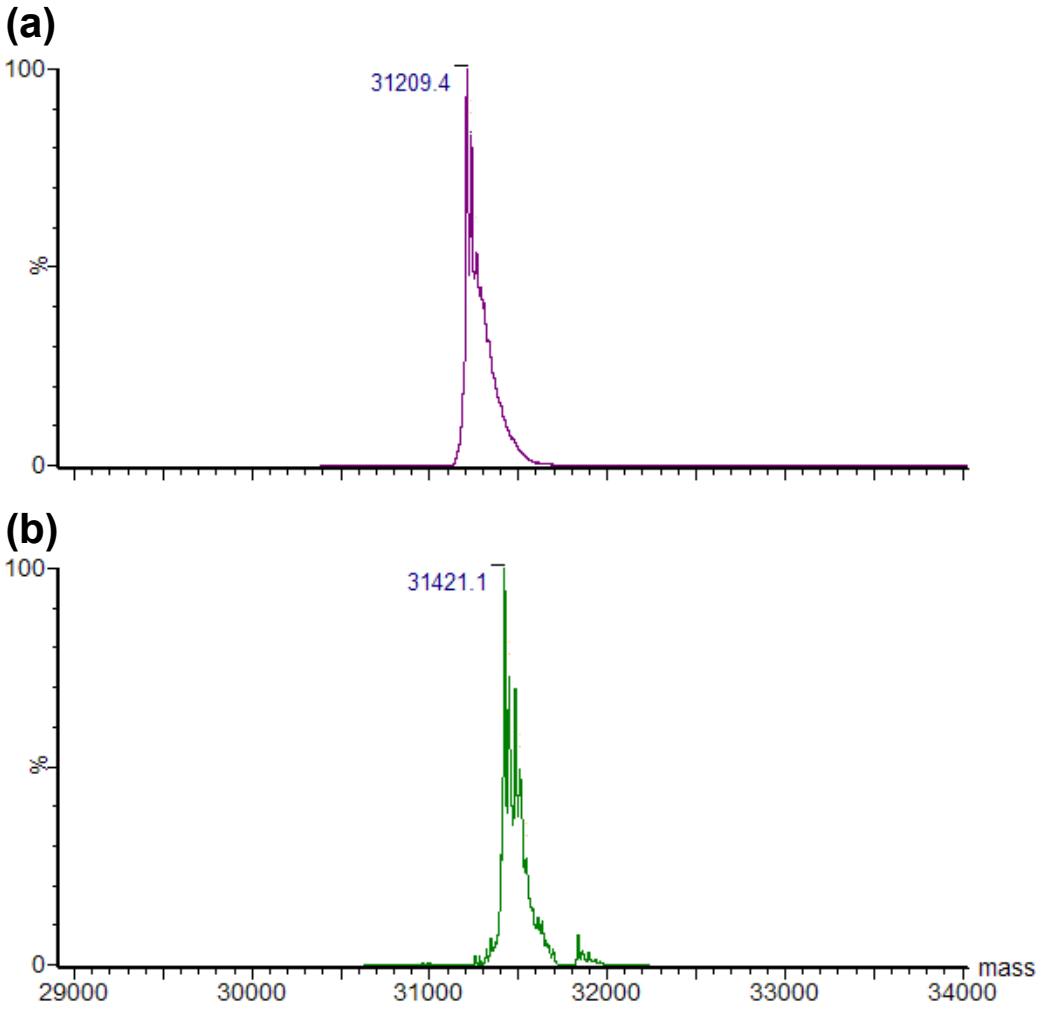

Figure 5.3: De-convoluted ESI mass spectra of (a) 6xHis_TEV_PenP_E166C/E168L, (b) 6xHis_TEV_PenP_E166Cb/E168L.

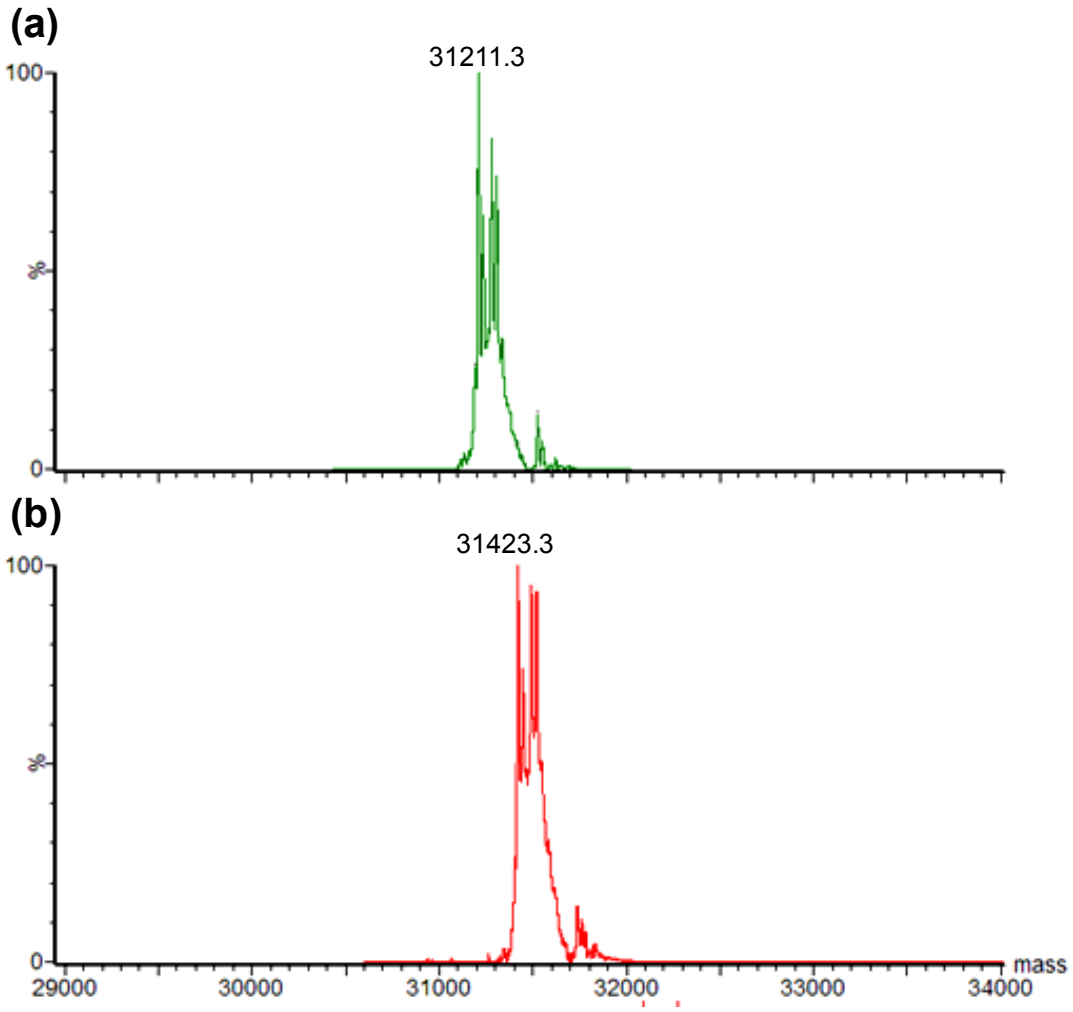

Figure 5.4: De-convoluted ESI mass spectra of (a) 6xHis_TEV_PenP_E166C/E168N, (b) 6xHis_TEV_PenP_E166Cb/E168N.

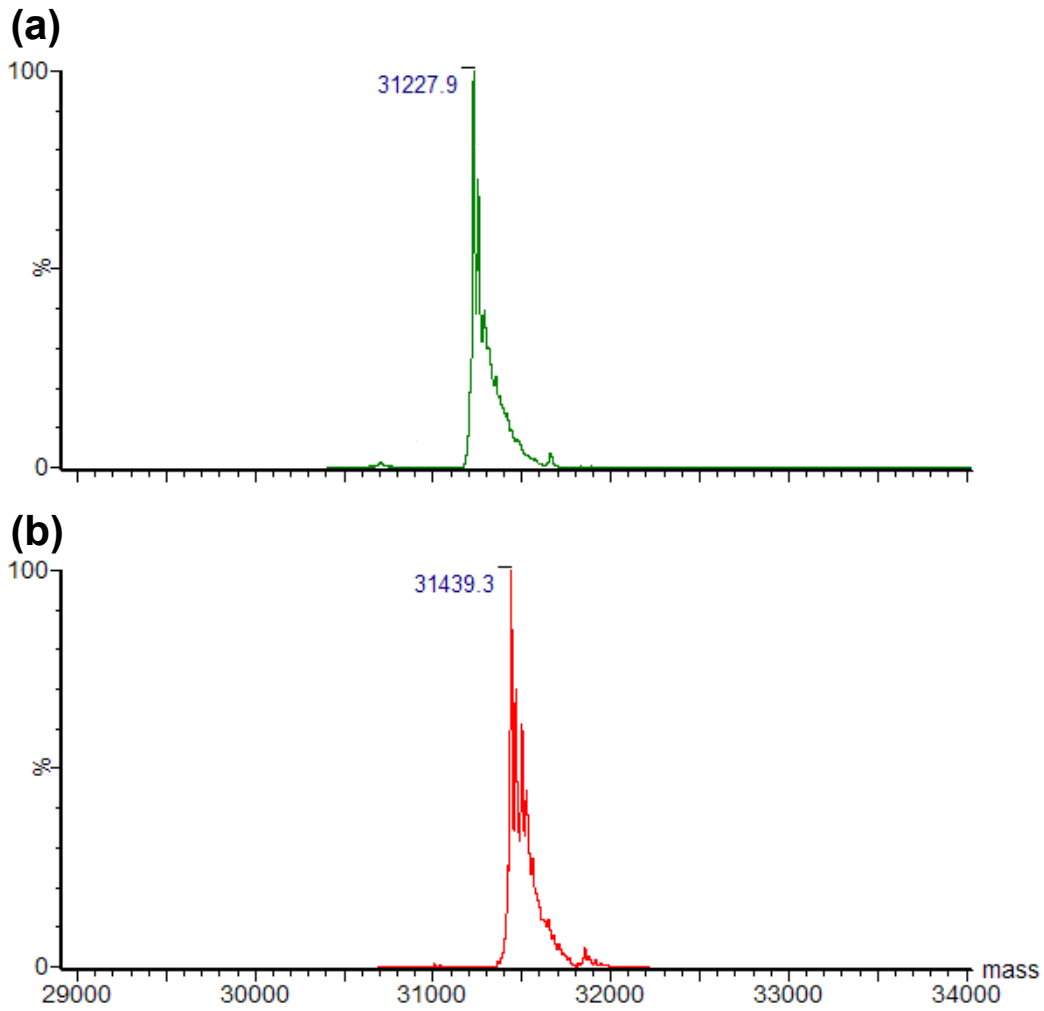

Figure 5.5: De-convoluted ESI mass spectra of (a) 6xHis_TEV_PenP_E166C/ L169D, (b) 6xHis_TEV_PenP_E166Cb/L169D.

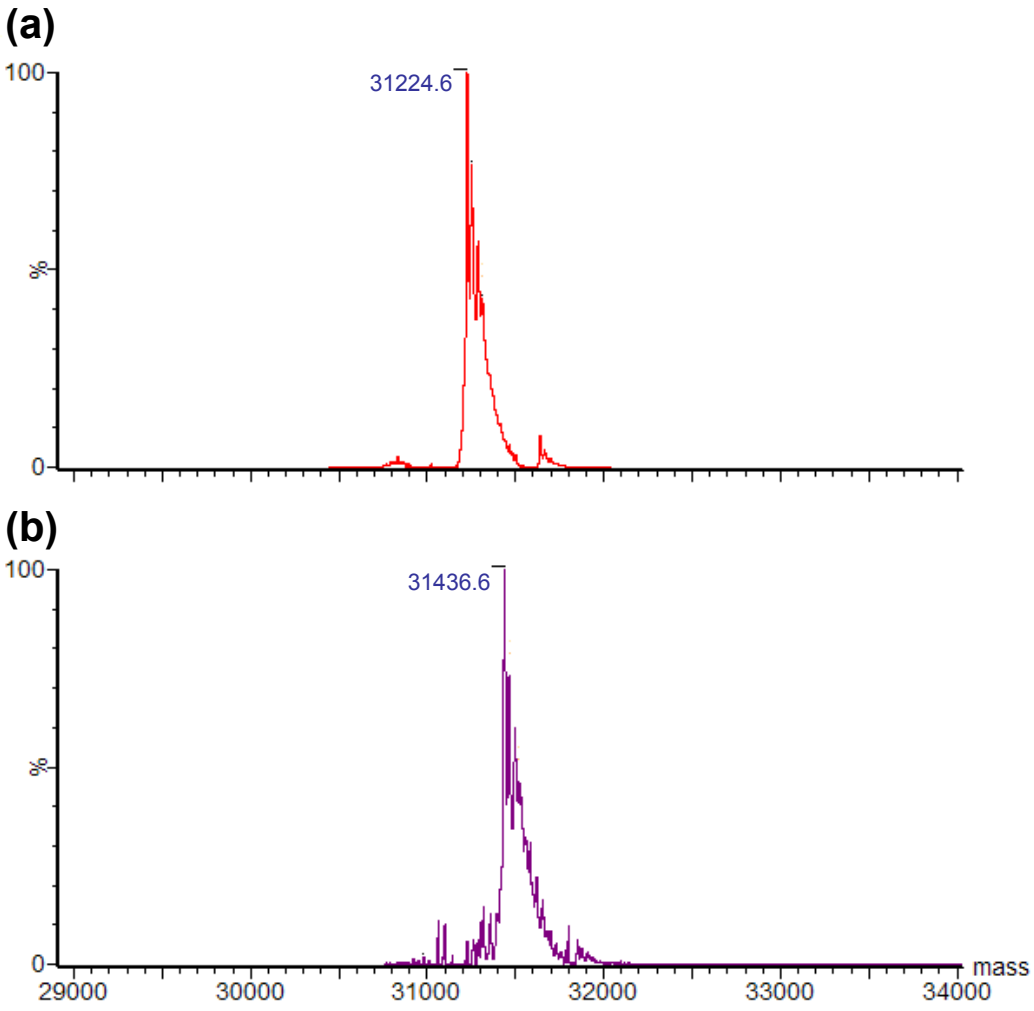

Figure 5.6: De-convoluted ESI mass spectra of (a) 6xHis_TEV_PenP_E166C/ L169N, (b) 6xHis_TEV_PenP_E166Cb/L169N.

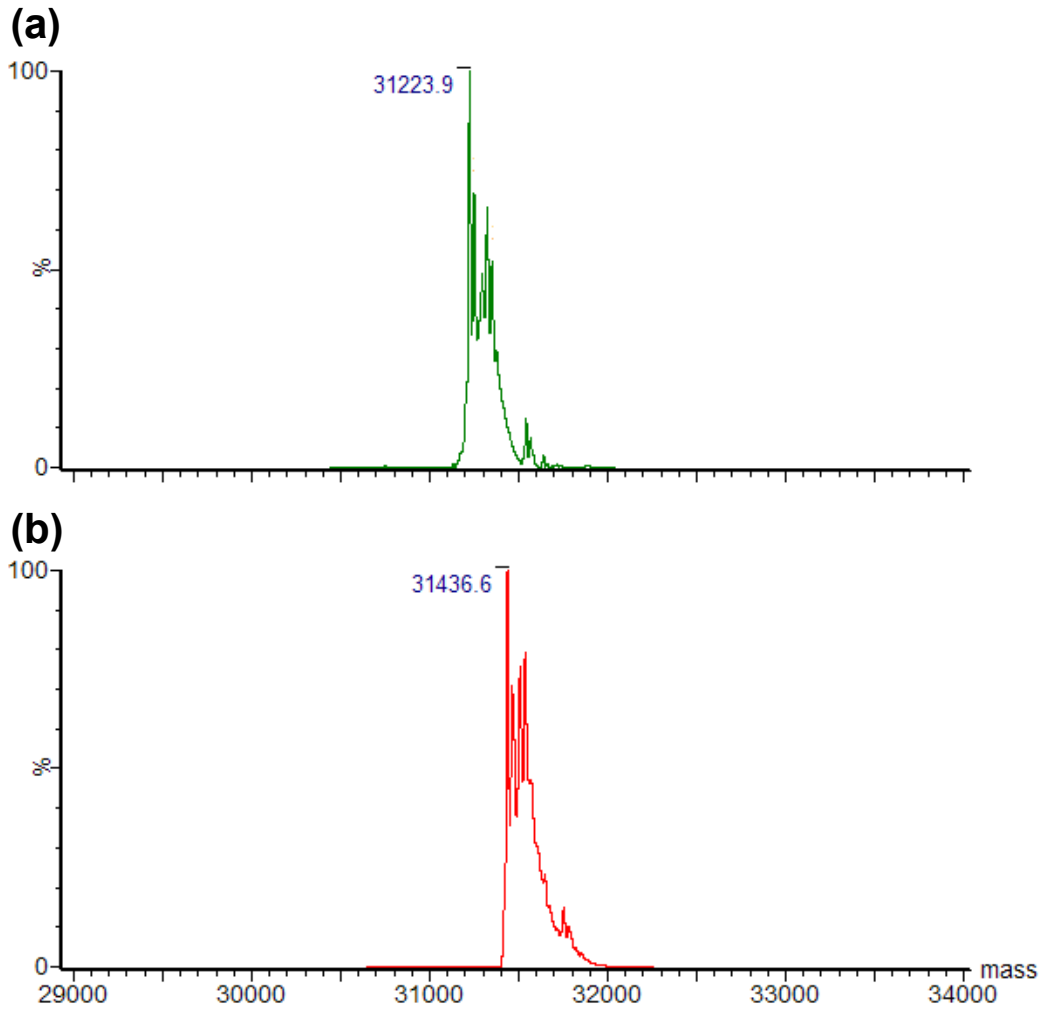

Figure 5.7: De-convoluted ESI mass spectra of (a) 6xHis_TEV_PenP_E166C/ N104L, (b) 6xHis_TEV_PenP_E166Cb/N104L.

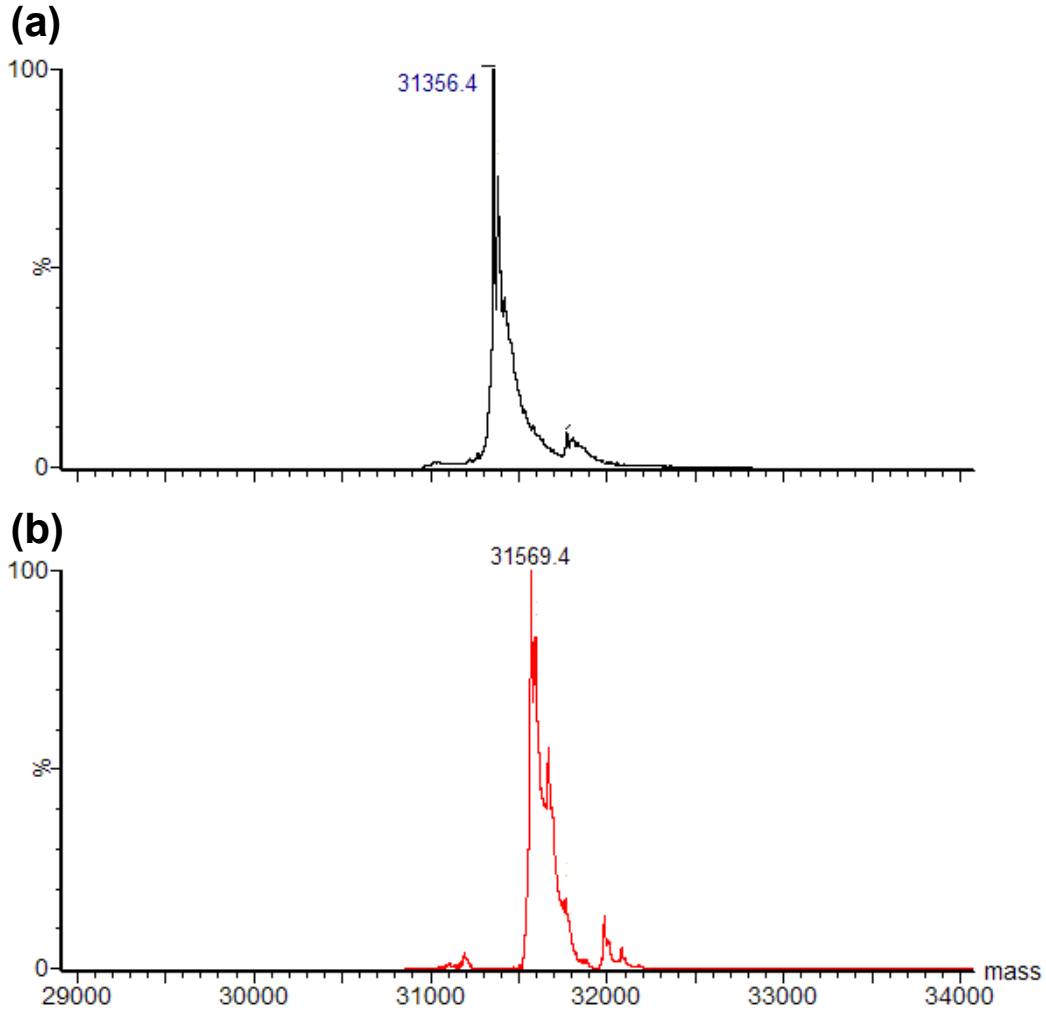

Figure 5.8: De-convoluted ESI mass spectra of (a) 6xHis_TEV_PenP_E166C/ L169N/N104L, (b) 6xHis_TEV_PenP_E166Cb/ L169N/N104L.

Table 5.8: Theoretical and calculated molecular mass vlaues of (a) PenP_E166C mutants and (b) PenP_E166Cb mutants.

(a)

Mutants	Calculated molecular mass (Da)	Experimental molecular mass (Da)
6xHis_TEV_PenP_E166C/E168L	31,209	31,209
6xHis_TEV_PenP_E166C/E168N	31,210	31,211
6xHis_TEV_PenP_E166C/L169D	31,227	31,227
6xHis_TEV_PenP_E166C/L169N	31,226	31,225
6xHis_TEV_PenP_E166C/N104L	31,224	31,224
6xHis_TEV_PenP_E166C/L169N/N104L	31,357	31,356

(b)

Mutants	Calculated molecular mass (Da)	Experimental molecular mass (Da)
6xHis_TEV_PenP_E166Cb/E168L	31,421	31,421
6xHis_TEV_PenP_E166Cb/E168N	31,422	31,423
6xHis_TEV_PenP_E166Cb/L169D	31,439	31,439
6xHis_TEV_PenP_E166Cb/L169N	31,438	31,437
6xHis_TEV_PenP_E166Cb/N104L	31,436	31,436
6xHis_TEV_PenP_E166Cb/L169N/N104L	31,569	31,569

5.3.2 Fluorescence scanning spectra of 6xHis_TEV_PenP_E166Cb/E168L

The fluorescence scanning spectra of 6xHis_TEV_PenP_E166Cb/E168L in the presence of 0.1 mM of cefotaxime, cefuroxime, ceftazidime, ceftriaxone, 7-ACA, cefoxitin, cephalothin, cephaloridine are shown in Figure 5.9 and the bar chart for the fluorescence change in the presence of various cephalosporins is shown in Figure 5.10. Generally the fluorescence signal changes upon addition of β-lactams were small and most of them were insignificant. The percentage changes in fluorescence intensities induced by the three oxyimino-cephalosporins (cefotaxinme, ceftazidime and ceftriaxone) decreased by approximately 70% in E166Cb/E168L. There were significant improvements on the fluorescence signals induced by 7-ACA, cefoxitin, cephaloridine and cephalothin. For cephaloridine, the signal was significantly improved from 0% to about 25%.

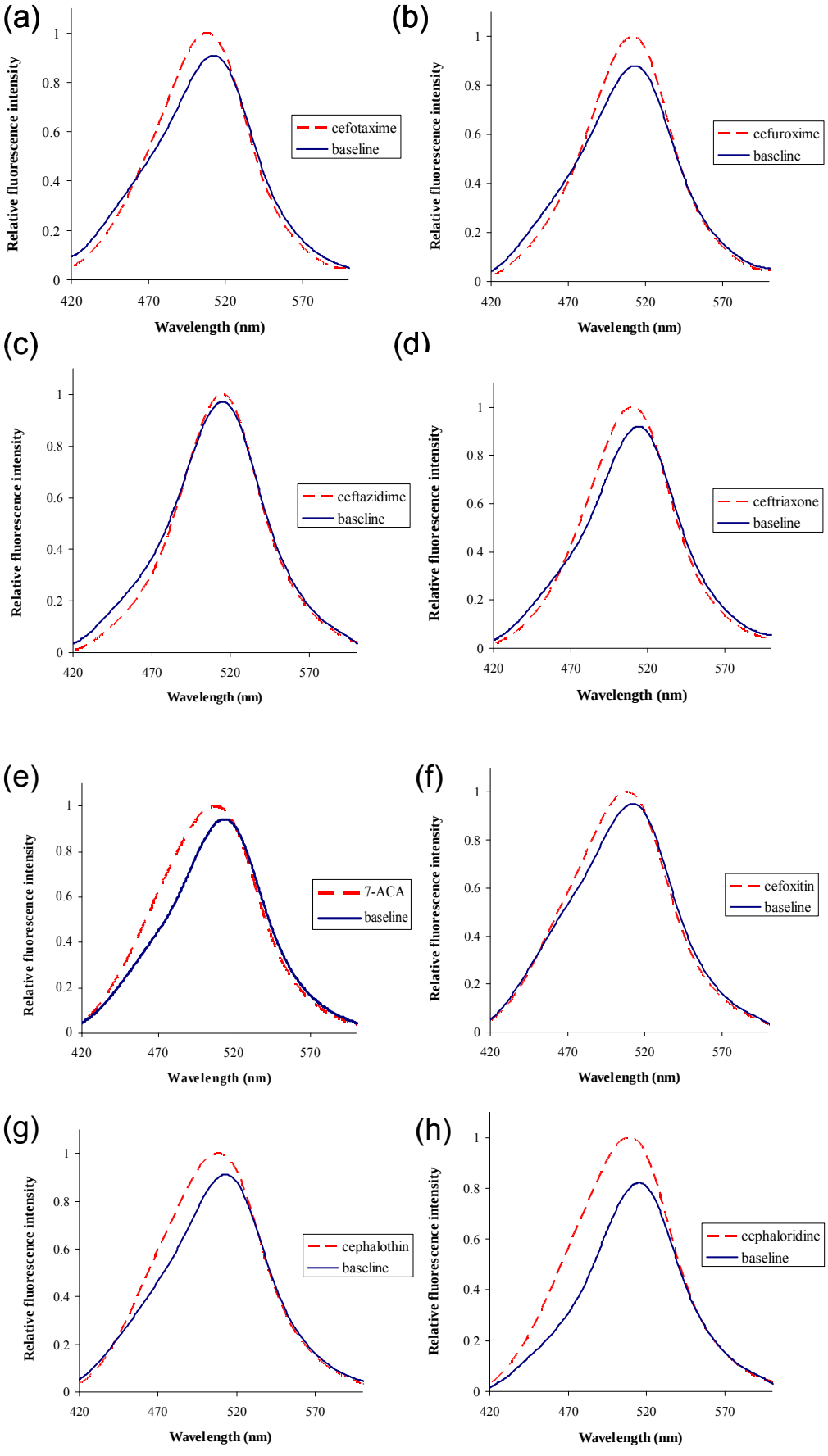
(a)
Relative fluorescence intensity
Wavelength (nm)
cefotaxime
baseline
(b)
cefuroxime
baseline
(c)
ceftazidime
baseline
(d)
ceftriaxone
baseline
(e)
7-ACA
baseline
(f)
cefoxitin
baseline
(g)
cephalothin
baseline
(h)
cephaloridine
baseline

Figure 5.9: Fluorescence spectra of 6xHis_TEV_PenP_E166Cb/E168L in the presence of 0.1 mM (a) cefotaxime, (b) cefuroxime, (c) ceftazidime, (d) ceftriaxone, (e) 7-ACA, (f) cefoxitin, (g) cephalothin, (h) cephaloridine.

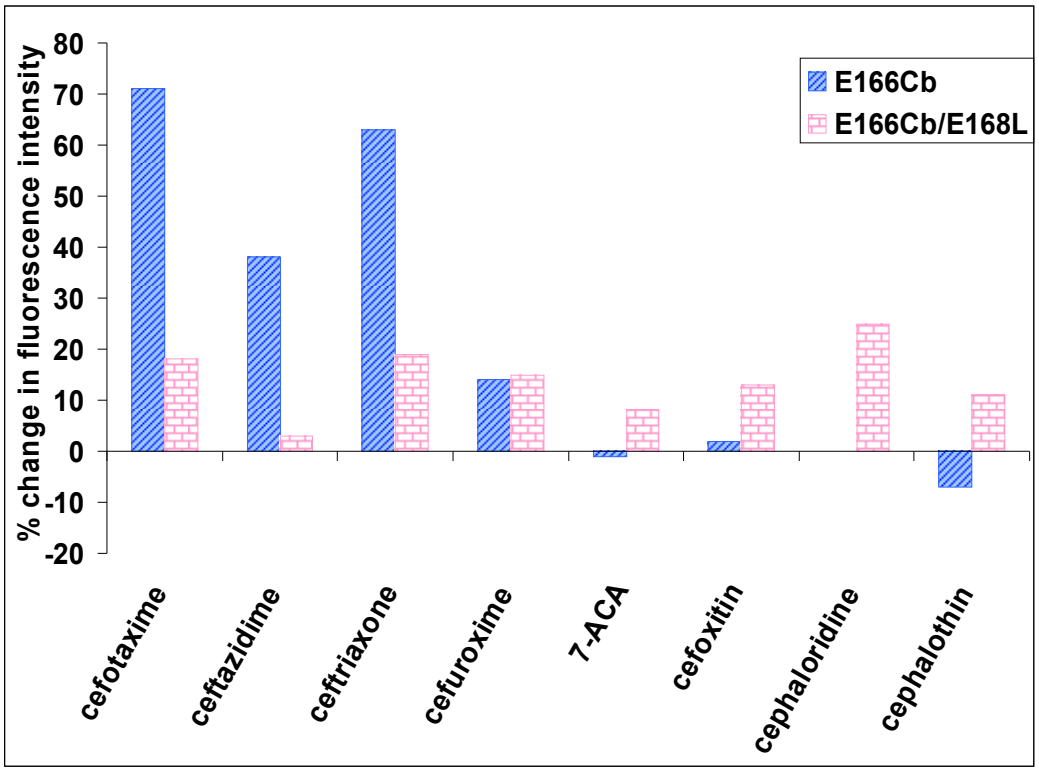

Figure 5.10: The percentage change in fluorescence intensity of 6xHis_TEV_PenP_E166Cb/E168L in the presence of various cephalosporins. Data were collected from a single measurement for each antibiotic used.

5.3.3 Fluorescence scanning spectra of 6xHis_TEV_PenP_E166Cb/E168N

The fluorescence scanning spectra of 6xHis_TEV_PenP_E166Cb/E168N in the presence of 0.1 mM of cefotaxime, cefuroxime, ceftazidime, ceftriaxone, 7-ACA, cefoxitin, cephalothin, cephaloridine are shown in Figure 5.11 and the bar chart for the fluorescence change in the presence of various cephalosporins is shown in Figure 5.12. The percentage changes in fluorescence intensities induced by the three oxyimino-cephalosporins (cefotaxinme, ceftazidime and ceftriaxone) decreased by 25-50% in E166Cb/E168N, whilst the signal for cefuroxime was unchanged. There were no significant improvements on the fluorescence signals induced by 7-ACA and cefoxitin but the signals for cephaloridine and cephalothin increased a lot, similar to that observed in E166Cb/E168L.

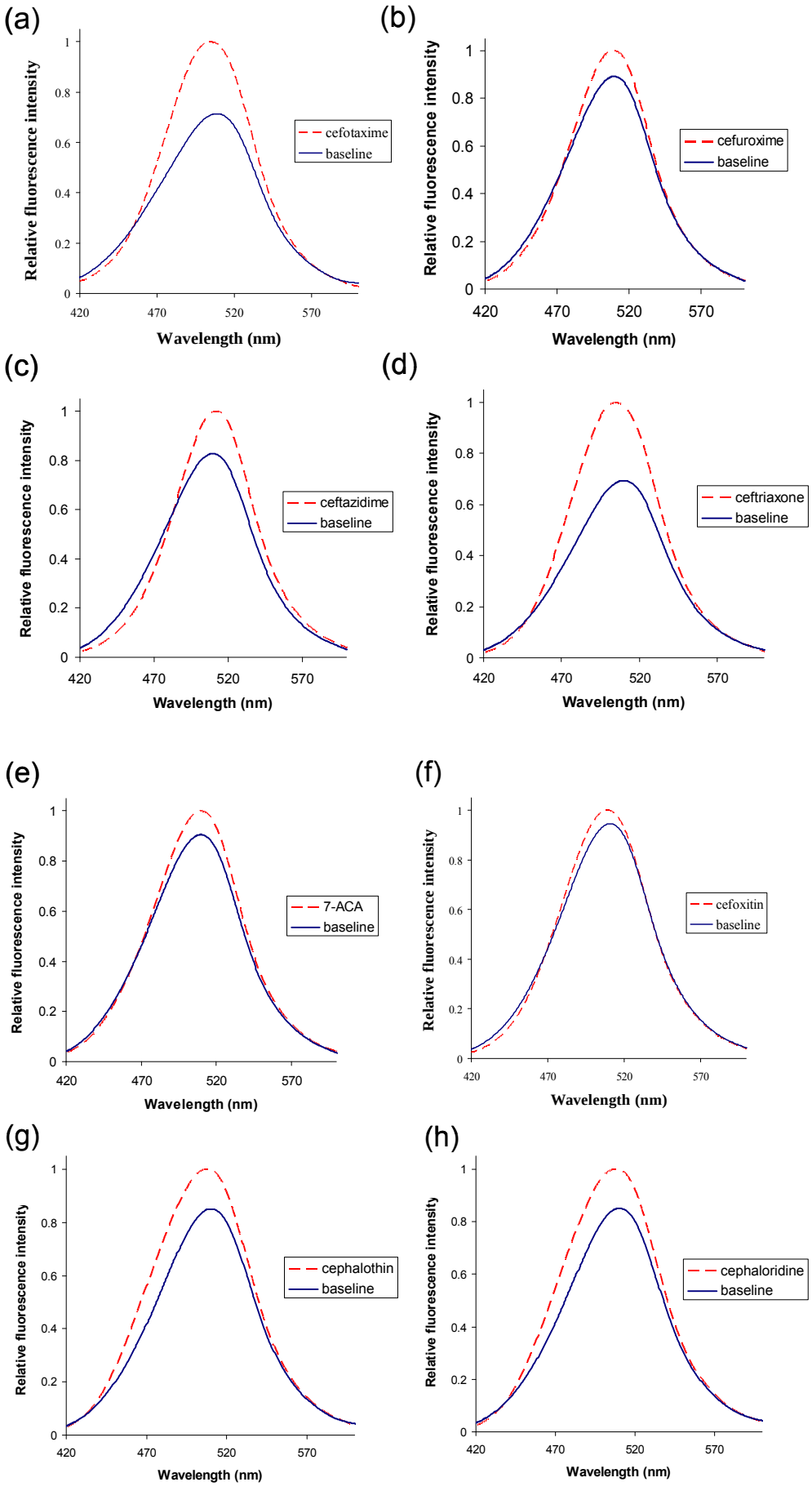
(a)
Relative fluorescence intensity
cefotaxime
baseline
Wavelength (nm)
(b)
Relative fluorescence intensity
cefuroxime
baseline
Wavelength (nm)
(c)
Relative fluorescence intensity
ceftazidime
baseline
Wavelength (nm)
(d)
Relative fluorescence intensity
ceftriaxone
baseline
Wavelength (nm)
(e)
Relative fluorescence intensity
7-ACA
baseline
Wavelength (nm)
(f)
Relative fluorescence intensity
cefoxitin
baseline
Wavelength (nm)
(g)
Relative fluorescence intensity
cephalothin
baseline
Wavelength (nm)
(h)
Relative fluorescence intensity
cephaloridine
baseline
Wavelength (nm)

Figure 5.11: Fluorescence spectra of 6xHis_TEV_PenP_E166Cb/E168N in the presence of 0.1 mM (a) cefotaxime, (b) cefuroxime, (c) ceftazidime, (d) ceftriaxone, (e) 7-ACA, (f) cefoxitin, (g) cephalothin, (h) cephaloridine.

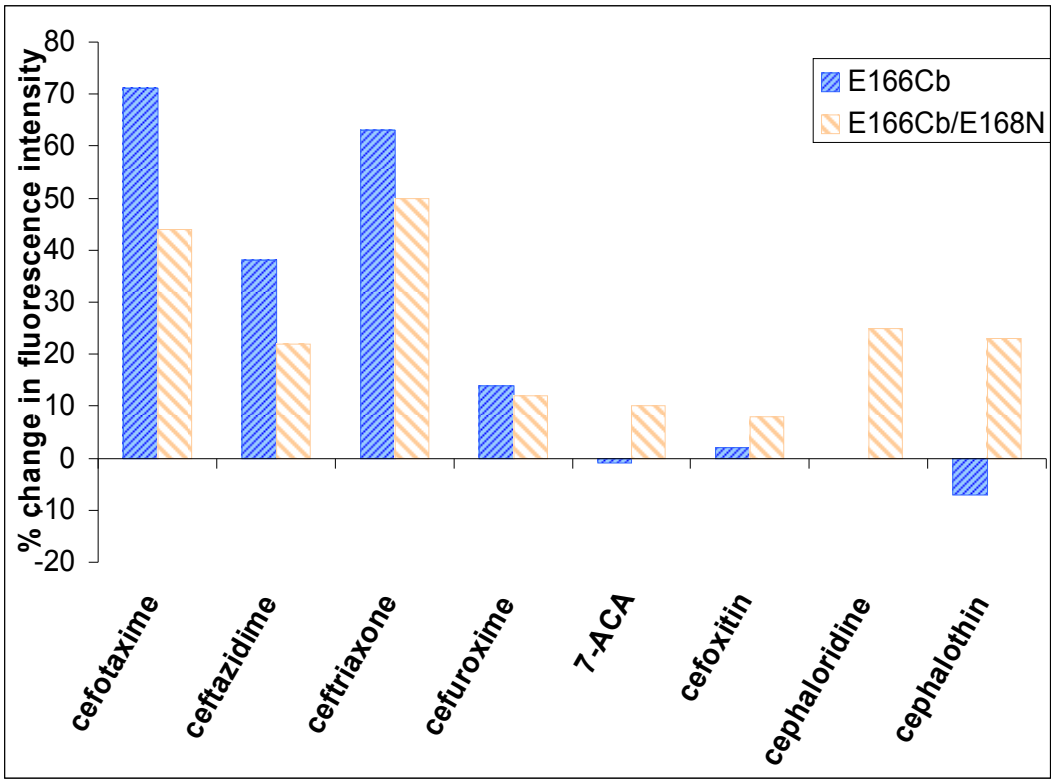

Figure 5.12: The percentage change in fluorescence intensity of 6xHis_TEV_PenP_E166Cb/E168N in the presence of various cephalosporins. Data were collected from a single measurement for each antibiotic used.

5.3.4 Fluorescence scanning spectra of 6xHis_TEV_PenP_E166Cb/L169D

The fluorescence scanning spectra of 6xHis_TEV_PenP_E166Cb/L169D in the presence of 0.1 mM of cefotaxime, cefuroxime, ceftazidime, ceftriaxone, 7-ACA, cefoxitin, cephalothin, cephaloridine are shown in Figure 5.13 and the bar chart for the fluorescence changes in the presence of different cephalosporins is shown in Figure 5.14. The percentage changes in fluorescence intensities induced by the three oxyimino-cephalosporins (cefotaxime, ceftazidime and ceftriaxone) decreased by >65% in E166Cb/L169D, similar to that observed in E166Cb/E168L, whilst the signal induced by cefuroxime only increased slightly. It was surprising that the fluorescence signals decreased upon binding of 7-ACA, cefoxitin, cephalothin and cephaloridine to mutant E166Cb/L169D.

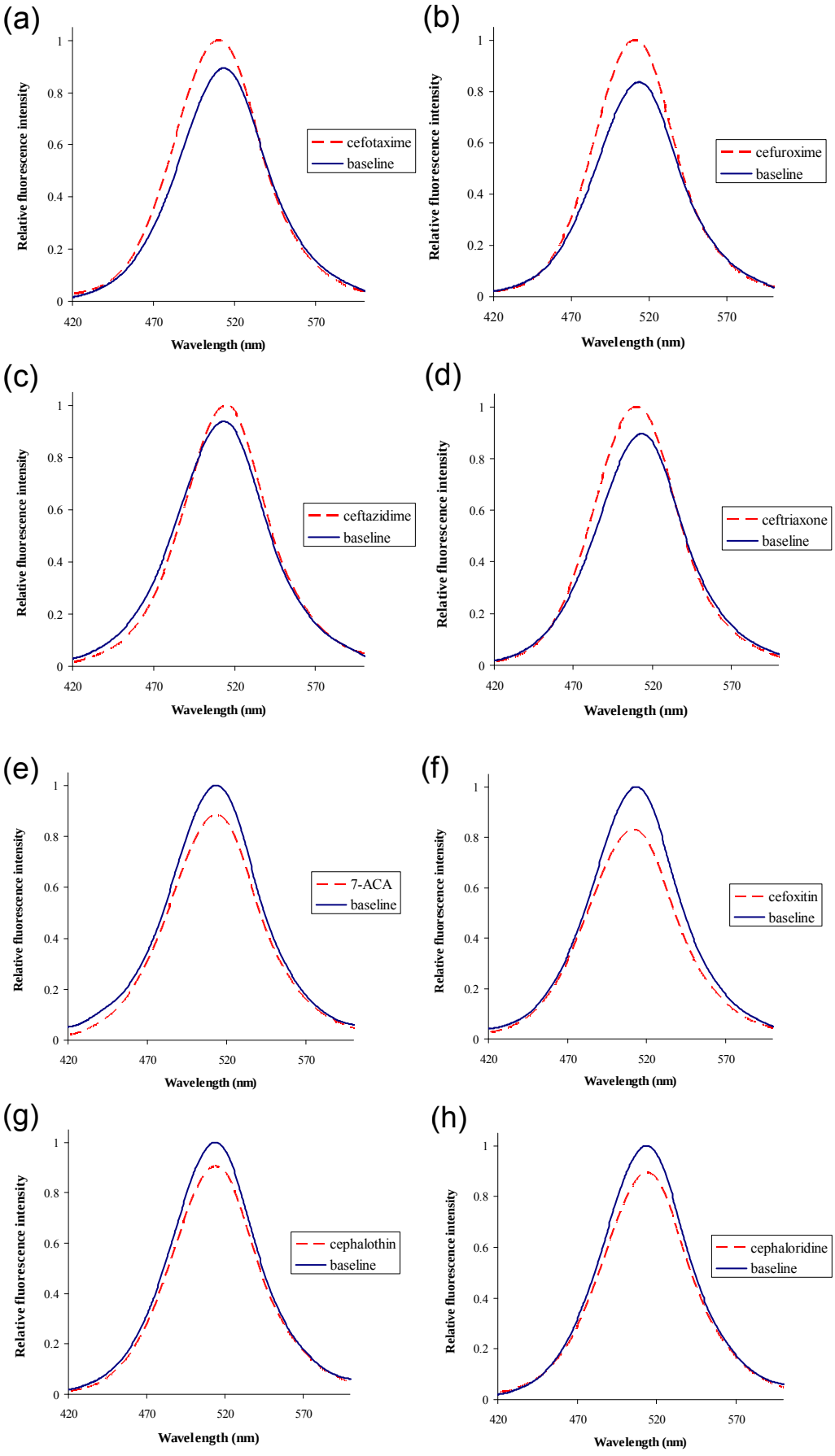
(a)
Relative fluorescence intensity
Wavelength (nm)
cefotaxime
baseline
(b)
Relative fluorescence intensity
Wavelength (nm)
cefuroxime
baseline
(c)
Relative fluorescence intensity
Wavelength (nm)
ceftazidime
baseline
(d)
Relative fluorescence intensity
Wavelength (nm)
ceftriaxone
baseline
(e)
Relative fluorescence intensity
Wavelength (nm)
7-ACA
baseline
(f)
Relative fluorescence intensity
Wavelength (nm)
cefoxitin
baseline
(g)
Relative fluorescence intensity
Wavelength (nm)
cephalothin
baseline
(h)
Relative fluorescence intensity
Wavelength (nm)
cephaloridine
baseline

Figure 5.13: Fluorescence spectra of 6xHis_TEV_PenP_E166Cb/L169D in the presence of 0.1 mM (a) cefotaxime, (b) cefuroxime, (c) ceftazidime, (d) ceftriaxone, (e) 7-ACA, (f) cefoxitin, (g) cephalothin, (h) cephaloridine.

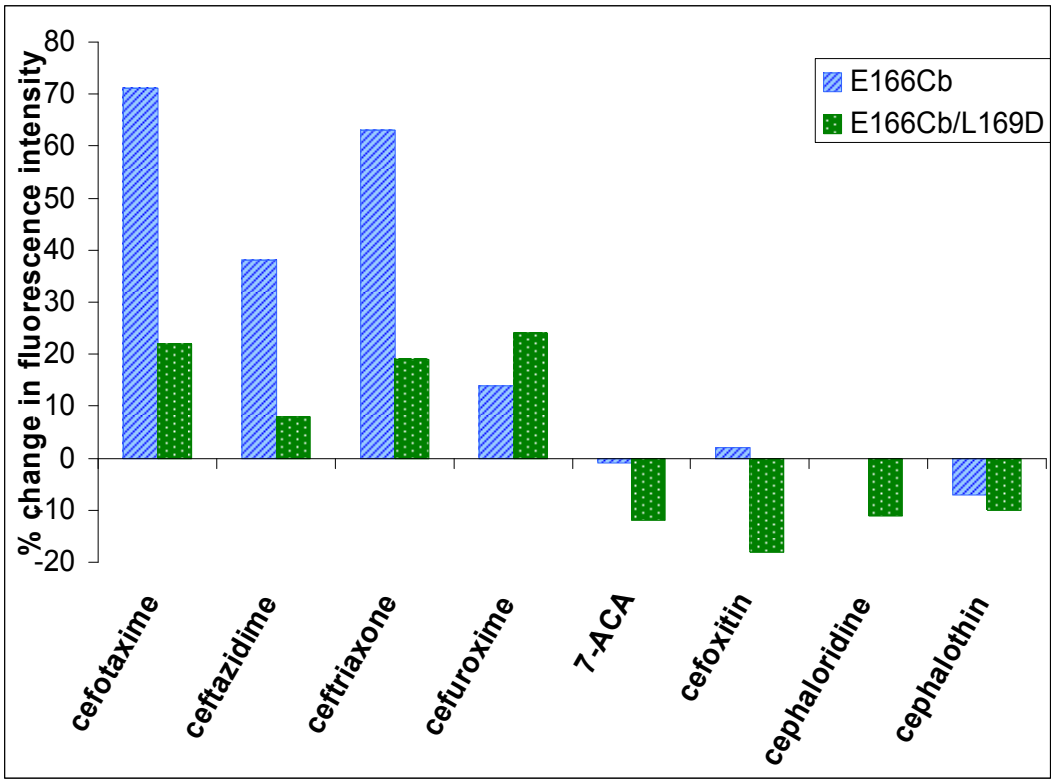

Figure 5.14: The percentage change in fluorescence intensity of 6xHis_TEV_PenP_E166Cb/L169D in the presence of various cephalosporins. Data were collected from a single measurement for each antibiotic used.

5.3.5 Fluorescence scanning spectra of 6xHis_TEV_PenP_E166Cb/L169N

The fluorescence scanning spectra of 6xHis_TEV_PenP_E166Cb/L169N in the presence of 0.1 mM of cefotaxime, cefuroxime, ceftazidime, ceftriaxone, 7-ACA, cefoxitin, cephalothin, cephaloridine are shown in Figure 5.15 and the bar chart for the fluorescence changes in the presence of various cephalosporins is shown in Figure 5.16. The percentage changes in fluorescence intensities induced by the three oxyimino-cephalosporins (cefotaxinme, ceftazidime and ceftriaxone) did not decrease much in E166Cb/L169N, whereas the signal of cefuroxime increased by approximately 4-fold. There were no improvements on the fluorescence signal induced by 7-ACA but those induced by cefoxitin, cephaloridine and cephalothin increased a lot.

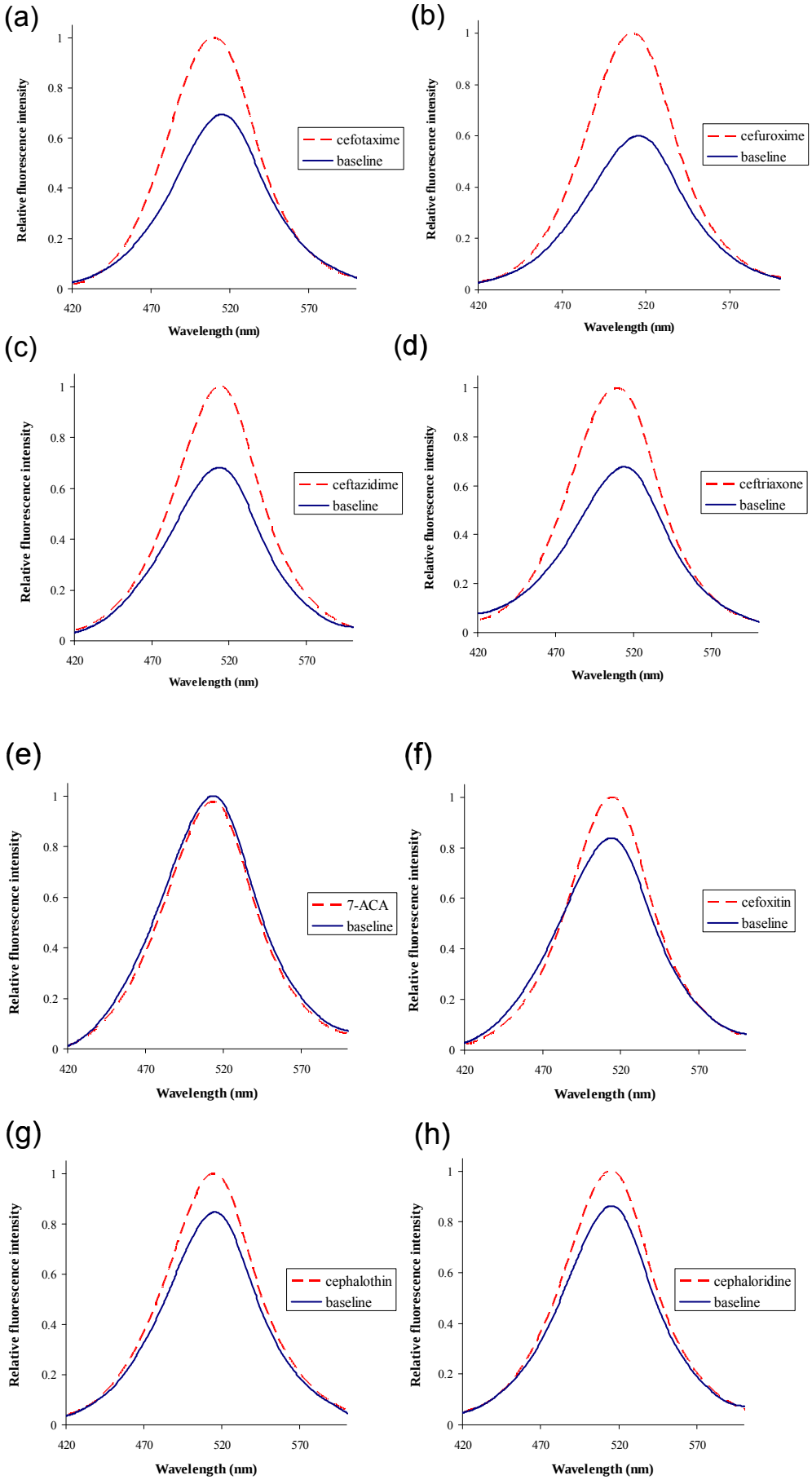
(a)
Relative fluorescence intensity
Wavelength (nm)
cefotaxime
baseline
(b)
cefuroxime
baseline
(c)
ceftazidime
baseline
(d)
ceftriaxone
baseline
(e)
7-ACA
baseline
(f)
cefoxitin
baseline
(g)
cephalothin
baseline
(h)
cephaloridine
baseline

Figure 5.15: Fluorescence spectra of 6xHis_TEV_PenP_E166Cb/L169N in the presence of 0.1 mM (a) cefotaxime, (b) cefuroxime, (c) ceftazidime, (d) ceftriaxone, (e) 7-ACA, (f) cefoxitin, (g) cephalothin, (h) cephaloridine.

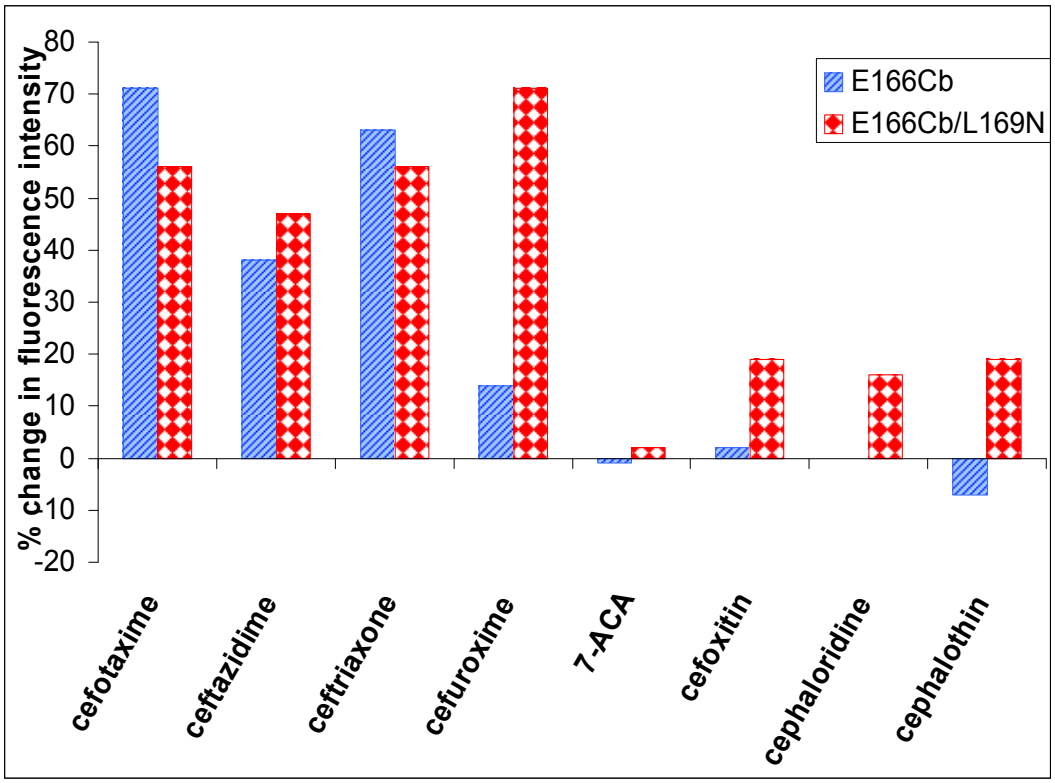

Figure 5.16: The percentage change in fluorescence intensity of 6xHis_TEV_PenP_E166Cb/L169N in the presence of various cephalosporins. Data were collected from a single measurement for each antibiotic used.

5.3.6 Fluorescence scanning spectra of 6xHis_TEV_PenP_E166Cb/N104L

The fluorescence scanning spectra of 6xHis_TEV_PenP_E166Cb/N104L in the presence of 0.1 mM of cefotaxime, cefuroxime, ceftazidime, ceftriaxone, 7-ACA, cefoxitin, cephalothin, cephaloridine are shown in Figure 5.17 and the bar chart for the fluorescence changes in the presence of various cephalosporins is shown in Figure 5.18. The percentage changes in fluorescence intensity for the three oxyimino-cephalosporins (cefotaxinme, ceftazidime and ceftriaxone) decreased moderately in E166Cb/N104L. The signal for cefuroxime increased by more than 1-fold. Similar to E166Cb/L169N, there were no improvements on the fluorescence signal of 7-ACA but the signals for cefoxitin, cephaloridine and cephalothin increased a lot.

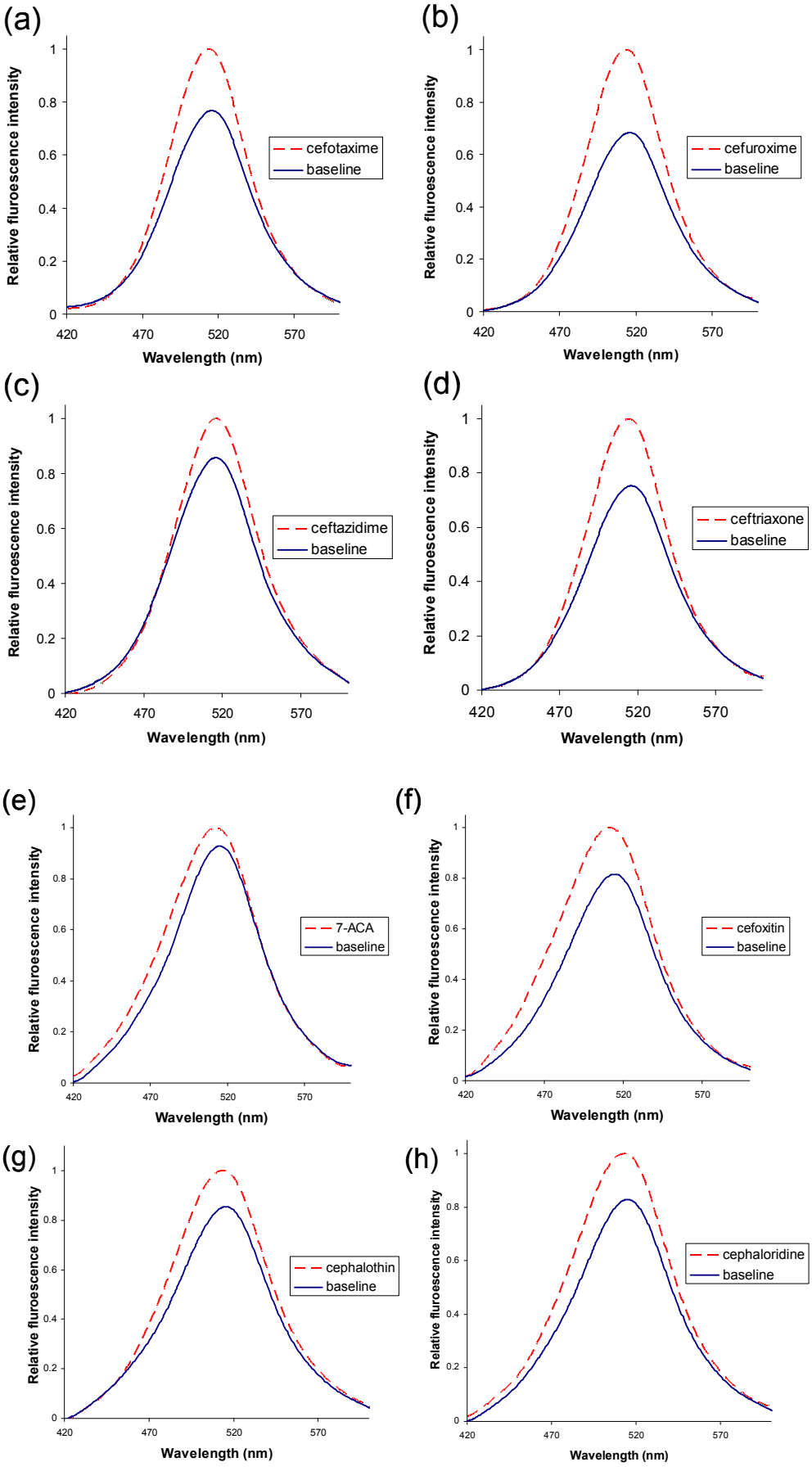
(a)
Relative fluroescence intensity
Wavelength (nm)
cefotaxime
baseline
(b)
cefuroxime
baseline
(c)
ceftazidime
baseline
(d)
ceftriaxone
baseline
(e)
7-ACA
baseline
(f)
cefoxitin
baseline
(g)
cephalothin
baseline
(h)
cephaloridine
baseline

Figure 5.17: Fluorescence spectra of 6xHis_TEV_PenP_E166Cb/N104L in the presence of 0.1 mM (a) cefotaxime, (b) cefuroxime, (c) ceftazidime, (d) ceftriaxone, (e) 7-ACA, (f) cefoxitin, (g) cephalothin, (h) cephaloridine.

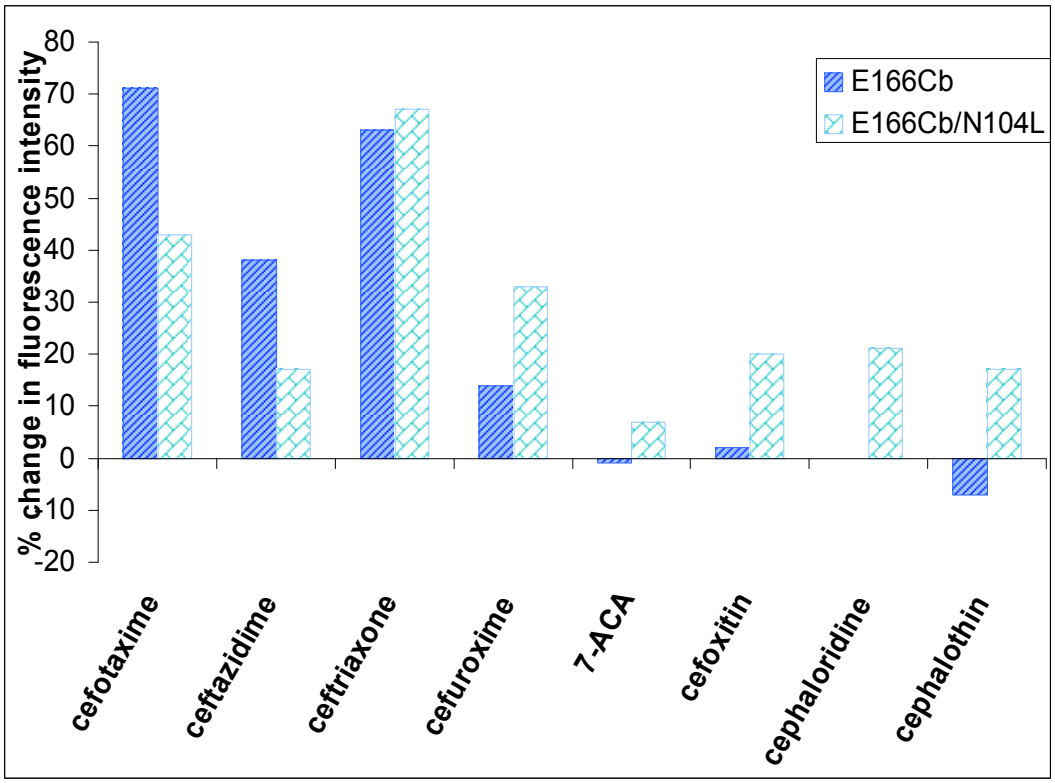

Figure 5.18: The percentage change in fluorescence intensity of 6xHis_TEV_PenP_E166Cb/N104L in the presence of various cephalosporins. Data were collected from a single measurement for each antibiotic used.

5.3.7 Fluorescence scanning spectra of 6xHis_TEV_PenP_E166Cb/ L169N/N104L

The fluorescence scanning spectra of 6xHis_TEV_PenP_E166Cb/ L169N/N104L in the presence of 0.1 mM of cefotaxime, cefuroxime, ceftazidime, ceftriaxone, 7-ACA, cefoxitin, cephalothin, cephaloridine are shown in Figure 5.19 and the bar chart for the fluorescence changes in the presence of various cephalosporins is shown in Figure 5.20. The percentage changes in fluorescence intensity induced by the three oxyimino-cephalosporins (cefotaxinme, ceftazidime and ceftriaxone) decreased by more than 50% in E166Cb/L169N/N104L. The signal for cefuroxime increased by 2-fold. Surprisingly, there was a large increase in the fluorescence signal induced by 7-ACA but not for cefoxitin and cephalothin. The fluorescence signal induced by cephaloridine was improved.

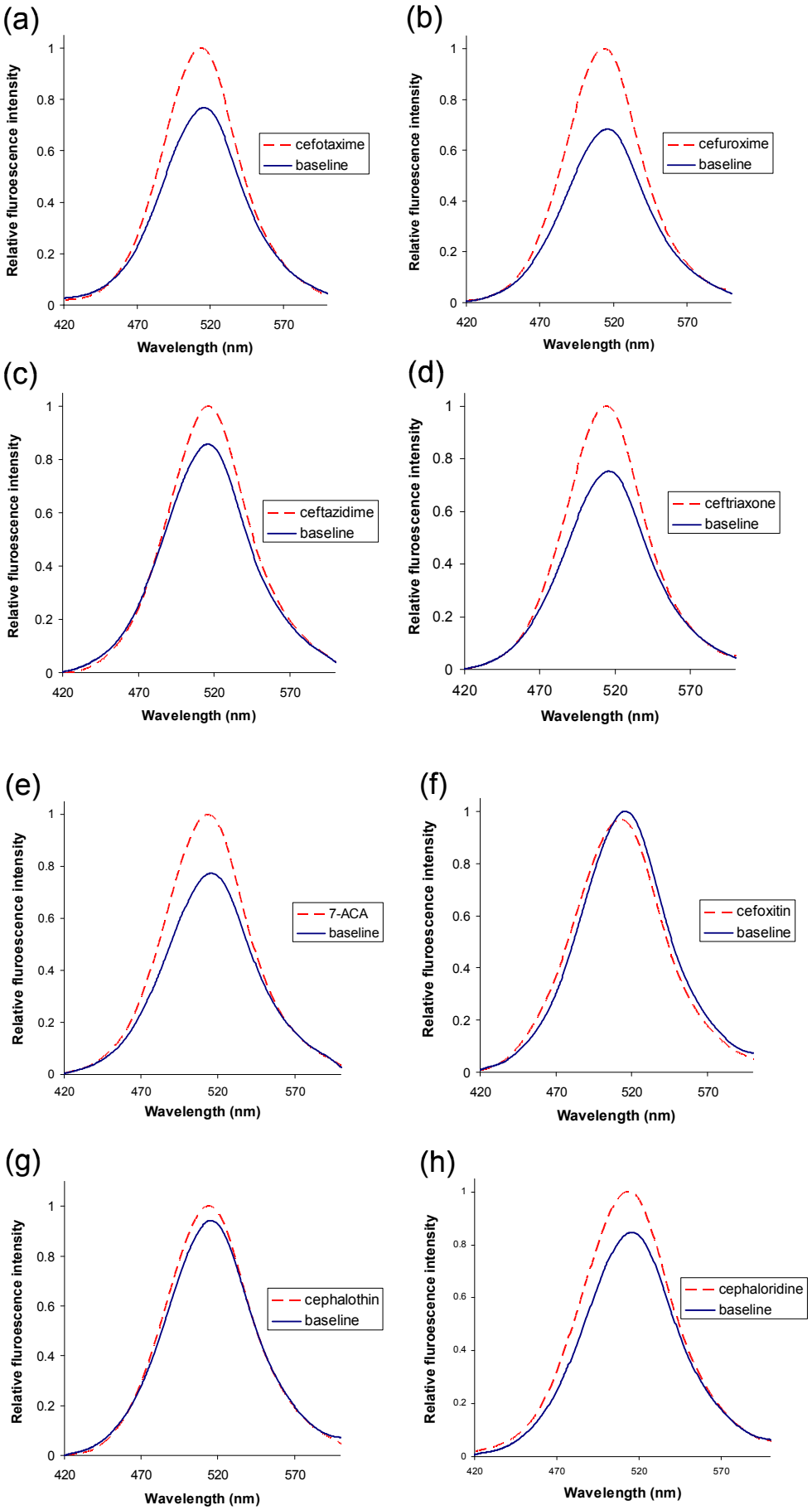
(a)
Relative fluroescence intensity
Wavelength (nm)
cefotaxime
baseline
(b)
cefuroxime
baseline
(c)
ceftazidime
baseline
(d)
ceftriaxone
baseline
(e)
7-ACA
baseline
(f)
cefoxitin
baseline
(g)
cephalothin
baseline
(h)
cephaloridine
baseline

Figure 5.19: Fluorescence spectra of 6xHis_TEV_PenP_E166Cb/ L169N/N104L in the presence of 0.1 mM (a) cefotaxime, (b) cefuroxime, (c) ceftazidime, (d) ceftriaxone, (e) 7-ACA, (f) cefoxitin, (g) cephalothin, (h) cephaloridine.

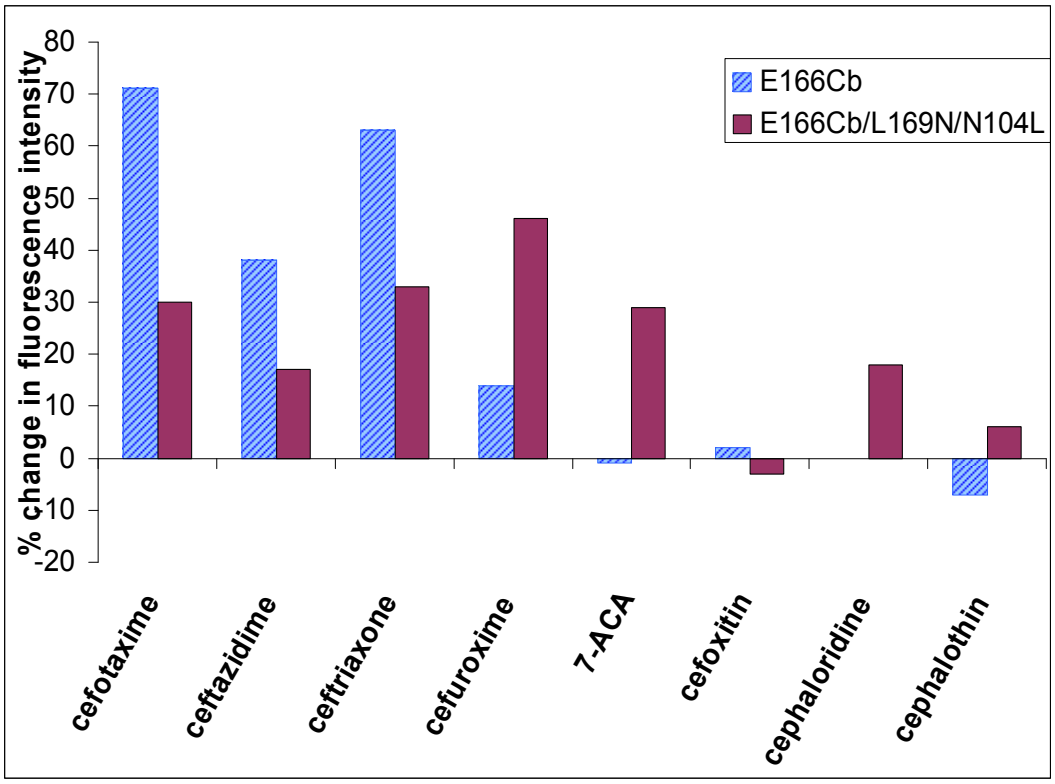

Figure 5.20: The percentage change in fluorescence intensity of 6xHis_TEV_PenP_E166Cb/L169N/N104L in the presence of various cephalosporins. Data were collected from a single measurement for each antibiotic used.

5.4 Discussion

In general, from the fluorescence signals of all the E166Cb mutants, it can be observed that mutations on residue 168 or 169 caused a decrease in the percentage change in the fluorescence intensity upon binding with oxyimino-cephalosporins when compare to the non-mutated E166Cb. On the other hand, most mutations gave rise to an improvement of the fluorescence signal for non-oxyimino-cephalosporins. The possible biosensing mechanism is discussed here. The overall percentage changes in fluorescence intensity of E166Cb, E166Cb/E168L, E166Cb/E168N, E166Cb/L169D, E166Cb/L169N, E166Cb/N104L and E166Cb/L169N/N104L in the presence of various cephalosporins are shown in Figure 5.21.

Effects of mutations on oxyimino-cephalosporin binding

From the crystal structure of PenP_E166Cb, Glu168 was in proximity to the badan molecule and it was believed that mutation on this site would alter the initial polarity of the surrounding environment of badan. Also, after binding to the oxyimino cephalosporin (e.g. cefotaxime), Glu168 was displaced from the protein interior to the solvent outside because of the steric clash with the oxyimino group of cefotaxime. This also caused the displacement of the other residues on the Ω-loop. The displacement of the negatively-charged side chain of Glu rendered the local environment of the fluorophore less polar, which led to an increase in the fluorescence signal. A mutation of Glu168 to Leu168 caused a significant decrease in the fluorescence signal. It is possible that when the charged carboxylate side chain of Glu168 was changed to a hydrophobic side

chain of Leu168, the local polarity of badan molecule would be reduced. In this case, after the binding of the oxyimino-cephalosporin, Leu168 should be also displaced to a more solvent-exposed position. However, the change in the local environment in E166Cb/E168L was not as large as that in E166Cb so that the fluorescence change was not as large as E166Cb. For the mutant E166Cb/E168N, since asparagine is a polar residue, the fluorescence signal change was in somewhere between Glu168 and Leu168 as the removal of the polar effect exerts on the local area is larger than Leu168 but smaller than Glu168. Although it was believed that Glu168 did not play a key part in catalysis (Madgwick and Waley 1987), it is the most important residue in our biosensing model because the fluorescence change was a result of the steric clash between Glu168 and the antibiotic side chain.

On the other hand, the crystal structure of PenP_E166Cb in complex with cefotaxime showed that Leu169 was moved from a more solvent exposed position to the protein interior after the binding of cefotaxime. It was predicted that the mutation of the leucine would cause a small change in the local environment of badan. From the fluorescence data, it can be seen that the mutation of leucine to aspartic acid or asparagine significantly decreased the fluorescence intensity upon binding of oxyimino-cephalosporins. When the hydrophobic Leu169 was changed to the charged Asp169, the overall environment became electrostatic so that the fluorescence intensity decreased. Similarly, asparagine is a polar residue so that the fluorescence signal change exhibited the same trend with Asp169. The polar effect of Asn169 exerted on the local area was larger than Leu169 but smaller than Asp169. It is possible that mutating residue 169 to more hydrophobic residues, such as methionine,

phenylalanine and tryptophan, might cause the fluorescence to increase by a larger extent.

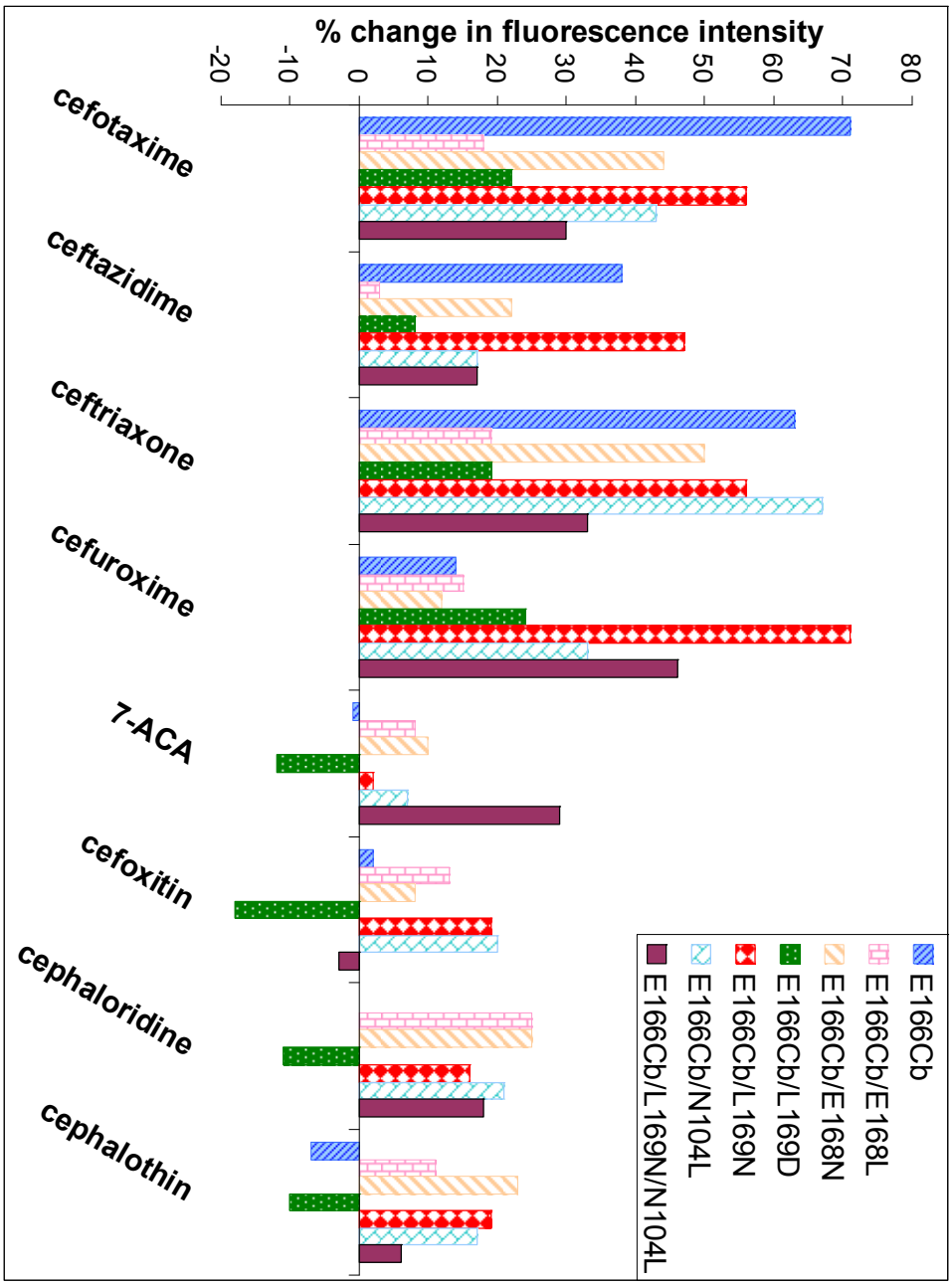

Figure 5.21: Percentage change in fluorescence intensity of E166Cb, E166Cb/E168L, E166Cb/E168N, E166Cb/L169D, E166Cb/L169N, E166Cb/N104L and E166Cb/L169N/N104L in the presence of various cephalosporins. Data were collected from a single measurement for each antibiotic used. This is a preliminary analysis and the measurements were repeated selectively.

Effects of mutations on non-oxyimino-cephalosporin binding

Mutations on Glu168, Leu169 and Asn104 also caused some significant changes in fluorescence intensity for non-oxyimino-cephalosporins. The crystal structures of PenP_E166Cb after binding with cefoxitin and cephaloridine revealed that the Ω-loop is highly dynamic and disordered. Therefore, we can only speculate the biosensing mechanism of non-oxyimino-cephalosporins. The fluorescence data of L169D and L169N show that when the local environment was changed from hydrophobic to charged, the fluorescence decreased. This indicates that a more hydrophobic environment would enhance the fluorescence signal. As observed in oxyimino-cephalosporins, some highly hydrophobic residues can be tested in future experiments (e.g. methionine, phenylalanine and tryptophan) to investigate how residue 169 affects the fluorescence signal.

On the other hand, Asn104 is in close proximity to badan but is not on the same side as Glu168 and Leu169. When Asn104 was changed to Leu104, the fluorescence increased after binding of non-oxyimino-cephalosporins. This implies that changing to a hydrophobic environment on the other side of badan is beneficial to the fluorescence enhancement. More surprisingly, it was predicted that the double mutations of L169N and N104L should have a synergistic effect on the fluorescence signal change. However, the observed fluorescence signal was not expected. The effects of the two mutations might have antagonized each other by turning the environment in one side of badan more polar and that in the other side more hydrophobic. This implies that only a small change in the local area may be very sensitive to the surrounding environment of badan and caused a large difference in the fluorescence signal. A double mutant of L169M/N104L or

L169F/N104L could be tested in the future to set-up a highly hydrophobic environment, which may be particularly useful for detecting non-oxyimino-cephalosporins. Further analysis on these mutations could be carried out by crystallization to investigate how the local environment is altered for the change in fluorescence signal.

β-lactam profiling using different PenP_E166Cb mutants

In summary, eight of the β-lactam antibioctics were tested by various mutated PenP_E166Cb biosensors. It can be observed that two kinds of β-lactam, oxyimino-cephalosporins and non-oxyimino-cephalosporins, were grouped in terms of fluorescence change in intensity. In Figure 5.21, the four β-lactams on left belong to oxyimino-cephalosporins while the four β-lactams on right belong to non-oxyimino-cephalosporins since the left ones generated significnat changes in fluorescence intensity. In addition, we found that the structures of β-lactams and the change in fluorescence signal could be closely related. In oxyimino-cephalosporins, cefotaxime has a similar structure with ceftriaxone. The only difference between them is the R1 side chain group on the C3 position (Figure 1.2). After binding to Ser70, the R1 side chain group rearranges and leaves (as described in Section 3.3.9) so that cefotaxime and ceftriaxone are identical to each other when they are bound to the active sites. Since ceftazidime is very different from them, the fluorescence signal generated was in a different pattern. Therefore, the fluorescence signal changes are very sensitive to the small differences in the chemical structures of the antibiotics. This can also be applied to non-oxyimino-cephalosporins since cefoxitin has a different structure from cephaloridine and cephalothin.

Based on these preliminary results, the mutants of PenP_E166Cb might have potential to be developed into differentiating biosensors to identify β-lactams present in testing samples, since different β-lactams show varying fluorescence patterns upon binding each of the mutants. To make it more precise and more powerful, each fluorescence measurement should be repeated several times to obtain an error bar and more β-lactams should be included in the measurement. The final fluorescence data could be a small library and could offer a profile for β-lactams with same structures after binding. PenP_E166Cb is a good candidate because of its high expression level for production, good thermostability for storage, high sensitivity for probing local environment and high specificity to β-lactams. This may offer a cheap and convenient method for testing of the presence of β-lactams in the future.

5.5 Concluding remarks

Several mutants for PenP β-lactamase were successfully expressed, purified and labeled with badan, namely 6xHis_TEV_PenP_E166Cb/E168L, 6xHis_TEV_PenP_E166Cb/E168N, 6xHis_TEV_PenP_E166Cb/L169D, 6xHis_TEV_PenP_E166Cb/L169N, 6xHis_TEV_PenP_E166Cb/N104L and 6xHis_TEV_PenP_E166Cb/L169N/N104L. The fluorescence scanning spectra and the percentage change of fluorescence intensity upon binding with various cephalosporins for all mutants were investigated.

Comparing E166Cb with other mutants, it was found that the tested mutations caused a significant decrease in the fluorescence intensity for oxyimino-cephalosporins. This fluorescence data supports our model on the environmental change induced by the movement of Glu168. The mutation of L169D shows that by changing the overall environment more electrostatic, the fluorescence signal of non-oxyimino-cephalosporin-bound biosensors decreased. This implies that hydrophobic environment may be particularly beneficial to the fluorescence enhancement induced by non-oxyimino-cephalosporins. The results indicate that badan is very sensitive to the local environment because only a small change in the local area can cause a large difference in the fluorescence signal. This study can provide new insights on the design of a new biosensor for β-lactams. The fluorescence pattern obtained from different combinations of β-lactams and PenP_E166Cb mutants might offer a profile for β-lactams with same structures after binding and might provide a good method for identification of β-lactams in testing samples.

Chapter 6: Characterization and structural study of PenP_E166Cf

6.1 Introduction

Fluorescein-5-maleimide (in short fluorescein) is one of the most common thiol-reactive fluorophores used for probing specific sites of proteins. It belongs to the group of "maleimide" in thiol-reactive probes, which is similar to iodoacetamide in terms of thiol modification but with higher selectivity. The optimum pH for the labeling reaction is at physiological pH (near 7.0). The reactivity of the maleimide group towards a free sulfhydryl is about 1,000 times higher than an amine (Bigelow and Inesi 1991). At a higher pH of 7.5, reactivity towards primary amines is increased. In order to achieve single site labeling, any substances interfering with the reaction, such as reducing agents should be avoided. Proteins that contain disulfide bonds should have reduction reaction carried out prior to labeling so that the free sulfhydryl groups will be present. A schematic diagram for the labeling reaction of fluorescein in PenP_E166C is shown in Scheme 4.

Scheme 4

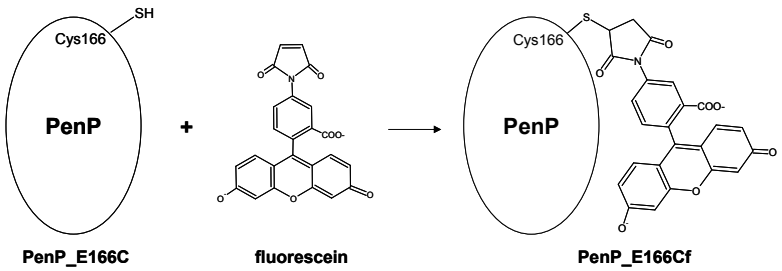

Scheme 4: The labeling reaction between PenP_E166C and fluorescein

Fluorescein has a larger size (M.W.: 427.37) than badan (M.W.: 292.17) and it has more conjugations. It was used in the previously published work (Chan *et al.* 2004; Chan *et al.* 2008), where the fluorescent protein was called PenPC_E166Cf. Fluorescein was also used in this project for comparison of the fluorescence profiles between PenP_E166Cf and PenP_E166Cb. The two fluorophores have very different properties in terms of enhancement in fluorescence intensity, wavelength at maximum emission and sensitivity to surrounding environment. The two fluorophores attached to the Ω-loop of β-lactamase respond differently, upon a change in the environment induced by the binding of the antibiotic.

The fluorophore-labeling techinique is an emerging approach. Similar to the approach described in our previously published biosensor, another biosensor that detects the binding of aminoglycoside antibiotics to an aminoglycoside resistant enzyme, aminoglycoside 6-N-acetyltransferase (AAC(6')) has been developed (Chu *et al.* 2008). A fluorescein-5-maleimide molecule is labeled onto a flexible loop close to the binding site so that the binding of the aminoglycoside antibiotic induces conformational changes to the labeled enzyme, then changes the surrounding environment of the fluorophore, and finally gives rise to an increase in the fluorescence intensity.

In this chapter, the crystal structures of the PenP_E166Cf and PenP_E166Cf in complex with cefotaxime were resolved in order to explain the corresponding fluorescence signal changes upon addition of β-lactams. The general biosensing mechanism is discussed based on the observed fluorescence

signals and crystal structures. This study provides hints and strategies to discover new biosensors for screening small ligands such as β-lactams.

6.2 Methods

6.2.1 Preparation and purification of 6xHis_TEV_PenP_E166C mutant

The expression and purification of 6xHis_TEV_PenP_E166C are described in Sections 3.2.2, 3.2.3 and 3.2.4.

6.2.2 Labeling of PenP_E166C by fluoresein-5-maleimide

To label PenP_E166C, a ten-fold molar excess of fluorescein-5-maleimide (Invitrogen) was dissolved in DMF (concentration: 20 mM) and then added to the protein solution drop by drop. The mixture was labeled in darkness with stirring for 1 h, and then dialysed against 50 mM potassium phosphate buffer (pH 7.0) at 4 ℃ several times in order to remove excess dyes. The protein solution was concentrated to less than 1 ml and loaded to the Superdex™ 75 gel filtration column (GE Healthcare). The running buffer contained 20 mM Tris-HCl and 50 mM NaCl (pH 7.5). The target fractions were pooled and concentrated by Amicon Ultra to 25 mg/ml. The protein was confirmed by ESI-MS as described in Sections 2.8.1 and 2.8.2.

6.2.3 Fluorescence scanning spectra and time-dependent fluorescence profiles

Different kinds of β-lactam antibiotics, namely cefotaxime, ceftriaxone, ceftazidime, cephaloridine, cephalothin, cefoxitin, cefuroxime, ampicillin and penicillin G, were used for the fluorescence scanning measurement for

PenP_E166Cf. The concentrations used for all antibiotics were 1 x 10^{-4} M to get a saturated fluorescence signal. The details of the measurement are described in Section 2.7.1. For the time-dependent fluorescence measurement, cefotaxime was chosen to be the candidate. Different concentrations of cefotaxime were tested (1 x 10^{-8} M, 5 x 10^{-8} M, 1 x 10^{-7} M, 1 x 10^{-6}, 1 x 10^{-5} M). Details are described in Section 2.7.2.

6.2.4 Crystallization of PenP_E166Cf and PenP_E166Cf in complex with cefotaxime

The crystallization of PenP_E166C and PenP_E166Cf was performed by the method described in Section 2.9.1. The protein concentration used for crystallization was 30 mg/ml. Hampton Screen was used and the crystallization conditions were screened for growing small crystals. Structures of PenP_E166C and PenP_E166Cf were compared. Crystals of PenP_E166Cf were soaked in the solution of 0.01 M cefotaxime for 20 minutes to obtain the acyl-enzyme intermediate complex. To confirm the crystals grown were PenP_E166Cf, purification of the crystals was conducted prior to SDS/PAGE analysis.

6.3 Results

6.3.1 Preparation, purification and labeling of PenP_E166C by fluorescein-5-maleimide

Preparation and purification of PenP_E166C are described in Sections 3.3.1, 3.3.2 and 3.3.3. PenP_E166C, with the 6xHis-tag removed, was labeled with fluorescein-5-maleimide according to the method described in Section 2.4.2. After labeling, the solution turned yellow, which was a good indicator of successful labeling. The best labeling condition was found among the different concentrations of GdnHCl, different reaction times and different temperatures for labeling. The labeling efficiency of each of the condition was calculated according to the equation shown in Section 2.8.2 and listed in Table 6.1. It can be seen that no GdnHCl was needed to unfold the protein before the labeling reaction. In the mass spectra, just a very small peak of unlabeled PenP_E166C could be observed. Moreover, neither the labeling duration nor the temperature affected the labeling efficiency.

Table 6.1: Labeling efficiency of PenP_E166Cf at different labeling conditions.

Conc. of GdnHCl	Labeling duration			Temperature
	30 min	1 h	2 h	
6 M GdnHCl	---	98%	---	**25℃**
4 M GdnHCl	---	98%	---	
2 M GdnHCl	---	97%	---	
0 M GdnHCl	96%	97%	97%	
	---	97%	---	**37℃**

The labeling efficiencies were checked by the transformed mass spectrum of PenP_E166Cf (Figure 6.1) shows a peak with a molecular mass value of 30,054 Da, which is (427+18) Da higher than E166C. The mass increment of (427+18) Da is approximately an addition of a fluorescein-5-maleimide molecule and a water molecule. The addition of a water molecule was likely due to the formation of a protein–water adduct during electrospray ionization, since formation of adducts between protein and small solvent molecules (e.g. H_2O) derived from the solvent or the buffer during electrospray ionization is a commonly observed phenomenon (Tolic *et al.* 1998; Vedadi *et al.* 2006). The measurement shows that the fluorescein was incorporated into the PenP_E166C mutant with a stiochiometry of 1:1 and the protein was labeled with fluorescein-5-maleimide in nearly 100% labeling efficiency.

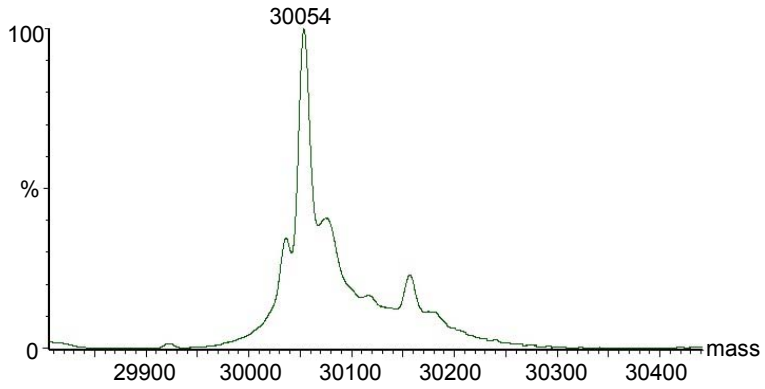

Figure 6.1: De-convoluted ESI mass spectra of labeled PenP_E166Cf. The

major peak shows the measured mass (30,054 Da), in good agreement with the calculated mass (30,053 Da).

6.3.2 Fluorescence scanning and time-dependent fluorescence spectra

Eight β-lactam antibiotics, namely cefotaxime, ceftriaxone, ceftazidime, cephaloridine, cephalothin, cefoxitin, cefuroxime, ampicillin, and penicillin G, were used in the fluorescence scanning measurement. The fluorescence scanning spectra for all these antibiotics are shown in Figure 6.2. It can be observed that all the cephalosporins used could generate significant increases of more than 20% in the fluorescence intensity. The percentage changes in fluorescence intensity for these cephalosporins are shown in Figure 6.3. A time-dependent fluorescence measurement of cefotaxime was done. The result shows that changes in fluorescence intensity were not significant when the cefotaxime concentration was 1 x 10^{-8} M (Figure 6.4). When the concentration of cefotaxime was at 5 x 10^{-8} M, the increase in fluorescence intensity could not achieve maximum value as at 10^{-6} M. When concentration was at 1 x 10^{-7} M, it took PenP_E166Cf about 500 s to achieve a maximum change in fluorescence intensity. In a high concentration such as 1 x 10^{-6} M, the fluorescence intensity increased to a maximum value within a few seconds.

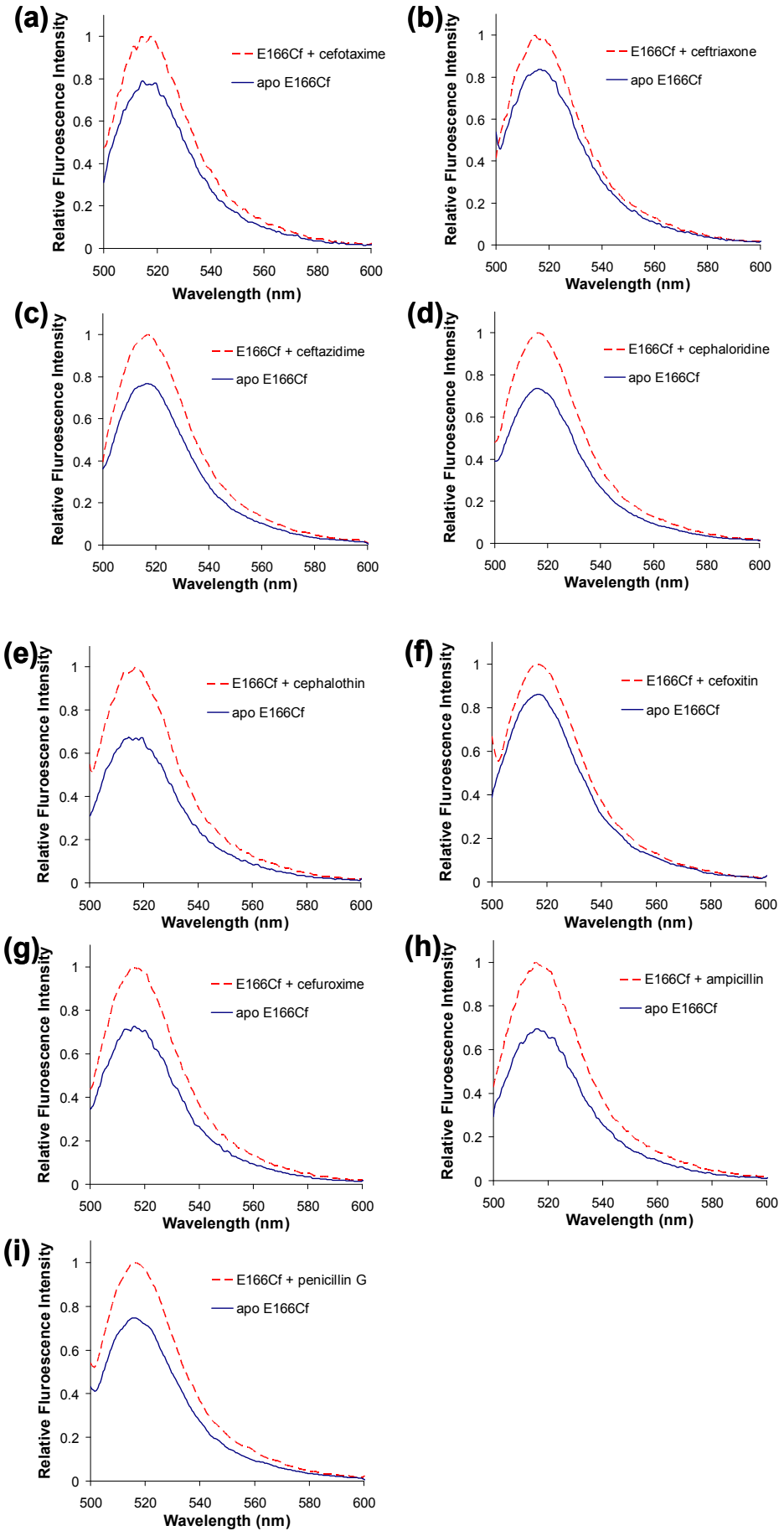
(a)
E166Cf + cefotaxime
apo E166Cf
(b)
E166Cf + ceftriaxone
apo E166Cf
(c)
E166Cf + ceftazidime
apo E166Cf
(d)
E166Cf + cephaloridine
apo E166Cf
(e)
E166Cf + cephalothin
apo E166Cf
(f)
E166Cf + cefoxitin
apo E166Cf
(g)
E166Cf + cefuroxime
apo E166Cf
(h)
E166Cf + ampicillin
apo E166Cf
(i)
E166Cf + penicillin G
apo E166Cf
Relative Fluroescence Intensity
Wavelength (nm)
0
0.2
0.4
0.6
0.8
1
500
520
540
560
580
600

Figure 6.2: Fluorescence spectra of PenP_E166Cf (0.1 μM) in the presence of 0.1 mM (a) cefotaxime, (b) ceftriaxone, (c) ceftazidime, (d) cephaloridine, (e) cephalothin, (f) cefoxitin, (g) cefuroxime, (h) ampicillin, and (i) penicillin G.

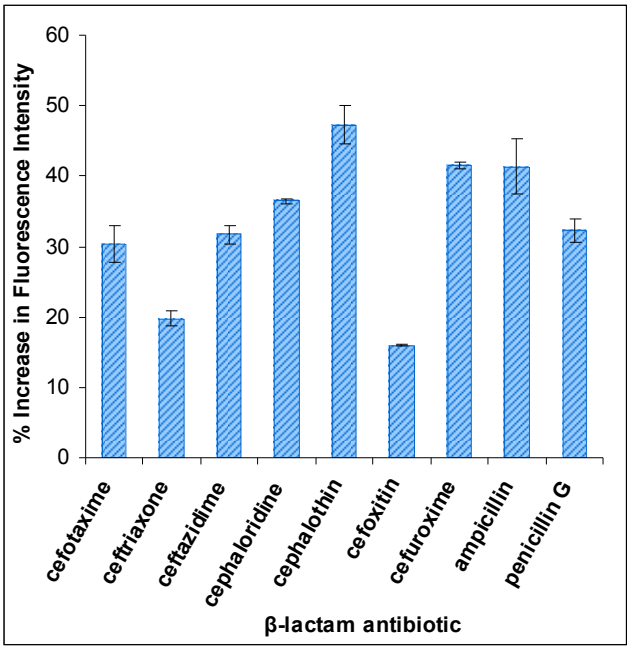

Figure 6.3: Percentage changes in fluorescence intensity upon addition of various cephalosporins. SD values were estimated using data from 3 measurements.

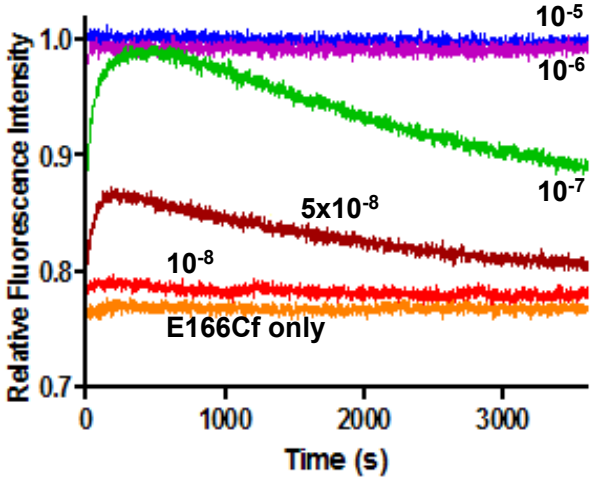

Figure 6.4: Time-dependent fluorescence spectra of PenP_E166Cf (0.1 μM) in the presence of 1 x 10^{-8} M, 5 x 10^{-8} M, 1 x 10^{-7} M, 1 x 10^{-6} M and 1 x 10^{-5} M cefotaxime.

6.3.3 Crystal structure of PenP_E166Cf

Crystals of PenP_E166Cf were grown by commercial screens from Hampton Research (Hampton Research, Aliso Viejo, California, USA). Small crystals were observed in CS10 after a few days. After optimization, a larger crystal was formed from the reservoir solution that contained 25% (w/v) PEG 4000, 0.1 M Hepes pH 7.2, 0.4 M NH_4Acetate and 0.2 M K_2HPO_4 from a protein concentration of 30 mg/ml. The crystal was tinted with yellow because of the presence of fluorophore. It was flash cooled with liquid nitrogen in the Rigaku MicroMax^{TM}-007HF X-ray machine (Figure 6.5). Diffraction data comprising 280 images were collected using an oscillation range of 0.5° and an exposure time of 240 s. Data were integrated and scaled by CrystalClear 1.3.5 SP2. The crystal belongs to the space group $P2_1$. The crystallographic data and refinement statistics are shown in Table 6.2. The crystal structure of PenP_E166Cf was determined by molecular replacement using the PDB entry 4BLM (Knox and Moews 1991) and refined at 2.2 Å. There were two molecules in an asymmetric unit. Several alternating rounds of refinement with Refmac5 and rebuilding with Coot in CCP4 program suite (Collaborative Computational Project, Number 4, 1994) converged with an R factor of 0.20 and a free R factor of 0.23. Fluorescein was built in molecule A by PRODRG (Schuttelkopf and van Aalten 2004). The structure of PenP_E166Cf was deposited in the PDB under accession code 3M2J. To confirm that the crystal was the labeled PenP_E166Cf, the fluorescence levels of the crystals were checked with the use of SDS/PAGE gel electrophoresis. Figure 6.6 shows the polyacrylamide gel and its corresponding fluorescence image. Protein with a correct mass (~ 30 kDa) with fluorescence signal was confirmed to be PenP_E166Cf.

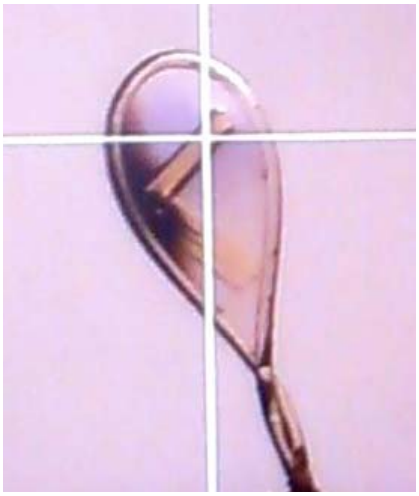

Figure 6.5: Crystal of PenP_E166Cf during flash cooling in the X-ray machine.

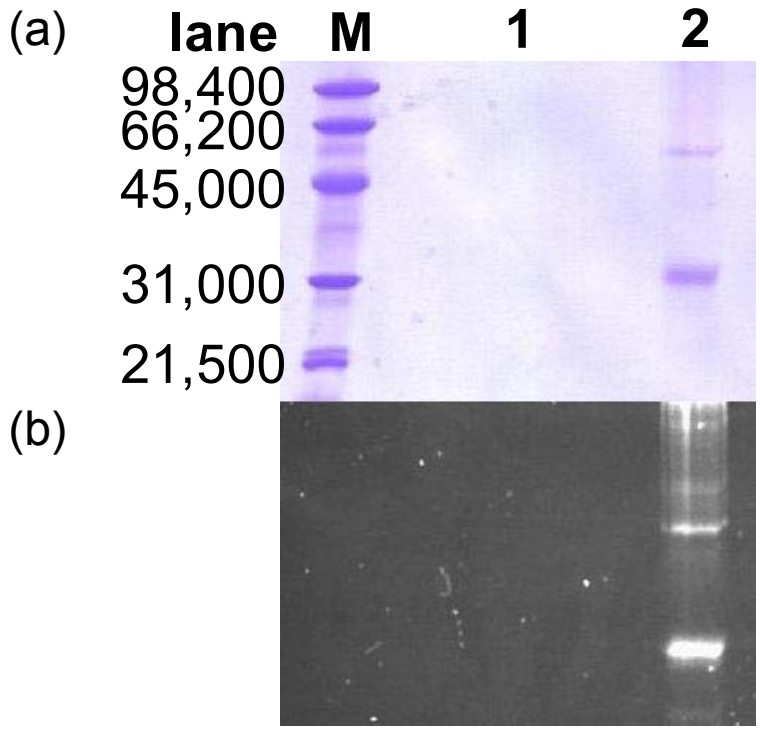

Figure 6.6: (a) 12% SDS/PAGE analysis of the purified crystal of PenP_E166Cf. M is the low-range marker: rabbit muscle phosphorylase b (97,400), bovine serum albumin (66,200), hen egg white ovalbumin (45,000), bovine carbonic anhydrase (31,000), soybean trypsin inhibitor (21,500); lane 1: final wash supernatant of the crystal; lane 2: Melted crystal of PenP_E166Cf. (b) Fluorescence image of the same polyacrylamide gel.

Table 6.2: X-ray data collection and structure refinement statistics for apo PenP_E166Cf and PenP_E166Cf in complex with cefotaxime

	E166Cf	E166Cf+cefotaxime
PDB code	3M2J	3M2K
Data collection		
Space group	$P2_1$	$P2_1$
Unit cell parameters (Å)		
a	43.3	43.5
b	92.3	91.4
c	66.3	66.1
β	104.82	104.52
Resolution range (Å)	52.0-2.15 (2.24-2.15)	45.0-2.80 (2.95-2.80)
No. of total reflections	79750	40611
No. of unique reflections	29537	12412
I/σ	7.1 (2.7)	6.3 (2.4)
Completeness (%)	97.0 (99.5)	99.8 (99.9)
R_{merge} (%)	9.7 (27.1)	11.8(32.0)
Structure refinement		
Resolution (Å)	50.0-2.20	45.0-2.80
R_{cryst}/R_{free} (%)	20.0/23.2	21.9/27.7
r.s.m.d. bonds (Å)/angles (°)	0.018/1.784	0.010/1.672
No. of reflections		
Working set	24217	11749
Test set	1291	647
No. of atoms		
Protein atoms	4011	3706
Water molecules	254	29
Average *B*-factor ($Å^2$)		
Main chain	24.70	16.96
Ligand molecules	48.40	42.46
Water	32.70	10.70

The overall crystal structure of a molecule of PenP_E166Cf is shown in a small picture on the left of Figure 6.7 (a). A scaled-up representation of the area containing the Ω-loop and active site is also shown nearby. It is the view of the f_o-f_c omit map with the refined molecular model of Phe165 to Asn170. The f_o-f_c electron density map was contoured at 2.0 σ. The modeled fluorescein-5-maleimide is displayed in green cylinder. However, the electron density for the fluorescein molecule is not well-defined. It is clear from the f_o-f_c omit map that the fluorescein is partly visible, especially around the connection site with the sulphur atom on Cys166 and the lower part with the three benzene rings, but there is no electron density in the middle part at any contour levels. In figure 6.7 (b), it is clear that the $2f_o$-f_c electron density for the side chains in the Ω-loop is of high quality. The calculation of the B factor by the CCP4 program suite shows that fluorescein-5-maleimide in chain A has the highest B factor (72.3) among all residues in the same molecule.

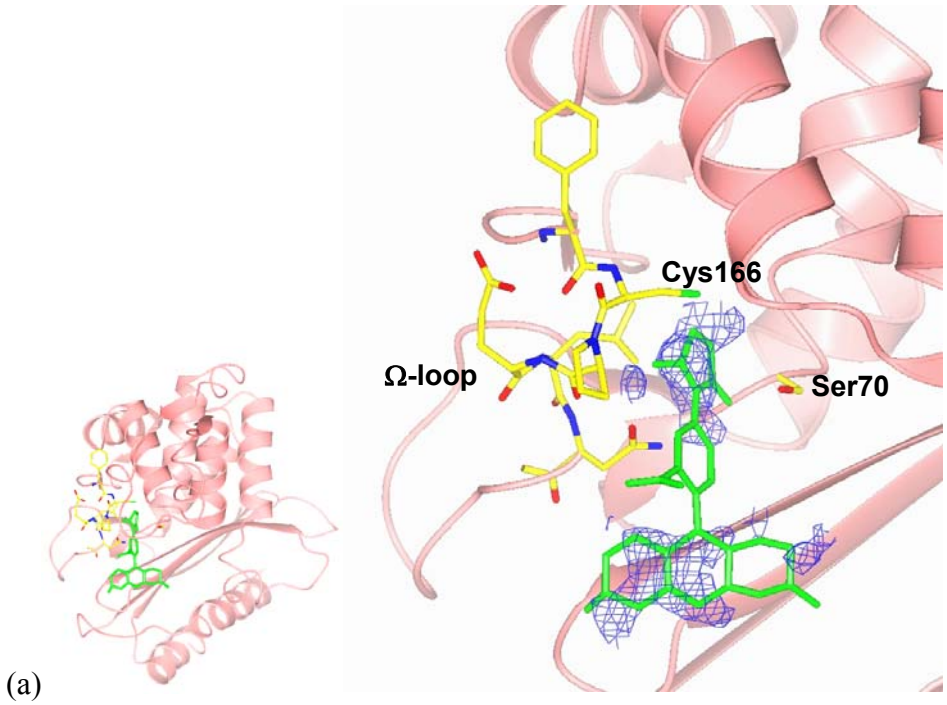

(a)

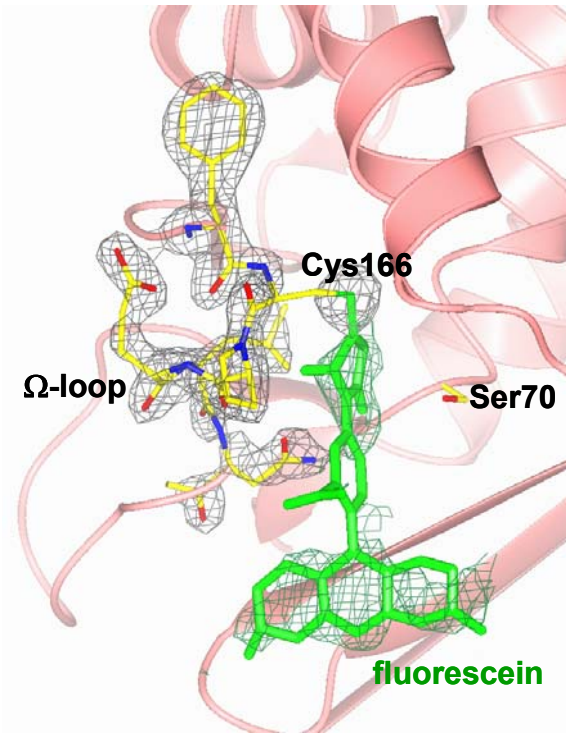

(b)

Figure 6.7: *(a)* f_o-f_c omit map of fluorescein-5-maleimide contoured at 2.0 σ and (b) $2f_o$-f_c map of Phe165 to Asn170 and fluorescein-5-maleimide contoured at 1.0 σ. Side chains of Phe165 to Asn170 and Ser70 are shown in cpk cylinder model. Fluorescein is shown in green cylinder model. The small picture on the left hand side in (a) is the scaled down version of the whole PenP_E166Cf molecule.

6.3.4 Crystal structure of PenP_E166Cf in complex with cefotaxime

The crystal structure of PenP_E166Cf in complex with cefotaxime was obtained by soaking the crystal of PenP_E166Cf in 0.01 M cefotaxime solution. After obtaining the crystal data, several alternating rounds of refinement with Refmac5 and rebuilding with Coot in the CCP4 program suite (Collaborative Computational Project, Number 4, 1994) converged with a R factor of 0.22 and a free R factor of 0.28. Cefotaxime was built in molecule A by PRODRG (Schuttelkopf and van Aalten 2004). The structure of PenP_E166Cf in complex with cefotaxime was deposited in the PDB under the accession code 3M2K.

The crystal structure of PenP_E166Cf in complex with cefotaxime shows that the overall structure for the main chain atoms are highly similar to that of the apo PenP_E166Cf. The electron density maps for most of the atoms are in high quality except in the Ω-loop region. It can be seen that the electron density is missing starting from Arg164 to Pro174. No fluorescein molecule is found in this structure. The f_o-f_c omit map of cefotaxime in PenP_E166Cf-cefotaxime complex contoured at 2.0 σ is shown in Figure 6.8. The whole cefotaxime molecule is obviously present and connected to the O^{γ} atom of Ser70.

Figure 6.9 shows the superimposition of the structure of spo PenP_E166Cf and PenP_E166Cf-cefotaxime. Due to the missing of the Ω-loop in the PenP_E166Cf-cefotaxime structure, the change of the position of the side chains before and after binding with cefotaxime cannot be interpreted. However, from the overlapping structures, it can be observed that the position of the fluorescein molecule before binding is occupied by the 7-amino substituent of

the cefotaxime after binding.

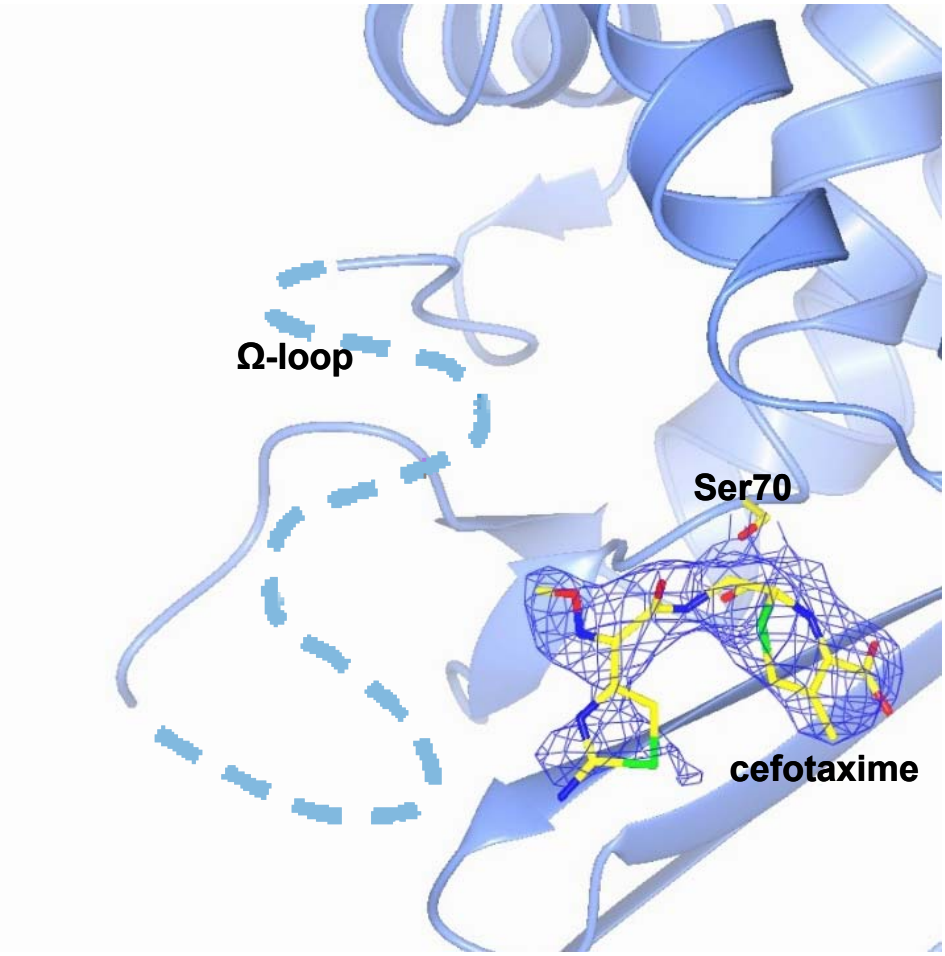

Figure 6.8: The f_o-f_c omit map of cefotaxime in PenP_E166Cf-cefotaxime complex contoured at 2.0 σ. Cefotaxime and Ser70 are shown in cpk cylinder model. The light blue dash line represents the distorted Arg164 to Pro174 due to the poor electron density.

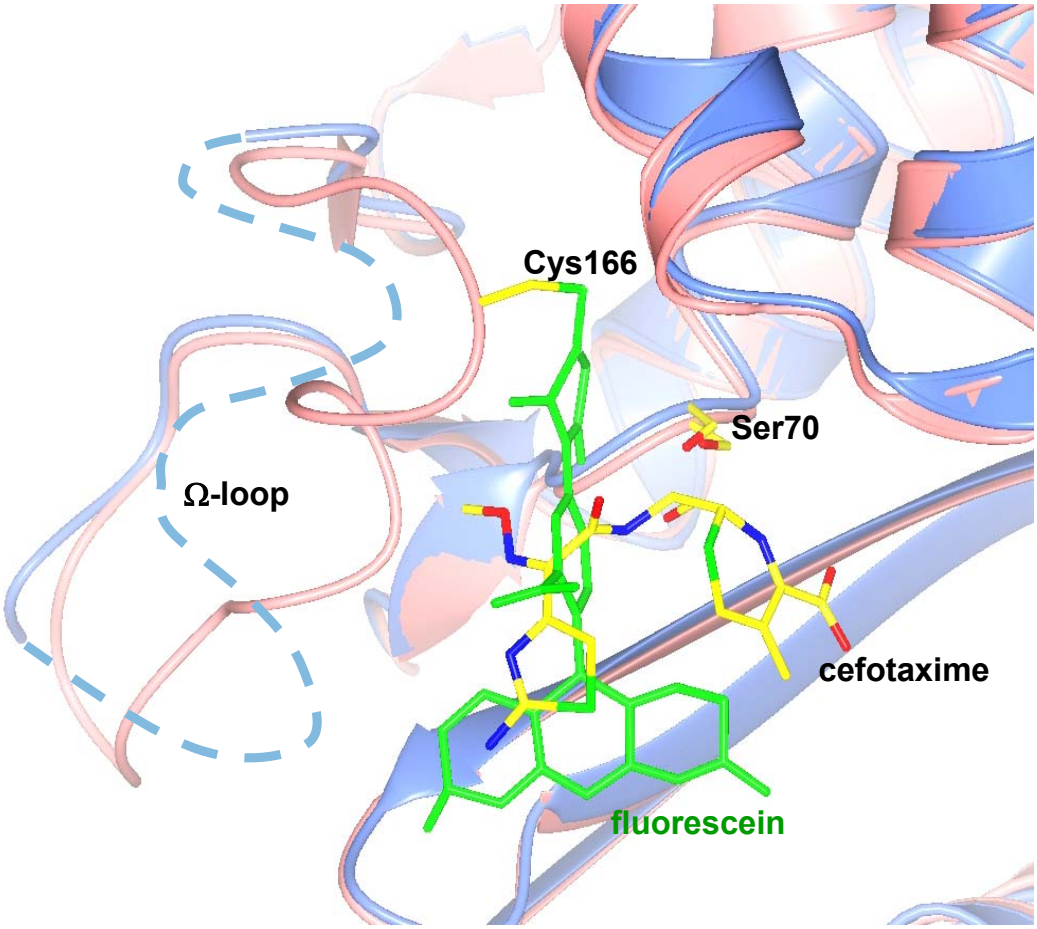

Figure 6.9: Overlaid structures of PenP_E166Cf-cefotaxime complex (blue) with apo PenP_E166Cf (pink). Cys166, Ser70 and cefotaxime are also shown in cpk cylinder model.

6.4 Discussion

6.4.1 Preparation of PenP_E166Cf

PenP_E166Cf was successfully prepared from PenP_E166C by labeling. No GdnHCl was needed to unfold the protein prior to the labeling process, which was different from the labeling of PenP_E166C by badan. When preparing PenP_E166Cb, a small amount of GdnHCl was essential for labeling to unfold the protein so that the thiol group of Cys166 could be more exposed to the solvent and the fluorophore could react with it more readily. Why labeling by fluorescein did not need to unfold the protein eventhough fluorescein has a larger size than badan? It seems that fluorescein-5-maleimide is a better fluorophore for labeling PenP_E166C, as the labeling efficiency does not depend on changes in labeling conditions, such as labeling duration, temperature and concentration of GdnHCl. This might be due to the different labeling mechanisms exhibited by fluroescein and badan: fluorescein undergoes an electrophilic addition (Means and Feeney 1990) while badan undergoes an electrophilic substitution (Bernatowicz and Matsueda 1986; Inman *et al.* 1991).

6.4.2 Fluorescence signals of PenP_E166Cf

The result of the fluorescence scanning spectra shows that all the cephalosporins tested were "signal-positive" towards PenP_E166Cf, with at least 20% fluorescence enhancement. It shows that PenP_E166Cf is a more universal biosensor than PenP_E166Cb, since PenP_E166Cb only detected the β-lactams selectively. Even for the β-lactams that generated poor signals in PenP_E166Cb (cephalothin, cephalodine, cefoxitin), PenP_E166Cf produced positive signals for them. For cephalodine and cephalothin, the fluorescence enhancements were more than 35%. Interestingly, the fluorescence changes of PenP_E166Cf for cefotaxime and ceftriaxone, which generated the highest fluorescence changes upon binding in PenP_E166Cb (~70%), were only about 30%. It seems that the fluorescein mechanism is different from the badan one, as E166Cf does not distinguish the oxyimino- and non-oxyimino cephalosporins. Moreover, the property of fluorescein is different from that of badan. This may be one of the reasons why some of the fluorescence signals generated by E166Cf were opposite to those by E166Cb.

6.4.3 Crystal structure of the apo PenP_E166Cf

The crystal structure of PenP_E166Cf shows that the Ω-loop after labeling with fluroescein-5-maleimide was highly similar to that in PenP_E166C. In the badan-labeled protein, the Ω-loop adapted a new conformation so that the upper part of it was rotated for about 180°. However, in PenP_E166Cf, no such a conformational change of the Ω-loop was observed. This might imply that when fluorescein was attached to the cysteine molecule, the intrinsic flexibility of the fluorescein might not affect the conformation of the Ω-loop. This result is supported by the kinetic data of PenPC_E166C, PenPC_E166Cf and PenPC_E166Cb for the hydrolysis of cefuroxime, which was determined by ESI-MS (Table 6.3) (Chan *et al.* 2008). The binding constant of E166C + cefuroxime was similar to that of E166Cf + cefuroxime, while it was significantly different from that of E166Cb + cefuroxime. The k_2/K_D of the badan labeled protein was about 150 times larger than that of the unlabeled protein. To explain this with the PenP crystal structure, it is inferred that the incorporation of badan molecule would induce a change in the conformation of the Ω-loop and increase the flexibility of the Ω-loop so that the binding of cephalosporins with large side chain will be much faster. In the fluorescein labeled protein, it is suggested that the flexibility of the Ω-loop would not change much upon the incorporation of the fluorescein molecule so that the binding rate of PenPC_E166Cf would not be as fast as that of PenPC_E166Cb. This can also be applied to the PenP_E166Cf structure and explain why the conformation of Ω-loop was highly similar to that of the unlabeled PenP_E166C in the crystal structure.

Table 6.3: Kinetic parameters of the PenPC_E166C, PenPC_E166Cf and PenPC_E166Cb for the hydrolysis of cefuroxime determined by ESI-MS. The kinetic data for E166C+cefuroxime and E166Cf+cefuroxime were previously published (Chan *et al.* 2008) while the data for E166Cb+cefuroxime are new.

	k_2 (s^{-1})	K_d (mM)	k_2/K_d (M^{-1} s^{-1})
E166C + cefuroxime	2.5 ± 0.2	2.9 ± 0.3	(0.9 ± 0.1) x 10^3
E166Cf + cefuroxime	1.9 ± 0.1	0.91 ± 0.09	(2.0 ± 0.2) x 10^3
E166Cb + cefuroxime	26.8 ± 2.3	0.20 ± 0.02	(134 ± 0.1) x 10^3

The flexibility of fluorescein-5-maleimide can be interpreted by the electron density map obtained in the structure. It is believed that the absence of fluorophore was a consequence of the highly dynamic nature of the fluorescein itself. However, the fluorescein was still modeled by hand in the most preferable position since it had nowhere to go as the protein interior was too crowded for the conjugation of a fluorescein molecule, which is about three times larger than the badan molecule. It is clear from the f_o-f_c electron density map that the fluorescein was not fully visible. There was no electron density in the middle part of the fluorescein at any contour levels that could have resulted from the reduced rigidity of the rotational moiety. The modeling result shows that fluorescein was adjacent to the active site pocket and moderately exposed to solvent. From the calculated B value by the CCP4 program suite, the fluroescein had the highest B factor among all residues because of its highly flexible property.

6.4.4 Crystal structure of PenP_E166Cf in complex with cefotaxime

The crystal structure of PenP_E166Cf-cefotaxime shows that the cefotaxime was successfully bound to the Ser70 in the active site. It is proved by the connected electron density between the O^{γ} atom of Ser70 and the C7 carbon atom of the cefotaxime. Nonetheless, there was no electron density observed for the fluorescein molecule and most of the residues in the Ω-loop. The electron density was absent starting from Arg164 to Pro174. Therefore the fluorescein failed to be built in this structure. It is inferred that after the binding of cefotaxime to the active site of the protein, the Ω-loop became highly flexible so that the whole Ω-loop was distorted in this crystal structure in both molecules A and B. This led to the high free R factor. The B factors calculated by the CCP4 program suite show that Glu163, Gly175 and Glu176, which were just next to the missing Ω-loop, had significantly higher B values than other residues. This implies that the distorted Ω-loop was indeed highly dynamic.

Although the fluorescein molecule in the PenP_E166Cf-cefotaxime complex was absent, the superimposition of two crystal structures (before and after binding with cefotaxime) could elucidate changes of the conformation in the local area upon binding with cefotaxime. It can be shown that the bound cefotaxime would collide with the lower part of the fluorescein molecule severely. The fluorescein on the flexible Ω-loop had to move away from the position where they collide. This led to a movement of the fluorescein to a new position, together with the movement of the flexible Ω-loop. Therefore, it is believed that the conformation of the Ω-loop after binding would be different from the original one. It is a good manifestation of the previous hypothesis that

fluorophore would move out from the active site and be more exposed to solvent upon binding with antibiotics (Chan *et al.* 2004). The fluorescein, covalently linked to the 166 position, could not be pushed to the interior region of the protein and consequently, it moved away from the active site cavity to avoid steric clash with the imcoming antibiotic and became more solvent exposed. The dramatic movement of the fluorescein led to an increase in its solvent accessible area and thus an increase in the fluorescence signal.

Fluorescein is a much larger molecule than badan. Therefore, it would be difficult for the covalently linked fluorescein to approach the interior of the protein. This might explain why the fluorescein was less sensitive to detect the local environmental changes induced by the binding of chemically distinct cephalosporins. This might be one of the factors to explain why the fluorescein gave enhancement in fluorescence intensity in all the cephalosporins tested but the badan only sensed them selectively. In other words, badan could sense the cephalosporins according to the structural difference of oxyimino- and non-oxyimino cephalosporins, while fluorescein could not distinguish the two types.

It is likely that in the biosensing mechanism of PenP_E166Cb, after the binding of the cefotaxime, the badan would be moved from the “near” position to the “far” position. However, the distance between the positions of “near” and “far” was small. Such a small difference would not be a significant factor for inducing a large change in the fluorescence signal. The fluorescence change was mainly due to the changing of the surrounding environment of the badan

molecule, while the change of the environment was attributed to the change of conformation of the Ω-loop that changed the local polarity. On the other hand, the fluorescein molecule was displaced by the incoming cefotaxime to a more solvent exposed position. However, it is highly likely that the Ω-loop would also become highly flexible and adopted different conformations upon binding with β-lactams, which might affect the local polarity of the fluorescein molecule. This would affect the change in fluorescence intensity. To investigate the detailed biosensing mechanism in the vicinity of the fluorescein, crystallization of PenP_E166Cf in complex with different β-lactams shoud be carried out in the future.

6.5 Concluding remarks

In conclusion, the fluorescein-labeled biosensor PenP_E166Cf was characterized with fluorescence spectrometry after addition of various cephalosporins. All the tested cephalosporins showed enhancement in fluorescence intensity after addition of the substrates to the biosensor protein solution. PenP_E166Cf did not differentiate the oxyimino and non-oxyimino cephalosporins as PenP_E166Cb did.

Crystal structures of the apo PenP_E166Cf and PenP_E166Cf complexed with cefotaxime were determined. The fluorescein molecule was not fully visible but the position of the fluorescein was predicted and built into the structure based on the broken block of electron density. PenP_E166Cf did not detect cephalosporins selectively because fluorescein was a larger molecule than badan and it would be displaced readily by the incoming antibiotic so that the fluorescein would be moved to a more solvent exposed area that generated an increase in the fluorescence intensity.

Chapter 7: Conclusions and suggestions for future research

The PenP β-lactamase mutant E166C has been successfully labeled with badan to form the biosensor PenP_E166Cb. The labeled mutant was characterized with fluorescence spectrometry after addition of different cephalosporins. About half of the tested β-lactam antibiotics showed significant enhancement in fluorescence intensity immediately after the binding of the substrates. PenP_E166Cb differentiated the oxyimino- and non-oxyimino-cephalosporins by generating significant enhancement in fluorescence intensity for oxyimino cephalosporins only. Kinetic study by mass spectrometry reveals that after conjugation of a badan fluorophore onto the Ω-loop of PenP β-lactamase, the binding rate of cefotaxime was significantly improved when compared to the badan-free enzyme. It is believed that the conjugation of badan increases the flexibility of Ω-loop, thus improving the binding of cephalosporins with large side chains. For example, the binding of cefotaxime to PenP_E166Cb was about 10 times faster compared to the unlabeled PenP_E166C.

Comparison of the crystal structures of PenP_E166C and PenP_E166Cb shows that the conjugation of a badan molecule to the cysteine residue at the 166 position caused a change in the conformation of the Ω-loop. The Ω-loop became more flexible and more amenable to the binding of cephalosporins with large side chains. Interestingly, the covalently linked badan exhibited two positions in the apo PenP_E166Cb structure, named as “near” and “far”, showing that badan is highly dynamic. The crystal structures of PenP_E166Cb complexed with two oxyimino-cephalosporins (cefotaxime and cefuroxime), and with three

non-oxyimino-cephalosporins (7-ACA, cephaloridine and cefoxitin) were determined. These structures showed that the significant fluorescence enhancement upon adding oxyimino-cephalosporins was not due to the spatial displacement of badan by the incoming antibiotic, but the change in configuration of key residues on the Ω-loop (e.g. Glu168 and Leu169) in proximity to the badan molecule. This small conformational change caused a change in the local polarity, which led to a change in the fluorescence signal. Non-oxyimino-cephalosporins do not have the branched methoxyimino moiety to displace Glu168, thus producing little, if any, fluorescence change. To better understand the biosensing mechanism, crystal structures of PenP_E166Cb complexed with ceftazidime, ceftriaxone and cephalothin could be resolved in the future. The structure of ceftriaxone-bound PenP_E166Cb should be the same as that with cefotaxime because the chemical structure of ceftriaxone and cefotaxime are identical after binding. Similarly, the structure of cephalothin-bound PenP_E166Cb should be the same as that with cephaloridine.

Several mutants of PenP β-lactamase were produced, including E166Cb/E168L, E166Cb/E168N, E166Cb/L169D, E166Cb/L169N, E166Cb/N104L and E166Cb/L169N/N104L, and their fluorescence profiles were compared with the PenP_E166Cb. These mutations caused significant reduction in fluorescence after binding of oxyimino-cephalosporins, whilst resulting in observable increase in fluorescence after binding of non-oxyimino-cephalosporins. It was also observed that a hydrophobic environment might be beneficial to the fluorescence enhancement induced by non-oxyimino-cephalosporins. Therefore, double mutants such as L169M/N104L or L169F/N104L, could be tested in the future. The results presented in this

thesis indicate that badan, covalently linked to the 166 position, is very sensitive to the local environment, because a small change in the local polarity can result in a very large difference in the fluorescence signal. This study can provide new insights into the design of a novel biosensor for β-lactams. The fluorescence pattern obtained from different combinations of β-lactams and PenP_E166Cb mutants might provide a profile for β-lactams with same structures after binding and a good method for identification of β-lactams in testing samples.

Another biosensor that we developed, namely PenP_E166Cf, generated fluorescence enhancements for all tested cephalosporins. Unlike PenP_E166Cb, PenP_E166Cf could not differentiate the oxyimino and non-oxyimino cephalosporins. As shown in the crystal structure of the apo PenP_E166Cf, the fluorescein molecule was only partly visible but the position of the fluorescein could be predicted. From the crystal structure of PenP_E166Cf in complex with cefotaxime, it can be seen that the incoming cefotaxime would clash severely with the fluorescein molecule. Therefore, PenP_E166Cf did not detect cephalosporins selectively because fluorescein is a large molecule that would be displaced readily by the incoming antibiotic. The fluorescein would move to a more solvent-exposed area, thus generating an increase in the fluorescence intensity.

Appendix I

Protein sequences of all mutants of 6xHis_TEV_PenP_E166C in this project

6xHis_TEV_PenP_E166C:

6XHis-tag TEV site

HHHHHHENLYFQMKTEMKDDFAKLEEQFDAKLGIFALDTGTNRTVA
YRPDERFAFA STIKALTVGVLLQQKSIEDL NQRITYTRDD LVNYNPI
TEK HVDTGMTLKELADASLRYSDNAAQNLILKQIGGPESLKKELRKI
E166C
GDEVTNPERFCPELNEVNPGETQDTSTARALVTSLR AFALEDKLPS
EKRELLIDWMKRNTTGDALIRAGVPDGWEVADKTGAASYGTRNDIA
IIWPPKGDPVVLAVLSSRDKKDAKYDDKLIAEATKVVMKALNMNGK

6xHis_TEV_PenP_E166C/E168L:

6xHis-tag TEV site

HHHHHHENLYFQMKTEMKDDFAKLEEQFDAKLGIFALDTGTNRTVA
YRPDERFAFA STIKALTVGVLLQQKSIEDL NQRITYTRDD LVNYNPI
TEK HVDTGMTLKELADASLRYSDNAAQNLILKQIGGPESLKKELRKI
E168L
GDEVTNPERFCPLLNEVNPGETQDTSTARALVTSLR AFALEDKLPS
EKRELLIDWMKRNTTGDALIRAGVPDGWEVADKTGAASYGTRNDIA
IIWPPKGDPVVLAVLSSRDKKDAKYDDKLIAEATKVVMKALNMNGK

6xHis_TEV_PenP_E166C/E168N:

6xHis-tag TEV site

HHHHHHENLYFQMKTEMKDDFAKLEEQFDAKLGIFALDTGTNRTVA
YRPDERFAFA STIKALTVGVLLQQKSIEDL NQRITYTRDD LVNYNPI
TEK HVDTGMTLKELADASLRYSDNAAQNLILKQIGGPESLKKELRKI
GDEVTNPERFCPNLNEVNPGETQDTSTARALVTSLR AFALEDKLPS
EKRELLIDWMKRNTTGDALIRAGVPDGWEVADKTGAASYGTRNDIA
IIWPPKGDPVVLAVLSSRDKKDAKYDDKLIAEATKVVMKALNMNGK

E168N

6xHis_TEV_PenP_E166C/L169D:

6xHis-tag TEV site

HHHHHHENLYFQMKTEMKDDFAKLEEQFDAKLGIFALDTGTNRTVA
YRPDERFAFA STIKALTVGVLLQQKSIEDL NQRITYTRDD LVNYNPI
TEK HVDTGMTLKELADASLRYSDNAAQNLILKQIGGPESLKKELRKI
GDEVTNPERFCPEDNEVNPGETQDTSTARALVTSLR AFALEDKLPS
EKRELLIDWMKRNTTGDALIRAGVPDGWEVADKTGAASYGTRNDIA
IIWPPKGDPVVLAVLSSRDKKDAKYDDKLIAEATKVVMKALNMNGK

L169D

6xHis_TEV_PenP_E166C/L169N

6xHis-tag TEV site

HHHHHHENLYFQMKTEMKDDFAKLEEQFDAKLGIFALDTGTNRTVA
YRPDERFAFA STIKALTVGVLLQQKSIEDL NQRITYTRDD LVNYNPI
TEK HVDTGMTLKELADASLRYSDNAAQNLILKQIGGPESLKKELRKI
GDEVTNPERFCPENNEVNPGETQDTSTARALVTSLR AFALEDKLPS
EKRELLIDWMKRNTTGDALIRAGVPDGWEVADKTGAASYGTRNDIA
IIWPPKGDPVVLAVLSSRDKKDAKYDDKLIAEATKVVMKALNMNGK

L169N

6xHis_TEV_PenP_E166C/N104L:

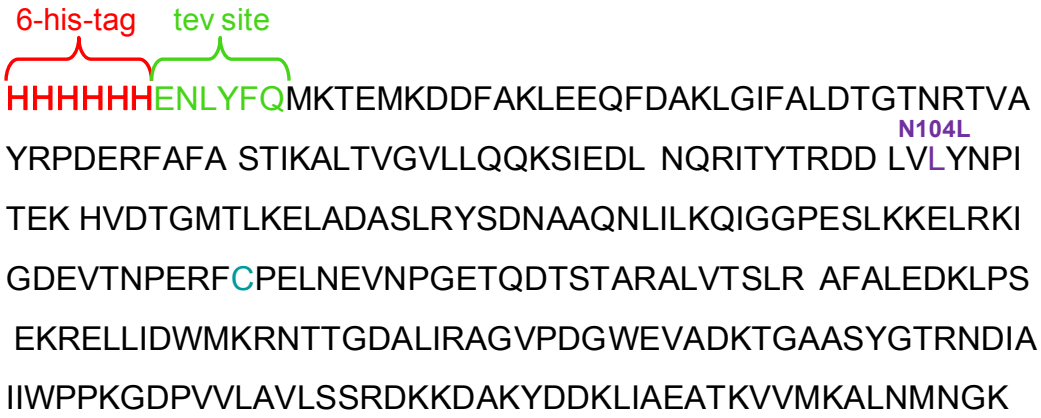

6xHis_TEV_PenP_E166C/L169N/N104L:

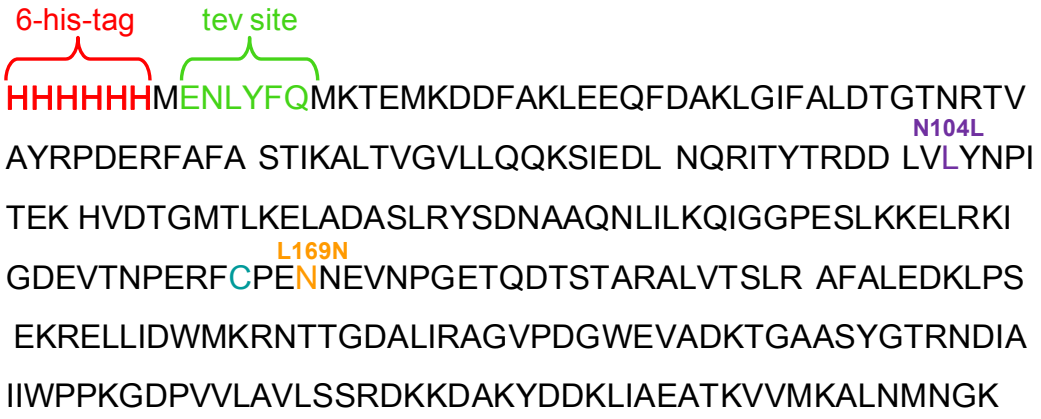

Appendix II

Plasmid map of 6xHis_TEV_PenP_E166C/L169N/N104L:

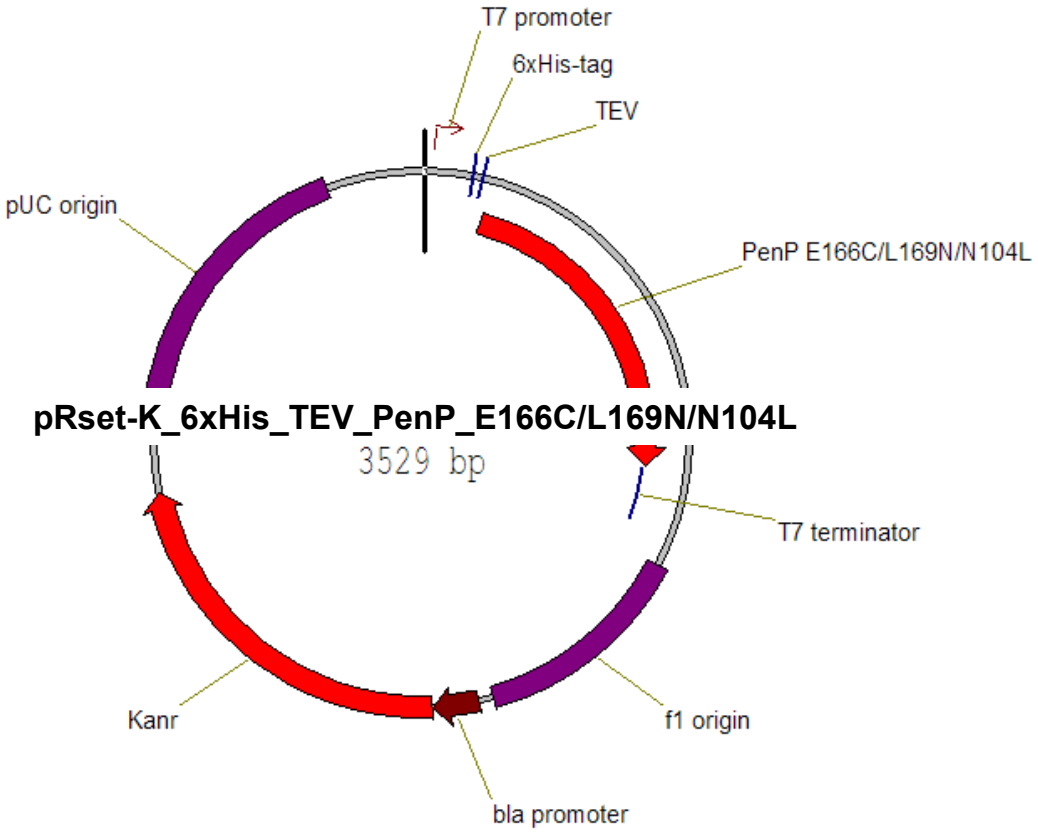

Appendix III

Crystal Screen Formulation

Hampton Research - Copyright 2006

Reagent #	[Salt 1]	[Salt 1] units	Salt	[Buffer]	[Buffer] units	Buffer	pH	Reagent #	[Precipitant 1]	[Ppt 1] units	Precipitant 1	[Ppt 2]	[Ppt 2] units	Precipitant 2
1	0.02	M	Calcium chloride dihydrate	0.1	M	Sodium acetate trihydrate	4.6	1	30	%v/v	(+/-)-2-Methyl-2,4-pentanediol			
2								2	0.4	M	Potassium sodium tartrate tetrahydrate			
3								3	0.4	M	Ammonium phosphate monobasic			
4				0.1	M	Tris hydrochloride	8.5	4	2	M	Ammonium sulfate			
5	0.2	M	Sodium citrate tribasic dihydrate	0.1	M	HEPES sodium	7.5	5	30	%v/v	(+/-)-2-Methyl-2,4-pentanediol			
6	0.2	M	Magnesium chloride hexahydrate	0.1	M	Tris hydrochloride	8.5	6	30	%w/v	Polyethylene glycol 4,000			
7				0.1	M	Sodium cacodylate trihydrate	6.5	7	1.4	M	Sodium acetate trihydrate			
8	0.2	M	Sodium citrate tribasic dihydrate	0.1	M	Sodium cacodylate trihydrate	6.5	8	30	%v/v	2-Propanol			
9	0.2	M	Ammonium acetate	0.1	M	Sodium citrate tribasic dihydrate	5.6	9	30	%w/v	Polyethylene glycol 4,000			
10	0.2	M	Ammonium acetate	0.1	M	Sodium acetate trihydrate	4.6	10	30	%w/v	Polyethylene glycol 4,000			
11				0.1	M	Sodium citrate tribasic dihydrate	5.6	11	1	M	Ammonium phosphate monobasic			
12	0.2	M	Magnesium chloride hexahydrate	0.1	M	HEPES sodium	7.5	12	30	%v/v	2-Propanol			
13	0.2	M	Sodium citrate tribasic dihydrate	0.1	M	Tris hydrochloride	8.5	13	30	%v/v	Polyethylene glycol 400			
14	0.2	M	Calcium chloride dihydrate	0.1	M	HEPES sodium	7.5	14	28	%v/v	Polyethylene glycol 400			
15	0.2	M	Ammonium sulfate	0.1	M	Sodium cacodylate trihydrate	6.5	15	30	%w/v	Polyethylene glycol 8,000			
16				0.1	M	HEPES sodium	7.5	16	1.5	M	Lithium sulfate monohydrate			
17	0.2	M	Lithium sulfate monohydrate	0.1	M	Tris hydrochloride	8.5	17	30	%w/v	Polyethylene glycol 4,000			
18	0.2	M	Magnesium acetate tetrahydrate	0.1	M	Sodium cacodylate trihydrate	6.5	18	20	%w/v	Polyethylene glycol 8,000			
19	0.2	M	Ammonium acetate	0.1	M	Tris hydrochloride	8.5	19	30	%v/v	2-Propanol			
20	0.2	M	Ammonium sulfate	0.1	M	Sodium acetate trihydrate	4.6	20	25	%w/v	Polyethylene glycol 4,000			
21	0.2	M	Magnesium acetate tetrahydrate	0.1	M	Sodium cacodylate trihydrate	6.5	21	30	%v/v	(+/-)-2-Methyl-2,4-pentanediol			
22	0.2	M	Sodium acetate trihydrate	0.1	M	Tris hydrochloride	8.5	22	30	%w/v	Polyethylene glycol 4,000			
23	0.2	M	Magnesium chloride hexahydrate	0.1	M	HEPES sodium	7.5	23	30	%v/v	Polyethylene glycol 400			
24	0.2	M	Calcium chloride dihydrate	0.1	M	Sodium acetate trihydrate	4.6	24	20	%v/v	2-Propanol			
25				0.1	M	Imidazole	6.5	25	1	M	Sodium acetate trihydrate			
26	0.2	M	Ammonium acetate	0.1	M	Sodium citrate tribasic dihydrate	5.6	26	30	%v/v	(+/-)-2-Methyl-2,4-pentanediol			
27	0.2	M	Sodium citrate tribasic dihydrate	0.1	M	HEPES sodium	7.5	27	20	%v/v	2-Propanol			
28	0.2	M	Sodium acetate trihydrate	0.1	M	Sodium cacodylate trihydrate	6.5	28	30	%w/v	Polyethylene glycol 8,000			
29				0.1	M	HEPES sodium	7.5	29	0.8	M	Potassium sodium tartrate tetrahydrate			
30	0.2	M	Ammonium sulfate					30	30	%w/v	Polyethylene glycol 8,000			
31	0.2	M	Ammonium sulfate					31	30	%w/v	Polyethylene glycol 4,000			
32								32	2	M	Ammonium sulfate			
33								33	4	M	Sodium formate			
34				0.1	M	Sodium acetate trihydrate	4.6	34	2	M	Sodium formate			
35				0.1	M	HEPES sodium	7.5	35	0.8	M	Sodium phosphate monobasic monohydra	0.8	M	Potassium phosphate monobasic
36				0.1	M	Tris hydrochloride	8.5	36	8	%w/v	Polyethylene glycol 8,000			
37				0.1	M	Sodium acetate trihydrate	4.6	37	8	%w/v	Polyethylene glycol 4,000			
38				0.1	M	HEPES sodium	7.5	38	1.4	M	Sodium citrate tribasic dihydrate			
39				0.1	M	HEPES sodium	7.5	39	2	%v/v	Polyethylene glycol 400	2	M	Ammonium sulfate
40				0.1	M	Sodium citrate tribasic dihydrate	5.6	40	20	%v/v	2-Propanol	20	%w/v	Polyethylene glycol 4,000
41				0.1	M	HEPES sodium	7.5	41	10	%v/v	2-Propanol	20	%w/v	Polyethylene glycol 4,000
42	0.05	M	Potassium phosphate monobasic					42	20	%w/v	Polyethylene glycol 8,000			
43								43	30	%w/v	polyethylene glycol 1500			
44								44	0.2	M	magnesium formate dihydrate			
45	0.2	M	Zinc acetate dihydrate	0.1	M	Sodium cacodylate trihydrate	6.5	45	18	%w/v	Polyethylene glycol 8,000			
46	0.2	M	Calcium acetate hydrate	0.1	M	Sodium cacodylate trihydrate	6.5	46	18	%w/v	Polyethylene glycol 8,000			
47				0.1	M	Sodium acetate trihydrate	4.6	47	2	M	Ammonium sulfate			
48				0.1	M	Tris hydrochloride	8.5	48	2	M	Ammonium phosphate monobasic			
49	1	M	Lithium sulfate monohydrate					49	2	%w/v	Polyethylene glycol 8,000			
50	0.5	M	Lithium sulfate monohydrate					50	15	%w/v	Polyethylene glycol 8,000			

Appendix III (cont')

Crystal Screen 2 Formulation

Hampton Research - Copyright 2006

Reagent #	[Salt 1]	[Salt 1] units	Salt	[Buffer]	[Buffer] units	Buffer	pH	Reagent #	[Precipitant 1]	[Ppt 1] units	Precipitant 1	[Ppt 2]	[Ppt 2] units	Precipitant 2
1	2.0	M	Sodium chloride					1	10	% w/v	Polyethylene glycol 6,000			
2	0.5	M	Sodium chloride					2	0.01	M	Hexadecyltrimethylammonium bromide			
	0.01	M	Magnesium chloride hexahydrate											
3								3	25	% v/v	Ethylene glycol			
4								4	35	% v/v	1,4-Dioxane			
5	2.0	M	Ammonium sulfate					5	5	% v/v	2-Propanol			
6								6	1	M	Imidazole pH 7.0			
7								7	10	% w/v	Polyethylene glycol 1,000	10	% w/v	Polyethylene glycol 8,000
8	1.5	M	Sodium chloride					8	10	% v/v	Ethanol			
9				0.1	M	Sodium acetate trihydrate	4.6	9	2	M	Sodium chloride			
10	0.2	M	Sodium chloride	0.1	M	Sodium acetate trihydrate	4.6	10	30	% v/v	(+/-)-2-Methyl-2,4-pentanediol			
11	0.01	M	Cobalt (II) chloride hexahydrate	0.1	M	Sodium acetate trihydrate	4.6	11	1	M	1,6-Hexanediol			
12	0.1	M	Cadmium chloride hydrate	0.1	M	Sodium acetate trihydrate	4.6	12	30	% v/v	Polyethylene glycol 400			
13	0.2	M	Ammonium sulfate	0.1	M	Sodium acetate trihydrate	4.6	13	30	% w/v	Polyethylene glycol monomethyl ether 2,000			
14	0.2	M	Potassium sodium tartrate tetrahydrate	0.1	M	Sodium citrate tribasic dihydrate	5.6	14	2	M	Ammonium sulfate			
15	0.5	M	Ammonium sulfate	0.1	M	Sodium citrate tribasic dihydrate	5.6	15	1	M	Lithium sulfate monohydrate			
16	0.5	M	Sodium chloride	0.1	M	Sodium citrate tribasic dihydrate	5.6	16	2	% v/v	Ethylene imine Polymer			
17				0.1	M	Sodium citrate tribasic dihydrate	5.6	17	35	% v/v	tert-Butanol			
18	0.01	M	Iron (III) chloride hexahydrate	0.1	M	Sodium citrate tribasic dihydrate	5.6	18	10	% v/v	Jeffamine M-600			
19				0.1	M	Sodium citrate tribasic dihydrate	5.6	19	2.5	M	1,6-Hexanediol			
20				0.1	M	MES monohydrate	6.5	20	1.6	M	Magnesium sulfate heptahydrate			
21	0.1	M	Sodium phosphate monobasic monohydrate	0.1	M	MES monohydrate	6.5	21	2	M	Sodium chloride			
	0.1	M	Potassium phosphate monobasic											
22				0.1	M	MES monohydrate	6.5	22	12	% w/v	Polyethylene glycol 20,000			
23	1.6	M	Ammonium sulfate	0.1	M	MES monohydrate	6.5	23	10	% v/v	1,4-Dioxane			
24	0.05	M	Cesium chloride	0.1	M	MES monohydrate	6.5	24	30	% v/v	Jeffamine M-600			
25	0.01	M	Cobalt (II) chloride hexahydrate	0.1	M	MES monohydrate	6.5	25	1.8	M	Ammonium sulfate			
26	0.2	M	Ammonium sulfate	0.1	M	MES monohydrate	6.5	26	30	% w/v	Polyethylene glycol monomethyl ether 5,000			
27	0.01	M	Zinc sulfate heptahydrate	0.1	M	MES monohydrate	6.5	27	25	% v/v	Polyethylene glycol monomethyl ether 550			
28								28	1.6	M	Sodium citrate tribasic dihydrate pH 6.5			
29	0.5	M	Ammonium sulfate	0.1	M	HEPES	7.5	29	30	% v/v	(+/-)-2-Methyl-2,4-pentanediol			
30				0.1	M	HEPES	7.5	30	10	% w/v	Polyethylene glycol 6,000	5	% v/v	(+/-)-2-Methyl-2,4-pentanediol
31				0.1	M	HEPES	7.5	31	20	% v/v	Jeffamine M-600			
32	0.1	M	Sodium chloride	0.1	M	HEPES	7.5	32	1.6	M	Ammonium sulfate			
33				0.1	M	HEPES	7.5	33	2	M	Ammonium formate			
34	0.05	M	Cadmium sulfate hydrate	0.1	M	HEPES	7.5	34	1	M	Sodium acetate trihydrate			
35				0.1	M	HEPES	7.5	35	70	% v/v	(+/-)-2-Methyl-2,4-pentanediol			
36				0.1	M	HEPES	7.5	36	4.3	M	Sodium chloride			
37				0.1	M	HEPES	7.5	37	10	% w/v	Polyethylene glycol 8,000	8	% v/v	Ethylene glycol
38				0.1	M	HEPES	7.5	38	20	% w/v	Polyethylene glycol 10,000			
39	0.2	M	Magnesium chloride hexahydrate	0.1	M	Tris	8.5	39	3.4	M	1,6-Hexanediol			
40				0.1	M	Tris	8.5	40	25	% v/v	tert-Butanol			
41	0.01	M	Nickel (II) chloride hexahydrate	0.1	M	Tris	8.5	41	1	M	Lithium sulfate monohydrate			
42	1.5	M	Ammonium sulfate	0.1	M	Tris	8.5	42	12	% v/v	Glycerol			
43	0.2	M	Ammonium phosphate monobasic	0.1	M	Tris	8.5	43	50	% v/v	(+/-)-2-Methyl-2,4-pentanediol			
44				0.1	M	Tris	8.5	44	20	% v/v	Ethanol			
45	0.01	M	Nickel (II) chloride hexahydrate	0.1	M	Tris	8.5	45	20	% w/v	Polyethylene glycol monomethyl ether 2,000			
46	0.1	M	Sodium chloride	0.1	M	BICINE	9.0	46	20	% v/v	Polyethylene glycol monomethyl ether 550			
47				0.1	M	BICINE	9.0	47	2	M	Magnesium chloride hexahydrate			
48				0.1	M	BICINE	9.0	48	2	% v/v	1,4-Dioxane	10	% w/v	Polyethylene glycol 20,000

References

Adachi, H., Ohta, T., and Matsuzawa, H. 1991. Site-directed mutants, at position 166, of RTEM-1 β-lactamase that form a stable acyl-enzyme intermediate with penicillin. *J Biol Chem* 266: 3186-3191.

Adachi, H., Ohta, T., and Matsuzawa, H. 1991. Site-directed mutants, at position 166, of RTEM-1 beta-lactamase that form a stable acyl-enzyme intermediate with penicillin. *J Biol Chem* **266:** 3186-3191.

Ayad, M.M., Shalaby, A.A., Abdellatef, H.E., and Elsaid, H.M. 1999. Spectrophotometric determination of certain cephalosporins through oxidation with cerium(IV) and 1-chlorobenzotriazole. *J Pharm Biomed Anal* **20:** 557-564.

Banerjee, S., Pieper, U., Kapadia, G., Pannell, L.K., and Herzberg, O. 1998. Role of the omega-loop in the activity, substrate specificity, and structure of class A beta-lactamase. *Biochemistry* **37:** 3286-3296.

Bernatowicz, M.S., and Matsueda, G.R. 1986. Preparation of peptide-protein immunogens using N-succinimidyl bromoacetate as a heterobifunctional crosslinking reagent. *Anal Biochem* **155:** 95-102.

Bigelow, D.J., and Inesi, G. 1991. Frequency-domain fluorescence spectroscopy resolves the location of maleimide-directed spectroscopic probes within the tertiary structure of the Ca-ATPase of sarcoplasmic reticulum. *Biochemistry* **30:** 2113-2125.

Bonomo, R.A., and Rice, L.B. 1999. Inhibitor resistant class A beta-lactamases. *Front Biosci* **4:** e34-41.

Brown, N.G., Shanker, S., Prasad, B.V., and Palzkill, T. 2009. Structural and biochemical evidence that a TEM-1 beta-lactamase N170G active site

mutant acts via substrate-assisted catalysis. *J Biol Chem* **284:** 33703-33712.

Brown, R.P., Aplin, R.T., and Schofield, C.J. 1996. Inhibition of TEM-2 beta-lactamase from Escherichia coli by clavulanic acid: observation of intermediates by electrospray ionization mass spectrometry. *Biochemistry* **35:** 12421-12432.

Caselli, E., Powers, R.A., Blasczcak, L.C., Wu, C.Y., Prati, F., and Shoichet, B.K. 2001. Energetic, structural, and antimicrobial analyses of beta-lactam side chain recognition by beta-lactamases. *Chem Biol* **8:** 17-31.

Chan, P.H., Chan, K.C., Liu, H.B., Chung, W.H., Leung, Y.C., and Wong, K.Y. 2005. Fluorescein-labeled beta-lactamase mutant for high-throughput screening of bacterial beta-lactamases against beta-lactam antibiotics. *Anal Chem* **77:** 5268-5276.

Chan, P.H., Liu, H.B., Chen, Y.W., Chan, K.C., Tsang, C.W., Leung, Y.C., and Wong, K.Y. 2004. Rational design of a novel fluorescent biosensor for beta-lactam antibiotics from a class A beta-lactamase. *J Am Chem Soc* **126:** 4074-4075.

Chan, P.H., So, P.K., Ma, D.L., Zhao, Y., Lai, T.S., Chung, W.H., Chan, K.C., Yiu, K.F., Chan, H.W., Siu, F.M., *et al.* 2008. Fluorophore-labeled beta-lactamase as a biosensor for beta-lactam antibiotics: a study of the biosensing process. *J Am Chem Soc* **130:** 6351-6361.

Chen, C.C., and Herzberg, O. 1999. Relocation of the catalytic carboxylate group in class A beta-lactamase: the structure and function of the mutant enzyme Glu166-->Gln:Asn170-->Asp. *Protein Eng* **12:** 573-579.

Chen, C.C., and Herzberg, O. 2001. Structures of the acyl-enzyme complexes of the Staphylococcus aureus beta-lactamase mutant Glu166Asp:Asn170Gln

with benzylpenicillin and cephaloridine. *Biochemistry* **40:** 2351-2358.

Chen, Y., Bonnet, R., and Shoichet, B.K. 2007. The acylation mechanism of CTX-M beta-lactamase at 0.88 a resolution. *J Am Chem Soc* **129:** 5378-5380.

Chu, X., Wu, L., Liu, X., Li, N., and Li, D. 2008. Detection of broad-spectrum aminoglycoside antibiotics through fluorescence-labeling aminoglycoside acetyltransferase(6')-Ii. *Anal Biochem* **376:** 144-150.

Cohen, B.E., McAnaney, T.B., Park, E.S., Jan, Y.N., Boxer, S.G., and Jan, L.Y. 2002. Probing protein electrostatics with a synthetic fluorescent amino acid. *Science* **296:** 1700-1703.

Cohen, B.E., Pralle, A., Yao, X., Swaminath, G., Gandhi, C.S., Jan, Y.N., Kobilka, B.K., Isacoff, E.Y., and Jan, L.Y. 2005. A fluorescent probe designed for studying protein conformational change. *Proc Natl Acad Sci U S A* **102:** 965-970.

Crichlow, G.V., Kuzin, A.P., Nukaga, M., Mayama, K., Sawai, T., and Knox, J.R. 1999. Structure of the extended-spectrum class C beta-lactamase of Enterobacter cloacae GC1, a natural mutant with a tandem tripeptide insertion. *Biochemistry* **38:** 10256-10261.

de Lorimier, R.M., Smith, J.J., Dwyer, M.A., Looger, L.L., Sali, K.M., Paavola, C.D., Rizk, S.S., Sadigov, S., Conrad, D.W., Loew, L., *et al.* 2002. Construction of a fluorescent biosensor family. *Protein Sci* **11:** 2655-2675.

Di Guilmi, A.M., Mouz, N., Petillot, Y., Forest, E., Dideberg, O., and Vernet, T. 2000. Deacylation kinetics analysis of Streptococcus pneumoniae penicillin-binding protein 2x mutants resistant to beta-lactam antibiotics using electrospray ionization- mass spectrometry. *Anal Biochem* **284:**

240-246.

Dideberg, O., Libert, M., Frere, J.M., Charlier, P., Zhao, H., and Knox, J.R. 1985. Crystallization and preliminary X-ray data for the exocellular beta-lactamase of Bacillus licheniformis 749/C. *J Mol Biol* **181:** 145-146.

Donato, L.J., and Noy, N. 2006. A fluorescence-based method for analyzing retinoic acid in biological samples. *Anal Biochem* **357:** 249-256.

Drawz, S.M., Bethel, C.R., Hujer, K.M., Hurless, K.N., Distler, A.M., Caselli, E., Prati, F., and Bonomo, R.A. 2009. The role of a second-shell residue in modifying substrate and inhibitor interactions in the SHV beta-lactamase: a study of ambler position Asn276. *Biochemistry* **48:** 4557-4566.

Eidam, O., Romagnoli, C., Caselli, E., Babaoglu, K., Pohlhaus, D.T., Karpiak, J., Bonnet, R., Shoichet, B.K., and Prati, F. Design, synthesis, crystal structures, and antimicrobial activity of sulfonamide boronic acids as beta-lactamase inhibitors. *J Med Chem* **53:** 7852-7863.

Escobar, W.A., Tan, A.K., Lewis, E.R., and Fink, A.L. 1994. Site-directed mutagenesis of glutamate-166 in beta-lactamase leads to a branched path mechanism. *Biochemistry* **33:** 7619-7626.

Faraci, W.S., and Pratt, R.F. 1986. Mechanism of inhibition of RTEM-2 beta-lactamase by cephamycins: relative importance of the 7 alpha-methoxy group and the 3' leaving group. *Biochemistry* **25:** 2934-2941.

Fisher, J.F., Meroueh, S.O., and Mobashery, S. 2005. Bacterial resistance to beta-lactam antibiotics: compelling opportunism, compelling opportunity. *Chem Rev* **105:** 395-424.

Fisher, J.F., and Mobashery, S. 2009. Three decades of the class A beta-lactamase acyl-enzyme. *Curr Protein Pept Sci* **10:** 401-407.

Fitter, J., and Haber-Pohlmeier, S. 2004. Structural stability and unfolding properties of thermostable bacterial alpha-amylases: a comparative study of homologous enzymes. *Biochemistry* **43:** 9589-9599.

Fonze, E., Vanhove, M., Dive, G., Sauvage, E., Frere, J.M., and Charlier, P. 2002. Crystal structures of the Bacillus licheniformis BS3 class A beta-lactamase and of the acyl-enzyme adduct formed with cefoxitin. *Biochemistry* **41:** 1877-1885.

Frate, M.C., Lietz, E.J., Santos, J., Rossi, J.P., Fink, A.L., and Ermacora, M.R. 2000. Export and folding of signal-sequenceless Bacillus licheniformis beta-lactamase in Escherichia coli. *Eur J Biochem* **267:** 3836-3847.

Goffin, C., and Ghuysen, J.M. 1998. Multimodular penicillin-binding proteins: an enigmatic family of orthologs and paralogs. *Microbiol Mol Biol Rev* **62:** 1079-1093.

Gray, O., and Chang, S. 1981. Molecular cloning and expression of Bacillus licheniformis beta-lactamase gene in Escherichia coli and Bacillus subtilis. *J Bacteriol* **145:** 422-428.

Hata, M., Fujii, Y., Tanaka, Y., Ishikawa, H., Ishii, M., Neya, S., Tsuda, M., and Hoshino, T. 2006. Substrate deacylation mechanisms of serine-beta-lactamases. *Biol Pharm Bull* **29:** 2151-2159.

Herzberg, O., and Moult, J. 1987. Bacterial resistance to beta-lactam antibiotics: crystal structure of beta-lactamase from Staphylococcus aureus PC1 at 2.5 A resolution. *Science* **236:** 694-701.

Hirshberg, M., Henrick, K., Haire, L.L., Vasisht, N., Brune, M., Corrie, J.E., and Webb, M.R. 1998. Crystal structure of phosphate binding protein labeled with a coumarin fluorophore, a probe for inorganic phosphate. *Biochemistry* **37:** 10381-10385.

Huang, W., Petrosino, J., Hirsch, M., Shenkin, P.S., and Palzkill, T. 1996. Amino acid sequence determinants of beta-lactamase structure and activity. *J Mol Biol* **258:** 688-703.

Ibuka, A.S., Ishii, Y., Galleni, M., Ishiguro, M., Yamaguchi, K., Frere, J.M., Matsuzawa, H., and Sakai, H. 2003. Crystal structure of extended-spectrum beta-lactamase Toho-1: insights into the molecular mechanism for catalytic reaction and substrate specificity expansion. *Biochemistry* **42:** 10634-10643.

Inman, J.K., Highet, P.F., Kolodny, N., and Robey, F.A. 1991. Synthesis of N alpha-(tert-butoxycarbonyl)-N epsilon-[N-(bromoacetyl)-beta-alanyl]-L-lysine: its use in peptide synthesis for placing a bromoacetyl cross-linking function at any desired sequence position. *Bioconjug Chem* **2:** 458-463.

Jacob, F., Joris, B., Lepage, S., Dusart, J., and Frere, J.M. 1990. Role of the conserved amino acids of the 'SDN' loop (Ser130, Asp131 and Asn132) in a class A beta-lactamase studied by site-directed mutagenesis. *Biochem J* **271:** 399-406.

Jacoby, G.A., and Munoz-Price, L.S. 2005. The new beta-lactamases. *N Engl J Med* **352:** 380-391.

Job, V., Carapito, R., Vernet, T., Dessen, A., and Zapun, A. 2008. Common alterations in PBP1a from resistant Streptococcus pneumoniae decrease its reactivity toward beta-lactams: structural insights. *J Biol Chem* **283:** 4886-4894.

Kim, K.M., Yi, E.C., Baker, D., and Zhang, K.Y. 2001. Post-translational modification of the N-terminal His tag interferes with the crystallization of the wild-type and mutant SH3 domains from chicken src tyrosine

kinase. *Acta Crystallogr D Biol Crystallogr* **57:** 759-762.

Knox, J.R. 1995. Extended-spectrum and inhibitor-resistant TEM-type beta-lactamases: mutations, specificity, and three-dimensional structure. *Antimicrob Agents Chemother* **39:** 2593-2601.

Knox, J.R., and Moews, P.C. 1991. Beta-lactamase of Bacillus licheniformis 749/C. Refinement at 2 A resolution and analysis of hydration. *J Mol Biol* **220:** 435-455.

Knox, J.R., Moews, P.C., Escobar, W.A., and Fink, A.L. 1993. A catalytically-impaired class A beta-lactamase: 2 A crystal structure and kinetics of the Bacillus licheniformis E166A mutant. *Protein Eng* **6:** 11-18.

Koehorst, R.B., Laptenok, S., van Oort, B., van Hoek, A., Spruijt, R.B., van Stokkum, I.H., van Amerongen, H., and Hemminga, M.A. Profiling of dynamics in protein-lipid-water systems: a time-resolved fluorescence study of a model membrane protein with the label BADAN at specific membrane depths. *Eur Biophys J* **39:** 647-656.

Koehorst, R.B., Spruijt, R.B., and Hemminga, M.A. 2008. Site-directed fluorescence labeling of a membrane protein with BADAN: probing protein topology and local environment. *Biophys J* **94:** 3945-3955.

Kong, K.F., Schneper, L., and Mathee, K. Beta-lactam antibiotics: from antibiosis to resistance and bacteriology. *Apmis* **118:** 1-36.

Kurokawa, H., Shibata, N., Doi, Y., Shibayama, K., Kamachi, K., Yagi, T., and Arakawa, Y. 2003. A new TEM-derived extended-spectrum beta-lactamase (TEM-91) with an R164C substitution at the omega-loop confers ceftazidime resistance. *Antimicrob Agents Chemother* **47:** 2981-2983.

Lee, J.H., Bae, I.K., and Hee Lee, S. New definitions of extended-spectrum beta-lactamase conferring worldwide emerging antibiotic resistance. *Med Res Rev*.

Lee, W., McDonough, M.A., Kotra, L., Li, Z.H., Silvaggi, N.R., Takeda, Y., Kelly, J.A., and Mobashery, S. 2001. A 1.2-A snapshot of the final step of bacterial cell wall biosynthesis. *Proc Natl Acad Sci U S A* **98:** 1427-1431.

Lenfant, F., Labia, R., and Masson, J.M. 1991. Replacement of lysine 234 affects transition state stabilization in the active site of beta-lactamase TEM1. *J Biol Chem* **266:** 17187-17194.

Leung, Y.C., Robinson, C.V., Aplin, R.T., and Waley, S.G. 1994. Site-directed mutagenesis of beta-lactamase I: role of Glu-166. *Biochem J* **299 (Pt 3):** 671-678.

Lewis, E.R., Winterberg, K.M., and Fink, A.L. 1997. A point mutation leads to altered product specificity in beta-lactamase catalysis. *Proc Natl Acad Sci U S A* **94:** 443-447.

Lietz, E.J., Truher, H., Kahn, D., Hokenson, M.J., and Fink, A.L. 2000. Lysine-73 is involved in the acylation and deacylation of beta-lactamase. *Biochemistry* **39:** 4971-4981.

Lim, D., Park, H.U., De Castro, L., Kang, S.G., Lee, H.S., Jensen, S., Lee, K.J., and Strynadka, N.C. 2001. Crystal structure and kinetic analysis of beta-lactamase inhibitor protein-II in complex with TEM-1 beta-lactamase. *Nat Struct Biol* **8:** 848-852.

Lim, D., and Strynadka, N.C. 2002. Structural basis for the beta lactam resistance of PBP2a from methicillin-resistant Staphylococcus aureus. *Nat Struct Biol* **9:** 870-876.

Llinas, A., Ahmed, N., Cordaro, M., Laws, A.P., Frere, J.M., Delmarcelle, M.,

Silvaggi, N.R., Kelly, J.A., and Page, M.I. 2005. Inactivation of bacterial DD-peptidase by beta-sultams. *Biochemistry* **44:** 7738-7746.

Loving, G., and Imperiali, B. 2008. A versatile amino acid analogue of the solvatochromic fluorophore 4-N,N-dimethylamino-1,8-naphthalimide: a powerful tool for the study of dynamic protein interactions. *J Am Chem Soc* **130:** 13630-13638.

Ma, L., Alba, J., Chang, F.Y., Ishiguro, M., Yamaguchi, K., Siu, L.K., and Ishii, Y. 2005. Novel SHV-derived extended-spectrum beta-lactamase, SHV-57, that confers resistance to ceftazidime but not cefazolin. *Antimicrob Agents Chemother* **49:** 600-605.

Madgwick, P.J., and Waley, S.G. 1987. beta-lactamase I from Bacillus cereus. Structure and site-directed mutagenesis. *Biochem J* **248:** 657-662.

McLachlin, D.T., and Dunn, S.D. 1996. A method of screening for mutant proteins containing cysteine residues using fluorescein-5-maleimide. *Protein Expr Purif* **7:** 275-280.

McWhinney, B.C., Wallis, S.C., Hillister, T., Roberts, J.A., Lipman, J., and Ungerer, J.P. Analysis of 12 beta-lactam antibiotics in human plasma by HPLC with ultraviolet detection. *J Chromatogr B Analyt Technol Biomed Life Sci* **878:** 2039-2043.

Means, G.E., and Feeney, R.E. 1990. Chemical modifications of proteins: history and applications. *Bioconjug Chem* **1:** 2-12.

Meroueh, S.O., Fisher, J.F., Schlegel, H.B., and Mobashery, S. 2005. Ab initio QM/MM study of class A beta-lactamase acylation: dual participation of Glu166 and Lys73 in a concerted base promotion of Ser70. *J Am Chem Soc* **127:** 15397-15407.

Michalet, X., Weiss, S., and Jager, M. 2006. Single-molecule fluorescence

studies of protein folding and conformational dynamics. *Chem Rev* **106:** 1785-1813.

Minasov, G., Wang, X., and Shoichet, B.K. 2002. An ultrahigh resolution structure of TEM-1 beta-lactamase suggests a role for Glu166 as the general base in acylation. *J Am Chem Soc* **124:** 5333-5340.

Mitchell, J.M., Griffiths, M.W., McEwen, S.A., McNab, W.B., and Yee, A.J. 1998. Antimicrobial drug residues in milk and meat: causes, concerns, prevalence, regulations, tests, and test performance. *J Food Prot* **61:** 742-756.

Moffatt, B.A., and Studier, F.W. 1987. T7 lysozyme inhibits transcription by T7 RNA polymerase. *Cell* **49:** 221-227.

Monera, O.D., Sereda, T.J., Zhou, N.E., Kay, C.M., and Hodges, R.S. 1995. Relationship of sidechain hydrophobicity and alpha-helical propensity on the stability of the single-stranded amphipathic alpha-helix. *J Pept Sci* **1:** 319-329.

Mouz, N., Di Guilmi, A.M., Gordon, E., Hakenbeck, R., Dideberg, O., and Vernet, T. 1999. Mutations in the active site of penicillin-binding protein PBP2x from Streptococcus pneumoniae. Role in the specificity for beta-lactam antibiotics. *J Biol Chem* **274:** 19175-19180.

Neu, H.C. 1992. The crisis in antibiotic resistance. *Science* **257:** 1064-1073.

Nukaga, M., Kumar, S., Nukaga, K., Pratt, R.F., and Knox, J.R. 2004. Hydrolysis of third-generation cephalosporins by class C beta-lactamases. Structures of a transition state analog of cefotoxamine in wild-type and extended spectrum enzymes. *J Biol Chem* **279:** 9344-9352.

Owenius, R., Osterlund, M., Lindgren, M., Svensson, M., Olsen, O.H., Persson, E., Freskgard, P.O., and Carlsson, U. 1999. Properties of spin and

fluorescent labels at a receptor-ligand interface. *Biophys J* **77:** 2237-2250.

Page, M.G. 2000. b-Lactamase inhibitors. *Drug Resist Updat* **3:** 109-125.

Palzkill, T., and Botstein, D. 1992. Identification of amino acid substitutions that alter the substrate specificity of TEM-1 beta-lactamase. *J Bacteriol* **174:** 5237-5243.

Palzkill, T., Le, Q.Q., Venkatachalam, K.V., LaRocco, M., and Ocera, H. 1994. Evolution of antibiotic resistance: several different amino acid substitutions in an active site loop alter the substrate profile of beta-lactamase. *Mol Microbiol* **12:** 217-229.

Paterson, D.L., and Bonomo, R.A. 2005. Extended-spectrum beta-lactamases: a clinical update. *Clin Microbiol Rev* **18:** 657-686.

Phan, J., Zdanov, A., Evdokimov, A.G., Tropea, J.E., Peters, H.K., 3rd, Kapust, R.B., Li, M., Wlodawer, A., and Waugh, D.S. 2002. Structural basis for the substrate specificity of tobacco etch virus protease. *J Biol Chem* **277:** 50564-50572.

Pires de Abreu, L.R., Ortiz, R.M., de Castro, S.C., and Pedrazzoli, J., Jr. 2003. HPLC determination of amoxicillin comparative bioavailability in healthy volunteers after a single dose administration. *J Pharm Pharm Sci* **6:** 223-230.

Poole, K. 2004. Resistance to beta-lactam antibiotics. *Cell Mol Life Sci* **61:** 2200-2223.

Potterton, E., Briggs, P., Turkenburg, M., and Dodson, E. 2003. A graphical user interface to the CCP4 program suite. *Acta Crystallogr D Biol Crystallogr* **59:** 1131-1137.

Riediker, S., and Stadler, R.H. 2001. Simultaneous determination of five beta-lactam antibiotics in bovine milk using liquid chromatography

coupled with electrospray ionization tandem mass spectrometry. *Anal Chem* **73:** 1614-1621.

Romano, A., Mayorga, C., Torres, M.J., Artesani, M.C., Suau, R., Sanchez, F., Perez, E., Venuti, A., and Blanca, M. 2000. Immediate allergic reactions to cephalosporins: cross-reactivity and selective responses. *J Allergy Clin Immunol* **106:** 1177-1183.

Salverda, M.L., De Visser, J.A., and Barlow, M. Natural evolution of TEM-1 beta-lactamase: experimental reconstruction and clinical relevance. *FEMS Microbiol Rev* **34:** 1015-1036.

Sauvage, E., Kerff, F., Terrak, M., Ayala, J.A., and Charlier, P. 2008. The penicillin-binding proteins: structure and role in peptidoglycan biosynthesis. *FEMS Microbiol Rev* **32:** 234-258.

Saves, I., Burlet-Schiltz, O., Swaren, P., Lefevre, F., Masson, J.M., Prome, J.C., and Samama, J.P. 1995. The asparagine to aspartic acid substitution at position 276 of TEM-35 and TEM-36 is involved in the beta-lactamase resistance to clavulanic acid. *J Biol Chem* **270:** 18240-18245.

Schindel, C., Zitzer, A., Schulte, B., Gerhards, A., Stanley, P., Hughes, C., Koronakis, V., Bhakdi, S., and Palmer, M. 2001. Interaction of Escherichia coli hemolysin with biological membranes. A study using cysteine scanning mutagenesis. *Eur J Biochem* **268:** 800-808.

Schneider, K.D., Ortega, C.J., Renck, N.A., Bonomo, R.A., Powers, R.A., and Leonard, D.A. Structures of the Class D Carbapenemase OXA-24 from Acinetobacter baumannii in Complex with Doripenem. *J Mol Biol*.

Schuttelkopf, A.W., and van Aalten, D.M. 2004. PRODRG: a tool for high-throughput crystallography of protein-ligand complexes. *Acta Crystallogr D Biol Crystallogr* **60:** 1355-1363.

Serrano, J.M., and Silva, M. 2007. Use of SDS micelles for improving sensitivity, resolution, and speed in the analysis of beta-lactam antibiotics in environmental waters by SPE and CE. *Electrophoresis* **28:** 3242-3249.

Shih, Y.P., Wu, H.C., Hu, S.M., Wang, T.F., and Wang, A.H. 2005. Self-cleavage of fusion protein in vivo using TEV protease to yield native protein. *Protein Sci* **14:** 936-941.

Shimamura, T., Ibuka, A., Fushinobu, S., Wakagi, T., Ishiguro, M., Ishii, Y., and Matsuzawa, H. 2002. Acyl-intermediate structures of the extended-spectrum class A beta-lactamase, Toho-1, in complex with cefotaxime, cephalothin, and benzylpenicillin. *J Biol Chem* **277:** 46601-46608.

Smyth, M.S., and Martin, J.H. 2000. x ray crystallography. *Mol Pathol* **53:** 8-14.

Strynadka, N.C., Adachi, H., Jensen, S.E., Johns, K., Sielecki, A., Betzel, C., Sutoh, K., and James, M.N. 1992. Molecular structure of the acyl-enzyme intermediate in beta-lactam hydrolysis at 1.7 A resolution. *Nature* **359:** 700-705.

Strynadka, N.C., Jensen, S.E., Johns, K., Blanchard, H., Page, M., Matagne, A., Frere, J.M., and James, M.N. 1994. Structural and kinetic characterization of a beta-lactamase-inhibitor protein. *Nature* **368:** 657-660.

Studier, F.W., Rosenberg, A.H., Dunn, J.J., and Dubendorff, J.W. 1990. Use of T7 RNA polymerase to direct expression of cloned genes. *Methods Enzymol* **185:** 60-89.

Therrien, C., Sanschagrin, F., Palzkill, T., and Levesque, R.C. 1998. Roles of amino acids 161 to 179 in the PSE-4 omega loop in substrate specificity and in resistance to ceftazidime. *Antimicrob Agents Chemother* **42:** 2576-2583.

Thomas, V.L., Golemi-Kotra, D., Kim, C., Vakulenko, S.B., Mobashery, S., and Shoichet, B.K. 2005. Structural consequences of the inhibitor-resistant Ser130Gly substitution in TEM beta-lactamase. *Biochemistry* **44:** 9330-9338.

Thomson, J.M., Distler, A.M., and Bonomo, R.A. 2007. Overcoming resistance to beta-lactamase inhibitors: comparing sulbactam to novel inhibitors against clavulanate resistant SHV enzymes with substitutions at Ambler position 244. *Biochemistry* **46:** 11361-11368.

Tolic, L.P., Bruce, J.E., Lei, Q.P., Anderson, G.A., and Smith, R.D. 1998. In-trap cleanup of proteins from electrospray ionization using soft sustained off-resonance irradiation with fourier transform ion cyclotron resonance mass spectrometry. *Anal Chem* **70:** 405-408.

Vakulenko, S., and Golemi, D. 2002. Mutant TEM beta-lactamase producing resistance to ceftazidime, ampicillins, and beta-lactamase inhibitors. *Antimicrob Agents Chemother* **46:** 646-653.

Vakulenko, S.B., Taibi-Tronche, P., Toth, M., Massova, I., Lerner, S.A., and Mobashery, S. 1999. Effects on substrate profile by mutational substitutions at positions 164 and 179 of the class A TEM(pUC19) beta-lactamase from Escherichia coli. *J Biol Chem* **274:** 23052-23060.

Vanhove, M., Houba, S., b1motte-Brasseur, J., and Frere, J.M. 1995. Probing the determinants of protein stability: comparison of class A beta-lactamases. *Biochem J* **308 (Pt 3):** 859-864.

Vanhove, M., Raquet, X., Palzkill, T., Pain, R.H., and Frere, J.M. 1996. The rate-limiting step in the folding of the cis-Pro167Thr mutant of TEM-1 beta-lactamase is the trans to cis isomerization of a non-proline peptide bond. *Proteins* **25:** 104-111.

Vanwetswinkel, S., Avalle, B., and Fastrez, J. 2000. Selection of beta-lactamases and penicillin binding mutants from a library of phage displayed TEM-1 beta-lactamase randomly mutated in the active site omega-loop. *J Mol Biol* **295:** 527-540.

Vazquez, M.E., Blanco, J.B., and Imperiali, B. 2005. Photophysics and biological applications of the environment-sensitive fluorophore 6-N,N-dimethylamino-2,3-naphthalimide. *J Am Chem Soc* **127:** 1300-1306.

Vedadi, M., Niesen, F.H., Allali-Hassani, A., Fedorov, O.Y., Finerty, P.J., Jr., Wasney, G.A., Yeung, R., Arrowsmith, C., Ball, L.J., Berglund, H., *et al.* 2006. Chemical screening methods to identify ligands that promote protein stability, protein crystallization, and structure determination. *Proc Natl Acad Sci U S A* **103:** 15835-15840.

Venkatraman, P., Nguyen, T.T., Sainlos, M., Bilsel, O., Chitta, S., Imperiali, B., and Stern, L.J. 2007. Fluorogenic probes for monitoring peptide binding to class II MHC proteins in living cells. *Nat Chem Biol* **3:** 222-228.

Wang, Z., Zheng, Y., Fan, Q., Chen, X., and Lu, J. [Expression, purification and application of bla(TEM-116) extended-spectrum beta-lactamase]. *Sheng Wu Gong Cheng Xue Bao* **26:** 256-263.

Weiss, S. 2000. Measuring conformational dynamics of biomolecules by single molecule fluorescence spectroscopy. *Nat Struct Biol* **7:** 724-729.

Wilke, M.S., Lovering, A.L., and Strynadka, N.C. 2005. Beta-lactam antibiotic resistance: a current structural perspective. *Curr Opin Microbiol* **8:** 525-533.

Wood, W.B. 1966. Host specificity of DNA produced by Escherichia coli: bacterial mutations affecting the restriction and modification of DNA. *J*

Mol Biol **16:** 118-133.

Yamada, M., Watanabe, T., Miyara, T., Baba, N., Saito, J., Takeuchi, Y., and Ohsawa, F. 2007. Crystal structure of cefditoren complexed with Streptococcus pneumoniae penicillin-binding protein 2X: structural basis for its high antimicrobial activity. *Antimicrob Agents Chemother* **51:** 3902-3907.

Yang, Y., Janota, K., Tabei, K., Huang, N., Siegel, M.M., Lin, Y.I., Rasmussen, B.A., and Shlaes, D.M. 2000. Mechanism of inhibition of the class A beta -lactamases PC1 and TEM-1 by tazobactam. Observation of reaction products by electrospray ionization mass spectrometry. *J Biol Chem* **275:** 26674-26682.

Zawadzke, L.E., Chen, C.C., Banerjee, S., Li, Z., Wasch, S., Kapadia, G., Moult, J., and Herzberg, O. 1996. Elimination of the hydrolytic water molecule in a class A beta-lactamase mutant: crystal structure and kinetics. *Biochemistry* **35:** 16475-16482.